The Dissertation Committee for Ke-Yi Lin Certifies that this is the approved version of the following dissertation:

Molecular Mechanism of Poly(ADP-ribosyl)ation Catalyzed by Human Poly(ADP-ribose) Polymerase-1

Committee:

Hung-wen Liu, Supervisor

Christian P. Whitman

Walter Fast

Rick Russell

Seongmin Lee

Molecular Mechanism of Poly(ADP-ribosyl)ation Catalyzed by Human Poly(ADP-ribose) Polymerase-1

by

Ke-Yi Lin, B.S.PHR.

Dissertation

Presented to the Faculty of the Graduate School of

The University of Texas at Austin

in Partial Fulfillment

of the Requirements

for the Degree of

Doctor of Philosophy

The University of Texas at Austin

August, 2015

Dedication

I dedicate this dissertation to my family, who gave me unconditional love, wholehearted caring, and tremendous support throughout my entire life.

Acknowledgements

I would like to express my sincere gratitude to my advisor Dr. Hung-wen (Ben) Liu for his guidance and inspiration during my graduate studies. The PARP project stands alone from other biosynthetic themes in the Liu lab, and is quite challenging. Even after 50 years of its discovery, there is still much to be learned from an enzymological perspective. I appreciate him for introducing me to this fascinating enzyme, giving me the freedom to explore and the encouragement to tackle problems fearlessly. I also thank my committee members Dr. Chris Whitman, Dr. Walter Fast, Dr. Rick Russell, and Dr. Seongmin Lee for their constructive comments and suggestions.

None of this work would be accomplished without interdisciplinary collaborations. Special thanks go to Dr. Brian Cannon and Dr. Rick Russell for providing instrumental support and insightful advice in the design of single-molecule experiments and data analysis. I am grateful to Dr. Jennifer Brodbelt, Julia Aponte, and Michael Cammarata for their assistance on mass spectrometry experiments. Former lab members Dr. Hak Joong Kim, Dr. Chih-Hau Chen, Dr. Sei-hyun Choi, Mark Nielsen, and current member Richiro Ushimaru are acknowledged for their contribution to chemical synthesis. I would like to thank Dr. Mark Ruszczycky for always being fair and offering critical interpretation of my experimental data. You are a role model showing me how to ask hypothesis-driven questions and think logically. I am indebted to Dr. Yung-nan Liu not only for helping me with the molecular biology techniques, but also for giving me the warmest greetings in my daily life. Last but not least, I deeply appreciate all the essential help from the former graduate coordinator Mickie Sheppard, current graduate coordinator Stephanie Crouch, and the division coordinator Debbie Foulds. They took great care of

my registration, my employment issues, my visa status, and most importantly, my graduation. Everything would not work out without you. Thanks a million.

I wish to thank all my friends' support and companion during my life in the US. Lung-I Cheng, thank you for helping me settle down when I first move to Austin. Erica Hung and Andrea Chou, I would not be able to adjust myself to the new environment so quickly without you guys. I still remember the first time we met and chatted on the bus. Thank you Chi-Ting Chiang, Ping-Chun Li, and Lun-Chieh Lung for always being my emotional outlets and hearing my life's ups and downs. Jennifer Feng, Lucy Ko, and Sophie Chen, thank you for making me relaxed during my busiest time. I don't feel alone in the biomedical research area at all because of my NTU Pharmacy classmates and friends Tsai-Yu Chen and Li-Hsin Chang. Thank you my longtime friend Joy Chen for introducing me to the internship opportunity at OncoMed Pharmaceuticals in Redwood City, California. I had the most memorable summer time in the US and I have learned tremendously from this experience. Thanks to all these lovely people, I had so much fun during my graduate student's life besides working in the lab. I cherish our friendship very much.

Finally, I would like to thank all my past and present colleagues at UT: current Liu lab members Dr. Chia-I Lin, Anthony Romo, Hak Joong Kim, Byung-sun Jeon, Yeonjin Ko, Geng-Min Lin, Aoshu Zhong, Shao-An Wang, Jon Gengler, Richiro Ushimaru, Yu-Cheng Yeh; former Liu lab members Dr. Eita Sasaki (thank you! my rotation "Sensei"), Dr. Cheng-Hao Liu, Dr. Grace Sun, Dr. Yasushi Ogasawara, Dr. Eta Isiorho, Dr. Jordi Calveras, Dr. Reid McCarty, Dr. Hui Huang, Dr. Wei-Chen Chang, Dr. Jess White-Phillip, and Dr. Namho Kim. My heartfelt appreciation is extended to the "PARP family" Dr. Zhihua Tao, Dr. Ying Zhou, Dr. Gao Peng, Dr. Steven Mansoorabadi, Dr. Christopher Thibodeaux, Dr. Meilan Wu and Jung-Kuei Chen. In

addition to performing serious research, the Liu lab has always been a warm and supportive place to work. I have learned so much from each of you and grown both personally and professionally. Thank y'all for the unselfish sharing over the years.

Molecular Mechanism of Poly(ADP-ribosyl)ation Catalyzed by Human Poly(ADP-ribose) Polymerase-1

Ke-Yi Lin, Ph.D.

The University of Texas at Austin, 2015

Supervisor: Hung-wen Liu

Human poly(ADP-ribose) polymerase-1 (PARP-1) is an abundant nuclear enzyme which catalyzes protein poly(ADP-ribosyl)ation upon binding to DNA. NAD^+ is used as a co-substrate in the reaction via iterative transfer of its ADP-ribose moiety to acceptor proteins including PARP-1 itself, yielding elongated and branched poly(ADP-ribose) (PAR) polymers. This type of protein posttranslational modification has been demonstrated in the regulation of diverse biological processes including DNA repair, gene expression, cell cycle, etc. Therefore, elucidating the catalytic mechanism of PARP-1 would not only advance our understanding of how its enzymatic activity is regulated under physiological and pathophysiological conditions, but also greatly benefit the development of novel therapeutics involving pharmacological manipulation of PARP-1.

In this dissertation, the molecular mechanism of DNA-dependent poly(ADP-ribosyl)ation by human PARP-1 was addressed from an enzymological perspective in terms of the allosteric ligand DNA, the substrate NAD^+, and the PARP-1 protein–DNA complex as a whole. By site-specific labeling of the DNA-binding domain AB of PARP-1 and DNA ligands with fluorophores, quantitative binding kinetics of AB with DNA was investigated by single-molecule fluorescence spectroscopy. Two binding modes, one involving a strongly-associated protein–DNA complex and the other being transient,

were suggested by the experimental data. To probe the catalytic mechanism of the initiation, elongation, and branching step of poly(ADP-ribosyl)ation with regard to NAD^+ substrate scope, analogues of NAD^+ with fluoro-substituted ribose ring were synthesized chemoenzymatically and employed as substrates. The results are consistent with the proposed mechanism that the ADP-ribosyl transfer reaction proceeds through an oxocarbenium-like transition state. Mass spectrometry and biochemical approaches were utilized to decipher the poly(ADP-ribosyl)ation sites on PARP-1 and the chemical nature of PAR–protein linkages. The data confirm the existence of automodification sites beyond domain D, and lysine could be the targeted residue for poly(ADP-ribosyl)ation, either enzymatically or nonenzymatically. The macromolecular mechanism of DNA-dependent PARP-1 automodification was established by an *in vitro* radioactivity-based poly(ADP-ribosyl)ation assay using structurally distinguishable PARP-1 mutants. The data support the model of an intermolecular process. Top-down MS analysis and crosslinking assay bolster the monomeric structure of domain C in solution and its participation in interdomain contacts during PARP-1 catalysis. Taken together, these mechanistic studies provide further insight into the catalytic strategies exploited by human PARP-1 complementary to recent reports of structural characterization, and may help discover better therapeutic agents modulating poly(ADP-ribosyl)ation.

Table of Contents

List of Tables

List of Figures

Chapter 1. Background and Significance

1.1 NAD^+ AND ADP-RIBOSYLATION

Nicotinamide adenine dinucleotide (NAD^+, and its reduced form NADH, Figure 1-1) is an important organic molecule found in all living organisms. It consists of two mononucleotides, adenosine 5′-monophosphate (AMP) and nicotinamide mononucleotide (NMN) joined together by a phosphodiester bond. It has been well-established that NAD^+ serves as a coenzyme for cellular redox reactions catalyzed by oxidoreductases, where two-electron chemistry occurs on the pyridine ring of the nicotinamide base (*1*). Additionally, NAD^+ can also be utilized as a co-substrate by transferases. These transfer reactions include adenylation and ADP-ribosylation, where the phosphodiester bond and the *N*-glycosidic bond involving nicotinamide are cleaved, respectively (Figure 1-1). NAD^+-dependent DNA ligases in many bacteria species catalyze NAD^+-dependent adenylation reactions. These enzymes use NAD^+ to form an adenylate-ligase intermediate, which then transfers the AMP moiety to the 5′-phosphate of nicked DNA ends. Adenylation of the 5′-end of DNA facilitates the subsequent DNA ligation, resulting in the release of free AMP (*2*). The majority of NAD^+-consuming enzymes catalyze ADP-ribosyltransfer reaction, or ADP-ribosylation reaction (*3*). Based on the target molecules they modify, ADP-ribosyltransferases can be categorized into three classes: protein ADP-ribosyltransferases, nucleic acid ADP-ribosyltransferases, and small molecule ADP-ribosyltransferases (*4*). The following sections will give a brief introduction of each class of enzymes and the chemistry involved therein.

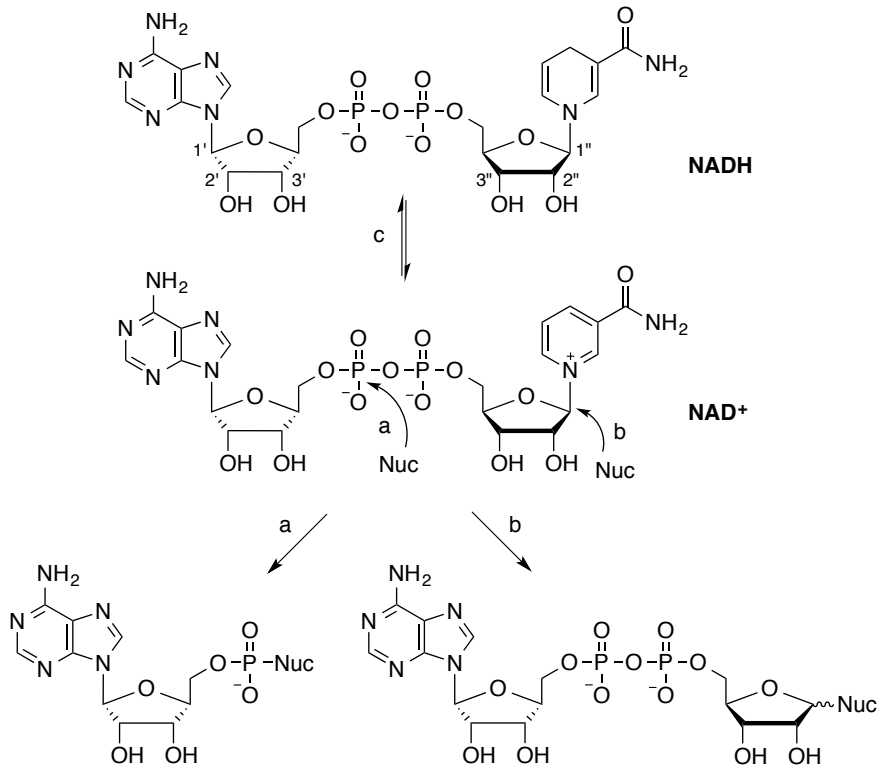

Figure 1-1. NAD^+-dependent enzymatic reactions. NAD^+ serves as a substrate in adenylation (pathway a) and ADP-ribosylation (pathway b) reactions. This is in contrast to its role as a coenzyme in redox reactions (pathway c).

1.1.1 Protein ADP-ribosyltransferases

Protein ADP-ribosyltransferases represent the largest group of all NAD^+-consuming enzymes. Protein ADP-ribosylation is an important type of protein posttranslational modifications which involves the transfer of ADP-ribose group(s) onto specific amino acid residues. Similar to phosphorylation, ADP-ribosylation of proteins can alter their enzymatic activities or molecular recognition properties, and thus modulate downstream biological effects. Enzymes that catalyze these reactions are poly(ADP-ribose) polymerases (*5-9*), mono-ADP-ribosyltransferases (*10*), and NAD^+-dependent deacetylases (*11*).

Poly(ADP-ribose) polymerases

Poly(ADP-ribose) polymerases (PARPs) carry out poly(ADP-ribosyl)ation mostly found in eukaryotes. The outcome of the reaction is the covalent attachment of multiple ADP-ribose groups from NAD^+ onto substrate proteins (Figure 1-2A). The first ADP-ribose group is typically added onto the carboxylate side chain of Glu or Asp residues on the substrate proteins, although recently ADP-ribosylation at lysine residue has also been found (*12, 13*). Following the initiation reaction, subsequent addition of ADP-ribose units can occur either on the 2′-hydroxyl group of the adenosine ribose, leading to linear elongation of poly(ADP-ribose) (PAR) polymer, or on the 2″-hydroxyl group of the nicotinamide ribose, creating a branching point (Figure 1-2A). Currently 17 PARPs have been identified in the human genome, with PARP-1 being the most extensively-studied member (*14*). PARPs exert myriad biological functions by covalently modifying their target proteins, or employing noncovalent interaction between PAR polymer and the recognition proteins (*15*). The detailed biochemistry and physiological functions of the PARP superfamily will be presented in later sections.

Mono-ADP-ribosyltransferases

Mono-ADP-ribosyltransferases (ARTs) catalyze the transfer of single ADP-ribose group onto substrate protein, similar to the first step of poly(ADP-ribosyl)ation reaction. The acceptor amino acid residues include Arg, Cys, Asn (less likely), and posttranslationally modified diphthamide (Figure 1-2B) (*16*). Mono(ADP-ribosyl)ation was originally discovered through studying bacterial toxins such as diphtheria toxin, cholera toxin, pertussin toxin, and pseudomonas exotoxin A (*16, 17*). In *Rhodospirillum rubrum* and other free-living photosynthetic bacteria, mono(ADP-ribosyl)ation by DraT is used to regulate the activity of enzyme involved in nitrogen fixation (*18*).

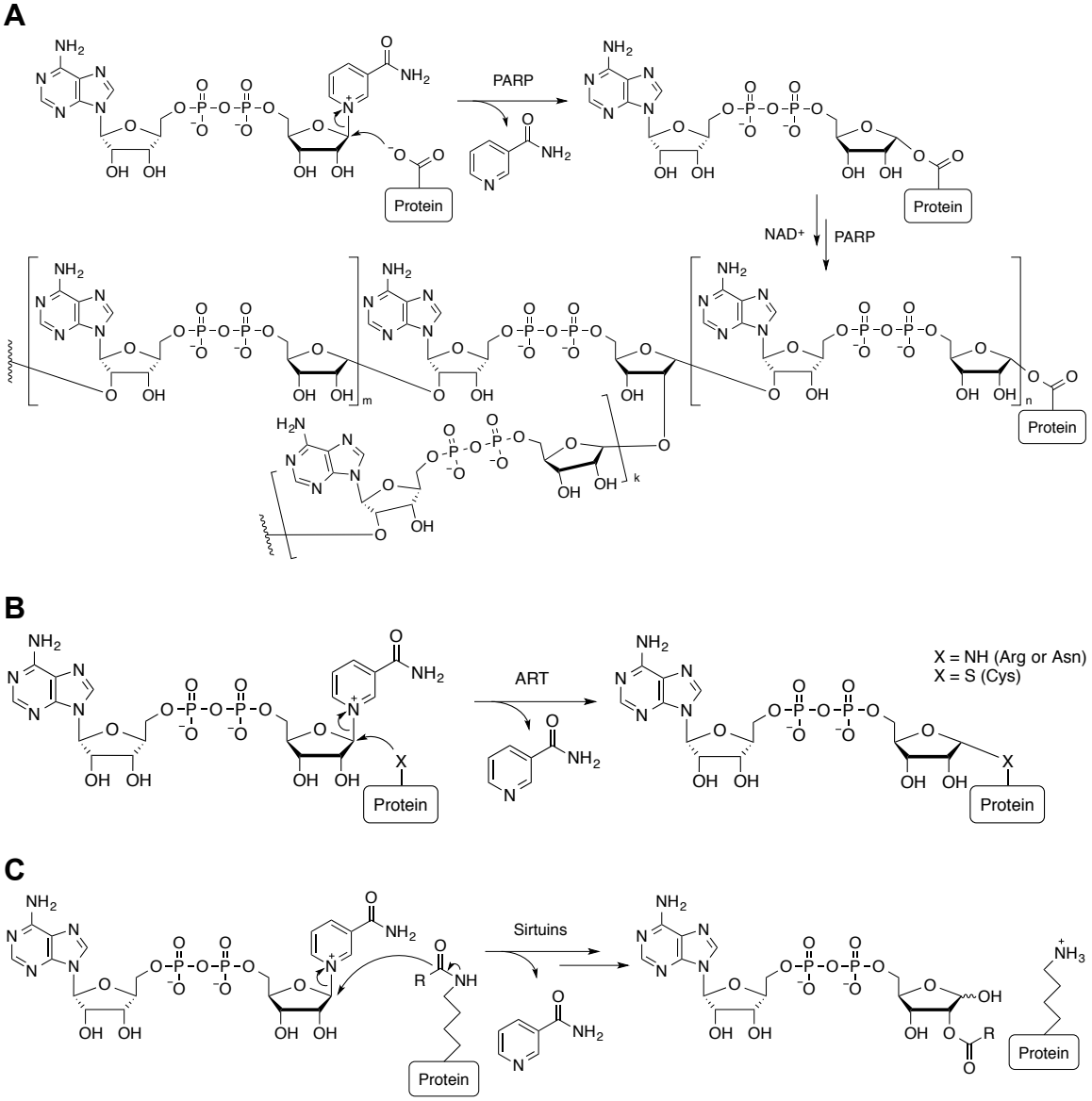

Figure 1-2. Enzymatic activities of protein ADP-ribosyltransferases. (A) PARPs catalyze the addition of multiple ADP-ribose groups onto Glu, Asp, or Lys residues, generating long and branched ADP-ribose polymers. (B) ARTs catalyze the addition of single ADP-ribose group onto Arg, Asn or Cys residues. (C) NAD^+-dependent deacetylases (sirtuins) catalyze lysine deacylation. The net reaction is the generation of free lysine and *O*-acylated ADP-ribose.

Eukaryotic ARTs have not been discovered until very recently (*8, 19*). Mammalian ART1-5 are the only ARTs that are structurally related and have been characterized to molecular level (*19*). They are ectoenzymes that catalyze extracellular mono(ADP-ribosyl)ation of integrins, defensins, and purinergic receptors, modulating cellular immune response (*10*). Intracellular mono(ADP-ribosyl)ation has been reported, but no definitive molecular characterization of enzymes responsible for this modification exists. Two groups of proteins may be involved in this process, the NAD^+-dependent deacylases (*20*) and members within the PARP superfamily possessing "PARP-like" feature (*21*).

NAD^+-dependent deacetylases

Protein acetylation, including histone acetylation, is an emerging posttranslational modification that correlates with not only gene expression but also metabolic regulation (*22, 23*). Histone deacetylases (HDAC) are Zn^{2+}-dependent protein deacetylase that use Zn^{2+} ion in the active site to activate a water molecule to perform amide bond hydrolysis (*24*). Another class of deacetylases is NAD^+-dependent, which couples protein deacetylation with the consumption of NAD^+ (Figure 1-2C). Sir2 (silencing information regulator 2) is the first discovered protein in this class, thus Sir2-like proteins have been collectively called "sirtuins." Sirtuins are evolutionarily conserved in all kingdoms, with seven homologues (SIRT1-7) identified in human (*20*). Sirtuins have been implicated in regulating various biological processes including metabolism and aging (*25*). In addition to its deacetylation activity, several sirtuins have been found to possess ADP-ribosyltransferase activity. However, such side activity may not be physiologically relevant (*26*). More recently, some sirtuins were found to be able to hydrolyze several newly identified lysine posttranslational modifications including succinylation,

malonylation, and palmitoylation very efficiently, suggesting this class of enzymes could catalyze protein "deacylation" reactions in general (*27, 28*).

1.1.2 Nucleic acid ADP-ribosyltransferases

There are only a few examples of ADP-ribosyltransferases that use nucleic acids as substrates. The first one is tRNA-dependent 2′-phosphotransferase Tpt1 found in yeast, whose function is to remove the 2′-phosphate group from the spliced tRNA in the presence of NAD^+ (Figure 1-3) (*29, 30*). The mechanism involves a two-step process, where the ADP-ribose group is first transferred to the 2′-phosphate of spliced tRNA, resulting in an ADP-ribosyl-tRNA intermediate (*31*). The second step is the attack of the phosphate linkage by the adjacent 2′-hydroxyl group, generating dephosphorylated tRNA and ADP-ribose-1′,2′-cyclic phosphate (*32*).

Pierisin-1, identified from the cabbage butterfly *Pieris rapae*, is an DNA ADP-ribosyltransferase. This enzyme has been shown to catalyze mono(ADP-ribosyl)ation of 2′-amino group of guanine residues in DNA and induces apoptosis in mammalian cells (*33*). The clam DNA ADP-ribosylating proteins (CARPs) and a secretory protein SCO5461 from *Streptomyces coelicolor* with similar activities have also been characterized (*34, 35*).

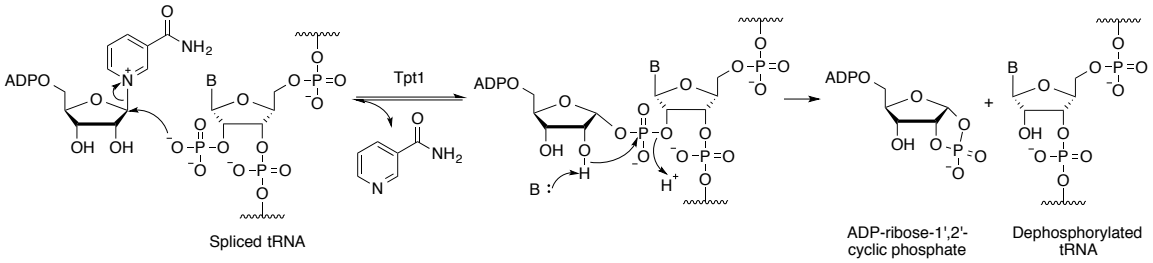

Figure 1-3. Proposed mechanism for NAD^+-dependent tRNA 2′-phosphotransferase.

1.1.3 Small molecule ADP-ribosyltransferases

Representative ADP-ribosyltransferases that modify small molecules include CobT from the biosynthetic pathway of cobalamin in bacteria (*36, 37*), rifampin ADP-ribosyltransferase Arr (*38*), and the special type ADP-ribosyl cyclases (*39*). CobT can use either NAD^+ or nicotinate mononucleotide (NaMN) as a substrate to modify 5,6-dimethylbenzimidazole (DMB), the base of the lower ligand of cobalamin (*40*). The Arr is responsible for the inactivation of antibiotic rifampin in mycobacteria species (*38*).

ADP-ribosyl cyclases use NAD^+ to generate cyclic ADP-ribose (cADPR, Figure 1-4A). The first ADP-ribosyl cyclase was identified from sea urchin egg homogenate (*41*). Mammalian cells contain two homologues identified so far, CD38 and CD157, both of which are ectoenzymes (*39*). Catalysis by ADP-ribosyl cyclases is initiated by forming an enzyme-stabilized oxocarbenium intermediate or a transient ADP-ribosyl-enzyme intermediate. The attack of such intermediate intramolecularly by the adenine base gives cADPR as a product (Figure 1-4A). Interestingly, ADP-ribosyl cyclases also catalyze the hydrolysis of cADPR (Figure 1-4A), and the base exchange reaction of nicotinamide with nicotinic acid in $NADP^+$ to produce nicotinate adenine dinucleotide phosphate ($NAADP^+$, Figure 1-4B). Both cADPR and $NAADP^+$ can serve as signaling molecules for the regulation of intracellular calcium concentration, distinct from inositol 1,4,5-triphosphate (IP_3) pathway (*42, 43*).

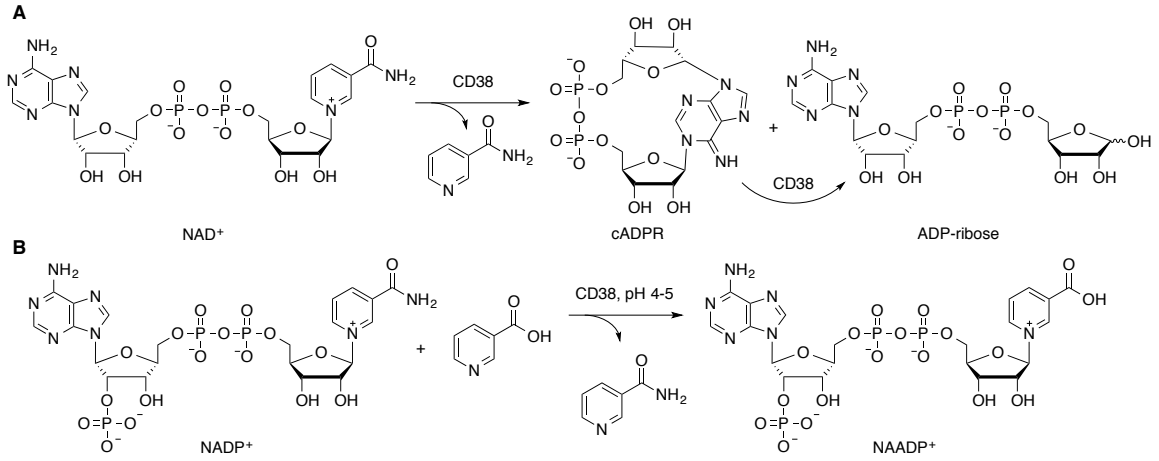

Figure 1-4. Enzymatic reactions catalyzed by mammalian CD38. (A) The formation of cADPR from NAD^+ and its hydrolysis. (B) The formation $NAADP^+$ from $NADP^+$.

In summary, ADP-ribosyltransferases are a diverse group of enzymes that use NAD^+ to modify a variety of molecules to induce a wide range of biological activities. Mechanistically, they also perform fascinating chemistry at the anomeric carbon of the nicotinamide ribose ring. More mechanistic details will be discussed in the following sections for poly(ADP-ribosyl)ation and the major enzyme that catalyzes the reaction, PARP-1.

1.2 BIOCHEMISTRY OF PROTEIN POLY(ADP-RIBOSYL)ATION

1.2.1 Discovery of poly(ADP-ribosyl)ation

The first report of poly(ADP-ribose) formation was published in 1963 by Chambon *et al*. (*44*). It was observed that the radioactivity of [*adenine*-^{14}C]- or [α-^{32}P]-labeled ATP was incorporated into the acid-insoluble fraction of hen liver nuclei upon the addition of NMN. The stimulated enzymatic activity was DNA-dependent, and the resulted product was resistant to DNase, RNase, or protease treatment, suggesting the

structure to be polyadenylate (poly(A)). This result was quickly confirmed by Sugimura *et al*., in which they used the similar nuclear preparation from rat liver and hepatoma cells (*45*).

Following the initial report, the same authors showed that radiolabeled NMN and ATP were incorporated into the polymer in equimolar amount (*46*). Therefore, previously observed stimulatory effect of NMN could be attributed to its capability to serve as the biosynthetic precursor of the substrate for the polymer formation. This suggests that NAD^+, whose biosynthetic precursors are NMN and ATP, is the immediate substrate for polymerization (*46*).

1.2.2 Structural features of poly(ADP-ribose) polymer

The structure of the polymer was first examined by degradation of the polymer using alkaline hydrolysis, acid hydrolysis, snake venom phosphodiesterases and alkaline phosphatase. The polymer was resistant to alkaline hydrolysis, ruling out the possibility of being poly(A). Complete digestion of the polymer yielded a mixture of adenine, ribose and phosphate with a ratio of 1:2:2, respectively, indicating ADP-ribose (or its isomer) as the monomer unit. This observation was later confirmed by Hayaishi *et al*. (*47, 48*) as well as Sugimura *et al*. (*49, 50*). The studies carried out by Hayaishi *et al*. also suggested that the polymer is composed of ADP-ribose units connected through ribose-ribose linkages (*48*).

Extensive characterizations of PAR polymer were done in the 1970s to gain new information about its chemical structure (Figure 1-5A). ^{13}C-NMR (nuclear magnetic resonance) studies carried out by Miwa *et al*. established that the ADP-ribose unit is connected through an α-(1″→2′)-ribose-ribose glycosidic bond (*51, 52*). Upon enzymatic

digestion with snake venom phosphodiesterase, the resulting compounds released from the polymer is 2′-(5″-phosphoribosyl)-5′-AMP (PRAMP, or *iso*-ADP-ribose), which is termed the elongation monomeric unit (*52*), together with 5′-AMP, to a lesser amount, which is derived from polymer termini (*53*). Therefore, it was proposed that PAR is a linear polymer, and the size of the polymer can be estimated by the ratio between PRAMP and AMP (*54*).

In 1978, Sugimura *et al*. reported that polymer with at least 65 residues by counting bands showing on the polyacrylamide electrophoresis gel, has an average chain length of about 30 residues as determined by the radioactivity ratio of the digested products (*55*). This implies the possibility of a branched polymeric structure with multiple 5′-AMP termini. Further studies by the same group provided definitive structural evidence of the branching unit, *O*-α-D-ribofuranosyl-(1‴→2″)-*O*-α-D-ribofuranosyl-(1″→2′)-adenosine-5′,5″,5‴-tris(phosphate) (*56, 57*), abbreviated as $(PR)_2AMP$. Visual evidence of a branched PAR polymer was also demonstrated subsequently by electron microscopy (Figure 1-5B) (*58, 59*).

The investigation of the three-dimensional conformation of PAR was hindered by its structural complexity. Specific antibodies have been raised successfully against PAR (*60*). Since they did not cross-react with DNA, RNA, or poly(A), it is possible that PAR adopts a unique conformation owing to its α-ribosyl linkages and branching units. Kun *et al*. have postulated the existence of helical structure of PAR based on CD spectroscopy (*61, 62*). However, recent NMR study indicated that free PAR appears to be devoid of inherent regular structure (*63*).

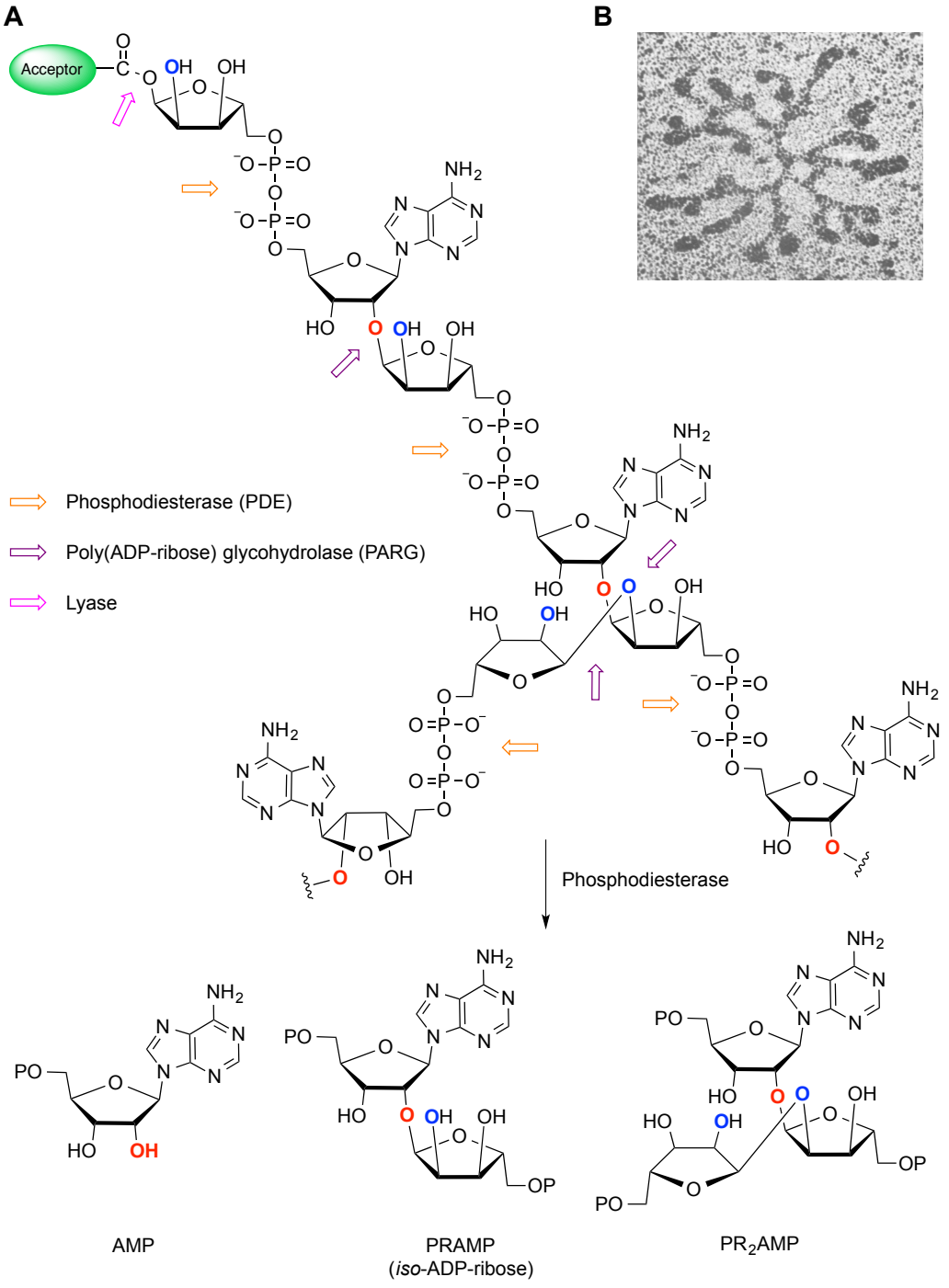

Figure 1-5. (A) Structure of PAR polymer and its enzymatic digestion products. Arrows indicate the cleavage site by specific enzyme. (B) An electron microscopic image of branched PAR structure adapted from (*58*).

The polymer size and average branching frequency can be estimated by the following formula,

$$\text{Average polymer size per molecule} = \frac{[\text{AMP}]+[\text{PRAMP}]+[(\text{PR})_2\text{AMP}]}{[\text{AMP}]-[(\text{PR})_2\text{AMP}]}$$

$$\text{Average number of branching points per molecule} = \frac{[(\text{PR})_2\text{AMP}]}{[\text{AMP}]-[(\text{PR})_2\text{AMP}]}$$

where AMP, PRAMP, and $(PR)_2AMP$ are produced by phosphodiesterase digestion. The size distributions of the polymers isolated from cell extracts are highly heterogeneous based on polyacrylamide gel electrophoresis (*55*). It was determined that the chain length of PAR polymer, generated *in vitro* or *in vivo*, ranges from a few oligomer up to 200 units, with branching point occurring every 20 to 50 units (*64*).

Shortly after the discovery of PAR, Hayaishi *et al*. revealed that PAR is associated with histones in the form ranging from monomer to oligomers, suggesting the possibility of covalent linkage to histones (*65*). This observation was confirmed and extended by a number of researchers both *in vitro* and *in vivo* (*66-68*). Based on the chemical instability to neutral hydroxylamine treatment and alkaline liability, it was proposed that an ester bond involving the carboxylate group of either Glu or Asp and the ADP-ribose moiety could be the covalent linkage (*69*). In the early 80s, several Glu residues and the terminal carboxylate group have been determined to be the sites of poly(ADP-ribosyl)ation on histones (*70, 71*). However, the automodification sites of PARP-1, the most abundant nuclear enzyme responsible for this reaction, remained unresolved until 2009 when our previous group member Dr. Zhihua Tao verified three ADP-ribosylation sites using mass spectrometry (MS) (*72*). More recent publication suggested that lysine could also serve as the acceptor residue for poly(ADP-ribosyl)ation in both PARP-1 and core histones (*12, 13, 73*).

1.2.3 Enzymes involved in poly(ADP-ribose) metabolism

Poly(ADP-ribosyl)ation is an important protein posttranslational modification that involves in the covalent attachment of ADP-ribose polymer onto specific amino acid residues of target proteins. The modification drastically changes the physicochemical properties of the substrate proteins to modulate their biological functions. This process appears to be highly dynamic and reversible *in vivo*, as long polymers generated upon DNA damage have a half-life of less than 1 min, in contrast to 7.7 h of constitutive short ADP-ribose polymers (*74*). In addition, the co-substrate of this reaction, NAD^+, is an essential coenzyme involved in energy metabolism and redox balance (*75*), underscoring the important connection between posttranslational modification and cellular metabolism. Therefore, the metabolism of PAR polymer is tightly controlled in eukaryotic cells (*5, 8*).

Three types of enzymes are involved in PAR metabolism (Figure 1-6) (*8*): PARPs which catalyze the synthesis of PAR polymer on the acceptor proteins, poly(ADP-ribose) glycohydrolase (PARG) or ADP-ribosylhydrolase 3 (ARH3) (*76*), which catalyzes the degradation of PAR into free polymer or ADP-ribose monomer, leaving the proteins mono(ADP-ribosyl)ated, and ADP-ribosyl protein glycohydrolase or ADP-ribosyl protein lyase, which removes the final ADP-ribose unit from the acceptor proteins.

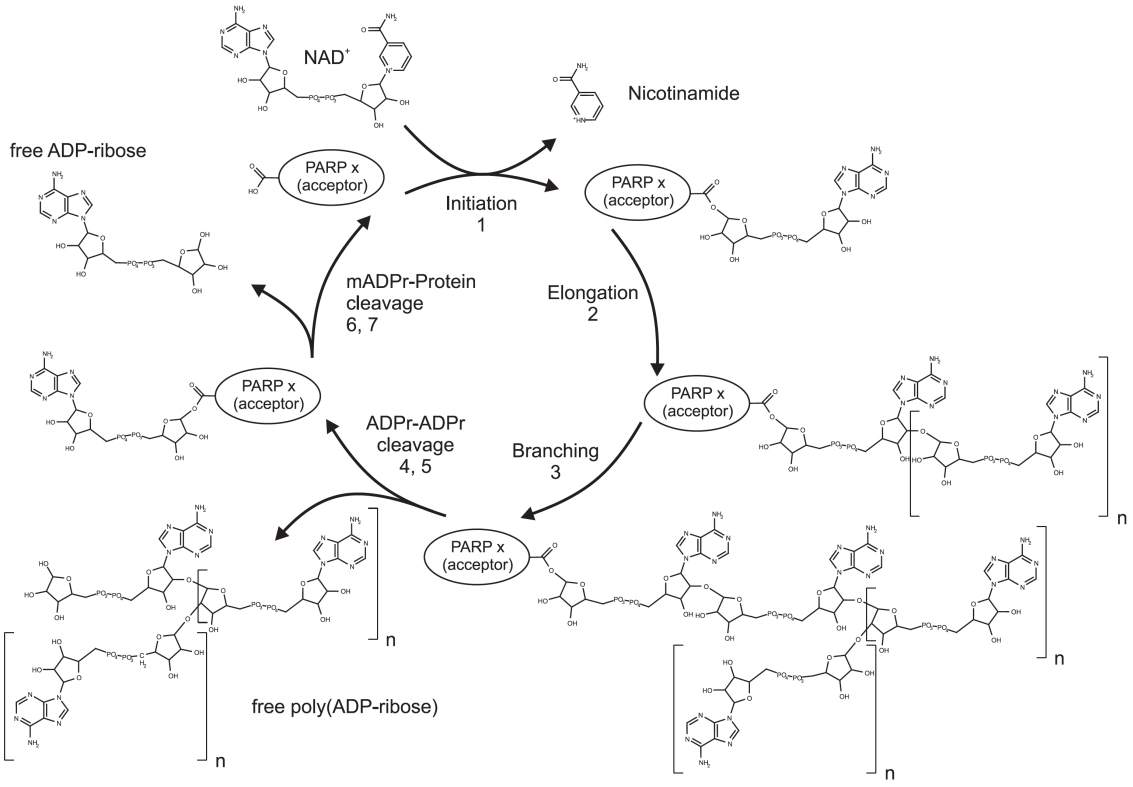

Figure 1-6. Metabolism of PAR polymer. (*8*). The synthesis of PAR polymer requires three steps: step 1, initiation, or mono(ADP-ribosyl)ation of the acceptor protein residues (Glu carboxylate is shown as an example); step 2, elongation of the polymer; and step 3, branching of the polymer. Step 1-3 are catalyzed by PARPs. The degradation process consists of step 4, the endoglycolytic and step 5, exoglycolytic cleavage catalyzed by PARG to give mono(ADP-ribosyl)ated proteins. The final stage of degradation involves step 6, cleavage of the terminal ADP-ribose unit from protein residues by TARG, or other macrodomain-containing hydrolases, or step 7, ADP-ribose lyase to complete the reaction cycle.

The PARP superfamily

The gene encoding human PARP-1 was first cloned in the late 80s (*77*). For many years, PARP-1 was believed to be the only PARP responsible for poly(ADP-ribosyl)ation. However, it was later found that *parp*-null mice cells could also synthesize PAR, suggesting the presence of other genes capable of producing PAR (*78, 79*). To date, a total of 17 genes have been identified as members of the "PARP superfamily" based on

their sequence homology to the "PARP signature" motif within the catalytic domains (Figure 1-7) (*7, 14*), but not all members within the family can synthesis PAR. Biochemical characterizations have shown that only PARP-1, PARP-2, tankyrase-1 and tankyrase-2 possess true polymerase activities. PARP-1 and PARP-2 can synthesize long and branched PAR polymers (*64, 79*), wherease tankyrase-1 could only synthesize linear polymers (*80*). Tankyrase-2 is also capable of forming poly(ADP-ribosyl)ated structures noticed as a smear on anti-PAR western blot, but its ability to introduce branching units has not been verified (*81*). A recent study aimed to establish the exact enzymatic activity of each member within the PARP superfamily showed that the majority of PARPs only generate mono-ADP-ribose, suggesting that the H-Y-E catalytic triad located within the active site is not the sole indicator of PARP activity (*82*). Indeed, there has been a call from the PARP research community to adopt a new nomenclature system toward mammalian ADP-ribosyltransferases according to their structural and biochemical features (*3*).

PARP-1 is the most abundant nuclear protein able to catalyze initiation, elongation, and branching reactions to synthesize PAR onto different acceptor proteins, including itself (*83*), with more than 90% of the overall cellular PAR found (*84*). PARP-1 is activated by single strand and double strand DNA breaks, giving rise up to a 500-fold increase in PAR level (*74, 85*). In addition to PARP-1, histones are also considered to be the major acceptors for PAR (*86*). A significant number of nuclear proteins have been identified as substrate proteins for poly(ADP-ribosyl)ation by PARP-1 including enzymes involved in DNA repair and transcription (*87*).

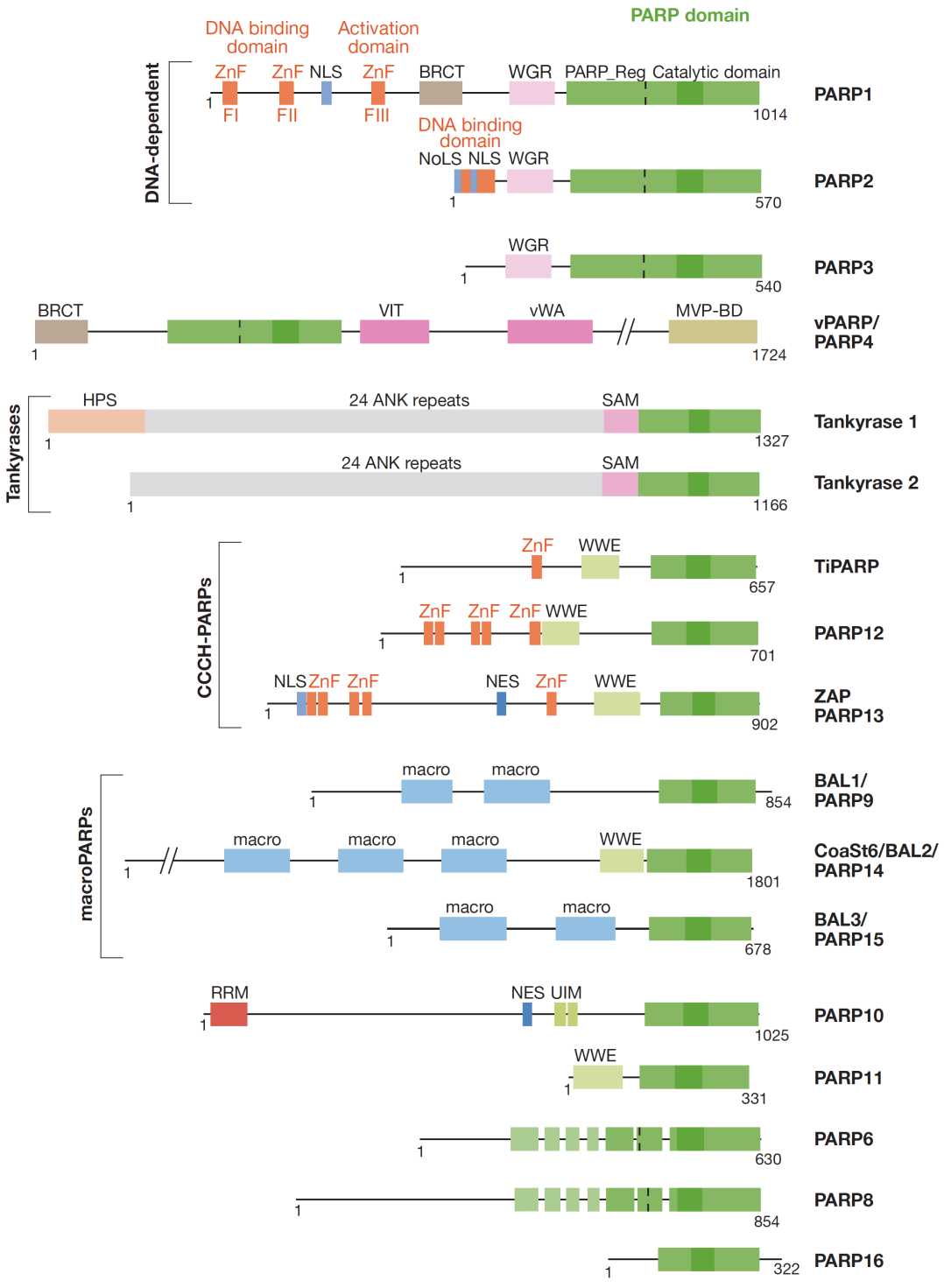

Figure 1-7. Domain organization of the PARP superfamily members (*88*).

Two other members, PARP-2 and PARP-3, belong to the same subgroup as PARP-1 because of the similarity of their domain architectures. PARP-2 activity can be activated by binding to RNA (*89*), whereas PARP-3 which lacks DNA-binding domain acts as a mono-ADP-ribosyltransferase and can in turn activate PARP-1 in the absence of DNA (*90*). Both PARP-2 and PARP-3 have been implicated to play a role in the DNA repair pathway (*91*).

Tankyrases are PARPs found to be associated with human telomeres that regulate telomere length, mitotic spindle formation, transcription, and protein degradation (*15, 92-94*). Relatively little is known about other members of the PARP superfamily. But several articles published recently have provided valuable insights into their biochemical properties as well as physiological functions in transcription, antiviral response, and stress granule assembly (*95-99*).

Poly(ADP-ribose) glycohydrolase

PARG is the principal enzyme responsible for the catabolism of PAR (*100, 101*). While multiple genes encode different PARPs, there is only one gene known to encode PARG (*102*). Mammalian cells contain several PARG isoforms located within various subcellular compartments, each of which is derived from alternative splicing of the same *parg* mRNA (*103*). Two isoforms are predominant: a 110-kDa full-length protein localized within nucleus, and a 60-kDa catalytically active isoform localized within cytoplasm/mitochondria (*103, 104*). Isoforms are different in the arrangement of the *N*-terminal regulatory domain and the presence or absence of cellular localization signal sequences, while the *C*-terminal catalytic domain is always conserved.

PARG has both exo- and endoglycosidase activities. Its reaction leads to monomeric ADP-ribose and free PAR polymers (Figure 1-5, the cleavage sites; Figure 1-

6, step 4 and 5) (*100, 105*). ADP-ribose could serve as a source for potential histone glycation or glycoxidation (*106*), whereas free PAR could interact noncovalently with PAR-recognition proteins and serve as a signaling molecule to induce downstream biological effects such as apoptosis (*107, 108*). Therefore, the dynamic interplay between PARPs and PARG could be vital for regulating many cellular processes (*101, 109*).

ADP-ribosyl protein lyase / ADP-ribose protein glycohydrolase

After PARG hydrolyzes the PAR polymer, one ADP-ribose residue remains attached to the proteins. To remove the very last ADP-ribose unit, it was hypothesized that an ADP-ribosyl protein lyase facilitates this reaction (Figure 1-7, step 6, 7). In the late 70s, Hayaishi *et al*. reported the observation of enzymatic activity capable of cleaving ADP-ribosyl histone linkage from partially purified rat liver cytosol (*110*), and an 83-kDa enzyme was subsequently purified to homogeneity by Oka *et al*. (*111*). However, no further characterization or genetic information of this enzyme was published ever since its discovery. It was until 2013 that a group of scientists identified a terminal ADP-ribose protein glycohydrolase (TARG) from patients with severe neurodegeneration attributable to the genetic abnormality of an unidentified enzyme involved in the cleavage of the bond between glutamate and ADP-ribose (*112*). It was noted that the enzyme TARG has a different molecular weight from 83-kDa, thus the existence of ADP-ribosyl lyase awaits to be confirmed.

1.2.4 Noncovalent protein interactions with poly(ADP-ribose)

Poly(ADP-ribosyl)ation is a posttranslational modification of target proteins with PAR polymers (*113*). While the covalent attachment of negatively-charged polymers may directly alter the physicochemical properties of the acceptor proteins, the size and

structural flexibility of the PAR polymers could also be exploited in noncovalent interactions with other proteins. Namely, the PAR polymer may serve as scaffolds for the assembly of multiprotein complexes or play roles in ligand binding-induced allosteric responses. Several evolutionarily conserved protein domains have been identified to be the recognition motifs for binding to PAR (*99, 113*).

PAR-binding motif

The phenomenon of noncovalent protein–PAR interaction was first observed for histones (*67, 114*), and later demonstrated *in vitro* using purified PAR polymers (*115*). Similar behavior was also noted for non-histone nuclear proteins such as p53, DNA-PK, and DNA ligase III, leading to the identification of a common PAR-binding motif (PBM) composed of an assortment of hydrophobic and basic amino acid residues downstream of a Lys- and Arg-rich region (Figure 1-8A) (*116*). Further alignments of this motif to better locate PBM in proteome had refined the types of hydrophobic residues around the dual K/R cores (Figure 1-8B) (*117*). The PBM is considered to be more of a physicochemical property pattern rather than exact amino acid sequence. No structural details of how PAR being recognized by PBM is available.

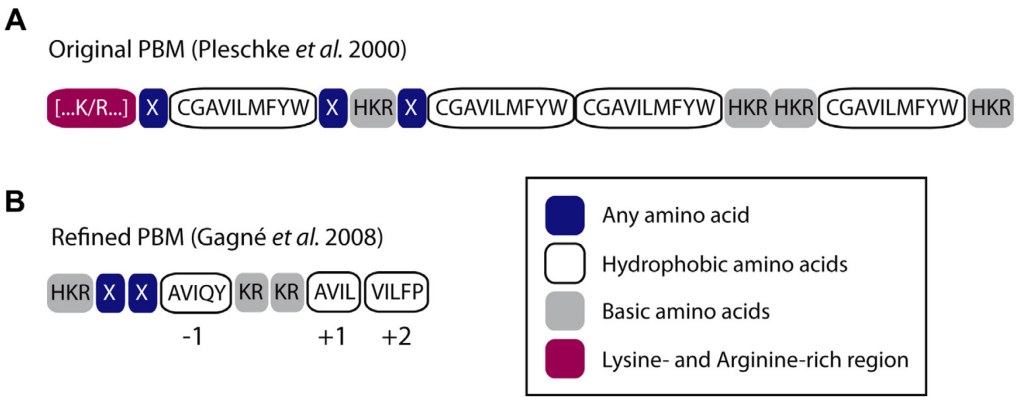

Figure 1-8. The noncovalent PAR-binding motif.

PBMs are present on the surface of a large number of proteins involved in chromatin-related processes such as DNA damage repair, DNA replication and transcription (*99, 116*). Thus PAR (protein-linked or free form) may function as a signal platform to recruit binding partners to chromatin where they execute biological tasks. Alternatively, PAR-binding can disrupt protein-ligand or protein–protein interactions, or even destabilize the folding of the domain to which it binds, so that protein functions may be modulated. As an example, PAR binding to apoptosis-inducing factor (AIF) is required for its release from the mitochondria to induce cell death in parthanatos (*118*). Given the fact that both nucleic acids and PAR have negatively-charged phosphate backbone and nucleobases, many more nucleic acids-interacting proteins could also bind PAR, adding another layer of regulation by poly(ADP-ribosyl)ation (*99*).

Macro domain

The macro domain was first reported for a core histone variant with unknown function (*119*). More than a decade later Karras *et al*. demonstrated that a macro domain homologue found in archaea can hydrolyze ADP-ribose-1″-phosphate to ADP-ribose and inorganic phosphate, and provided structural support for its ability to bind ADP-ribose (*120*). Subsequent studies showed that some macro domains could not only interact with ADP-ribose, but also with PAR, making it a novel PAR-interaction protein module (*121-123*). In spite of minimal sequence homology, the structure of PARG solved lately exhibited a similar macro fold housing the PARG signature GGG-X_{6-8}-QEE binding motif for ADP-ribose which is critical for its exo- and endoglycolytic activity (*124, 125*). In addition to cleaving the glycosidic bond of PAR, a group of macro domain-containing proteins were also demonstrated to be capable of hydrolyzing ADP-ribose derivatives including *O*-acetyl-ADP-ribose and mono(ADP-ribosyl)ated protein carboxylate side

chains (*126-128*). Collectively, macro domains are ADP-ribose-binding module with or without hydrolytic enzymatic activities.

PAR-binding zinc finger

Zinc fingers with PAR-binding affinity were discovered in a subgroup of proteins related to PAR metabolism in eukaryotes (*129*). Three human proteins carrying PAR-binding zinc finger (PBZ) motif identified so far are the aprataxin and PNK-like factor (APLF), the checkpoint protein with FHA and RING (really interesting new gene) domains (CHFR), and the DNA cross-link repair 1A protein (DCLRE1A) (*129*). PBZ motif has been shown to recognize α-(1″→2′)-ribosyladenosine, the core structure of PAR elongation unit (*130*). Upon UV irradiation, APLF is rapidly recruited to DNA damage site in a PAR-dependent manner via its PBZ domain to facilitate non-homologous end-joining (NHEJ) repair (*129*). CHFR is involved in mitotic checkpoint (*131*), but the function of DCLRE1A is unknown.

WWE domain

The WWE domain, named after its most conserved Trp and Glu residues, is a common module found in E3 ligases and a subset of PARP members, implying the potential cross-talk between ubiquitylation and poly(ADP-ribosyl)ation systems (*132*). Crystal structure and biochemical studies confirmed that some WWE domains, not all, could bind PR-AMP, the PAR elongation unit (*133*). The identification of Iduna/RNF146, a RING family E3 ligase containing the WWE domain, provided direct evidence that PAR-binding through the WWE domain is required for Iduna's E3 ligase activity which catalyzes the ubiquitylation of PARP-1 and other proteins associated with DNA repair (*134, 135*). Poly(ADP-ribosyl)ation of axin catalyzed by tankyrase can also trigger its activity for targeting proteasome degradation and regulating the Wnt signaling

pathway (*136*). PAR-binding induced conformational change of the RING domain reveals a new mechanism of how noncovalent protein–PAR interaction controls protein functions (*137*).

Miscellany

More PAR binding modules have been discovered in the last two years, including the FHA domain (*138*), the BRCT domain (*139*), the oligonucleotide/oligosaccharide-binding (OB) fold (*140*), and the PAR-binding regulatory motif (*141*). The FHA and BRCT domain have been established to be phospho-Ser/Thr-binding domains involved in the regulation of cell cycle and DNA damage response (*142*); OB fold is a single strand DNA or RNA binding domain found in prokaryotes and eukaryotes (*143*). The capability of these domains to recognize PAR polymer is not surprising owing to the high similarity of the structural elements between PAR and nucleic acids. It is also noteworthy that not all proteins containing the abovementioned domains can bind PAR. Hence, biochemical characterization of each individual protein is still needed to verify the predicted properties.

1.2.5 Cellular functions and therapeutic implications

Since the first discovery of PAR in rat liver nuclei and its association with chromatin, poly(ADP-ribosyl)ation has been postulated to play a regulatory role in the biological processes in relation to nuclei (*54*). Indeed, a significant body of literature published over the years indicated that poly(ADP-ribosyl)ation is crucial to stress response, maintenance of genome stability, and cell survival, dictated by genetic manipulations and pharmacological perturbations on enzymes involving PAR metabolism (*6, 144*).

DNA repair and other DNA-dependent biological processes

DNA repair is a collection of nuclear processes found in all cellular organisms that have evolved to cope with ubiquitously occurring DNA damage and to maintain genome integrity (*145*). The mechanism of PAR formation during DNA repair was first reported in a seminal paper by Lindahl, *et al*. in 1992 (*146*). It is now well-established that under low to moderate levels of DNA damage caused by alkylating agents, oxidation, or ionizing radiation, PARP-1 binds to DNA lesions and its activity is rapidly activated to produce long and branched PAR polymers onto itself and various substrate proteins including histones. PAR polymers generated thereafter can facilitate DNA repair processes as a result of covalent modifications of proteins involved or through noncovalent interactions with other proteins. The automodified PARP-1 has decreased affinity for DNA and therefore dissociates from DNA, allowing DNA repair enzymes such as DNA polymerase β, XRCC1 (X-ray repair cross-complementing protein 1), and DNA ligase III to have access to lesions. The PAR polymers can also attract histones from the nucleosomes and expose DNA to the repair enzymes, suggesting chromatin remodeling being a PAR-regulated process (*147*). Recent findings further demonstrated that PARP-1 is an architectural protein for chromatin and automodified PARP-1 promotes nucleosome assembly and thereby facilitates chromatin remodeling (*148, 149*). The effect of poly(ADP-ribosyl)ation is terminated by the removal of PAR polymers by PARG or other PAR-degrading enzymes.

DNA damage response (DDR) is a complex signaling pathway from sensing the aberrations, transducing the signals to downstream effectors and coordinating this whole process spatiotemporally (*150*). Poly(ADP-ribosyl)ation is one of the earliest posttranslation modifications in response to DNA single-strand or double-strand breaks (SSBs or DSBs) (*151*). In SSB or single-strand DNA damage, only one of the two strands

of a double helix has a defect, and this type of damage can be reversed by base excision repair (BER) pathway, in which PARP-1 is directly involved as mentioned earlier. DSBs are more deleterious to cells as these breaks can cause genome rearrangement or collapse of DNA replication fork, leading to developmental disorders and cancer. There are three mechanisms to repair DSBs: non-homologous end-joining (NHEJ), microhomology-mediated end joining (MMEJ) or alternative NHEJ, and homologous recombination (HR) (*151*). Accumulating evidence implicates that poly(ADP-ribosyl)ation participates in the determination of appropriate repair mechanisms to counteract DNA lesions (*152*). Poly(ADP-ribosyl)ation either provides a docking site for the targeted proteins, or modulates their conformation, stability, or enzymatic activity. Studying the molecular mechanisms of poly(ADP-ribosyl)ation in DDR has led to the development of novel therapeutic agents against certain types of cancer with inherent defects in DNA repair (*94*). Such cancer cells can only rely on PARP-1-dependent DNA repair pathway for survival, thus inhibition of PARP-1 creates a phenomenon referred to as "synthetic lethality."

In addition to DNA repair, poly(ADP-ribosyl)ation has also been suggested in other DNA-dependent processes including chromatin remodeling, transcription, replication, recombination, mitosis (*152-155*). PARP-1 can affect chromatin structure, be part of the transcription complexes, or control the actions of insulator. PARP-1 also controls the progression of replication fork in the presence of DNA damage. PARP-1 and PARP-2 catalytic activity may indirectly contribute to V(D)J recombination in immune cells. PARP-1 and other PARPs are associated with centrosomes and regulate spindle formation during mitosis. These results further underscore the importance and universality of poly(ADP-ribosyl)ation in chromatin-related processes and epigenetics.

Cell death

Contrary to the preservative role of poly(ADP-ribosyl)ation under low levels of DNA damage, PARP-1 activation in the presence of moderate to severe DNA damage promotes cell death (*156*). Early studies of PARP-1's involvement in cell death pathways focused on caspase-dependent apoptosis. It has been shown that PARP-1 cleavage by caspase-3 or 7 is the hallmark of cells undergoing apoptosis (*157*). Loss of enzymatic activity in the cleaved PARP-1 fragments is believed to be important for preserving energy for apoptosis.

PARP-1 also plays a pivotal role in caspase-independent apoptotic pathway mediated by apoptosis-inducing factor (AIF) (*158*). PAR polymers generated by PARP-1 in response to moderate DNA damage serve as a death signal and triggers the release of AIF from the mitochondria outer membrane, resulting in its translocation into nucleus to induce DNA fragmentation (*107, 108*).

When cells encounter severe DNA damage or other types of acute injury, PARP-1 hyperactivation may cause cell necrosis. The phenomenon is attributed to the depletion of cellular NAD^+ or ATP pool, leading to energy imbalance and mitochondria dysfunction (*159, 160*), and can be attenuated by treating cells with PARP inhibitors (*161*). This model connects poly(ADP-ribosyl)ation with cellular metabolism in terms of NAD^+ metabolome, which can be altered during ischemic reperfusion injury and cancer development (*75*).

Stress response

From a stress-coping perspective, the role of poly(ADP-ribosyl)ation (or specifically, PARP-1) in determining cell fate depends on the type, strength and duration of the stress stimuli (Figure 1-9). PARP-1 activation under mild stress conditions would lead to transcription and DNA repair responses that help reverse the damage, promote

transient inflammatory response, re-establish homeostasis, and maintain cell survival. Moderate to severe extent of stress gives cell death programs a cue to execute either apoptosis or necrosis. The regulatory effect of poly(ADP-ribosyl)ation in response to stress stimuli can happen at the DNA level, affecting transcription and other chromatin-related processes, or at the posttranslational level, or the protein–PAR interactions. Growing evidence published in the past few years also shed light on the emerging role of poly(ADP-ribosyl)ation in RNA biology, including noncoding RNA in gene regulation, RNA processing, and ribosome biogenesis (*162-164*). Taken together, poly(ADP-ribosyl)ation exerts its cellular functions at essentially all steps of central dogma, and elucidation of the underlying mechanisms at physiological or pathophysiological conditions could have tremendous impact on its therapeutic applications.

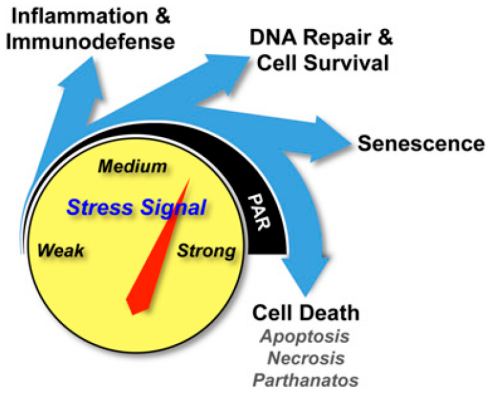

Figure 1-9. PARP-1 functions as a gauge of cellular stress response (*156*).

PARP inhibitors

Given the multifaceted roles of poly(ADP-ribosyl)ation in a wide range of physiological processes, it is of great interest to develop small molecules capable of modulating PARP activity as therapeutic agents (*165*). 3-Aminobenzamide (3-AB, Figure 1-10), a nicotinamide analogue, is the first reported PARP inhibitor which enhances the

cytotoxicity of DNA alkylating agents in murine leukemia cells. Its mode of action inspires the development of PARP inhibitors as sensitizing agents for chemotherapy (*166, 167*). Since then, a plethora of medicinal chemistry programs began to develop nicotinamide mimetic scaffolds as NAD^+ competitive inhibitors for PARP-1 (Figure 1-10) (*168*). Historically, the research effort has been devoted mostly to PARP-1 inhibition, but more and more data now suggest that other PARPs also have distinct biological functions. A Swedish group recently showed that most PARP inhibitors being used in research or evaluated clinically lack specificity and have promiscuous inhibitory activity (*169*). As a result, chemical optimization for isoform-specific PARP inhibitors is needed to assess whether cross-inhibitory activity is therapeutically relevant, and to dissect the biological functions of those poorly studied PARPs.

At present, seven PARP inhibitors are under active clinical trials as a single agent or in combination with other chemotherapeutic agents, with all indications against tumors (Table 1-1). Rucaparib was the first PARP inhibitor to enter human clinical trial in 2003 along with alkylating agent temozolomide to treat patients with advanced solid tumors (*170*). Iniparib, unlike others, was identified as a noncompetitive PARP-1 inhibitor which disrupts PARP-1 zinc finger/DNA interaction, preventing PARP-1 activation (*171*). The compound was brought into clinics and gained success in phase 1 and phase 2 trials without firm characterization of its mechanism of action. It was until the report of failure in a large-scale phase 3 trial of iniparib that prompted researchers to re-examine the preclinical data and found that this compound was not a *bona fide* PARP inhibitor after all (*172*). This result again reminds scientists that sufficient preclinical data, proof-of-mechanism studies, criteria for patient selection, and careful interpretation of clinical outcomes are all key to the success of drug development (*173*). Despite the downside of

iniparib, olaparib (Lynparza™), developed by AstraZeneca, was granted approval by the FDA in December 2014 for the treatment of ovarian cancer with BRCA mutation (*174*).

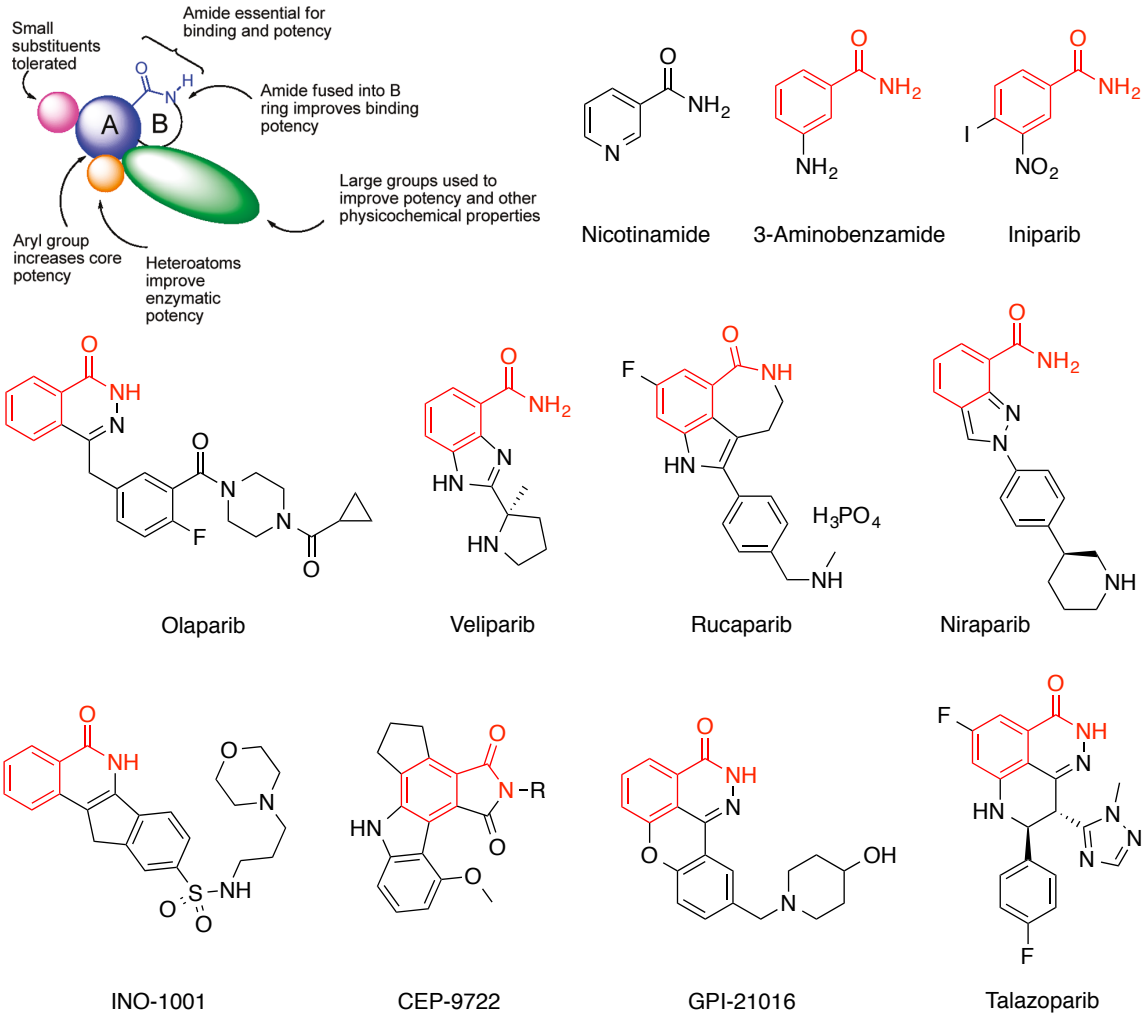

Figure 1-10. PARP-1 pharmacophore (*168*) and chemical structures of PARP inhibitors.

Beyond oncologic indications, the therapeutic effect of PARP inhibition has also been explored in the field of anti-inflammation and cytoprotection (*175*). As hyperactivation of PARP-1 causes cellular energy failure and induces necrosis, inhibition of PARP was expected to alleviate the cytotoxicity elicited by oxidative stress (*176*).

INO-1001 was the only PARP inhibitor that entered clinical studies for cardiac ischemia, particularly ST-elevated myocardial infarction, but unfortunately no significant response was observed (*168*). The "no-go" decision of this drug highlights the challenges in this clinical path and warrants further fundamental studies of the functions of poly(ADP-ribosyl)ation in stress response.

Poly(ADP-ribosyl)ation has been implicated in various cellular pathways and compelling evidence substantiates the therapeutic benefits of PARP inhibition. While elucidation of the mechanism of action of existing PARP inhibitors could provide important insights into PARP biology (*177*), the molecular mechanism of enzymatic catalysis, especially for PARP-1, is still unsettled. Learning the mechanistic details could have significant impact on the development of specific PARP-1 inhibitor with novel mechanism of action. The following sections will describe the current understandings of PARP-1 with an emphasis on mechanistic enzymology.

PARP inhibitor	Company	Status	Indication
AG-014699/Rucaparib	Pfizer/Clovis	Phase 2, 3	Solid tumors, melanoma
BSI-201/Iniparib	BiPAR/Sanofi-aventis	Phase 3 (terminated)	Triple negative breast cancer
INO-1001	Inotek/Genentech	Phase 1 (terminated)	Melanoma
GPI-21016/E-7601	MGI Pharma/Eisai	Phase 2	Melanoma
ABT-888/Veliparib	Abbott/AbbVie	Phase 3	Solid, hematological tumors
AZD-2281/Olaparib	AstraZeneca	Approved	BRCAmutant ovarian cancer
CEP-9722	Cephalon/Teva	Phase 1, 2 (terminated)	Solid tumors
MK-4827/Niraparib	Merck/Tesaro	Phase 3	Solid, hematological tumors
BMN-673/Talazoparib	BioMarin	Phase 2, 3	Solid, hematological tumors

Table 1-1. PARP inhibitors under clinical trials (*168, 176*).

1.3 Overview of Human PARP-1

1.3.1 Modular organization of human PARP-1

PARP-1 is the founding member of the PARP superfamily and the best characterized enzyme for poly(ADP-ribosyl)ation in eukaryotes. It is the most abundant nuclear protein after histones. The 113-kDa polypeptide chain can be separated into three distinct functional units by limited proteolysis: the DNA-binding domain, the automodification domain, and the substrate binding/catalytic domain (*178*). Multiple sequence alignment across species can further divide PARP-1 into six subdomains (Figure 1-11) (*179*).

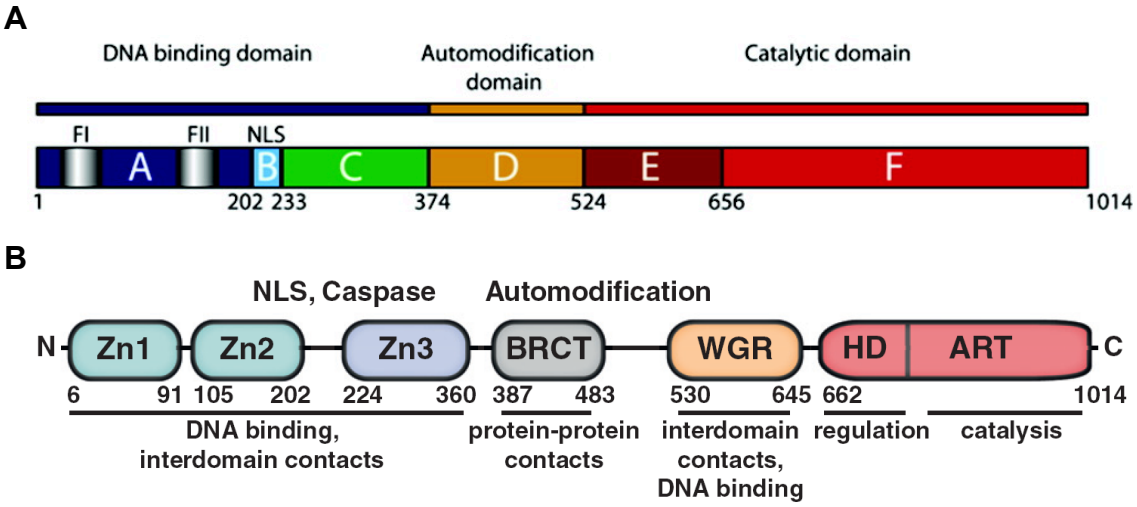

Figure 1-11. Modular structure of human PARP-1. (A) Classical naming system divides PARP-1 into six domains in alphabetic order according to their functions. (B) Naming with specific structural motifs (*180*).

Domain A contains two unusually long $CX_2CX_{28/30}HX_2C$ zinc finger motifs, termed zinc finger I (FI) and zinc finger II (FII), which can recognize a large set of different DNA lesions with high affinity rather than specific nucleotide sequence (*181-183*). This protein–DNA interaction triggers the catalytic activation of PARP-1. FI has

also been shown to be important for PARP-1 activation, as PARP-1 FII deletion mutant only showed reduced DNA binding affinity but remained catalytic active (*181*). These "PARP-like" zinc fingers have only been found to be present in a small number of proteins including DNA ligase IIIα and DNA 3′-phosphodiesterase from *Arabidopsis thaliana* (AtZDP) (*184*).

Domain B is a short oligopeptide region with a bipartite nuclear localization signal (NLS) in the form of KRK-X_{11}-KKKSKK. This sequence is essential for targeting PARP-1 to the nucleus (*185*). Within the NLS eleven amino acid linker X_{11} harbors the caspase-3 cleavage site $D_{211}EVD_{214}$. The cleaved enzyme fragment possesses only basal activity and can no longer be activated in the presence of damaged DNA (*157*). PARP-1 cleavage by caspase-3 has been considered to be one of the hallmarks of apoptosis (*157*).

Domain C has been known to be important for PARP-1 activity (*186*). In 2008, both X-ray crystallographic (*187*) and NMR study (*188*) unraveled that domain C contains a novel $CX_2CX_{12}CX_9C$ zinc-binding motif, termed zinc finger III (FIII). Unlike FI and FII, FIII alone does not bind to DNA, however, it is required for DNA-dependent PARP-1 activation (*187, 188*). It was proposed that interdomain contact mediated by domain C could be crucial to PARP-1 activity. Domain C forms a homodimeric structure in the crystal, but exists as a monomer in solution NMR study. Following structure-guided mutagenesis showed that residues located in the dimeric interface are not required for DNA-dependent PARP-1 activation (*189*). Whether full-length PARP-1 function as a monomer or dimer upon activation by DNA remains elusive, and will be part of the focus of this dissertation. The discrepancy between two structural studies could be due to the effect of crystal packing. In Chapter 4 of this dissertation, a MS-based approach used to probe the solution structure of domain C will be presented.

Domain D was first called the automodification domain attributed to its high occurrence of Glu and Asp residues as potential automodification sites (*190-193*). Recently, multiple automodification sites within this region have been confirmed by MS (*72, 73, 112, 194, 195*), and surprisingly a significant number of sites are present beyond domain D. The domain also contains a breast cancer 1 protein (BRCA1) *C*-terminus (BRCT) fold which also presents in many DNA damage repair and cell cycle checkpoint proteins, and is critical for mediating protein–protein interactions (*196*). It has been thought that the BRCT motif is the dimerization interface of PARP-1 upon activation. But a recent solution NMR and small-angle X-ray scattering (SAXS) study indicated that the BRCT fold exists as a monomer and no interactions could be detected either with other BRCT-containing proteins or PARP-1 itself (*197*), casting doubt of its role in the molecular mechanism of PARP-1 catalysis.

Domain E contains a WGR motif, which was named after the conserved Trp, Gly and Arg amino acid residues. This domain is essential for PARP-1 activity (*12, 198*). Recent findings demonstrated that domain E is capable of binding to short RNAs, PAR polymer, and double strand DNA (*198, 199*). Structural studies also provided evidence for its DNA-induced interdomain contacts with FI, FIII, and the helical subdomain (HD) within domain F (*200*).

Domain F is referred to as the minimal catalytic domain and is responsible for the basal level of DNA-independent activity of PARP-1 (*201*). Many important amino acid residues involving NAD^+ binding and catalysis are located within this domain. The single active site can catalyze the initiation, elongation, and branching reactions for the synthesis of PAR polymer, as well as the hydrolysis of NAD^+ to produce free ADP-ribose (*83*). In human PARP-1, the region spanning from residue 859 to 908 enclosing NAD^+ binding is phylogenetically well conserved in the PARP superfamily and thus designated

as the "PARP-signature" fold (*179*). The *N*-terminal section of domain F is the α-helical PARP regulatory domain (PRD, or HD), and its detailed function during DNA-dependent PARP-1 activation is to destabilize the catalytic domain as demonstrated in a recent structural study (*200*). Crystal structure of the PARP-1 catalytic domain displayed a striking homology to bacterial toxins that act as mono-ADP-ribosyltransferase (*202, 203*). The reaction mechanism will be discussed in Section 1.5.

1.3.2 Posttranslational modifications

Like other proteins that play key roles in regulating physiological processes, PARP-1 is subject to numerous posttranslational modifications, including poly(ADP-ribosyl)ation, acetylation, phosphorylation, ubiquitylation, and SUMOylation (*204*). PARP-1 is poly(ADP-ribosyl)ated by itself, PARP-2, and perhaps other PARPs. Extensive automodification inhibits its DNA binding and catalytic activities (*5*). Acetylation of PARP-1 by p300/CREB-binding protein regulates NF-κB-dependent gene transcription in immune cells (*205*). Phosphorylation of PARP-1 by ERK1/2 reinforces or promotes sustained catalytic activity under stress conditions (*206, 207*). SUMOylation of PARP-1 affects its function as a transcription co-activator of hypoxia-responsive genes (*208*), and this modification is stimulated by PARP-1 binding to intact, undamaged DNA (*209*). Polyubiquitylation of PARP-1 promotes its degradation and therefore regulating its overall activity (*210*).

1.3.4 Substrate proteins for PARPs

PARP-1 acts as the major acceptor in the cell for over 90% of PAR synthesized under stress stimuli (*84*). However, several nuclear substrate proteins have also been

identified *in vitro* and *in vivo*, which are predominantly involved in the metabolism of nucleic acids and in the maintenance of chromatin structure (*5*). With the advance of analytical technology, proteomic profiling of substrate proteins for ADP-ribosyltransferases or PARPs have made significant progress in the past five years (*211*). Di Girolamo *et al*. reported a method using an ADP-ribose-binding macro domain to enrich the ADP-ribosylated proteins in mammalian cell lysates and identified ART substrates by MS (*212*). In our laboratory, we have taken effort to screen PARP-1 substrates using both yeast and human proteome microarray and found a number of ribosomal proteins being modified by PARP-1, implying the potential regulatory function of poly(ADP-ribosyl)ation in ribosome biogenesis (*164*). Similar strategy has been applied for the identification of PARP-2 substrates (*213*). Poirier *et al*. adopted an antibody affinity purification coupled with MS analysis to profile the interactome of PARP-1, PARP-2, and PARG in human cancer cell lines (*214*). However, this procedure cannot distinguish between protein covalent poly(ADP-ribosyl)ation, noncovalent protein–PAR interaction, and direct protein–protein interaction. The same group later profiled the poly(ADP-ribosyl)ation proteome using anti-PAR 10H antibody. The experiment was carried out with the enrichment of poly(ADP-ribosyl)ated proteins by inactive (macro domain-like) PARG mutant and MS was used as the analytic tool to provide time-resolved information of cellular proteins associated with PAR under genotoxic insult (*215*). A SILAC- (stable isotope labeling by amino acids in cell culture) based quantitative proteomic analysis was also developed to discover poly(ADP-ribosyl)ated proteins under different stress conditions (*216*).

The concept of chemical biology has influenced the PARP field and stimulated newly designed experiments (*211, 217*). Lin *et al*. chemically synthesized clickable NAD^+ analogues and biotin affinity tag to profile PARP-1 and tankyrase-1 substrates and

found not only nuclear but also mitochondrial proteins being poly(ADP-ribosyl)ated (*218*). Recently a method featuring boronate resin-enrichment combined with hydroxylamine elution was developed to specifically convert Glu- and Asp-poly(ADP-ribosyl)ated residues into hydroxamic tags, which greatly facilitates their detection by MS (*195*). The results revealed a number of poly(ADP-ribosyl)ated proteins with specific modification sites, including PARP-1. Inspired by the "bump-and-hole" strategy in identifying kinase substrates, Cohen *et al*. applied the same idea onto PARP-1 and PARP-2 to engineer orthogonal enzyme-substrate pairs for substrate profiling (*219*). Their data suggested semi-complementary yet distinct targets for PARP-1 and PARP-2 under stress paradigms.

Despite the unfolding of ADP-ribosylation proteome, the identified substrate pools remain partially overlapped among different experimental conditions and procedures. Methods capable of differentiating specific amino acid linkage are still lacking. Nevertheless, protein poly(ADP-ribosyl)ation promises to be an active research area in the near future.

1.4 DNA BINDING PROPERTIES OF HUMAN PARP-1

1.4.1 Differential roles of DNA binding motifs in PARP-1

It is well known that intracellular PARP-1 activity is strongly stimulated in the presence of DNA lesions, and the activity is dependent on the number or types of DNA strand breaks, not the nucleotide sequence (*220-222*). The robust activation of PARP-1 enzymatic activity is mainly mediated by DNA binding to the two unique zinc fingers, FI and FII, located within PARP-1 *N*-terminal domain (*223*). They belong to a small family of "PARP-like" zinc fingers which were initially found to recognize DNA nicks as

evidenced by an electron microscope study (*224*). Thus, PARP-1 has been referred to as the "nick-sensor" (*179*).

The two zinc fingers appear to have differential roles in DNA recognition. While existing consecutively in PARP-1, phylogenetic analysis indicates that they are divergent (*184*). In early 90s, de Murcia and colleagues first showed by site-direct mutagenesis that disruption of the metal binding ability of FII dramatically reduced its binding to DNA single-strand break, whereas mutations of the corresponding FI zinc coordinating amino acid residues only slightly affects its DNA binding ability (*182*). Using DNA footprinting they also demonstrated that polypeptide containing FI and FII binds at the single-strand break via FII, and perhaps as a dimer (*182*). After less than a year, Ikejima *et al*. published their findings that both FI and FII are required for PARP-1 activation by single-strand breaks, but activation by double-strand breaks requires only FI (*181*).

The abovementioned studies provided a rough picture of the differential roles of the PARP-1 zinc fingers in terms of binding affinity for different DNA structures and subsequent catalytic activation. FI appears to be less important in binding to single-strand breaks and may prefer double-strand breaks. However, it is essential for all kinds of DNA-induced PARP-1 activation perhaps through interdomain interactions. FII is primarily responsible for protein–DNA interaction and is dispensable for PARP-1 activation by double-strand breaks. A novel zinc-ribbon fold distinct from FI and FII has recently been identified in domain C, named FIII (*187, 188*). FIII does not have DNA binding affinity, but it is required for DNA-dependent PARP-1 activation (*187, 188*).

In addition to three zinc-binding motifs, other regions of the PARP-1 molecule have been shown to be able to bind DNA. The existence of a double-strand DNA binding (DsDB) domain was confirmed by Satoh *et al*. (*199*). The DsDB domain is a highly basic 60-amino acid stretch located between the BRCT and WGR domain (around the

boundary of domain D and E, residues 480–540), which possesses weak double-strand DNA binding affinity relative to FI and FII, as well as medium PAR binding affinity. PAR binding to the DsDB domain can displace double-strand DNA and results in the dissociation of PARP-1 from DNA. DsDB domain may also control PAR synthesis, as illustrated in an experiment that a truncated PARP-1 construct containing the WGR and catalytic domain can produce long PAR polymers in the presence of dumbbell DNA, whereas construct containing additional DsDB domain only produced short PAR polymers. It is proposed that DsDB domain may assist in the overall DNA binding of PARP-1 by stabilizing intact double-strand DNA adjacent to the lesion sites. The exact function of DsDB domain in the context of full-length PARP-1 during the catalytic cycle remains to be verified.

From a recent SAXS study of full-length PARP-1 complexed with 8-mer DNA carried out by our laboratory, we discovered that the *C*-terminal end of the WGR domain (residues 626–645) can enhance PARP-1's binding to DNA, and is important in the following catalytic activation (*198*). The detailed structural studies of how PARP-1 recognizes different DNAs will be discussed in the later section.

1.4.2 Interactions with various DNA structures

PARP-1 is capable of interacting with a variety of DNA structures including damaged, intact, or even non-B DNA structures (*225*). PARP-1 shows low nanomolar affinity for DNA with nicks, overhangs, as well as blunt ends (*226*), but the corresponding catalytic power (estimated by V_{max}, units per mg protein) is not necessarily proportional to its DNA binding affinity. A systematic examination of the binding modes of PARP-1 DNA-binding domain (residues 1–234) towards different DNA substrates and

their correlation with PARP-1 enzymatic activation was performed by Bombarda *et al*. (*227*). The analysis indicated that PARP-1 can distinguish 3′-overhang (5′-recessive end) from 5′-overhang (3′-recessive end) DNA, with higher catalytic activity induced by binding to 3′-overhang. DNA with blunt ends gave stimulatory activity similar to DNase I-treated activated DNA mixtures. Intrinsic tryptophan fluorescence intensity and anisotropy measurements afforded 2:1 and 1:1 protein–DNA binding stoichiometry for 3′-overhang and 5′-overhang, respectively. The higher catalytic activity could be explained by the potential dimerization of PARP-1 at the 3′-overhang lesion site. Moreover, DNA intra- or interstrand cross-links created by alkylating agents such as cisplatin can promote PARP-1 binding and trigger downstream cytotoxic response (*228*). These data clearly suggested that PARP-1 can adopt different recognition modes according to the DNA damage types and exert structure-specific activity.

Apart from damaged DNA, PARP-1 can occupy intact DNA such as promoter regions, regulating gene transcription and chromatin structure through poly(ADP-ribosyl)ation (*148*). Numerous non-B DNA structures including hairpins, cruciforms, and the stably unpaired regions (loops) are all effective activators of PARP-1 automodification and heteromodification of histone 1 (*183*). More recently, PARP-1 was shown to be capable of binding to the G-quadruplex structure in the human *c-myc* gene's promoter and participates in its conversion into transcriptionally more active B-DNA form (*229*). From a chromatin perspective, PARP-1 also possesses nucleosome binding properties and functions as a chromatin architectural protein (*230-232*). The binding is dependent on nucleosome particles and does not involve free DNA ends or linkers. Automodified PARP-1 has the ability to sequester histones and assemble nucleosomes *in vitro* (*149*). This model suggests that PARP-1 automodification not only loosens chromatin for the recruitment of DNA repair machinery or transcription complex, but

also facilitates the re-establishment of chromatin structure through histone chaperone activity (*149*).

1.4.3 Structural evidence for PARP-1–DNA interactions

The exact mechanism of how PARP-1 recognizes DNAs and the binding stoichiometry are largely debated in light of the modular nature of PARP-1 molecule and its binding flexibility toward various DNA structures. Nevertheless, several crystal and NMR structures published in the past five years have significantly improved our understandings of this complex protein–DNA interaction.

Pascal *et al*. first determined the structures of individual zinc fingers FI and FII in complex with an 8-bp or 10-bp blunt end DNA as a mimic of double-strand break (*233*). FI and FII both bind to DNA in a similar fashion, with the phosphate backbone grips interacting with the minor groove of DNA near the 3′-end, and the base stacking loop extending 90° from the phosphate backbone grip, capping the 5′-end terminal base (Figure 1-12A, B). Both proteins associated with duplex DNA in monomeric form. The residues responsible for protein–DNA interactions were probed biochemically by site-directed mutagenesis. But based on the observed structural similarity it remains difficult to explain the differential roles of FI and FII, such as FI rather than FII is essential for blunt end DNA-induced PARP-1 activation, and FII has stronger affinity than FI for blunt end DNA (*233*).

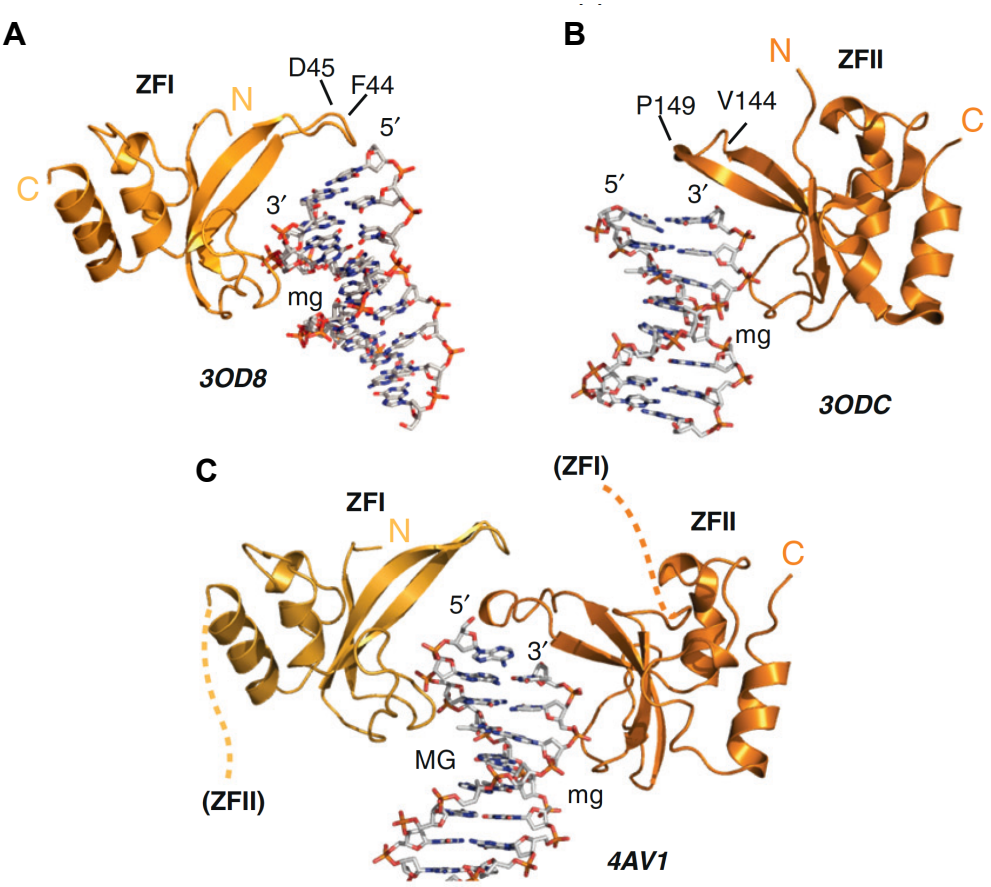

Figure 1-12. Crystal structures of human PARP-1 zinc fingers in complex with DNAs (*234*). (A) Zinc finger I complexed with a 10-bp duplex DNA (PDB: 3OD8) (*233*). (B) Zinc finger II complexed with a 8-bp duplex DNA (PDB: 3ODC) (*233*). (C) PARP-1 DNA-binding domain (residues 5–202) containing FI and FII complexed with a 11-bp single-base 5′ overhang duplex DNA (PDB: 4AV1) (*235*). mg, minor groove; MG, major groove.

A clearer picture of how these two zinc fingers cooperate to recognize DNA strand breaks can be seen from a following report where the authors used a protein construct bearing both FI and FII to crystallize with a duplex DNA containing single-base 5′-overhang mimicking DNA single-strand break (*235*). In their structure, FII binds to DNA in the same way as isolated domain, but FI binds to the opposite side of DNA, with its phosphate backbone grip interacting with the major groove and base stacking loop on

top of the corresponding loop in FII (Figure 1-12C). Unlike the 3′ recessed strand, the 5′-terminus is free from protein obstruction and the phosphate backbone can extend beyond the lesion site, implying the suitability of the current structure model for PARP-1 binding to single-strand DNA breaks. More importantly, the observed FI and FII proteins at the lesion site must come from different polypeptide chains, as the linker between FI and FII is too short to connect each other (Figure 1-12C). *In vivo* DNA damage site recruitment studies and *in vitro* gel shift, GST pull-down experiments confirmed the requirement of FI and FII protein–protein interactions for the assembly of a functional PARP-1 DNA-binding domain in response to DNA damage. DNA-induced dimerization of PARP-1 is therefore proposed to operate at the discontinued DNA damage site, facilitating intermolecular poly(ADP-ribosyl)ation reaction.

Despite the observed dimerization of the PARP-1 DNA-binding domain *in crystallo*, biophysical analyses in solution suggested a different recognition mode for PARP-1–DNA interaction. Analytical ultracentrifugation and SAXS data modeling showed that PARP-1 fragments containing both zinc fingers or with extra FIII and BRCT domain bind to model DNAs in a 1:1 stoichiometry (*236, 237*). Perturbations of NMR chemical shift signals indicated that FII binds to single-strand DNA in an identical way regardless of whether the protein fragment includes FI or not (*237*). The discrepancy among these studies could be attributed to different protein and DNA constructs used in the specific experiments. However, the general notion is that FI is absolutely required for DNA-induced PARP-1 activity and FII is primarily responsible for DNA recognition (perhaps mainly single-strand DNA breaks). FI, despite its weaker DNA binding affinity, can further strengthen the overall DNA binding or serve as a surrogate for DNA recognition in the absence of FII, leading to weaker enzymatic activation.

1.5 CATALYTIC MECHANISMS OF HUMAN PARP-1

1.5.1 Activation mechanisms

DNA-dependent activation

DNA-dependent PARP-1 activation has been well-documented and represents the mechanistic paradigm for this intriguing enzyme. It has been proposed that DNA ligand-induced protein conformational changes allosterically activate PARP-1 enzymatic activity, but evidence regarding the protein–DNA binding stoichiometry and the reaction molecularity (intra- vs intermolecular) is still equivocal (Figure 1-13 and 1-14). Early biochemical studies suggested the possible dimer formation and/or macromolecular association upon DNA binding (*182, 238*). A kinetic study of PARP-1 automodification reaction using radiolabeled NAD^+ as substrate showed that the initial rate measured by the incorporation of radioactivity into PARP-1 increases with the square of the enzyme concentration, suggesting a second-order kinetic behavior, or an intermolecular process is operating (*239*). Maximal production of PAR was also observed *in vitro* at PARP-1 to DNA molar ratio of 2:1 (*240*). Moreover, 3′-overhang DNA-induced dimerization of PARP-1 DNA binding domain (residues 1–234) was observed using fluorescence spectroscopy and correlated with elevated enzyme activity (*227, 241*). Therefore, the mechanism in which DNA ligand-induced dimerization and subsequent intermolecular *trans*-modification of PARP-1 molecule prevails in the PARP field. Consistent with this model, two PARP-1 molecules could dimerize at the DNA lesion site through FI from one molecule and FII from the other as detected in the crystal structure, thereby permitting *trans*-modification (Figure 1-13) (*235*).

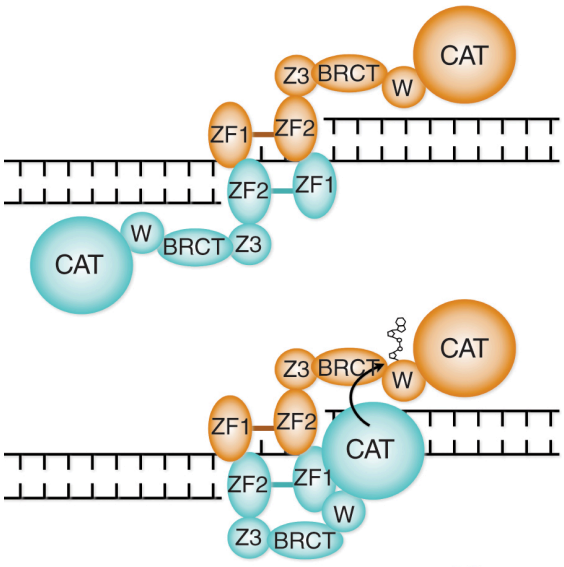

Figure 1-13. Proposed model for DNA-dependent PARP-1 dimerization and intermolecular *trans*-modification reaction (*235*).

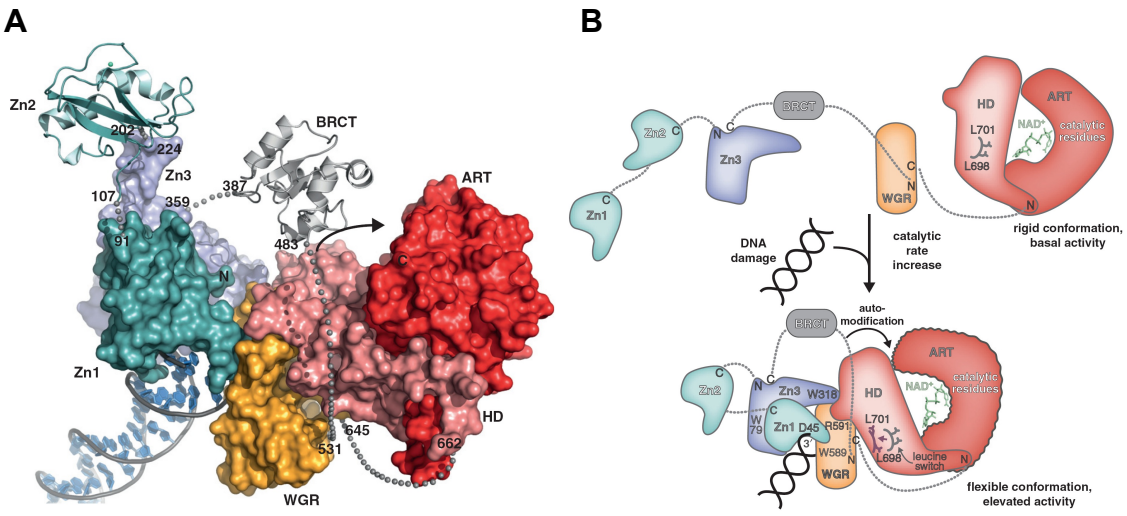

Figure 1-14. DNA-dependent PARP-1 activation: a monomeric perspective (*180*). (A) Crystal structure of PARP-1 domains in complex with blunt end DNA (PDB: 4DQY). FII (Zn2) and BRCT are computer-modeled in and not present in the real crystal. (B) A beads-on-a-string model where PARP-1 domains are engaged with blunt end DNA in the monomeric form. DNA binding destabilizes the catalytic domain (ART), leading to increased protein flexibility poised for higher catalytic turnover.

Although the structure of PARP-1 DNA-binding domain together with DNA provided a snapshot of how PARP-1 zinc fingers recognize DNA lesions, it is still unclear how DNA binding correlates to the catalytic activation of poly(ADP-ribosyl)ation. In a groundbreaking paper published in *Science*, Pascal and colleagues solved the crystal structure of PARP-1 multiple domains in complex with a 26-bp blunt end DNA mimicking double-strand break (*200*). These domains, comprised of FI, FIII, and the WGR-CAT domain (residues 518–1014, domain E and F), represent the minimal catalytic components for DNA-dependent PARP-1 activity. As shown in Figure 1-14A, FI, FII, and the WGR domain collapse onto DNA blunt end, creating a compact network of interdomain contacts. FI binds to the DNA minor groove side and the base stacking loop capping the 5′ terminal base in the way similar to its isolated form; FIII binds to the DNA phosphate backbone adjacent to FI, contrary to the negative result obtained from biochemical experiments with isolated FIII (*188*); the WGR domain occupies the other side of DNA, interacting with the 5′-end phosphate backbone. FI, FIII, and one face of the WGR domain form extensive interdomain contacts central to the DNA end. The opposite face of the WGR domain is in contact with the regulatory HD domain (*N*-terminus of domain F). Upon DNA-binding the HD domain is perturbed through its hydrophobic core, which in turn destabilizes the catalytic domain and results in elevated enzymatic activity (Figure 1-14B). Based on the amino acid linkage, the BRCT domain with multiple automodification sites is in proximity toward the catalytic domain so that the preference of PARP-1 for self-modification can be readily explained (Figure 1-14B). The model also confirmed the importance of several amino acid residues involved in interdomain contacts and paved the way for designing inhibitors targeting domain–domain interactions (*242*).

The monomeric structure of near full-length PARP-1 domains complexed with a blunt end DNA is in stark contrast to the previous reported dimerization of FI and FII in the presence of an overhang DNA (*235*). It is noteworthy that the exclusion of FII in the crystallization experiment, perhaps due to technical difficulty, might result in an incomplete view of DNA-dependent PARP-1 activation process. Monomeric PARP-1–DNA complex may possibly represent binding to double-strand break whereas dimeric PARP-1 DNA-binding domain is more relevant to single-strand break recognition. Nonetheless, SAXS studies using *N*-terminal partial (residues 1–486) or full-length PARP-1 with DNA ligands all suggested a compact conformational change upon DNA binding (*198, 236*). A stretch of amino acid residues 626 to 645 within the WGR domain (domain E) was found to support the DNA-binding ability of the DEF domain (residues 374-1014) of PARP-1 and crucial to the overall enzymatic activity based on the SAXS modeling of full-length PARP-1 with 8-bp DNA (*198*), but it is not seen in direct contact with DNA in the crystal structure (*200*). It is likely that residues assisting interdomain contacts could indirectly reinforce the overall DNA binding ability, leading to PARP-1's catalytic activation. It may be difficult to entirely deconvolute the effect of interdomain interactions in the context of DNA-binding affinity and catalytic activity. These contrasting models of DNA-dependent PARP-1 activation in terms of binding stoichiometry and reaction molecularity provided the founding hypotheses that would be examined in the later chapters.

DNA-independent activation

Free DNA is not the only stimulatory factor for PARP-1 activity; nucleosomes, RNAs, and protein posttranslational modifications can also activate PARP-1 poly(ADP-ribosyl)ation. PARP-1 is capable of binding to nucleosome particles through histones H3

and H4, and the *N*-terminal tail of H4 triggers PARP-1 activity independently of DNA (*231*). Single-strand RNAs such as poly(rA), poly(U), and poly(rC) can bind to the WGR domain of PARP-1 and activate the enzymatic activity of the WGR-CAT domain more than single-strand DNAs do (*199*). PARP-3, a mono-ADP-ribosyltransferase, can interact with PARP-1 *in vitro* through its *N*-terminal WGR domain and activate PARP-1's poly(ADP-ribosyl)ation activity in the absence of DNA (*90*); SIRT6 can mono-ADP-ribosylate PARP-1 on Lys521 and further stimulates its activity to a higher extent in the presence of DNA (*243*). Mono-ADP-ribosylation of PARP-1 by PARP-3, SIRT6, and perhaps other cellular PARPs possessing mono-ADP-ribosyltransferase activity may thus function as a "kickstart" for PARP-1-mediated poly(ADP-ribosyl)ation.

Posttranslational modifications other than poly(ADP-ribosyl)ation can also modulate PARP-1 activity (see Section 1.3.2). Phosphorylation of PARP-1 by ERK1/2 is required for maximal PARP-1 activation after DNA damage (*206, 207*). Moreover, phosphorylated ERK2 can direct interact with PARP-1 and promotes its activation more than damaged DNA does at NAD^+ concentration lower than physiological condition (*206, 207*). These results suggest that a mechanism of protein-mediated PARP-1 activation could resemble the effect of DNA lesions as allosteric regulators for PARP-1 activity.

1.5.2 Reaction mechanisms

PARP-1-catalyzed poly(ADP-ribosyl)ation produces long, branched PAR polymers attached to substrate proteins. The reaction can be divided into three steps: initiation, elongation, and branching (Figure 1-15A). Initiation involves the formation of a covalent bond between the attacking carboxyl group of glutamate or aspartate (or the ε-amino group of lysine) from the substrate protein and the anomeric carbon of the NMN

moiety in NAD^+, cleaving the ribose–nicotinamide glycosidic bond. Next, elongation happens when the 2′-hydroxyl group of the adenosine moiety from the just added ADP-ribose becomes the nucleophile to attack another NAD^+ molecule at the same anomeric position, extending the modification with one more ADP-ribose unit. In contrast to elongation, branching reaction takes place when the 2″-hydroxyl group of the original NMN ribose moiety serves as the nucleophile to branch out from the linear PAR chain. These newly formed glycosidic linkages are believed to be in α-stereochemistry. In addition, PARP-1 can also catalyze the hydrolysis of NAD^+, though to a less extent as compared to the polymerase activity (*83*). The distinction between initiation, elongation, branching, and hydrolysis reactions can be perceived as the transfer of ADP-ribose group onto different acceptors, i.e., protein amino acid residues, 2′-hydroxyl of the adenosine ribose, 2″-hydroxyl of the NMN ribose, and water molecule, respectively.

Early studies regarding the catalytic mechanism of PARP-1-catalyzed poly(ADP-ribosyl)ation were based on the sequence similarities between PARP-1 catalytic domain and those of ADP-ribosylating bacterial toxins including diphtheria toxin and *Pseudomonas aeruginosa* exotoxin A (*244*). In the toxins, a conserved glutamate was found to be essential for the attachment of a single ADP-ribose moiety onto specific host protein. Mutation of this residue impaired the ADP-ribosyltransferase activity and toxicity, while having little effect on NAD^+ binding (*245*). This result suggested a catalytic role for the active site glutamate. Similarly, the role of a conserved Glu-988 found in the catalytic domain of PARP-1 in catalyzing the formation of PAR polymer was investigated by site-directed mutagenesis (*246*). By estimating the amount of enzyme-digested components of PAR (see Section 1.2.2), the E988Q and E988A mutants were found to have limited reduction in initiation reaction, but almost incapable of performing chain elongation. E988D, on the other hand, could still produce PAR

polymers with branches, although to a shorter length. These data led to a proposed reaction mechanism for PARP-1 involving catalytic Glu-988, which is reminiscent of bacteria ADP-ribosylating toxins (Figure 1-15A). Glu-988 could serve in initiation by hydrogen bonding to position the incoming acceptor nucleophile or the donor NAD^+ molecule. Acidic nucleophiles such as glutamate or aspartate carboxylic groups are presumably ionized at neutral pH, and may not require the activation by Glu-988, as implied by the minor effect in chain initiation of the E988A and E988Q mutants. For chain elongation, the 2′-hydroxyl group of the adenosine ribose is activated by the general base Glu-988 to perform nucleophilic attack to the donor NAD^+ molecule. The activation process could involve a proton relay system which also includes the 3′-hydroxyl group of the ribose, because PARP-1 automodification reaction using 3′-deoxy NAD^+ analogues as substrates can only form either mono-ADP-ribosylated PARP-1 or protein-bound ADP-ribose oligomers (*247-249*).

Later, the crystal structure of human PARP-1 catalytic domain complexed with carba-NAD^+, an NAD^+ analogue, revealed the striking homology of the active site architecture between PARP-1 and diphtheria toxin (*250*). Although only the electron density of the adenosine moiety within carba-NAD^+ can be seen, it is believed that carba-NAD^+ occupies the acceptor site which the terminal ADP-ribose from a PAR chain would typically reside. By modeling in the donor NAD^+ molecule from the diphtheria toxin–NAD^+ co-crystal, the snapshot of the elongation reaction can be envisioned and the catalytic role of Glu-988 is justified (Figure 1-15B).

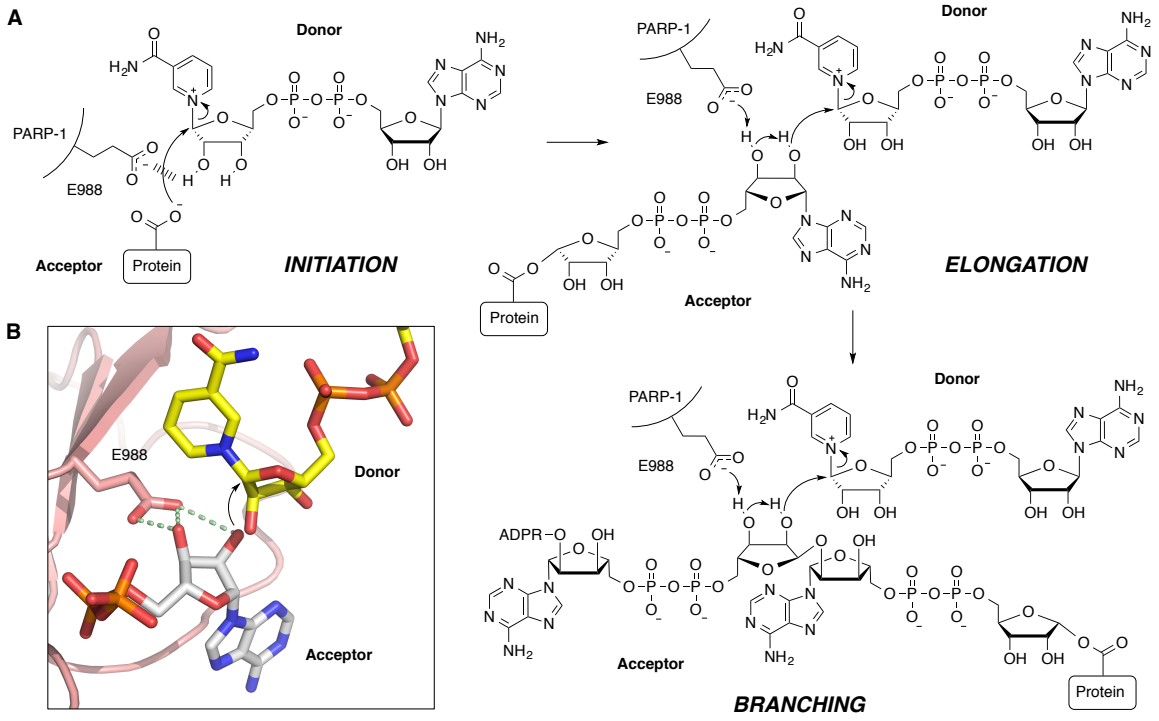

Figure 1-15. Reaction mechanism of protein poly(ADP-ribosyl)ation catalyzed by PARP-1. (A) Proposed mechanisms for initiation, elongation, and branching reactions. Glu988 is the catalytic base. (B) Structure view of human PARP-1 catalytic domain in complex with carba-NAD^+ (PDB: 1A26) (*250*). The donor NAD^+ (yellow) was modeled from the alignment of diphtheria toxin–NAD^+ crystal structure (PDB: 1TOX) (*251*).

The mechanism of PAR branching is somewhat implicit. Based on the chemical linkage, the NMN moiety from NAD^+ is assumed to occupy the same position as the adenosine moiety, and Glu-988 can facilitate the nucleophilic attack by the 2″-hydroxyl group in a similar fashion as the elongation reaction (Figure 1-15A). However, it is difficult to account for the low branching frequency (ca. 2%) in the overall polymerized ADP-ribose residues. One possible explanation based on the available crystal structure information is that the orientation of the nascent PAR polymer chain when entering the active site determines whether elongation or branching reaction would occur (Figure 1-16). It is the pyrophosphate group rather than the adenosine moiety that is fixed by a

more extensive hydrogen bond network, thus giving the flexibility for the terminal ADP-ribose unit to position differently. Catalysis proceeds through elongation or branching reaction depends on whether the terminal adenosine ribose or internal NMN ribose is closer to the donor NAD^+ binding site, respectively (*250*) (Figure 1-15). Consistent with this hypothesis, Tyr-986, which forms hydrogen bond with the pyrophosphate group, was found to be an important residue to modulate the branching frequency of PAR in a random mutagenesis study of PARP-1 (*252*). While the Y986H mutant retained 14% of the wild-type enzyme activity, the branching frequency was about 15-fold higher. It is proposed that the histidine mutant could have more favorable hydrogen bond with the pyrophosphate group, augmenting the symmetry of the acceptor binding site. Enhanced symmetrical binding of the terminal ADP-ribose unit in two orientations gives the increased branching frequency, despite the fact that shortened polymer was produced. The model is also in agreement with distal addition mechanism during polymer elongation/branching (*247*, *253*).

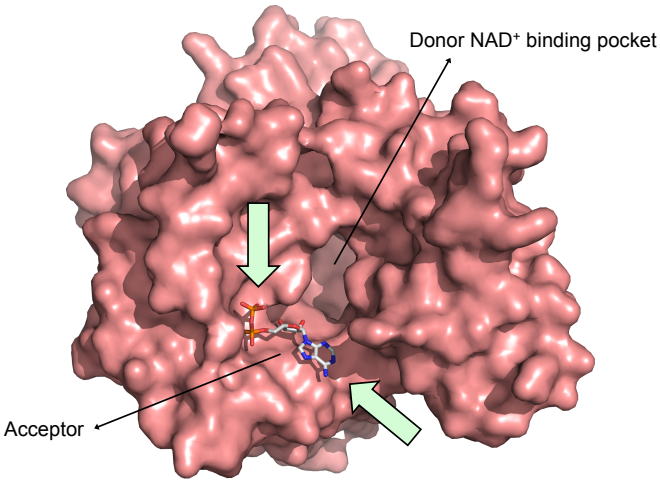

Figure 1-16. Surface representation of human PARP-1 catalytic domain in complex with carba-NAD^+ (PDB: 1A26) (*250*). The light green arrows indicate the possible two orientations of incoming acceptor PAR polymer.

1.5.3 Regulation of PARP-1 activity

While PARP-1 activity is stimulated by binding to damaged DNA, negative charges from the PAR polymers are rapidly accumulated on PARP-1 as a result of automodification. PARP-1 activity is inhibited consequently. Ebisuzaki *et al*. first studied the mechanism of how PARP-1 is inactivated following automodification. They showed that automodified PARP-1 has decreased affinity for DNA by sucrose gradient differential centrifugation, and the addition of PARG into the reaction reactivates PARP-1 by degrading PAR polymers and restoring PARP-1–DNA complex (*254*). These data suggested a "PARP shuttling" model where electrostatic repulsion between the newly formed PAR polymers and DNA leads to the dissociation of automodified PARP-1 from DNA (*5*). Subsequently, PARG can hydrolyze the PAR polymers presented on PARP-1, allowing a new catalytic cycle to begin. The presence of PARG could have important regulatory effect on PARP-1 activity, as demonstrated *in vitro* where sustained PARP-1 activity can be achieved (*255*).

Several other cellular components can also regulate PARP-1 activity. Histones, including H1 and core histones, can affect the size distribution of PAR polymers and the modification proportion among different acceptor proteins (*256*). Small molecules or bivalent cations such as Mg^{2+} and Ca^{2+}, polyamines, and ATP were demonstrated to be allosteric regulators for PARP-1 in addition to DNA (*257*). The effects of posttranslational modifications on PARP-1 activity have already been discussed in Section 1.3.2.

1.6 THESIS STATEMENT

PARP-1-catalyzed poly(ADP-ribosyl)ation is a protein posttranslational modification reaction implicated in various cellular processes including DNA repair,

inflammation, and cell death. The enzymatic activity of PARP-1 is allosterically stimulated by binding to DNA, resulting in the synthesis of PAR polymers from NAD^+ onto specific proteins. Despite its discovery over fifty years ago, the molecular mechanism used by PARP-1 remains unsettled. Work presented in this dissertation aims to provide further mechanistic details regarding PARP-1 catalysis from three different perspectives. Chapter 2 describes the DNA binding properties of PARP-1 in a quantitative way using single-molecule fluorescence spectroscopy and enzyme kinetics. Chapter 3 and chapter 4 address the mechanistic issues with an emphasis on the role of NAD^+. In chapter 3, fluorinated NAD^+ analogues were designed and synthesized to investigate the distinct steps of poly(ADP-ribosyl)ation involving the cleavage of the NAD^+ ribose–nicotinamide glycosidic bond. The result is consistent with the proposed mechanism that an oxocarbenium-like transition state is formed during enzyme catalysis. In chapter 4, biochemical and analytical methods were applied to locate the automodification sites of PARP-1 and characterize the chemical nature of ADP-ribose–protein linkages. MS data confirm the existence of automodification sites beyond domain D in PARP-1. However, whether poly(ADP-ribosyl)ation of lysine residues is attributed to the ADP-ribosyltransferase activity of the enzyme remains an open question. In chapter 5, a radioactivity-based assay using two structurally distinguishable protein constructs was developed to interrogate the molecularity of DNA-dependent PARP-1 automodification. The results support a bimolecular, intermolecular process. Moreover, structural characterization of domain C by top-down MS analysis excludes the possibility of a domain C-mediated dimerization of PARP-1. Instead, interdomain contacts involving domain C are important for catalysis.

Chapter 2. Quantitative Binding Kinetics of Human PARP-1 with DNA

2.1 INTRODUCTION

The poly(ADP-ribosyl)ation activity of PARP-1 is strongly activated by binding to DNA strand breaks (*179*), and its binding repertoire is highly diverse in terms of DNA structures rather than sequence dependence (*225*). There are three zinc fingers present in human PARP-1 (Figure 1-11), with FI and FII mainly responsible for the recognition of DNA (*181*). It has been proposed that these two zinc fingers have differential roles in DNA recognition. PARP-1 lost its ability to bind to DNA single-strand breaks when FII was structurally disrupted by mutations, whereas little effect was observed for the corresponding mutations in FI (*182*). Another report, however, suggested that both FI and FII are required for PARP-1's binding to and subsequent enzymatic activation by single-strand breaks, but only FI is required for similar effect induced by double-strand breaks (*181*). Therefore, how the two zinc fingers cooperate to recognize different DNA structures and stimulate PARP-1 activity is still unclear.

Recent structural characterizations of PARP-1 DNA-binding domains in complex with DNA ligands provided a visual aid to understanding the mechanism of this recognition process. Pascal *et al*. reported that FI or FII alone binds to the minor groove of a double-strand blunt end DNA, capping the end base in an identical fashion (Figure 1-12A, B) (*233*). On the contrary, Oliver *et al*. found that when using a single polypeptide comprising the two zinc fingers to crystallize with a duplex DNA containing 5′ single-base overhang, FI and FII clustered at the same side of the DNA, with FI flipping its polarity from the minor groove to the major groove (Figure 1-12C). Considering the amino acid connectivity of the protein in the crystal also implied that the two zinc fingers do not come from the same polypeptide chain. Mutation of amino acid residues involved

in contouring the hydrophobic interface between FI and FII abolished the relocalization of the mutant protein to DNA damaged site. These results support a model of DNA-induced dimerization of PARP-1 via cooperation of FI and FII. Interestingly, another crystal structure of PARP-1 domains complexed with a blunt-end DNA duplex, omitting FII and the BRCT domain, showed that FI, FIII, the WGR domain all collapsed onto the same DNA end (*200*). The overall PARP-1 molecule and the DNA interact in a 1:1 ratio. These studies shed light on the mechanistic details of how PARP-1 recognizes DNA, but on the other hand created controversy regarding the binding stoichiometry of PARP-1 versus different DNA structures.

To study the DNA-binding properties of PARP-1 from a different perspective, single-molecule fluorescence colocalization technique was employed to address this question in a quantitative way. Using a Cy3-labeled PARP-1 DNA-binding domain AB and a Cy5-labeled DNA ligand, protein–DNA interactions can be directly visualized in real time under the single-molecule platform. Binding rate constants can be deduced from the analysis of dwell-time distributions of combined individual binding event. Unlike ensemble biochemical techniques which measure averaged signal from the sample, single-molecule technique allows the identification of heterogeneity in binding properties. Based on the experimental data, two binding modes were suggested for the PARP-1 AB domain–DNA interactions, one involving a strongly-associated protein–DNA complex and the other being transient. Specific time trajectories revealed some binding events involving multiple proteins. In addition, a continuous kinetic assay was developed to monitor the enzyme activity of PARP-1, and the effect of DNA ligands was also estimated.

2.2 MATERIALS AND METHODS

2.2.1 Preparation of Cy3-labeled AB domain of PARP-1

Preparation of Cy3-labeled AB domain of PARP-1 was conducted by Dr. Meilan Wu in our laboratory. The protein construct used in the experiments, termed AB-150, contains a six amino acid mutations LC*TPSR at residues 150–155 of AB domain of PARP-1 (residues 1–232), where C* denotes a formylglycine residue generated *in vivo* by coexpression with His-tagged formylglycine generating enzyme (FGE) (*258*). The formylglycine-containing AB domain, termed Fgly-AB-150, was cloned in the form of His-tagged maltose-binding protein (MBP) fusion protein at the *N*-terminal of AB, separated by a tobacco etch virus (TEV) protease cleavage sequence. The resulting plasmid His_6-FGE/MBP-Fgly-AB-150/pET was used to transform *E. coli* BL21 CodonPlus (DE3)-RP or Rosetta strain. The expression and purification of Fgly-AB-150 was following similar procedures described in Section 3.2.4 and Section 4.2.1. The existence of an aldehyde group on the protein was confirmed by reacting with biotin-hydrazide followed by immunoblotting using horseradish peroxidase (HRP)-conjugated streptavidin (Pierce) and colorimetric 1-Step TMB-Blotting substrate solution (Pierce).

The site-specific labeling of Cy3 to Fgly-AB-150 was accomplished by incubating Fgly-AB-150 with 16- to 20-fold molar excess of Cy3-hydrazide (GE Healthcare). The unreactive dye was removed by dialysis. The labeling yield was determined by UV absorbance at 280 nm and 555 nm using NanoDrop. Typical labeling efficiency was about 60%.

2.2.2 Preparation of Cy5-labeled DNA ligands

Single-strand DNA primers were all purchased from IDT. The sequences are listed in Table 2-1. To generate double-strand DNA duplex 66G (66-mer duplex with a single base gap in the center) and 32B (32-mer duplex with blunt ends) (Figure 2-1), corresponding single-strand primers were diluted to a 25 μM final concentration in the annealing buffer containing 30 mM HEPES, pH 7, and 100 mM potassium acetate. The mixtures were heated at 95°C for 2 min and then slowly cooled down to room temperature. The DNAs were aliquoted and stored at −20°C until further use.

DNA duplex	Primers used	Primer sequence
66G	66-bpR	5′-AAGGGCAAGGCTGCTGTGGACCCTGCTGTGGGC TGGAGAACAAGGTGATCTGCGCCCTGGTCCTGG-3′
	33-bp	5′-GCCCACAGCAGGGTCCACAGCAGCCTTGCCCTT-3′
	32-bp	5′-CCAGGACCAGGGCGCAGATCACCTTGTTCTC**C**-3′
32B	32-bp	5′-CCAGGACCAGGGCGCAGATCACCTTGTTCTC**C** -3′
	32-bpR	5′-GGAGAACAAGGTGATCTGCGCCCTGGTCCTGG-3′

Table 2-1. Primer sequences for the DNA ligands used in the experiments. Base underlined and in boldface was labeled with Cy5 at its 3′-end.

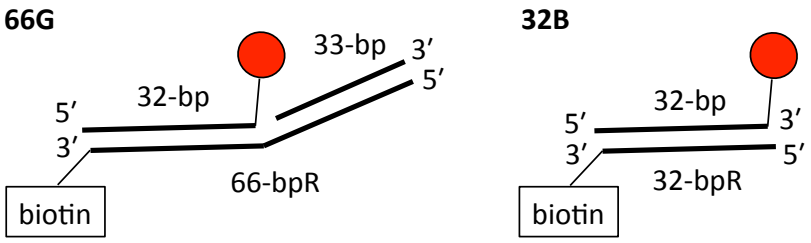

Figure 2-1. Diagrams for the DNA duplex 66G and 32B used in the experiments.

2.2.3 Single-molecule fluorescence colocalization experiments

Biotinylated Cy5-DNA duplexes were immobilized onto a surface-passivated quartz slide via streptavidin conjugation. Briefly, the quartz slide was passivated with a mixture of methoxy polyethylene glycol (mPEG) and biotinylated mPED (1-2%), which allowed the immobilization of streptavidin on the slide. Biotinylated Cy5-DNA was then captured by streptavidin, forming a three-layer sandwich.

A typical image chamber (0.5 × 1.5 cm) sealed with double-sided tape was made between the quartz slide surface and a cover slip. Typically, a 50-μL sample of 50 pM DNA duplex in the loading buffer containing 50 mM Tris-HCl, pH 8.0, and 250 mM NaCl was loaded onto the slide which had been pre-treated with streptavidin. Unbound DNA was washed out by loading buffer. Various concentrations of Cy3-labeled AB-150 proteins diluted in a buffer containing 50 mM Tris-HCl, pH 8.0, and 25 mM NaCl were used for imaging. To extend the fluorescence lifetime during experiments, an oxygen scavenging system consisting of 0.6 mM Trolox, 11% glucose, 0.1 mg/mL glucose oxidase, 0.05 mg/mL catalase, 1 mM $MgCl_2$, and 10 mM DTT was pre-mixed with AB-150 protein before loading into the chamber. PEGylated slides, the oxygen scavenging system, and the access to a microscope equipped with a total internal reflection fluorescence (TIRF) platform were all kindly provided by Dr. Rick Russell in the Department of Molecular Biosciences at UT-Austin.

Protein–DNA binding events were recorded in real time by mounting the imaging chamber beneath the prism-type total internal reflection (TIR) microscopy consisting of an inverted Olympus IX-71 microscope connected to an I-PentaMAX IIC CCD camera with a cooling unit (Princeton Instruments). For fluorescence colocalization experiment, Cy3-labeled proteins were directly excited with a 532 nm laser (Crystalaser). The excitation was conducted continuously with 10 frames per second and data acquisition for

90 s. Alternatively, it was done with a 2-s on/2-s off pulsed excitations manner for a total of 300 s of 1 frame per second data acquisition. To confirm the existence of immobilized Cy5-labeled DNA molecules, the chamber was excited with a 637 nm laser (Coherent) for 10 s at the end of each movie. Movies were taken from random fields of view for each protein concentration. All the single-molecule experiments were conducted with the assistance of Dr. Brian Cannon, a postdoctoral associate in Dr. Rick Russell's laboratory.

2.2.4 Single-molecule experiments data analysis

Fluorescence produced from each field of view was splitted into Cy3 (donor) and Cy5 (acceptor) intensity signals by a pair of dichroic mirrors. Colocalized signals from Cy3 and Cy5 dyes were matched using an affine transformation that was based on pre-determined fiducial markers using fluorescent nanobeads (*259*). Raw intensity time trajectories of the colocalized Cy3 and Cy5 signals were generated for each movie using a in house single-molecule data analysis program written by Dr. Brian Cannon. For the pulse-type excitation experiments, the dwell time of individual binding event was manually identified based on the appearance and disappearance of the Cy3 or Cy5 signals above average background threshold of each time trace. The combined cumulative dwell-time histograms from each individual binding event were fitted to a single- or double-exponential cumulative function ($f(t) = \Sigma A_i [1 - \exp(-k_i t)]$, where $i = 1$ or 2) to obtain binding rate constants.

2.2.5 Continuous kinetic assay for poly(ADP-ribosyl)ation

An enzyme-coupled continuous kinetic assay was developed to monitor poly(ADP-ribosyl)ation activity (Figure 2-2). A nicotinamide molecule is produced for

each round of NAD^+ turnover, which can be converted to nicotinic acid and ammonia by *E. coli* nicotinamidase PncA. The resulting ammonia can be further used in a second coupled reaction where α-ketoglutarate (α-KG) is reductively aminated to glutamate by glutamate dehydrogenase (GDH) from *Proteus* sp. in the presence of NADPH. The reaction can be continuously monitored at 340 nm UV absorbance, reflecting the consumption of NADPH which is correlated to the consumption of NAD^+ by PARP-1.

Briefly, a 100-μL reaction containing varying concentrations of NAD^+, 1 mg/mL DNA, 150 μM NADPH, 3.5 μM PncA, 5 mM α-KG, 1 unit GDH, 100 mM Tris-HCl, pH 8.0, and 10 mM DTT was premixed for 5 min to equilibrate the background signal. The reaction was initiated by adding PARP-1 into the mixture. Initial rate was obtained by monitoring the reaction at 340 nm. For steady-state kinetics with regard to DNA, 1 mM NAD^+ was used with varying concentrations of DNA. In some cases, PARP-1 was substituted by equimolar of AB and CDEF domains to reconstitute a functional PARP complex *in trans*.

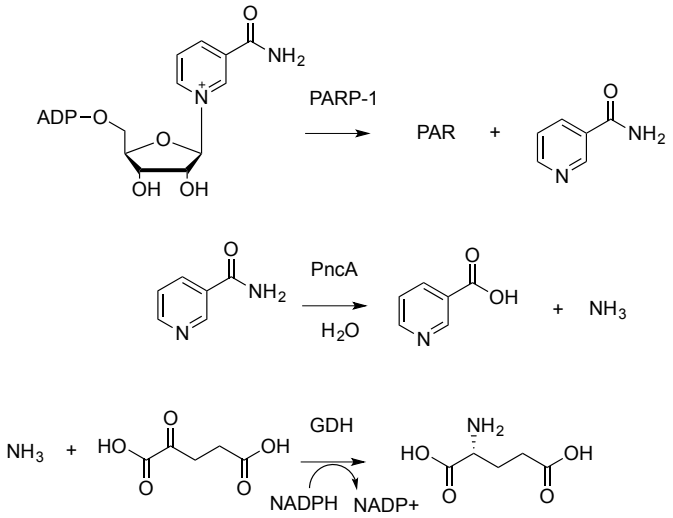

Figure 2-2. Enzyme-coupled continuous assay for monitoring poly(ADP-ribosyl)ation of PARP-1.

2.3 RESULTS

2.3.1 Rationale of generating AB with site-specific labeled Cy3 fluorophore

To study the DNA binding kinetics of PARP-1, the DNA-binding domain AB was selected to be the protein construct in use, considering the major functions of the two zinc fingers and the feasibility of *in vitro* protein purification. The labeling positions of fluorophores were based on the crystal structure of FI or FII in complex with a duplex DNA (Figure 1-12A and B). By putting the fluorophore at the base-stacking loop of FII (residue 151), and the 3′-end of double-strand DNA, a colocalization signal and/or fluorescence resonance energy transfer (FRET) phenomenon was expected.

To site-specific label a fluorophore onto the protein, a technique applying bioorthogonal reaction was adopted from the literature (*258*). A stretch of amino acid between residues 150 and 155 was replaced by a characteristic sequence LCTPSR. This short peptide motif can be recognized by the formylglycine generating enzyme (FGE) from *Mycobacterium tuberculosis*, where the cysteine residue is coverted to a formylglycine moiety by this enzyme. The resulting aldehyde tag (Fgly) allows the functionalization with different probes carrying a hydrazide group, such as biotin-hydrazide and Cy3-hydrazide.

The generation of Cy3-labeled AB-150 protein was achieved by *in vivo* coexpression with the FGE followed by *in vitro* labeling with Cy3-hydrazide. Control reactions using biotin-hydrazide as a probe confirmed the transformation of cysteine to Fgly by immunoblotting. The DNA-binding property of AB-150 was comparable to wild-type AB domain using electrophoretic mobility shift assay.

2.3.2 Overview of the single-molecule fluorescence colocalization experiment

The design of the single-molecule fluroesence colocalization experiment was to monitor the binding process of a free Cy3-labeled protein interacting with a immobilized Cy5-labeled DNA molecule in a small chamber created on the quartz slide in real time (Figure 2-3). The DNA was first immobilized through a biotin-streptavidin affinity complex. Cy3-labeled protein, AB-150 in this case, was then loaded into the chamber. The binding process was monitored by a prism-type total internal reflection fluorescence microscopy (TIRF, Figure 2-4A). TIRF microscopy confines laser to a 100-nm thin layer above the glass slide, which greatly improves the signal-to-noise performance of fluorescence detection (*260*). The fluorescence signal was splitted into two channels (Cy3 and Cy5) and was recorded simultaneously (Figure 2-4B).

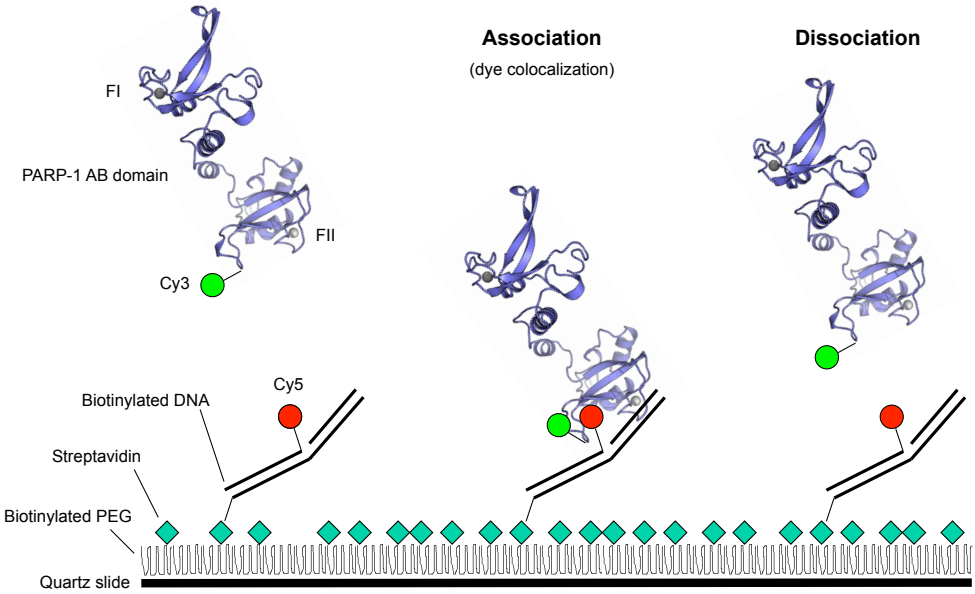

Figure 2-3. Schematic diagram of Cy3-labeled PARP-1 AB domain interacting with Cy5-labeled DNA at the single-molecule platform.

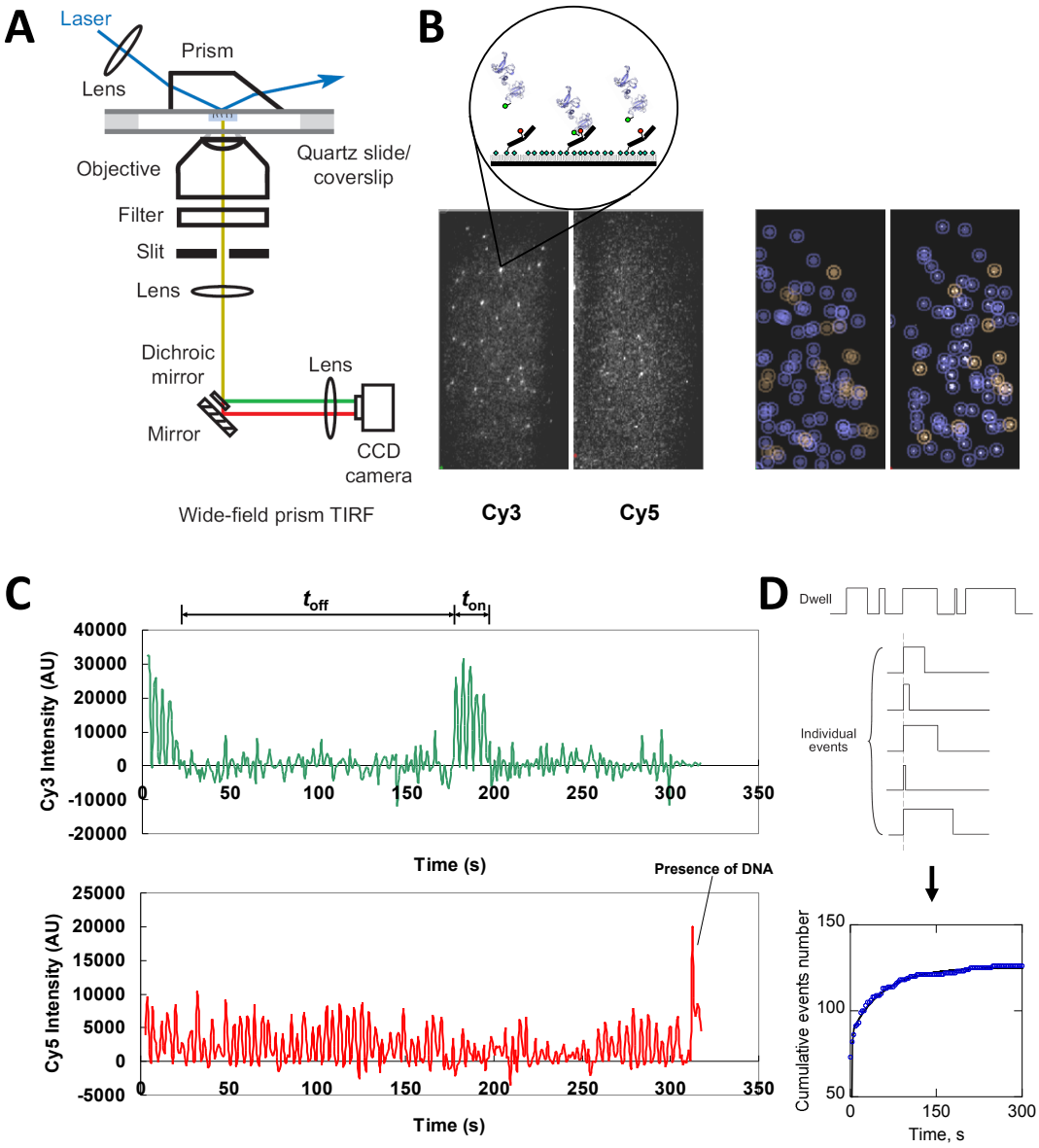

Figure 2-4. Experimental setup for the single-molecule fluorescence colocalization study. (A) Schematic diagram of a prism-type total internal reflection fluorescence microscopy (*261*). (B) Left, example of a field view in both Cy3 and Cy5 channels; right, mapping protein–DNA complexes in the Cy3 channel based on the locations of DNA molecules in the Cy5 channel. (C) Representative time traces for a specific protein/DNA molecule. t_{on} and t_{off} are protein on-time, off-time, respectively. (D) Dwell-time analysis of individual binding events leads to a cumulative histogram, which can be fitted to a cumualtive exponential function to obtain binding constants.

For the initial 300 s, a 532 nm laser was used in a pulsed manner (2-s on/2-s off) to excite the protein. Binding (association) of the protein onto DNA would result in an increase of Cy3 fluorescence signal, whereas dissociation would result in a decrease of the signal. At 305 s, the locations of DNA molecules were visualized by direct excitation with a 637 nm laser for 10 s. This also caused the photobleaching of Cy5 dyes. The number of DNA molecules was used as basis to search for effective protein–DNA complexes presented in the Cy3 channel. The colocalized Cy3 and Cy5 signals were matched according to a calibration procedure using fluorescent nanobead markers (*259*). The time trajectories for each spot were then generated by an in house written program (Figure 2-4C). The duration of each binding events was manually identified from the Cy3 fluorescence channel, as exemplified by t_{on} and t_{off}. The combined dwell time (either "on" or "off") were used to construct a cumulative histogram, where the binding constants can be estimated by fitting the data to either a cumulative single- or double-exponential function, assuming a one-step binding model (Figure 2-4D). Fitting the "on-time" would give dissociation constant, whereas fitting the "off-time" would afford association constant. Fluorescent intensities of each binding events were also examined as an indicator for protein multimerization. Control experiments using Cy3-coated nanobeads revealed the fluorophore blinking off rate $k_{\text{blink off}}$ to be 0.0096 s^{-1}. No Cy3 signal was observed when no DNA was immobilized on the slide, supporting that the observed signals truly came from the protein–DNA binding.

2.3.3 Binding kinetics of PARP-1 AB domain with DNA

Presented in Table 2-2 are the data obtained from AB-150 interacting with either 66G or 32B DNA assuming a one-step binding model (Protein+DNA <-> P-D) (Figure 2-

1). In the case of 66G, which mimicks DNA single-strand break, fitting the combined "dwell-on" time histogram with single-exponential function gave a dissociation constant k_{off} a value of 0.027 s^{-1}. For 32B which mimicks DNA double-strand break, the cumulative histogram was best fit with double-exponential function, affording two dissociation constants, with 0.039 s^{-1} representing the averaged slow phase population ($k_{off, slow}$) and 0.65 s^{-1} describing the fast phase population ($k_{off, fast}$). Two binding modes can thus be assigned to each rate constant. Association constants were also obtained by fitting the "dwell-off" time, but low event numbers may hamper further interpretation. The fast-phase rate constant for 32B is comparable to the one for 66G. By estimating the amplitude of each exponential term, it suggests that about 60% of the population of AB-150/32B complex accounts for a weakly-associated protein–DNA complex with a maximum lifetime of 3 s due to the pulsed time limit. The other 40% population represents strongly-associated AB-150/32B complex similar to the AB-150/66G complex, and is kinetically more stable than the blinking rate of Cy3 dye ($k_{blink\ off}$ = 0.0096 s^{-1}).

		66G	32B					
Rate (s^{-1})		k_{off}	$k_{off, slow}$	A_1	$k_{off, fast}$	A_2	$^{app}k_{on}$	A
[Protein]	0.1 nM	0.018	0.036	44.51	0.41	57.50	0.022	24.38
	1 nM	0.026	0.040	41.12	0.76	33.89	0.040	23.97
	10 nM	0.036	0.040	49.59	0.79	56.40	0.098	29.11
Average rate (s^{-1})		0.027	0.039		0.65			

Table 2-2. Binding constants for AB-150 with DNA ligands.

2.3.4 Steady-state enzyme kinetics of PARP-1

A steady-state continuous enzyme kinetic assay was developed to evaluate PARP-1 automodification activity (Figure 2-2). For each round of ADP-ribosyl transfer reaction, equimolar of nicotinamide is produced, which can be converted in a coupled enzyme reaction catalyzed by PncA to nicotinic acid and ammonia. The free ammonia can be further used in a GDH-catalyzed reductive amination of α-KG to glutamate in the presence of NADPH. Therefore, the consumption of NAD^+ by PARP-1 can be correlated to the consumption of NADPH by continuous monitoring at 340 nm UV absorbance.

To ensure that PARP-1 is limiting the reaction, varying concentrations of PARP-1 were used to see if there is a linear relationship between the PARP-1 concentration and enzyme activity readout. Figure 2-5A shows that between 10 and 100 nM PARP-1, the enzyme activity (μM/s) is proportional to the enzyme concentration. This result indicates that the coupled enzyme reactions are not rate limiting, supporting the measured activity attributed to PARP-1. By varying NAD^+ concentrations, steady-state kinetic constants of PARP-1 can be obtained by fitting to Michalis-Menten equation, with a k_{cat} and K_M value of 1.39 s^{-1} and 46 μM, respectively (Figure 2-5B).

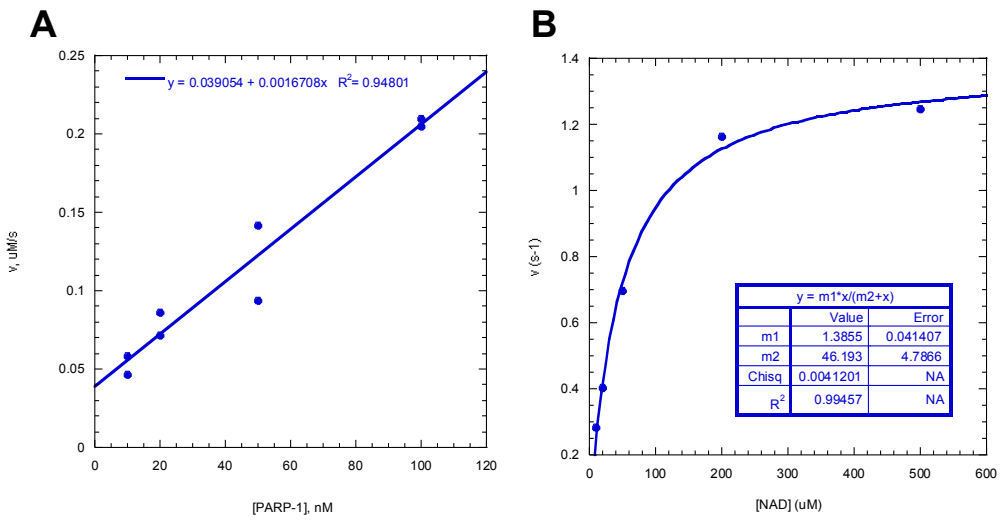

Figure 2-5. Steady-state kinetics of PARP-1 automodification reaction with respect to NAD^+.

It has been shown by previous group member Dr. Peng Gao and other laboratories that using PARP-1 truncated domains complementary to each other can reconstitute PARP-1 activity. In the previous single-molecule experiments, only binding constants were evaluated. Here, the activity of AB in the presence of CDEF was investigated using similar kinetic assay using 66G as the DNA activator. Fluorophore-labeled AB or 66G counterparts were also tested for the effect of carrying a bulky chemical group on enzyme activity. The data are shown in Figure 2-6 and the kinetic parameters are summarized in Table 2-3. The k_{cat} values are comparable to the wild type PARP-1. K_M values are in nanomolar range, indicating tight binding of DNA with the protein. However, there seems to be some variations of K_M values among samples, ranging from 8 to 36 nM. There is no obvious trend in terms of the effect of fluorophore labeling, but the similar k_{cat}/K_M values obtained from all four samples suggest that the interference of fluorophore labeling with enzyme activity is minimal.

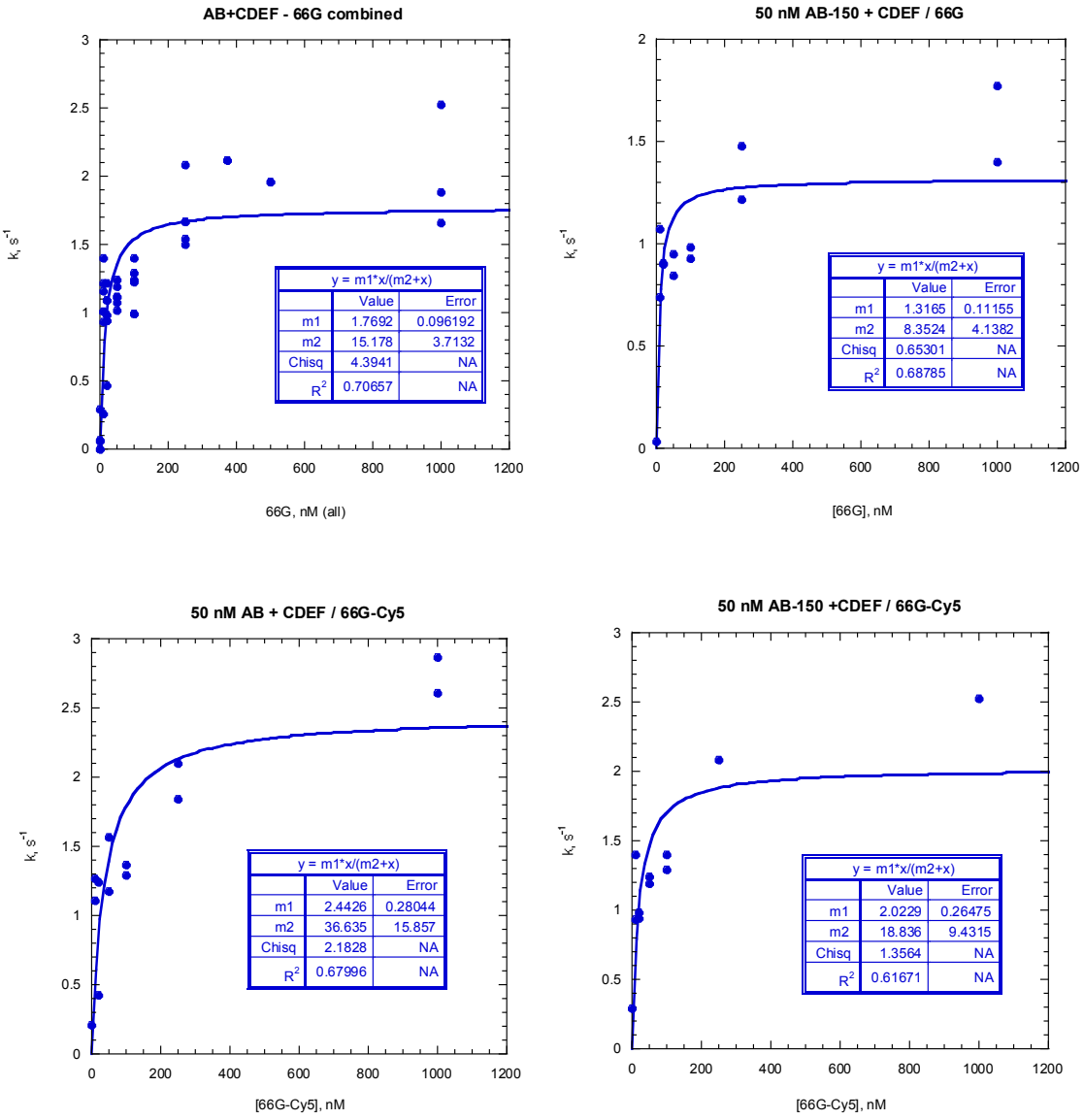

Figure 2-6. Steady-state kinetics of PARP-1 automodification reaction in the form of AB/CDEF protein complex with respect to DNA.

Protein	DNA	k_{cat} (s^{-1})	K_M (nM)	k_{cat}/K_M ($s^{-1}nM^{-1}$)
AB	66G	1.77	15.2	0.116
AB-150	66G	1.32	8.35	0.158
AB	66G-Cy5	2.44	36.6	0.067
AB-150	66G-Cy5	2.02	18.8	0.107

Table 2-3. Steady-state kinetic parameters of AB/CDEF and 66G with respect to DNA.

2.4 DISCUSSION

2.4.1 Study of PARP-1–DNA interactions using single-molecule technique

Single-molecule fluorescence microscopy has become an emerging technique to study biological problems (*262*). The advantage of single-molecule over traditional bulk biochemical approach is that it can follow the dynamic change over time for each individual molecule, which is impossible for ensemble methods because it requires all molecules to be synchronized over the observational trajectories. Rapid mix or rapid quench apparatus used to study transient kinetics of biological systems at ms scale, but single-molecule fluorescence spectroscopy can have a wider time scale, ranging from μs to even days. The ability of this method to monitor the entire time trajectory can reveal hidden intermediates or multiple pathways within the system. In addition, TIRF microscopy further reduced the background signal significantly, allowing possible assignment of signals to a "single molecule." These features all support single-molecule techniques to become more useful to address biological questions in a quantitative way (*263*).

It is well known that PARP-1 is activated upon binding to DNA. Despite early biochemical studies of its functions or with regard to individual domain or single amino acid residue, the overall picture of how the DNA-binding domains cooperate to recognize

DNA and relays this allosteric activating signal to the active site remains elusive. Furthermore, recent structural characterizations using different protein fragments and DNA constructs showed contradicting results in terms of protein–DNA stoichiometry (*198, 200, 235, 236*). These issues prompted us to investigate this complex protein–DNA recognition process using a novel single-molecule technique.

Single-molecule fluorescence spectroscopy has been proven useful in the studies of protein–DNA interactions (*260, 264*). One of the challenges when we were facing at the initial stage of this study is to determine where to label the fluorophore on the protein, and which protein construct to work with. We decided to label the Cy3 fluorophore at the base-stacking loop of FII based on its proximity to DNA and the solvent accessibility without disrupting protein folding from the crystal structure report (*233*). Domain AB was chosen to be the protein construct used in the experiments considering its small size (ca. 26 kDa) and major function in DNA recognition.

Once the location has been derermined, another important technical aspect of the experiment is the preparation of site-specifically labeled protein. A widely used method for protein labeling is to utilize the chemical reactivity of cysteine toward maleimide. The desired location must be a cysteine residue, and all the other Cys need to be mutated to Ala or other residues. This method, however, may not be applicable to PARP-1 AB domain, due to the potential reactivity of Zn^{2+}-coordinating Cys toward labeling reagents, resulting in disruption of protein structure.

Alternatively, engineering proteins to carry a functional group capable of performing bioorthogonal reactions has been rapidly developed (*265*). Among them, a genetically encoded aldehyde tag was selected for this study (*258*). A stretch of six amino acid in the base-stacking loop of FII was mutated to LCTPSR which can be recognized by a bacterial FGE enzyme. By coexpression with the enzyme, Cys was converted to

formylglycine (Fgly) *in vivo*. Control experiments successfully verified the labeling of biotin-hydrazide onto the aldehyde-containing protein by immunoblotting, and the labeled protein AB-150 behaves similarly to the wild type in terms of DNA binding ability. This bioorthogonal protein labeling method has recently been demonstrated in a single-molecule experimental setup as well (*266*).

2.4.2 Two binding modes were identified for PARP-1–DNA complexes

With the materials in hand, single-molecule fluorescence colocalization experiments were conducted. The 2-s on/2-s off pulse-type excitation method was adopted mainly for the purpose of extending the photostability of Cy3 and Cy5 dyes. Despite sacrificing minimal resolution between binding events (3 s apart), binding events with intensities higher than the averaged background can still be manually selected. There are several technical issues that may complicate the data analysis. One example is the photostability of Cy5-DNA molecules used as the basis for identifying true protein–DNA complexes. The current method is to directly excite the Cy5 dyes to locate these molecules while they emit fluorescent signals. The rapid photobleaching of Cy5-DNA molecules may result in the low numbers of countable protein–DNA complexes. Low numbers of molecules present in each view may require more movies to be taken. The extended experimental acquisition time may render the oxygen scavenging system ineffective, which in turn accelerate the photobleaching of Cy3 dyes. The solution to this problem is to constantly replenishing new oxygen scavenging system to maintain the photostability of the cyanine dyes.

Another complication is the concentration limit. To avoid strong background signals, the reaction chamber was set to have minimal volume. However, the highest

tolerable concentration at which individual fluorescent molecule can be resolvable is at the order of 10 nM. Due to diffraction limit, concentration used above 10 nM may result in multiple molecules present at a single spot, complicating the interpretation of a single binding event involving multermerized proteins, or more than one event happens at the same spot.

The experimental results suggest that there is one binding mode for AB-150 interacting with 66G, whereas there are two binding modes for 32B. It is unclear that the two binding modes are intercovertible, or there are two binding site present on the very 32B DNA duplex. Nonetheless, the biphasic distribution of the cumulative histograms uncovered the potential multiple protein–DNA complexes with distict lifetime, which would otherwise be invisible using ensemble experiments.

The averaged dissociation constants of the strongly-associated species is about 0.027 s^{-1} and 0.039 s^{-1} for 66G and 32B, respectively. A reported PARP-1–DNA binding kinetics using surface plasmon resonance techniques showed a dissociation constant (k_{off}) value of 0.0034 s^{-1} for double-strand break DNA duplex, which is an order tigher than the data reported here (*267*). The weaker binding of domain AB could be due to the disruption of the base-stacking loop important for capping DNA end (Figure 1-12). After the initiation of the current study, an X-ray crystal structure using FI and FII within the same polypeptide in complex with a 5′-overhand duplex DNA revealed a striking dimerization composition of FI and FII, underscoring the significance and versatility of the base-stacking loop not only in DNA end capping, but also in protein–protein interactions (*235*).

While discrepancy in kinetic numbers can be attributed to different protein constructs being used, it is also possible that there exists additional protein–DNA complex within the recognition process. Recently, a loop within PARP-1 residues 480–

540 contains a double-strand break-binding domain (*199*). Dr. Meilan Wu also reported that the amino acid stretch of residues 626–645 is also important for DNA-binding (*198*). It is possible that protein domains beyond AB also contribute to the over DNA affinity of PARP-1.

Regarding the fluorescence intensities of each binding events, it is evident that some event may involve protein multimerization (Figure 2-7). The close proximity of Cy3 and Cy5 dyes may also induce FRET to occur. Detailed analysis to clearly dissecting the fluorescence intensities regarding whether it is resulted from FRET or crossover excitation is currently underway.

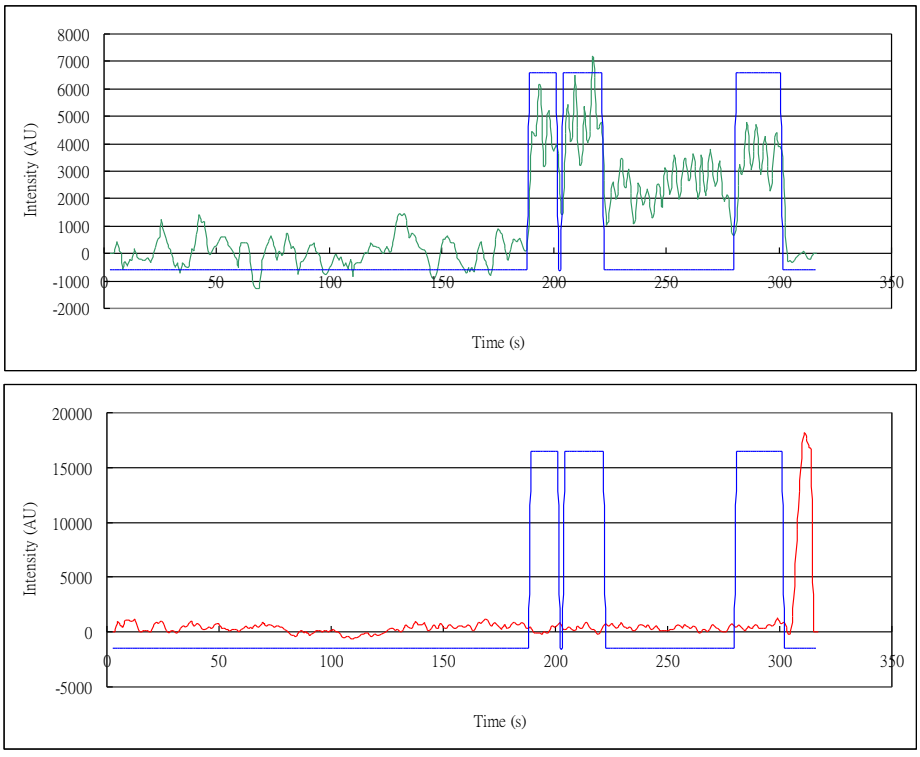

Figure 2-7. Representative time trace of AB-150 interacting with 32B showing possible multimerization of the protein. The fluorescence intensity from the Cy3 channel is colored in green, and the Cy5 channel is colored in red.

2.4.3 Steady-state kinetics of PARP-1

Measuring the incorporation of radioactivity signal into PARP-1 proteins using ^{32}P-NAD$^+$ represents the paradigmatic method to determine the activity of PARP-1. However, this method in discontinuous in its nature. An HPLC-based method has also been reported to estimate PARP-1 activity (*218*), it is also discontinuous. To complement the current methods for PARP-1 steady-state kinetics, an enzyme-coupled continuous assay involving the bacterial nicotinamidase PncA and GDH was developed. The result showed that by properly adjusting the concentration of each reaction component can make the PARP-1 activity rate-limiting (Figure 2-5A). The reported k_{cat} and K_M values are comparable to the literature (0.41 s^{-1} and 59–278 μM for k_{cat} and K_M, respectively) (*268*). Note that the assay cannot distinguish between the NADase activity and the poly(ADP-ribosyl)ation acitivity, since both reactions produce nicotinamide as by-product.

To apply this method for the estimation of the effect of fluorophore-labeling of protein and/or DNA constructs on the enzyme activity, equimolar of AB and CDEF were used in the automodification in the presence of 66G. The results showed that fluorophore-labeling did not have a significant effect on the enzyme activity. The fitting of the data to Michalis-Menten model with regard to the concentration of allosteric DNA ligands may be puzzling. But the estimated K_M within nanomolar range is consistent with other reports that PARP-1 has strong affinity for DNA.

Chapter 3. Investigation of Human PARP-1 Catalytic Mechanism Using Fluorinated NAD^+ Analogues

3.1 INTRODUCTION

PARP-1 catalyzes protein poly(ADP-ribosyl)ation reaction in which PAR polymers are synthesized from NAD^+ onto substrate proteins, with itself being the major acceptor (*269*). The reaction is catalyzed by a single active site located within domain F (or the catalytic domain, Figure 1-11), and can be dissected into three steps: initiation, elongation, and branching. Each step can be viewed as the cleavage of the ribose–nicotinamide glycosidic bond and the concomitant transfer of ADP-ribose moiety to different nucleophilic acceptors. Based on the sequence homology of PARP-1 catalytic domain to bacterial ADP-ribosylating toxins and available crystal structures, a reaction mechanism involving Glu-988 as the general base has been proposed (Figure 1-15). The γ-carboxylate of the glutamate serves as an anchor for positioning donor and/or acceptor substrates, or directly activates the acceptor hydroxyl groups for nucleophilic attack (*246*).

The mechanism of how enzymes catalyze the nicotinamide–ribosyl bond cleavage has been the subject of research by several groups. Early study carried out by Oppenheimer and colleagues provided substantial insight into the mechanism of chemical and enzymatic hydrolysis (by calf spleen NAD^+ glycohydrolase) of NAD^+ using a series of NAD^+ analogues containing H, NH_2, OH, N_3 and F at the 2′-position, either in ribose or arabinose configuration (*270*). Analogues with arabinose configuration cannot be hydrolyzed by the enzyme and instead are slow binding inhibitors. The log of the rate constants of the reactions forms a linear relationship with the corresponding inductive Taft constants. The log of the V_{max} of the enzymatic reaction using natural NAD^+ (OH at the 2′-position) would directly fall on the line defined by other analogues only with the

choice of an alkoxide Taft constant, not neutral hydroxyl group. These results suggested that the anionic character developed at the 2′-hydroxyl group may inductively stabilize the oxocarbenium intermediate (or oxocarbenium-like transition state) during enzyme catalysis (*271*). An active site base, later confirmed to be Glu-988 in PARP-1, could facilitate the inductive stabilization through interacting with the 2′-hydroxyl group. Schramm *et al*. measured the kinetic isotope effect (KIE) of diphtheria toxin-catalyzed NAD^+ hydrolysis and the data is consistent with an A_ND_N mechanism in which both leaving group and nucleophile participate in the reaction coordinate (*272*). Quantum mechanics/molecular mechanics (QM/MM) simulation study of the hydrolysis of NAD^+ by PARP-1 showed that the cleavage of nicotinamide–ribosyl bond proceeds through a dissociative S_N2 mechanism via an oxocarbenium-like transition state structure (or intermediate), in agreement with previous linear free energy and KIE studies (*273*). Moreover, Lim *et al*. also performed density functional theory (DFT) calculations combined with continuum dielectric methods to systematically assess the roles of pyrophosphate, the nucleophilicity of different attacking nucleophiles, and the medium in affecting the NAD^+ non-redox reaction pathways and demonstrated their contributions to accelerating the reaction in general (*274*).

Experimental evidence regarding the NAD^+ substrate scope of poly(ADP-ribosyl)ation reaction is somewhat limited for PARP-1. Radiolabeled adenosine deoxyribose analogues of NAD^+ have been enzymatically synthesized in the 80s in order to characterize the mechanism of chain elongation catalyzed by PARP-1 (*275*). While 3′-deoxy-NAD^+ can be incorporated into oligomeric PAR polymers (*247*), 2′-deoxy-NAD^+ was not a substrate for PARP-1 as no radiolabeled protein was detected following the incubation. Instead, it was shown to be a noncompetitive inhibitor for PARP-1 with a K_i

value of 32 μM (*275*). This compound, however, could be processed by an arginine-specific mono-ADP-ribosyltransferase from turkey erythrocytes (*276*).

In order to gain further insight into the reaction mechanism of each step of poly(ADP-ribosyl)ation, fluorinated NAD^+ analogues were designed and synthesized in our laboratory to study the PAR polymer formation. Fluorine-containing compounds are useful small molecule probes to elucidate enzymatic reaction mechanisms (*277*). The electronegativity and van der Waals radius of fluorine render it an effective hydroxyl group mimic. Our interest mainly lies in examining the stepwise mechanism of poly(ADP-ribosyl)ation during PAR polymer growing. Replacement of the 2′-hydroxyl group of the adenosine ribose with fluorine (2′-deoxy-2′-fluororibo-NAD^+, 2AF-NAD^+) is expected to prevent chain elongation (Figure 3-1). Likewise, replacement of the 2″-hydroxyl group of the NMN ribose with fluorine (2″-deoxy-2″-fluororibo-NAD^+, 2NF-NAD^+) could potentially block branching reaction, generating linear PAR polymers (Figure 3-1). In this chapter, fluorinated NAD^+ analogues were synthesized and detailed characterizations of the reaction outcomes with human PARP-1 were carried out with our focus set on 2NF-NAD^+, since the biological significance of the branching reaction has not been fully addressed. The data indicate that 2NF-NAD^+ is not a substrate for PARP-1, whereas 2AF-NAD^+ has minor inhibitory effect on PAR formation. This result, however, is consistent with the proposed catalytic mechanism of ADP-ribosyltransferase reaction that an oxocarbenium-like transition state is formed during enzyme catalysis. A fluorine atom present at the C2 position of the nicotinamide ribose hampers the formation of such intermediate, rendering no catalytic turnover of the compound.

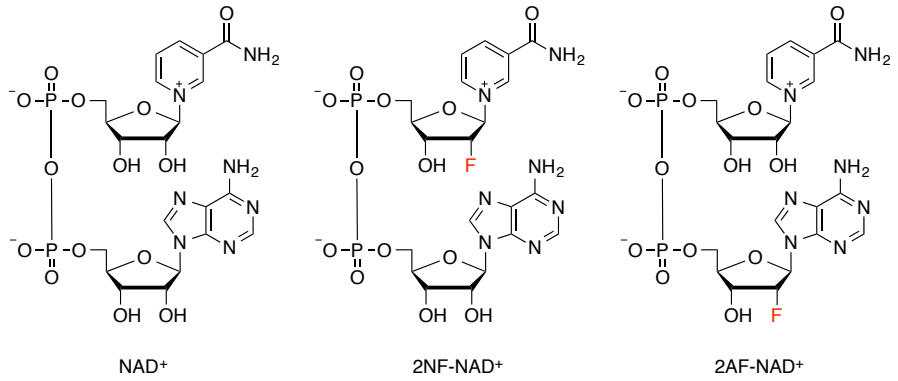

Figure 3-1. Structures of NAD^+ analogues as mechanistic probes for PARP-1.

3.2 MATERIALS AND METHODS

3.2.1 Expression and purification of human NMNAT-1 in *E. coli*

The cDNA encoding human nicotinamide/nicotinate mononucleotide (NMN/NaMN) adenylyltransferase-1 (NMNAT-1), a gift from Dr. Hong Zhang in UT Southwestern Medical Center, was subcloned into pET-28b(+) vector (Novagen) by Dr. Peng Gao. Expression of the protein was carried out in *Escherichia coli* (*E. coli*) BL21-CodonPlus strain (Stratagene). A glycerol stock of cells transformed with NMNAT-1/pET-28b(+) was re-streaked onto a Luria-Bertani (LB) agarose plate containing 50 μg/mL ampicillin and incubated at 37 °C overnight. A single colony was selected to produce a 10 mL, overnight small culture subsequently used to inoculate a 1 L large culture of LB medium containing the same selection antibiotic. Cells were grown at 37 °C with shaking at 200 rpm until OD_{600} reached 0.6. Protein expression was induced by the addition of isopropyl β-D-1-thiogalactopyranoside (IPTG) to a final concentration of 1.0 mM, and the cells were allowed to grow for an additional 12-18 h at 18 °C with

shaking at 125 rpm. Cells were then harvested by centrifugation at 4500 × *g* for 30 min and stored at −80 °C until lysis.

All the protein purification procedures were performed at 4 °C. Thawed cells were re-suspended in lysis buffer containing 50 mM sodium phosphate, 300 mM NaCl, 10 mM imidazole, 1 mM β-mercaptoethanol and 10% glycerol at pH 8.0. Sonication for ten 10-sec bursts with 30-sec cooling interval was used to completely disrupt cells. Cell debris was removed by centrifugation at 16,000 × *g* for 30 min, and the supernatant was incubated with Ni-NTA agarose resin (Qiagen) on a tube rotator for 1 h. The lysate mixture was transferred onto a column, gravity drained, and washed with lysis buffer. The His_6-tagged NMNAT-1 protein was then eluted with elution buffer (lysis buffer with 250 mM imidazole). The desired fractions were checked by Bradford reagent (Bio-Rad), pooled, and dialyzed against lysis buffer. Purity of the protein was analyzed by sodium dodecyl sulfate polyacrylamide gel electrophoresis (SDS-PAGE). Purified His-tagged NMNAT-1 was aliquoted, flash-frozen in liquid nitrogen, and stored at −80 °C.

3.2.2 NMNAT-1 activity assay

To test the activity of purified human NMNAT-1, a high-performance liquid chromatography (HPLC)-based assay was developed to monitor the production of NAD^+ in the presence of NMN, ATP, and NMNAT-1. Briefly, a 200-μL reaction mixture containing 120 μM NMN, 10 mM ATP, 30 μM purified NMNAT-1, 2 units inorganic pyrophosphatase, 10 mM $MgCl_2$, and 50 mM sodium phosphate at pH 7.4 was incubated at 37 °C for 2 h. The reaction mixture was filtered through a Microcon centrifugal filter unit YM-10 (EMD Millipore) to remove the enzyme. The filtrate was subjected to HPLC analysis using System Gold HPLC (Beckman Coulter) equipped with a Luna C18(2) 5

μm 250 × 4.6 mm analytical column (Phenomenex). The sample was eluted with the mobile phase consists of 10 mM ammonium acetate (solvent A) and acetonitrile (solvent B). The gradient started from 0 to 10% B over 20 min, 10 to 70% B over 2 min, and 70 to 0% B over 2 min before re-equilibration for 6 min. The flow rate was 1 mL/min and the eluent was monitored by UV absorbance at 260 nm. Product peaks were verified by co-elution with standards.

3.2.3 Chemoenzymatic synthesis of fluorinated NAD$^+$ analogues

2NF-NAD$^+$ was chemoenzymatically synthesized according to the scheme shown in Figure 3-2 with the input from Dr. Chi-Hau Chen. The fluorinated NMN moiety (compound **6**) was chemically synthesized with the assistance of Richiro Ushimaru. Enzymatic coupling of **6** with ATP using NMNAT-1 gave the final product 2NF-NAD$^+$.

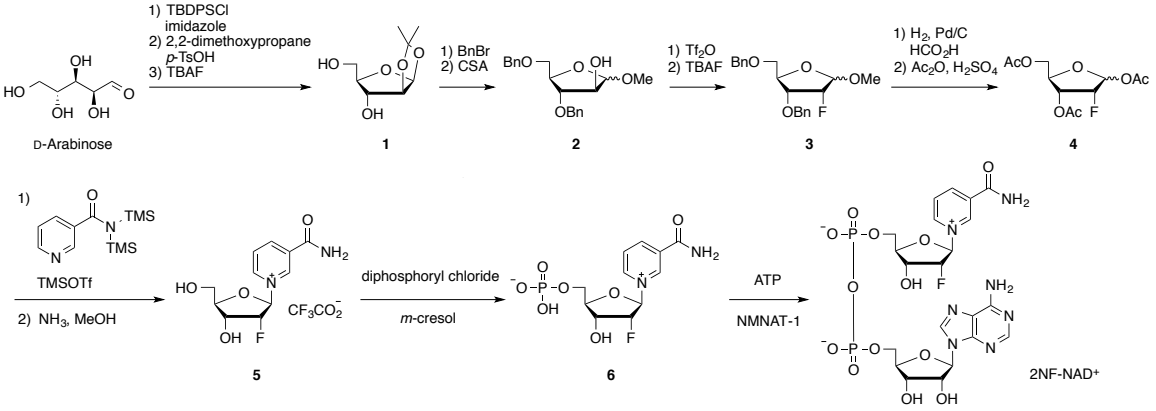

Figure 3-2. Synthetic scheme for 2NF-NAD$^+$.

Synthesis of compound 5

D-Arabinose was selectively protected to leave 2′-hydroxyl available. Fluorine was introduced by tetra-*n*-butylammonium fluoride (TBAF), affording compound **3** with

a ribose configuration. Change of protecting group to acetyl moiety at the anomeric position enhanced its reactivity and facilitated the installation of nicotinamide base. The resulting compound **5** is a mixture of α- and β-nucleosides and the desired β-form was further purified by HPLC using a Nucleosil C18 5 μm 250 × 10.0 mm semi-preparative column (Phenomenex) and a gradient elution consists of 0.1% TFA in water (solvent A) and 0.1% TFA in acetonitrile (solvent B). Following injection, the column was eluted with 0 to 5% B over 15 min and washed with 100% B before re-equilibrating back to 100% A for 4 min. The flow rate was 4 mL/min and the eluent was monitored by UV absorbance at 260 nm. Peak corresponding to the β-form of compound **5** (retention time ~7 min) was collected, neutralized with saturated sodium bicarbonate, lyophilized and verified by NMR and ESI-MS analysis (*278*).

Synthesis of compound 6

Selective phosphorylation of the primary hydroxyl group of **5** was carried out according to the literature (*279*). The resulting nucleotide **6** was purified by semi-preparative HPLC similar to **5**. The mobile phase consists of 10 mM ammonium acetate (solvent A) and acetonitrile (solvent B). The gradient elution was 0 to 10% B over 10 min. Peak corresponding to **6** (retention time ~3.5 min) was collected, lyophilized, and verified by NMR and ESI-MS analysis (*278*).

Synthesis of 2NF-NAD$^+$

The synthesis of 2NF-NAD$^+$ was accomplished using an enzymatic coupling reaction catalyzed by NMNAT-1 between **6** and ATP. The reaction was carried out according to the literature with some modifications (*278*). Purified NMNAT-1 was added (final concentration 30 μM) to a 1-mL reaction containing 3.8 mM compound **6**, 10 mM ATP, 20 units inorganic pyrophosphatase, 10 mM $MgCl_2$, and 50 mM sodium phosphate

at pH 7.4. The reaction mixture was incubated at 37 °C for 1 h and then quenched by adding 3 μL 0.1% TFA. Quenched reaction was filtered through a Microcon centrifugal filter YM-10 unit to remove proteins. The filtrate was subjected to semi-preparative HPLC purification following the same procedure for compound **5** except for the gradient elution starting from 0 to 5% B over 10 min. Peak corresponding to 2NF-NAD^+ (retention time ~9.3 min) was collected, lyophilized, and verified by NMR and ESI-MS analysis (*278*).

Synthesis of 2AF-NAD^+

The synthesis of 2AF-NAD^+ (Figure 3-1) was accomplished by Dr. Peng Gao.

3.2.4 Cloning, expression, and purification of human full-length PARP-1 and the E988Q mutant using baculovirus expression vector system in insect cells

The human PARP-1 gene was cloned from PARP-1/pET-28b(+) into the NdeI and XhoI restriction sites of an intermediate pFastBac HT B/MBP-Tev vector generated in our laboratory by Dr. Yung-nan Liu from the pFastBac HT B vector (Invitrogen). The pFastBac HT B/MBP-Tev vector contains an engineered decahistidine-tagged maltose-binding protein (MBP, molecular weight ~42.5 kDa) sequence followed by a tobacco etch viruse (TEV) protease cleavage site *N*-terminal to the gene of interest for expression. The resulting pFastBac HT B/MBP-Tev-PARP plasmid was amplified in *E. coli* DH5α competent cells (Stratagene) for downstream purpose. E988Q mutant construct was generated in house by Dr. Zhihua Tao using site-directed mutagenesis (*72*) and followed by the same procedures mentioned above.

To generate the recombinant baculovirus shuttle vector "bacmid" for the MBP-Tev-PARP construct, MAX Efficiency DH10Bac *E. coli* competent cells (Invitrogen)

were transformed with pFastBac HT B/MBP-Tev-PARP according to the manufacturer's instructions for the Bac-to-Bac Baculovirus Expression System. Successful transformants were selected by blue/white colony screening on LB agar plates containing 50 μg/mL kanamycin, 7 μg/mL gentamicin, 10 μg/mL tetracycline, 100 μg/mL Bluo-gal, and 40 μg/mL IPTG. Following the incubation of the streaked LB agar plates at 37 °C for 48 h, white colonies were selected, re-streaked on a fresh LB agar plate containing the same additives, and incubated at 37 °C overnight to confirm the white colony phenotype. A single white colony was then used to inoculate an LB medium containing 50 μg/mL kanamycin, 7 μg/mL gentamicin, and 10 μg/mL gentamicin. The liquid culture was incubated at 37 °C overnight with shaking at 250 rpm. The resulting recombinant bacmid DNA was subsequently purified using the Purelink HiPure Plasmid DNA Miniprep Kit (Invitrogen) and confirmed by PCR based on the manufacturer's protocol.

The bacmid DNA containing MBP-fused PARP-1 gene was used to transfect Sf21 insect cells using Cellfectin II Reagent (Invitrogen). When the cells displayed signs of late stage infection (cytopathic effect) roughly 72-96 h after transfection, the medium was collected by centrifugation at 1,000 × *g* for 5 min. The resulting P1 viral stock was then used to generate P2 viral stock by infecting Sf21 cells grown in suspension.

For the expression of MBP-PARP-1 fusion protein, P2 viral stock was used to infect Sf21 insect cells grown in serum-free SF-900 II SFM medium at 27 °C with shaking at 100 rpm. At 72 h post infection, the infected cells were harvested by centrifugation at 4,000 × *g* for 10 min. Cells were re-suspended and washed with PBS twice and stored at −80 °C until further usage.

Protein purification was carried out at 4 °C as follows. Harvested cells were thawed and re-suspended in lysis buffer containing 20 mM HEPES, 1 M NaCl, 10 mM imidazole, 1% Triton X-100, 1 mM β-mercaptoethanol, and 10% glycerol at pH 7.5.

Cells were disrupted by sonication and debris was removed by centrifugation at 4,000 × *g* for 20 min. The resulting supernatant was incubated for 1 h on a tube rotator with 10 mL Ni-NTA agarose resin (Qiagen) which had been pre-equilibrated with the lysis buffer. The mixture was then loaded onto a column for gravity drainage and washed extensively with at least 10× column volume wash buffer (lysis buffer containing 20 mM imidazole). To facilitate the washing process for large-scale preparation, the mixture could be centrifuged at 500 × *g* for 3 min and buffer-exchanged with wash buffer twice before loading onto the column for gravity drainage. The MBP fusion protein was eluted with elution buffer (lysis buffer containing 250 mM imidazole and 300 mM NaCl). Fractions containing desired protein were checked by Bradford reagent (Bio-Rad), pooled and dialyzed against 2 × 1 L lysis buffer. His_6-tagged TEV protease was added into the protein solution to a final concentration of 5% (w/w) 2 h after the start of dialysis, for the cleavage of the His_{10}-MBP tag. The mixture was continued to undergo dialysis with 1 L fresh buffer for 24 h at 4 °C.

To remove the cleaved MBP tag from the non-tagged protein, the protein mixture was slowly passed through a column containing 10 mL Ni-NTA agarose resin. The protein recovered in the flow through was concentrated using an Amicon Ultra-15 centrifugal filter unit with a 10-kDa cut-off (EMD Millipore). The desired protein construct contains two additional amino acid residues, glycine followed by histidine, at the protein *N*-terminus owing to the engineered TEV cleavage sequence. Depending on specific experiment, further purification was performed by size-exclusion chromatography using AKTA FPLC system equipped with a Superdex 200 column (GE Healthcare). The elution buffer contains 10 mM sodium phosphate, 100 mM NaCl, and 10% glycerol at pH 7.5. Purified protein was aliquoted, flash-frozen in liquid nitrogen, and stored at –80 °C.

3.2.5 PARP-1 automodification assay

In vitro PARP-1 automodification assay was carried out by adding PARP-1 (final concentration 0.5-5 μM) to a reaction mixture containing varying concentrations of NAD^+ or NAD^+ analogues in the 10-μL PARP reaction buffer (25 μg/mL calf thymus DNA (Sigma-Aldrich), 250 μM dithiothreitol (DTT), 10 mM $MgCl_2$, 100 mM Tris-HCl at pH 8.0). The mixture was incubated at room temperature for 30 to 60 min and then quenched by 2× SDS-PAGE loading buffer. To assess the effect of fluorinated NAD^+ analogues on the wild-type poly(ADP-ribosyl)ation reaction, either a mixture of NAD^+ and NAD^+ analogues was included in the same reaction, or a 30-min pre-incubation of NAD^+ analogues with PARP-1 and other reaction components was performed before the addition of natural NAD^+ to initiate poly(ADP-ribosyl)ation. The reaction was analyzed by SDS-PAGE and visualized by SYPRO Ruby protein gel stain (Invitrogen) or Western blotting. The blots were probed with anti-PAR polymer monoclonal antibody (Trevigen) followed by incubation of horseradish peroxidase-conjugated anti-mouse IgG secondary antibody (Sigma-Aldrich), and the protein bands were visualized using Amersham ECL Prime Western Blotting chemiluminescence substrate (GE Healthcare).

A radioactivity-based PARP-1 automodification assay was also adopted to achieve higher detection sensitivity. Total volume of 6 μL reactions were conducted under the same condition described above in the presence of a mixture of cold NAD^+ and [*adenylate*-^{32}P]NAD^+ (^{32}P-NAD^+, American Radiolabeled Chemicals). The ratio of NAD^+ to ^{32}P-NAD^+ was 0.1 mM–0.1 μCi μL^{-1}. The samples were resolved by a 16 × 16 cm SDS-PAGE gel, exposed on a storage phosphor screen (GE Healthcare) and detected by Typhoon FLA 9500 (GE Healthcare). Gel images were processed by ImageJ (National Institutes of Health).

3.2.6 Sequencing gel-based poly(ADP-ribose) polymer analysis

Characterization of PAR polymers generated by PARP-1 automodification in the presence of fluorinated NAD^+ analogues was carried out according to the literature with some modifications (*64*). Briefly, a 100-μL automodification reaction containing varying concentrations of fluorinated NAD^+ analogues were pre-incubated with 0.2 μM PARP-1 in the PARP reaction buffer (see Section 3.2.5) at room temperature for 30 min prior to the addition of 100 μM NAD^+ and 0.1 μCi ^{32}P-NAD^+. The reaction was allowed to proceed for 10 min before quenching by equal volume of 20% (w/v) trichloroacetic acid (TCA). Protein precipitates were collected by centrifugation and washed twice with ice-cold ethanol. The precipitates were then digested in a 30-μL solution containing 0.5 M KOH and 50 mM EDTA at 37 °C for 15 min. After base digestion, the solution was brought to neutral pH by adding Tris-HCl buffer. Cleaved PAR polymers were extracted by equal volume of phenol/chloroform/isoamyl alcohol (25:24:1, v/v/v, saturated with 10 mM Tris, pH 8.0 and 1 mM EDTA). The aqueous layer was collected and the extraction was repeated twice. The combined aqueous layer was mixed with 2× PAR loading buffer (40% urea, 25 mM NaCl, 4 mM EDTA, 0.02% bromophenol blue, and 0.02% xylene cyanol) and resolved by 20% Tris-borate-EDTA PAGE system followed by phosphorimaging. Gel images were processed by ImageJ (National Institutes of Health).

3.2.7 HPLC-based poly(ADP-ribose) polymer analysis

For HPLC-based PAR polymer analysis, nonradioactive NAD^+ was used. A 300-μL automodification reaction was set up as described in Section 3.2.6, except for using 1 μM PARP-1 and 1 mM NAD^+, or a mixture of 500 μM NAD^+ and 500 μM fluorinated NAD^+ analogues. A solution of 50 μg/mL histone H1 was also included to enhance overall PAR production. Steps leading to the generation of aqueous solution containing

free PAR polymers after extraction by organic solvent were followed according to Section 3.2.6. PAR polymers were precipitated at –20 °C overnight by adding ethanol to a final concentration of 70% (w/w). The precipitates were collected by centrifugation at 16,000 × *g*, washed by ether, dried by speedvac, and stored at –20 °C until further process.

To digest the PAR polymers into monomeric subunits (Figure 1-5), the pellets were first re-dissolved in 56 μL 0.1 M ammonium bicarbonate and 2 mU phosphodiesterase (PDE) was added to the solution for 2 h incubation at 37 °C. Alkaline phosphatase (AP) was added subsequently to convert digestion products into their corresponding nucleoside forms. The digestion was allowed to proceed overnight at 37 °C. After removing enzymes by YM-10 membrane filtration, the filtrate was subjected to C18 analytical HPLC analysis using 10 mM ammonium acetate (solvent A) and methanol (solvent B) as mobile phase components. The gradient program started from 7 to 14% B over 35 min. The flow rate was 1 mL/min and the elution was monitored by UV absorbance at 260 nm. Product peaks were verified by co-elution with standards and collected for ESI-MS analysis.

3.2.8 Analysis of PARP-1 initiation reaction using HPLC

To confirm if the initiation step occurred during protein poly(ADP-ribosyl)ation, automodification reaction (50 μL) of PARP-1 or the E988Q mutant was set up according to the same procedures described in Section 3.2.5, in the presence of 500 μM NAD^+ or NAD^+ analogues. The reaction was incubated at 37 °C for 1 h. PAR polymer was then cleaved by the addition of purified PARG enzyme (kindly provided by Dr. Yung-nan Liu) for overnight incubation at 37 °C, leaving the proximal ADP-ribose attached to

proteins. The samples were passed through a YM-10 filtering unit to filter out ADP-ribose produced by PARG digestion. The filtrate (sample *a*) was saved for subsequent C18 analytical HPLC analysis. After washing with 0.1 M ammonium bicarbonate, the remaining proteins were further digested with PDE for 3 h followed by AP for 1 h at 37 °C. Proteins were again filtered out by YM-10 filtering unit, and the filtrate (sample *b*) was subjected to C18 analytical HPLC analysis using 10 mM ammonium acetate (solvent A) and acetonitrile (solvent B) as mobile phase. The gradient elution were 0 to 10% B over 20 min and 7 to 12% B over 25 min for sample *a* and *b*, respectively. The flow rate was 1 mL/min and the elution was monitored by UV absorbance at 260 nm. Product peaks were verified by co-elution with standards.

3.2.9 NAD^+-dependent redox reaction assay

To test if fluorinated NAD^+ analogues can serve as redox cofactors, NAD^+-dependent oxidation of ethanol to acetaldehyde catalyzed by alcohol dehydrogenase (ADH) from yeast (YADH) was used as the model reaction. A 100-μL solution contains 0.33 M ethanol, 8.3 mM NAD^+ or NAD^+ analogues, and 50 mM sodium pyrophosphate, pH 9.2. The reaction was initiated by adding 1 μL YADH (2 μg/mL in 0.1 M sodium phosphate, pH 7.5 and 0.1% BSA) and monitored continuously fore every 10 sec by UV absorbance at 340 nm using Agilent 8453 Spectrophotomer (Agilent Technologies) for 350 sec. Reactions using 2NF-NAD^+ as cofactor was monitored by NanoDrop (Thermo Scientific) before and 350 sec after the addition of the enzyme.

3.3 RESULTS

3.3.1 Chemoenzymatic synthesis of fluorinated NAD^+ analogues

The key steps to synthesize 2NF-NAD^+ are the preparation of the fluorinated NMN moiety in the ribose configuration, and the formation of pyrophosphate linkage between NMN and AMP. The fluorinated NMN moiety was prepared chemically starting from D-arabinose. After a series of selective introductions of protecting groups, nucleophilic fluorination of compound **2** at 2′ position was carried out using triflic anhydride and TBAF, generating compound **3** with ribose configuration. Changing from methoxy group to acetyl group at the anomeric carbon increased the reactivity of compound **4** for the introduction of nicotinamide base. The reaction to generate nucleoside **5** with exclusive β-configuration was performed according to the literature (*280*). However, a mixture α- and β-form was observed by the crude NMR of the reaction, potentially due to the substitution of fluorine for the hydroxyl group at 2′-position. The desired β-form was then purified by semi-preparative HPLC and converted to nucleotide **6** by phosphorylation of the primary alcohol.

The final coupling of the fluorinated NMN moiety (**6**) with AMP was accomplished by the enzyme NMNAT-1. To test the activity of *in vitro* overexpressed NMNAT-1, the production of NAD^+ was examined using natural β-NMN and ATP. In the presence of enzyme, a peak at ~11.6 min was observed, which co-eluted with NAD^+ (Figure 3-3), suggesting that the purified NMNAT-1 was active. With the active enzyme in hand, the coupling of fluorinated NMN (**6**) with ATP was conducted, and the product was purified by semi-preparative HPLC. As shown in Figure 3-4, the peak eluted at ~9.2 min was collected and subjected to ESI-MS and NMR analysis. The data are consistent with the chemical structure of 2NF-NAD^+ (see Appendix). The reaction was not complete

even in the presence of ~2.6-fold molar excess of ATP, and compound **6** can be recovered for further conversion.

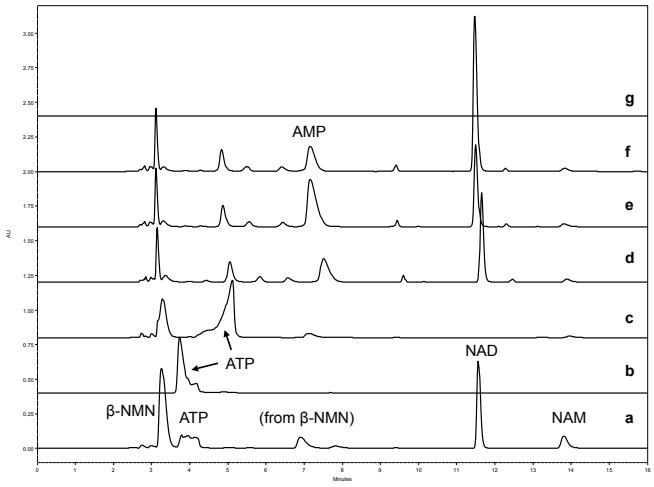

Figure 3-3. HPLC analysis of NMNAT-1 activity assay. (a) Mixture of chemical standards. NAM, nicotinamide. (b) ATP. (c) Reaction in the absence of NMNAT-1. (d) Reaction in the presence of NMNAT-1. (e) Co-injection of the reaction (trace *d*) with AMP. (f) Co-injection of the reaction (trace *d*) with NAD^+. (g) NMNAT-1 only.

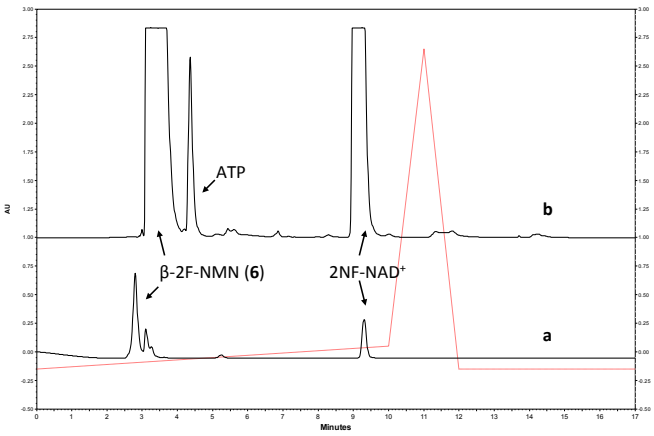

Figure 3-4. Semi-preparative HPLC chromatograms of the production of 2NF-NAD^+ by NMNAT-1-catalyzed reaction. (a) 10-μL injection of the reaction. (b) 400-μL injection of the reaction.

2AF-NAD^+ has been synthesized in our laboratory previously, and the compound was verified by ESI-MS.

3.3.2 Poly(ADP-ribosyl)ation of PARP-1 using fluorinated NAD^+ analogues

To test if fluorinated NAD^+ analogues are substrates for PARP-1, *in vitro* poly(ADP-ribosyl)ation reaction of PARP-1 was carried out and resolved by SDS-PAGE. Western blotting using anti-PAR monoclonal antibody was performed to detect the formation of PAR polymer, whereas PARP-1 protein was stained by SYPRO Ruby dye.

The results of PARP-1 automodification reactions using either NAD^+ and/or 2NF-NAD^+ as substrates are shown in Figure 3-5. PARP-1 was poly(ADP-ribosyl)ated in the presence of NAD^+, as revealed by anti-PAR immunoblotting (lane 2-5, Figure 3-5A) and the smear in the protein stain (lane 1-5, Figure 3-5B). However, no PAR polymer was formed in the presence of 2NF-NAD^+ alone, and no protein smear was observed (lane 6-9, Figure 3-5). Longer exposure of the gel did not show any PAR signal. To further confirm the observation, similar reactions with increased PARP-1 concentration was carried out. Neither PAR polymer signal was detected, nor protein band shift was observed (Figure 3-5C). The results suggest that no PAR polymer was produced by PARP-1 in the presence of 2NF-NAD^+ alone.

To assess if 2NF-NAD^+ has any effect on native poly(ADP-ribosyl)ation, automodification of PARP-1 was conducted using a mixture of NAD^+ and 2NF-NAD^+, or pre-incubation of PARP-1 with 2NF-NAD^+ prior to the addition of NAD^+. All reactions showed comparable level of poly(ADP-ribosyl)ation as those using NAD^+ alone (lane 10-14, Figure 3-5A, B; lane 8-12, Figure 3-5C). Reactions with higher molar ratio of 2NF-NAD^+ to NAD^+ (up to 20:1) did not show significant difference of protein smear as

compared to reactions using NAD^+ only (Figure 3-5D). The results indicate that 2NF-NAD^+ has minimal perturbation on native poly(ADP-ribosyl)ation reaction.

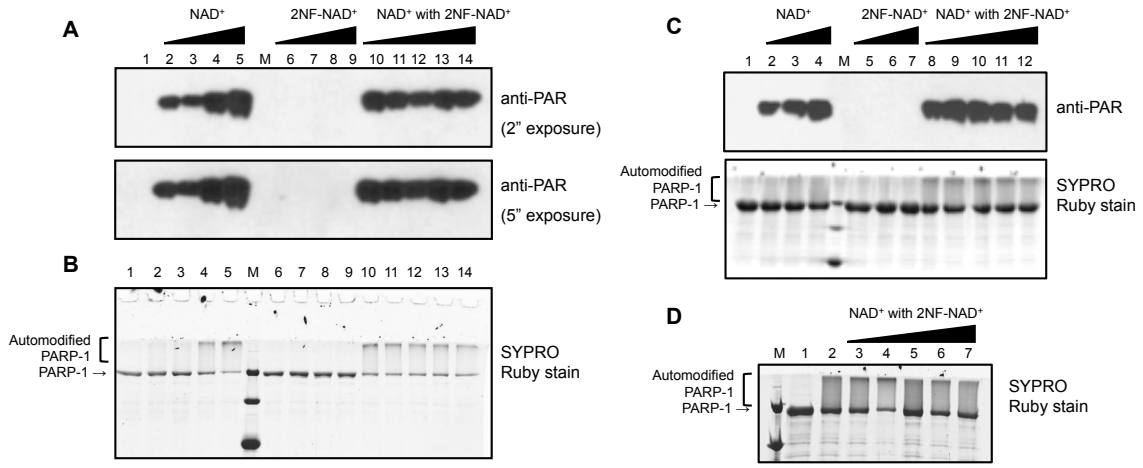

Figure 3-5. Poly(ADP-ribosyl)ation of PARP-1 using NAD^+ or 2NF-NAD^+ as substrates. (A) Automodification reactions of 0.5 μM PARP-1 detected by anti-PAR monoclonal antibody. Lane 1, no NAD^+; lanes 2-5, increasing NAD^+ concentrations of 5, 10, 50, 100 μM, respectively; lanes 6-9, increasing 2NF-NAD^+ concentrations of 5, 10, 50, 100 μM, respectively; lanes 10-14, increasing 2NF-NAD^+ concentrations of 5, 10, 50, 100, 200 μM respectively in the presence of 50 μM NAD^+. M, molecular weight marker. (B) Same reactions performed in (A) detected by SYPRO Ruby stain. (C) Automodification reactions of 5 μM PARP-1. Lane 1, no NAD^+; lanes 2-4, increasing NAD^+ concentrations of 50, 100, 200 μM, respectively; lanes 5-7, increasing 2NF-NAD^+ concentrations of 50, 100, 200 μM, respectively; lanes 8-12, pre-incubation of 50, 100, 200, 500, 1000 μM 2NF-NAD^+, respectively for 30 min before the addition of 200 μM NAD^+. *Top*, anti-PAR Western blot. *Bottom*, SYPRO Ruby stain. (D) Automodification reactions of 1 μM PARP-1. Lane 1, no NAD^+; lane 2, 50 μM NAD^+; lanes 3-7, increasing 2NF-NAD^+ concentrations of 10, 50, 100, 500, 1000 μM, respectively in the presence of 50 μM NAD^+.

To gain further insight into the effect of 2NF-NAD^+ on poly(ADP-ribosyl)ation, radioactivity-based automodification reactions were performed to achieve higher detection sensitivity. In the presence of ^{32}P-NAD^+, PARP-1 was poly(ADP-ribosyl)ated

and shifted toward the gel interface. Poly(ADP-ribosyl)ation still occurred as the concentration of 2NF-NAD^+ increases, and the intensity did not change significantly (Figure 3-6). However, more ADP-ribose was produced, suggesting that NAD^+ hydrolysis could be more efficient than PAR polymer elongation in the presence of 2NF-NAD^+.

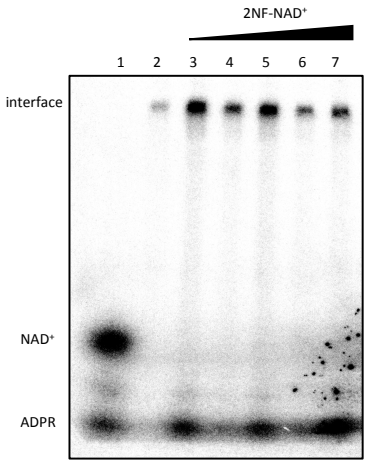

Figure 3-6. Radioactivity-based PARP-1 automodification reactions in the presence of 2NF-NAD^+. Lane 1, NAD^+ only; lane 2, PARP-1 + 50 μM NAD^+; lanes 3-7, increasing 2NF-NAD^+ concentrations of 10, 50, 100, 500, 1000 μM, respectively in the presence of 50 μM NAD^+. Interface indicates the boundary between the stacking and the separating gel. ADPR, ADP-ribose.

2AF-NAD^+, another fluorinated analogue with fluorine atom substituted at the C2 position of the adenosine ribose ring, was assessed for its ability to poly(ADP-ribosyl)ate PARP-1 in a similar way to 2NF-NAD^+. PARP-1 incubated with 2AF-NAD^+ alone was not able to generate PAR polymers detected by anti-PAR Western blot (lane 2, Figure 3-7). 2AF-NAD^+ also did not have significant effect on the native poly(ADP-ribosyl)ation reaction, as protein smear was observed for all reactions up to 20-fold molar excess of the analogue (lane 3-7, Figure 3-7). These results suggest that no PAR polymers were formed

in the presence of 2AF-NAD^+ alone, and no significant effect of 2AF-NAD^+ on PARP-1 automodification in the presence of natural substrate NAD^+.

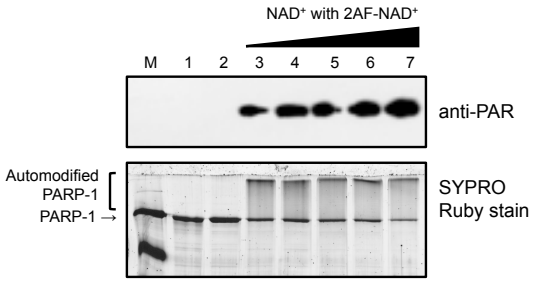

Figure 3-7. Poly(ADP-ribosyl)ation of PARP-1 using NAD^+ or 2AF-NAD^+ as substrates. Lane 1, PARP-1 only; lane 2, 25 μM 2AF-NAD^+; lanes 3-7, increasing 2AF-NAD^+ concentrations of 0, 10, 50, 100, 500 μM, respectively in the presence of 25 μM NAD^+. *Top*, anti-PAR immunoblotting. *Bottom*, SYPRO Ruby stain. M, molecular weight marker.

3.3.3 PAR polymer analysis

PARP-1 incubated with fluorinated NAD^+ analogues alone were not able to produce PAR polymers, but the possibility that these analogues can be incorporated into the growing polymer in the presence of natural NAD^+ still cannot be ruled out. If 2NF-NAD^+ was incorporated into the PAR polymer, the composition and branching frequency of the polymer could be altered. Therefore, detailed analyses of the PAR polymer in the presence of fluorinated NAD^+ analogues were conducted.

To estimate the size distribution of the *in vitro* synthesized PAR polymers, a modified sequencing gel-based assay was adopted. PARP-1 automodification reactions were performed in the presence of ^{32}P-NAD^+ and fluorinated NAD analogues. PAR polymers attached on the proteins were chemically cleaved and purified with a method similar to the purification of nucleic acids. Radiolabeled PAR polymers were resolved on

a TBE-buffered PAGE gel and visualized by phosphorimaging analysis. Radioactivity can be observed at the origin of each well, representing highly branched PAR polymers which cannot enter into the gel. A ladder of PAR polymers were observed according to their size, with the shortest one migrated to the bottom of the gel. 2NF-NAD^+ seemed to have minimal effect on the distribution of PAR polymers (lane 2-4, Figure 3-8), whereas reduced level of highly branched polymers as well as linear polymers were observed with increasing concentrations of 2AF-NAD^+ (lane 6-8, Figure 3-8).

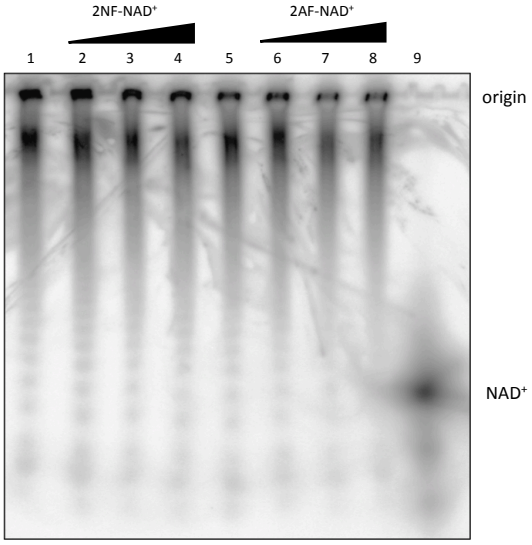

Figure 3-8. PAR polymer analysis using modified sequencing PAGE gel in the presence of ^{32}P-NAD^+. Lanes 1 and 5, 100 μM NAD^+ only; lanes 2-4, increasing 2NF-NAD^+ concentrations of 50, 100, 500 μM, respectively in the presence of 100 μM NAD^+; lanes 6-8, increasing 2AF-NAD^+ concentrations of 50, 100, 500 μM, respectively in the presence of 100 μM NAD^+; lane 9, NAD^+ only.

The composition of PAR polymers can be analyzed by digesting the polymers with PDE and AP, producing nucleoside version of AMP, PR-AMP and PR_2-AMP (Figure 1-5). The resulting monomeric units can be separated by HPLC. If any

fluorinated analogue was incorporated into the growing polymer, a different elongation unit should be detected.

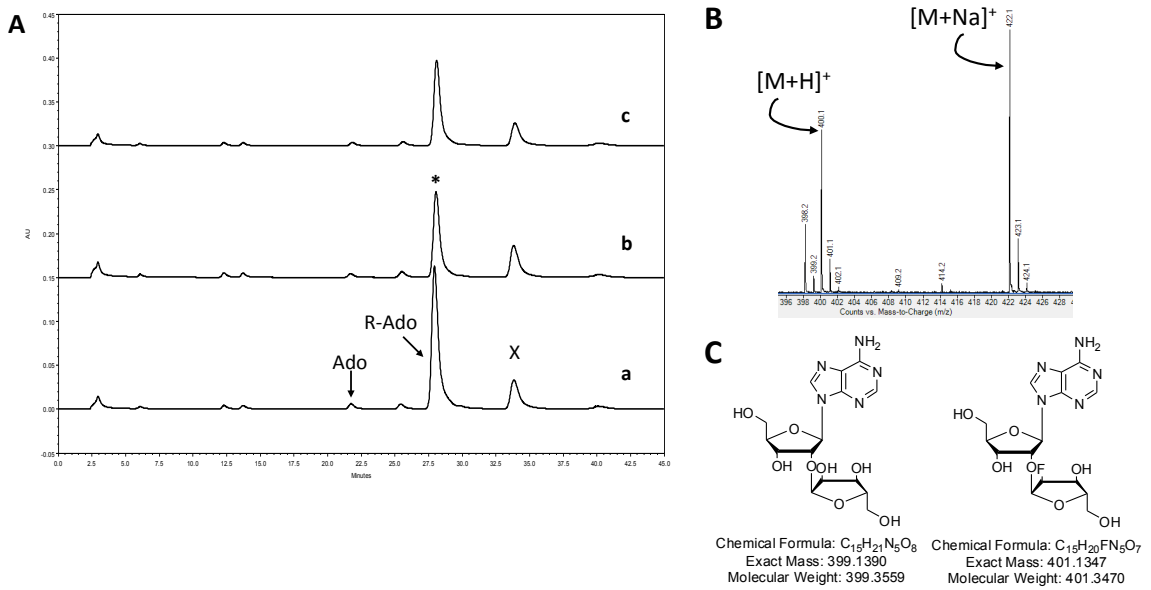

Figure 3-9. Analyses of the composition of PAR polymers. (A) HPLC profiling of monomeric units derived from enzymatic digestion of PAR polymers. (a) Samples derived from PARP-1 automodification using 1 mM NAD^+. (b) Samples derived from PARP-1 automodification using 500 μM NAD^+ and 500 μM 2NF-NAD^+. (c) Co-injection of *a* and *b*. Ado, adenosine; R-Ado, ribosyladenosine; X, unknown peak. (B) ESI-MS analysis of the peak denoted with an asterisk (*) in A. (C) Chemical structures of ribosyladenosine (left) and the fluorinated ribosyladenosine (right).

The result of HPLC analysis was shown in Figure 3-9A. Enzymatic digestion of samples derived from native PAR polymers gave UV-detectable adenosine (terminal unit) and ribosyladenosine (elongation unit) (trace *a*). The amount of branching unit was below UV detection limit. Enzymatic digestion of PAR polymers in the presence of a mixture of NAD and 2NF-NAD also gave similar profile (trace *b*). Co-injection of trace *a* and *b* resulted in the same HPLC profile (trace *c*). To confirm the identity of the asterisk

peak (retention time ~27.6 min) and to rule out the possibility of peak overlapping between ribosyladenosine and its fluorinated analogue, the peak was collected and submitted to ESI-MS analysis. The result is consistent with ribosyladenosine and no signals corresponding to its fluorinated analogue were observed (calculated $[M+H]^+$ = 400.2, found 400.1, Figure 3-9B).

3.3.4 Analysis of the initiation step of poly(ADP-ribosyl)ation by PARP-1

Protein poly(ADP-ribosyl)ation reaction can be dissected into three steps: initiation, elongation, and branching. Based on the results presented in the previous sections, incubation of PARP-1 with either 2NF-NAD^+ or 2AF-NAD^+ alone was not able to produce PAR polymers derived from these NAD^+ analogues. However, the methods used to detect PAR polymer formation (anti-PAR immunoblotting and protein smear detection) did not provide information regarding the initiation reaction, that is, a single ADP-ribose (or its fluorinated version) unit attaching onto the protein. The absence of PAR polymer formation does not necessarily mean that initiation reaction, or mono-ADP-ribosylation of PARP-1 does not occur. To provide evidence for the occurrence of initiation step of PARP-1 poly(ADP-ribosyl)ation, an HPLC-based method was developed to monitor the production of adenosine, which is derived from enzymatic digestion of the proximal ADP-ribose unit attached to the protein after initial mono-ADP-ribosylation. The E988Q mutant of PARP-1, which only catalyzes mono-ADP-ribosylation reaction, was included as a positive control. Reactions omitting either PARP-1 or substrate NAD^+s further served as negative controls to account for background signal during sample process. After 30-min incubation of the reaction mixtures, the modified proteins were separated from the remaining solution by passing through a molecular

weight cutoff centrifugal unit. Both the proteins and the filtrate were saved for HPLC analyses to examine the possibility of any NAD^+ substrate turnover. The modified proteins were treated with PARG to trim PAR polymers down to one ADP-ribose unit. Subsequent digestion with PDE and AP released the adenosine moiety from the protein-proximal ADP-ribose. The filtrate was analyzed by HPLC directly without further treatment.

The HPLC traces from the enzymatic digestion of modified proteins are shown in Figure 3-10A. A peak eluted at ~7.2 min in trace *a* was confirmed to be adenosine, as expected for PARP-1 automodification using NAD^+. A larger peak of adenosine was observed in trace *d* for the reaction of E988Q and NAD^+. This is consistent with the notion that the mutant can only catalyze mono-ADP-ribosylation. A relatively small peak corresponding to adenosine was observed for PARP-1 or E988Q incubated with 2NF-NAD^+ (trace *b* and *e*), as well as reactions with PARP-1 proteins (trace *c* and *f*) or substrate NAD^+s alone (trace *g* and *h*). The results indicate that there is residual amount of NAD^+ remained on the membrane of the centrifugal unit, or binding to the proteins even after buffer wash. Therefore, analyses of modified proteins are not sufficient to conclude that there is turnover of 2NF-NAD^+ or not.

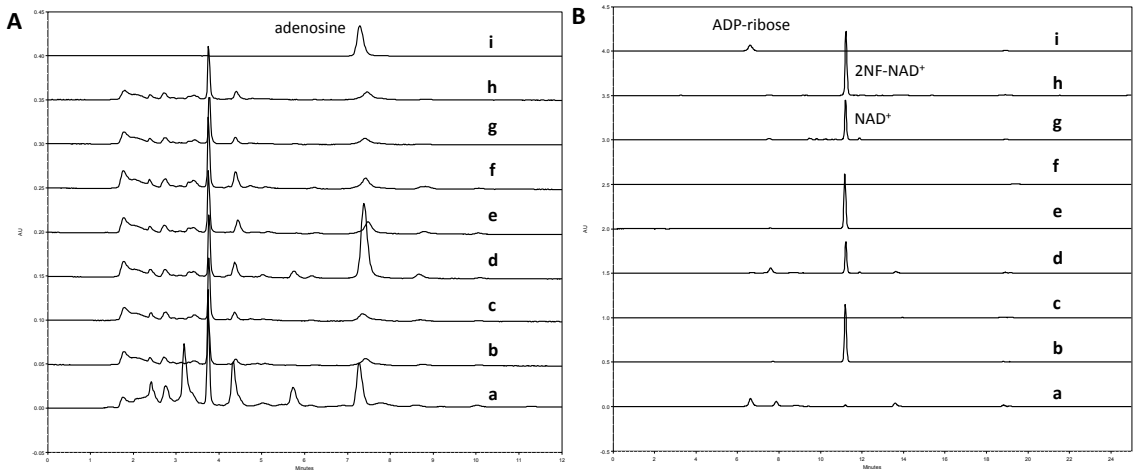

Figure 3-10. HPLC analysis of the initiation step of poly(ADP-ribosyl)ation catalyzed by PARP-1 or its mutant E988Q. (A) Samples derived from enzymatic digestion of the modified PARP-1 or control reactions omitting either PARP-1 or substrate NAD^+s. (B) Samples derived from the remaining filtrate after removing PARP-1 which had undergone automodification. Reaction conditions for each trace are as follows: (a) PARP-1 with NAD^+, (b) PARP-1 with 2NF-NAD^+, (c) PARP-1 only, (d) E988Q with NAD^+, (e) E988Q with 2NF-NAD^+, (f) E988Q only, (g) NAD^+ only, (h) 2NF-NAD^+ only, (i) Chemical standard of adenosine and ADP-ribose in A and B, respectively.

The HPLC traces from the filtrate of the reaction mixtures are shown in Figure 3-10B. For the PARP-1 reaction with NAD^+, almost all NAD^+ was consumed and the production of ADP-ribose (retention time ~6.5 min) was observed due to the NAD^+ hydrolysis side reaction (trace *a*). A small peak of NAD^+ was eluted at ~11 min in the E988Q reaction filtrate (trace *d*), consistent with the fact that less turnover of NAD^+ compared to wild-type PARP-1. However, a peak corresponding to 2NF-NAD^+ was observed for both PARP-1 and the E988Q mutant (trace *b* and *e*). No ADP-ribose was noticed, suggesting that enzyme-catalyzed hydrolysis of 2NF-NAD^+ did not take place under the experimental condition. Enzyme only controls omitting substrate NAD^+s indicated no small molecule contamination (trace *c* and *f*), therefore the small peaks

observed in Figure 3-8A trace *c* and *f* should be derived from residual NAD^+s bound to the membrane of the centrifugal unit. Together with the HPLC analyses of modified PARP-1 proteins, it is concluded that no initiation step, i.e., mono-ADP-ribosylation of PARP-1 happened in the presence of 2NF-NAD^+.

3.3.5 Test of 2NF-NAD^+ as a redox cofactor utilized by alcohol dehydrogenase

Since the nicotinamide part is unchanged in the structure of 2NF-NAD^+, its ability to serve as a redox cofactor was assessed in a model redox reaction catalyzed by alcohol dehydrogenase (ADH) from yeast (YADH). In control reaction using NAD^+ as the cofactor, the oxidation of ethanol to acetaldehyde was continuously monitored by UV absorbance at 340 nm, reflecting the reduction of NAD^+ to NADH. The result of the kinetic experiment reveals that about 2 ng of YADH can reduce 0.00125 μmol of NAD^+ per min, corresponding to an activity of 625 unit/mg enzyme (Figure 3-11A).

Similar reaction was conducted using 2NF-NAD^+ as the cofactor. However, the high UV background at 340 nm (> 1.0) prevented the monitor of 2NF-NAD^+ reduction continuously. Instead, the whole spectra were monitored by NanoDrop before and after the reaction. No significant elevated absorbance at 340 nm was observed, indicating that no turnover of 2NF-NAD^+ by this enzyme (Figure 3-11B).

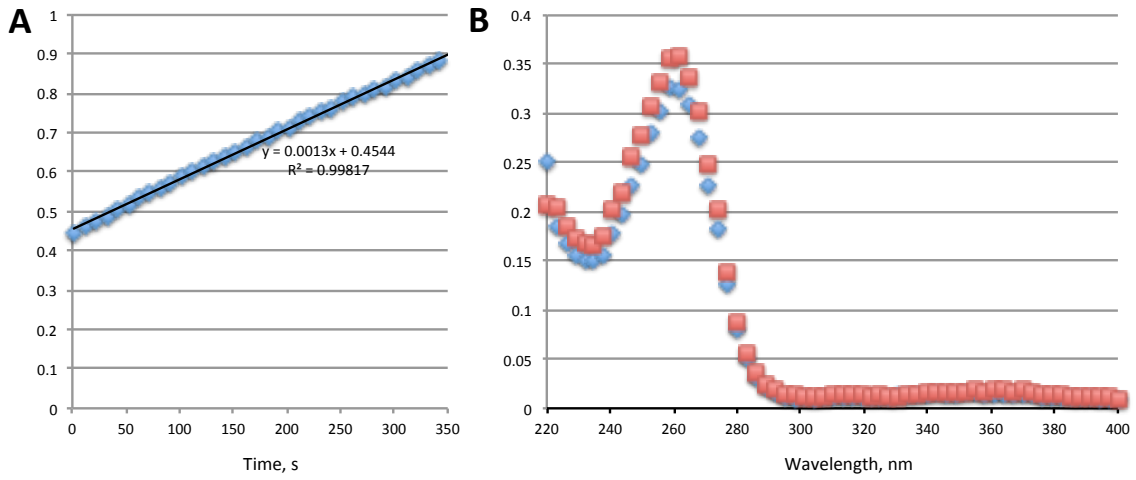

Figure 3-11. Oxidation of ethanol to acetaldehyde catalyzed by alcohol dehydrogenase from yeast. (A) Progress curve of reaction using NAD^+ as the cofactor monitored by UV absorbance at 340 nm. (B) UV spectra of samples using 2NF-NAD^+ as the cofactor. Square (■), before the addition of enzyme; diamond (◆), 350 sec after the addition of enzyme.

3.4 DISCUSSION

3.4.1 2NF-NAD^+ is not a substrate for PARP-1 automodification reaction

Poly(ADP-ribosyl)ation consists of three steps: initiation, elongation, and branching, each of which involves the breakage of nicotinamide–ribose glycosidic bond and the transfer of ADP-ribose unit onto different nucleophilic acceptors. To provide insight into the mechanism of such complicated reaction, fluorinated NAD^+ analogues substituted at different ribose hydroxyl groups were designed and synthesized as mechanistic probes for the individual steps of PARP-1-catalyzed poly(ADP-ribosyl)ation.

Fluorinated NAD^+ could be useful to stop poly(ADP-ribosyl)ation at different stages. Fluorine substitution at the C2 position of the nicotinamide ribose could prevent PAR polymer chain from branching, leading to linear polymers (Figure 3-12A). Fluorine

substitution at the C2 position of the adenosine ribose could stop chain elongation, generating mono-ADP-ribosylated proteins (Figure 3-12B).

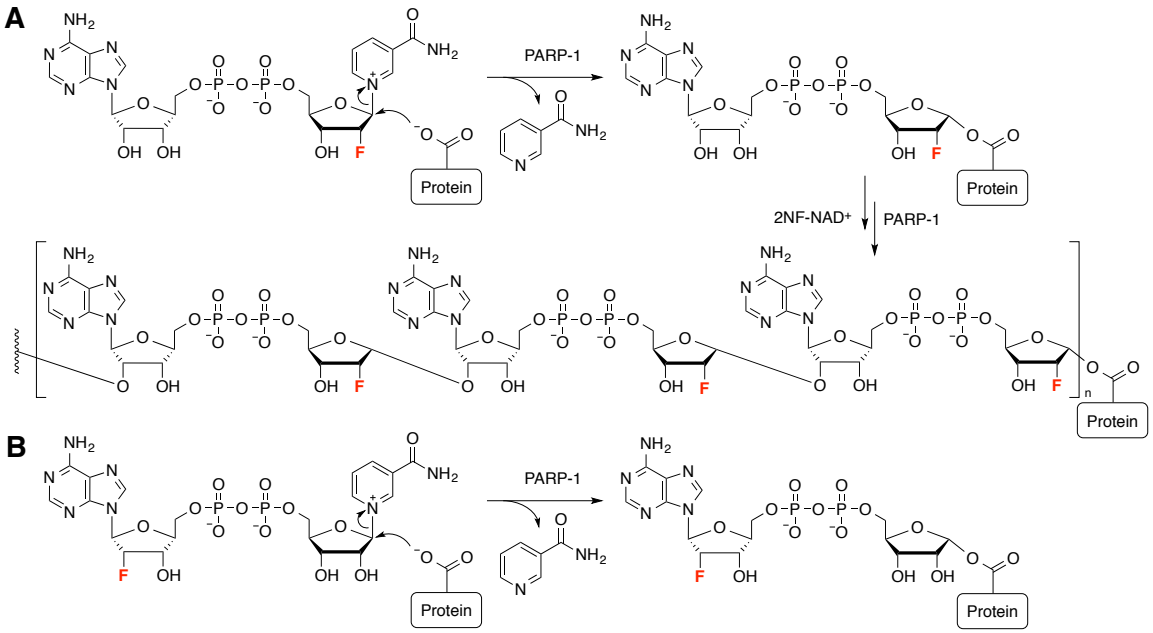

Figure 3-12. Expected outcomes of poly(ADP-ribosyl)ation of PARP-1 using fluorinated NAD^+ analogues as substrates. (A) Linear PAR polymers generated from the reaction of 2NF-NAD^+ with PARP-1. (B) Mono-ADP-ribosylation of PARP-1 by 2AF-NAD^+.

Since poly(ADP-ribosyl)ation is a protein posttranslational modification, it is not straightforward to isolate the enzymatic reaction products, which are heterogeneous PAR polymers. Instead, macromolecule-based methods were first chosen for the detection of protein-attached PAR polymers. PAR polymers can be visualized by Western blot analysis using anti-PAR antibody. Poly(ADP-ribosyl)ated proteins would have higher molecular weight than the unmodified ones. Moreover, the modified proteins would have different molecular weight dependent on the size of the polymers. Therefore, poly(ADP-ribosyl)ated protein species with different molecular weight could be resolved on an

SDS-PAGE gel, forming a smear as detected by sensitive protein stain such as SYPRO Ruby stain. In addition to staining, poly(ADP-ribosyl)ated proteins can be directly visualized by radioactivity-based imaging technique when using ^{32}P-NAD$^+$ as a substrate. All of the abovementioned methods were used to detect the formation of PAR polymers in the presence of fluorinated NAD$^+$ analogues.

2NF-NAD$^+$ was incubated with PARP-1 to see if PAR polymers can be produced. Western blot analysis as well as SYPRO Ruby stain indicated no PAR polymers were produced, as no signal was detected by anti-PAR immunoblot (Figure 3-5A), and the resulting PARP-1 protein maintained its original molecular weight (Figure 3-5B).

It is a discouraging finding that 2NF-NAD$^+$ could not be processed by PARP-1, but it may still be able to compete with NAD$^+$ and perturb native poly(ADP-ribosyl)ation, or it can be incorporated into the growing polymers once the initiation has been primed by natural NAD$^+$. To assess any potential effect of 2NF-NAD$^+$ on PARP-1 poly(ADP-ribosyl)ation, competition and pre-incubation experiments were set up. Increasing molar ratio of 2NF-NAD$^+$ to NAD$^+$ up to 20-fold or changing the amount of enzyme to facilitate the detection showed no significant effect on poly(ADP-ribosyl)ation (Figure 3-5), even with radioacitivity-based assay (Figure 3-6). Pre-incubation of 2NF-NAD$^+$ with PARP-1 also failed to hinder the formation of native PAR polymer chains (Figure 3-5C). These results ruled out the possibility of the covalent modification of the active site base Glu-988 by 2NF-NAD$^+$, which has been observed in the case of bovine CD38, an ADP-ribosyl cyclase (*281-284*).

Although no significant change of poly(ADP-ribosyl)ation of PARP-1 was observed using protein-based detection methods, direct analysis of the enzymatic reaction products was also carried out in order to unambiguously verify any possible incorporation of 2NF-NAD$^+$ into PAR polymers. To do so, PAR polymers produced using a mixture of

NAD^+ and 2NF-NAD^+ were purified and analyzed by a modified DNA sequencing PAGE method. By doping with radiolabeled NAD^+, PAR polymers can be directly visualized by phosphorimaging. The result, however, showed insignificant change of the polymer distribution pattern in the presence of 2NF-NAD^+, suggesting that polymer length or branching frequency was not altered by 2NF-NAD^+ (Figure 3-8).

To provide chemical evidence of the composition of PAR polymers in the presence of 2NF-NAD^+, polymers were again purified from large-scale *in vitro* PARP-1 automodification reaction, and further digested by PDE and AP, generating terminal, elongation, and branching unit which can be monitored by analytical HPLC. The result confirmed the production of PAR polymers in the presence of equimolar of NAD^+ and 2NF-NAD^+, but ESI-MS analysis of the isolated elongation unit only showed signals consistent with ribosyladenosine, the natural elongation unit (Figure 3-9). These results concluded that 2NF-NAD^+ cannot be processed by PARP-1, nor it can be incorporated into the growing polymer to modulate polymer pattern.

Despite the fact that 2NF-NAD^+ cannot be used in the elongation or branching step of poly(ADP-ribosyl)ation, one remaining possibility is that PARP-1 can be mono-ADP-ribosylated by 2NF-NAD^+, which means the initiation step is operating. To test this hypothesis, a novel HPLC-based assay suitable for the analysis of the initiation step of poly(ADP-ribosyl)ation reaction was developed. The rationale behind this assay is that mono-ADP-ribosylated proteins can be verified by producing adenosine from the ADP-ribose unit attached on the proteins. All other components present in the reaction mixture after removing the proteins were also subjected to HPLC analysis to capture any production of small molecules derived from the turnover of 2NF-NAD^+. Taking advantage of its mono-ADP-ribosylation activity, the PARP-1 mutant E988Q was also included as a positive control for the assay. Adenosine was detected for both PARP-1-

and E988Q-catalyzed reactions using NAD^+ as a substrate, confirming the assay was functional. A small peak eluted around the adenosine region was observed for both reactions using 2NF-NAD^+ as a substrate and negative controls (Figure 3-10A). Further analysis of the filtrate demonstrated that the adenosine should come from residual binding of NAD^+ to the filtering unit, and 2NF-NAD^+ remained intact after incubation with PARP-1 or E988Q, as opposed to NAD^+ which had been (partially) converted to ADP-ribose (Figure 3-10B). These results suggest that 2NF-NAD^+ is not a substrate for PARP-1-catalyzed poly(ADP-ribosyl)ation at all steps, i.e., initiation, elongation, and branching.

3.4.2 2NF-NAD^+ cannot serve as a redox cofactor for yeast alcohol dehydrogenase

To explore the competence of fluorinated NAD^+ analogues as redox cofactors, ethanol oxidation catalyzed by ADH from yeast was chosen as the model reaction. Despite the intact nicotinamide ring, 2NF-NAD^+ could not serve as a redox cofactor for yeast alcohol dehydrogenase (Figure 3-11). Modification of the nicotinamide ribose of NAD^+ has been demonstrated to affect both the redox potential of the pyridinium ring and the binding of the cofactor to the dehydrogenases (*285*). It is unclear to what aspect that the effect of fluorine substituent at the C2 position may have. However, the result is in accordance with the notion that perturbation of the microenvironment of the NMN moiety may have greater impact on the redox properties of NAD^+. Novel NAD^+ analogues with modifications at the AMP moiety have been successfully prepared and proved to be useful in engineering bioorthogonal redox systems (*286*).

3.4.3 2AF-NAD$^+$ has minor inhibitory effect on PARP-1 poly(ADP-ribosyl)ation

NAD$^+$ analogues with modification on the adenosine ribose have been explored only to the scope of deoxy-analogues in the past according to the literature. 2′-Deoxy-NAD$^+$ was not a substrate for PARP-1, whereas 3′-deoxy-NAD$^+$ only gave rise to mono-ADP-ribosylated or oligo-modified proteins (*247, 275, 276*). 2AF-NAD$^+$ has been synthesized in our laboratory, and here its effect on poly(ADP-ribosyl)ation was tested. In the presence of 2AF-NAD$^+$ alone, no PAR polymers were produced (Figure 3-7). However, a minor inhibitory effect on the formation of native PAR polymers was observed in the radioactivity-based experiment (Figure 3-8). The presence of 2AF-NAD$^+$ functioning as a polymer chain terminator could reduce the overall level of PAR polymers being produced. In addition, these results did not rule out the possibility that 2AF-NAD$^+$ can be processed by PARP-1 during the initiation step of poly(ADP-ribosyl)ation, generating mono-ADP-ribosylated proteins. Consistent with this hypothesis, a paper published recently reported the successful labeling of PARP-1 and histone H1.2 *in vitro* using clickable NAD$^+$ analogues bearing 2′-deoxy or 2′,3′-dideoxyadenosine moiety (*249*). Therefore, with further experiments to confirm the mono-ADP-ribosylation ability of 2AF-NAD$^+$, novel NAD$^+$ analogues can be designed in order to simplify the heterogeneous poly(ADP-ribosyl)ation reaction.

3.4.4 Mechanistic implication

The consequence of non-turnover of 2NF-NAD$^+$ by PARP-1 and the inhibitory effect of 2AF-NAD$^+$ limited the use of these fluorinated NAD$^+$ analogues in poly(ADP-ribosyl)ation reaction. Nonetheless, a mechanistic rationale can still be formulated based on the current experimental data. The substitution of fluorine for hydroxyl group at the C2 position of the nicotinamide ribose ring may have significant electron-withdrawing

effect, which in turn destabilizes the oxocarbenium intermediate, or increases the energy of the oxocarbenium-like transition state. The result is the inability of PARP-1 to break the nicotinamide–ribosyl bond of 2NF-NAD^+. Furthermore, fluorine substitution could disrupt the hydrogen bond stabilization effect provided by the catalytic glutamate residue. This may also decrease the binding affinity of this compound for PARP-1, but it is purely speculative at this point. Reduced binding affinity of 2NF-NAD^+ could explain the poor inhibitory effect of this compound in the presence of natural NAD^+, and the fact that the compound was not hydrolyzed by PARP-1 neither.

Significantly reduced rate of enzymatic hydrolysis of 2NF-NAD^+ has been observed for NAD^+-glycohydrolases (*270, 287*). The formation of an alkoxide-like hydroxyl group possessing partially anionic character was proposed to facilitate the reaction to proceed. Similar catalytic mechanism has also been proposed for the diphtheria toxin-catalyzed ADP-ribosylation diphthamide (*272*). The experimental data provided in this chapter are consistent with the mechanism that an oxocarbenium intermediate, or an oxocarbenium-like transition state is formed during the catalysis. Catalytic residue Glu-988 may provide necessary stabilization effect through hydrogen bonding to the 2′-hydroxyl group of the nicotinamide ribose. Both hydroxyl groups on the adenosine ribose ring are important for the elongation/branching step, as the reduced PAR polymer formation was observed herein and in the literature (*247, 249, 275*).

Chapter 4. Characterization of Poly(ADP-ribose)–Protein Linkages

4.1 INTRODUCTION

PARP-1 is known to be the major acceptor for poly(ADP ribosyl)ation, and the automodification sites were thought to be confined within domain D (Figure 1-11). The exact amino acid residues to which the PAR polymer is attached remain largely unknown owing to the difficulty in the characterization of such heterogeneous biopolymers. Previous group member Dr. Zhihua Tao had initiated an effort into the identification of automodification sites in PARP-1 by MS (*72*). Using the E988Q mutant which only catalyzes mono-ADP-ribosylation reaction, domain D protein construct was found to be the primary site for modification *in vitro* by the mutant enzyme. Tryptic digestion of the purified, mono-ADP-ribosylated protein followed by MS analysis revealed that Asp-387, Glu-488, and Glu-491 are the ADP-ribosylation sites. Unexpectedly, PARP-1 with domain D deleted is still catalytically active, and full length PARP-1 carrying point mutations of the aforementioned three residues can still undergo self-modification. These results suggest that there exist additional modification sites beyond domain D.

Recently, Hottiger *et al*. reported that PARP-1 bearing three lysine-to-arginine point mutations within domain D has a significantly reduced level of automodification. It was also found that additional mutations of eight glutamate to glutamine located between residues 484 to 557 in PARP-1 with deleted BRCT domain (which is a part of domain D) did not alter the automodification signal (*12*). Therefore they argued that lysine is the true acceptor for PAR polymers rather than glutamate or aspartate. In order to identify other potential automodification sites in PARP-1, and to verify that lysine can also be an acceptor for PAR polymer, MS techniques were adopted to locate the possible ADP-ribosylation sites in PARP-1 peptides and domains.

As described in this chapter, synthetic peptides containing previously reported automodification sites were not modified by PARP-1 or the E988Q mutant based on HPLC and MS analysis. These findings suggest that short peptides may not be able to compete with full-length protein as PARP-1 substrates. Direct MS analysis the *in vitro* automodification of PARP-1 confirmed that there are ADP-ribosylation sites present within domains A and B. Experiments to probe the chemical nature of poly(ADP-ribose)–protein linkage were also performed. For poly(ADP-ribosyl)ated proteins, the failure of detection of carbonyl groups derived from Amadori rearrangement of the ADP-ribose–lysine linkage suggests that lysine residues in domain D may not necessarily be the true modification sites. Instead, they may be important for catalysis in terms of maintaning the protein structure and/or binding with DNA.

4.2 MATERIALS AND METHODS

4.2.1 Cloning, expression, and purification of human PARP-1 fragments in *E. coli*

The gene encoding domain D of human PARP-1 (residues 374–525) was cloned into pET-28b(+) (Novagen) at the *Nde*I and *Hind*III restriction sites by Dr. Zhihua Tao (*72*). Protein expression and purification were carried out essentially the same as described in the original paper. A 10-mL overnight culture of *E. coli* Rosseta2 BL21(DE3) (Stratagene) transformed with D/pET-28b(+) was used to inoculate 1 L LB medium containing 50 μg/mL kanamycin. The cells were grown at 37 °C with shaking at 250 rpm until OD_{600} reached 0.6. Protein expression was then induced by the addition of IPTG to a final concentration of 0.2 mM, and the cells continued to grow for an additional 24 h at 18 °C with shaking at 125 rpm. Cells were harvested and re-suspended in lysis buffer containing 20 mM HEPES, 300 mM NaCl, 10 mM imidazole, and 10%

glycerol at pH 7.5. Sonication was used to disrupt cells. After removal of cell debris by centrifugation, the supernatant was incubated with pre-equilibrated Ni-NTA resin on a tube rotator at 4 °C for 1 h. The mixture was then loaded onto a column and washed with lysis buffer. The *N*-terminal His_6-tagged domain D was then eluted with elution buffer (lysis buffer with 250 mM imidazole). Fractions containing the desired protein were pooled and dialyzed against 3 × 1 L lysis buffer. Purified domain D was aliquoted, flash-frozen in liquid nitrogen, and stored at –80 °C.

DNA encoding domains A and B (AB) of human PARP-1 (residues 1–232) was cloned into the MalE-pET vector generated in house by Dr. Peng Gao at the *Nde*I and *Xho*I restriction sites. Construction of the MalE-pET vector was achieved by engineering a pET-24b(+) vector (Novagen) with an decahistidine MBP tag followed by a TEV cleavage site, similar to the pFastBac HT B/MBP-Tev vector (see Section 3.2.4). AB/MalE-pET was used to transform *E. coli* BL21 CodonPlus (DE3)-RP competent cells (Stratagene) for protein expression. Conditions for protein expression were the same as described for domain D. Harvested cells were re-suspended with lysis buffer containing 20 mM HEPES, 1 M NaCl, 10 mM imidazole, 1 mM β-mercaptoethanol, and 10% glycerol at pH 7.5. The remaining purification steps were similar to those described for MBP-tagged full-length PARP-1 (see Section 3.2.4).

4.2.2 ADP-ribosyl)ation of peptide substrates by the E988Q mutant

The reaction was performed according to the literature with some modifications (*72*). Briefly, a 50-μL reaction containing 2 μM E988Q, 1 mM synthetic peptides (Table 4-1, American Peptide Company), 100 μM or 1 mM NAD^+, 50 μg/mL calf thymus DNA or GGAATTCC 8-mer double-strand DNA, 250 μM DTT, 100 mM Tris-HCl, pH 8, and

10 mM $MgCl_2$ was incubated at 37 °C for 30 min. The reactions using PARP-1 as the enzyme were further treated with PARG before filtering out the proteins with YM-10 centrifugal unit (10-kDa cutoff). The filtrate was subject to C18 analytical HPLC analysis using 0.1% trifluoroacetic acid in water (TFA, solvent A) and 0.1% TFA in acetonitrile (solvent B) as mobile phase components. The flow rate was 1 mL/min and the elution was monitored by UV absorbance at both 214 nm and 260 nm. Samples were also directly submitted for MS analysis.

Peptide	Sequence	Molar Mass	m/z=+1	m/z=+2	m/z=+3
P1	A**D**^{387}KPLSNMK	1003.18	1003.50	502.27	335.18
P2	KA**E**^{488}PV**E**^{491}VVAPR	1194.39	1194.68	597.85	398.90
PK1	G**K**^{498}SGAALS**K**^{505}KS**K**^{508}	1161.40	1161.70	581.35	387.90
PK2	SE**K**^{521}RM**K**^{524}LTLK	1233.60	1233.73	617.37	411.92

Table 4-1. Peptides used in the PARP-1 heteromodification reactions. Amino acid residues that are possible modification sites are underlined and in boldface; numbers represent the corresponding amino acid residue number of human PARP-1.

4.2.3 Poly(ADP-ribosyl)ation of PARP-1 and PARP-1 domains

PARP-1 domains AB or D (10 μM) were poly(ADP-ribosyl)ated by 1 μM PARP-1 in the presence of 100 μM NAD^+, 10 μg/mL GGAATTCC 8-mer double-strand DNA, 250 μM DTT, 100 mM Tris-HCl, pH 8, and 10 mM $MgCl_2$ at 37 °C for 90 min. Under specific conditions, enzyme and substrate concentration will be stated otherwise. For MS analysis, the reactions were treated with PARG for an additional 1 h before sample cleaning. Automodification of PARP-1 followed by PARG treatment was also conducted for the same analysis.

4.2.4 MS analysis of ADP-ribosylated peptides or proteins

Protein disulfide bonds were reduced by incubation with equimolar amounts of DTT followed by alkylation with iodoacetamide at room temperature. Trypsin digestion was carried out at a 20:1 (w/w) ratio of protein to enzyme (Promega) at 37 °C overnight. The digest sample was then cleaned using a C18 spin column (Pierce) prior to nano LC-MS/MS analysis.

Samples were analyzed using an Orbitrap Elite dual-pressure linear ion trap mass spectrometer (Thermo Scientific) equipped with a Dionex UltiMate 3000 RSLCnano LC system (Thermo Scientific). Tryptic peptides of the protein digest were separated using an in-house C18 packed nanotip column (New Objective) at a 0.3 μL/min flow rate. The following mobile phases were used: LC-grade water with 0.1% formic acid (solvent A) and LC-grade acetonitrile with 0.1% formic acid (solvent B). After injection of 1 μg of total protein onto the column, mobile phases were applied using a 60-min linear gradient from 3% to 40% B, followed by a 10-min increase to 90% B. CID (collision-induced dissociation) spectra were acquired using an isolation width of 2 Da and a *q* value of 0.25 during a 10 ms activation period (35% normalized collision energy, NCE). Data was analyzed using Mass Matrix to determine the sequence coverage of proteins. The peptide/protein MS experiments were performed by Julia Aponte, a graduate student in Dr. Jennifer Brodbelt's laboratory in the Department of Chemistry, UT-Austin.

4.2.5 Analysis of poly(ADP-ribose)–histone H1 chemical linkage

To analyze the chemical nature of poly(ADP-ribose)–H1 linkage, H1 (20 μM, Calbiochem) was first poly(ADP-ribosyl)ated by PARP-1 (0.5 μM) in the presence of either 0.2 mM or 1 mM NAD^+ and PARP-1 reaction buffer (50 μg/mL GGAATTCC 8-mer double-strand DNA, 250 μM DTT, 100 mM Tris-HCl, pH 8, and 10 mM $MgCl_2$), at

37 °C for 15 min. The reactions mixtures were divided into four sets for 1-h further treatment with water, PARG, 0.9 M NH_2OH, pH 7, and 0.45 M KOH/45 mM EDTA, respectively. For the NH_2OH and KOH/EDTA treatment sets, proteins were concentrated by YM-10 filtering unit. The samples were resolved by SDS-PAGE and probed with anti-PAR monoclonal antibody (Trevigen).

4.2.6 Model studies of peptide glycation by ADP-ribose

Peptides PK1 or PK2 (1 mM) were incubated with 1 mM ADP-ribose in 50 mM potassium phosphate buffer (pH 7.5) at 37 °C for 1 h. The reactions were analyzed by C18 HPLC according to the method described in Section 4.2.2.

4.2.7 Model studies of protein glycation by ADP-ribose

BSA and histone H1 were used as model substrates for protein glycation by ADP-ribose. The reactions were carried out according to the literature with some modifications (*288*). Briefly, BSA (1.5 mg/mL, Thermo Scientific) or H1 (1.0 mg/mL) was incubated with 1 mM ADP-ribose in 50 mM potassium phosphate buffer (pH 7.5) at 37 °C for either 1 d or 7 d in dark. The samples were further reacted with solution containing 5 mM 2,4-dinitrophenylhydrazine (DNP) in 10% TFA, 2 M Tris-HCl, and 30% glycerol at room temperature for 1 h. Proteins were resolved by SDS-PAGE, stained with Coomassie Blue or probed with anti-DNP antibody (Novex).

4.2.8 Detection of protein carbonylation by DNP derivatization

Both the protein glycation reactions (Section 4.2.7) and poly(ADP-ribosyl)ation reactions of PARP-1 and domain D were analyzed for protein carbonylation. Glycation of

BSA or H1 was carried out as described in Section 4.2.7. Poly(ADP-ribosyl)ation of 50 μM domain D using 5 μM PARP-1, or automodification of 10 μM PARP-1 was performed following similar procedures described in Section 4.2.3, with additional PARG treatment. Derivatization of protein carbonyl groups with DNP was carried out as described in Section 4.2.7. Proteins were analyzed by analytical HPLC equipped with a 300 × 7.8 mm Bio-Sil SEC 125-5 gel filtration column (Bio-Rad) with isocratic elution using 200 mM sodium phosphate buffer, pH 6.5. The flow rate was 1 mL/min and the elution was monitored by UV absorbance at both 280 nm and 360 nm.

4.3 RESULTS

4.3.1 No modification of peptides substrates by the E988Q mutant

To verify that Asp-387, Glu-488, and Glu-491 are the automodification sites of PARP-1 as reported by Dr. Zhihua Tao (*72*) and other potential lysine automodification sites, synthetic peptides bearing these residues were used as substrates in ADP-ribosylation reactions catalyzed by the E988Q mutant which only generated mono-ADP-ribosylated species. The reactions were analyzed by HPLC at UV absorbance of 214 nm and 260 nm for peptide bonds and ADP-ribose, respectively. As shown in Figure 4-1, no change was observed for all four peptides under 214 nm absorbance, and no new peak appeared under 260 nm absorbance. The concentration of NAD^+ of the reactions was raised from 100 μM to 1 mM to see if it may increase the yield of modified peptides. No new peak was produced in the presence of the enzyme, except for P2 (Figure 4-2A and B, trace c, arrow). However, the low abundance of the peak prevented further characterization. Based on HPLC chromatograms, short peptides seem to be poor substrates and could not be modified by the E988Q mutant.

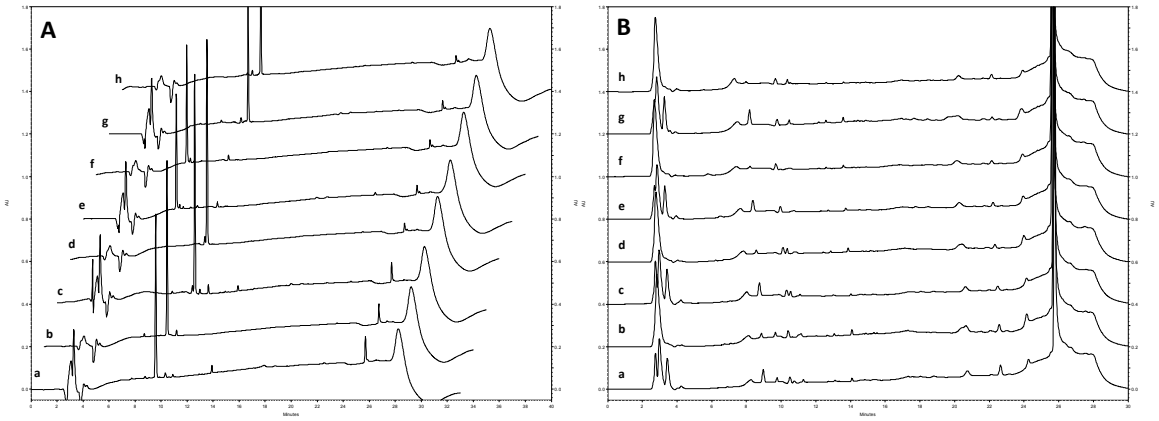

Figure 4-1. HPLC chromatograms of poly(ADP-ribosyl)ation reaction of synthetic peptides by the E988Q mutant using 100 μM NAD^+. The elution was monitored at (A) 214 nm and (B) 260 nm. (a) P1+E988Q (b) P1. (c) P2+E988Q. (d) P2. (e) PK1+E988Q. (f) PK1. (g) PK2+E988Q. (h) PK2.

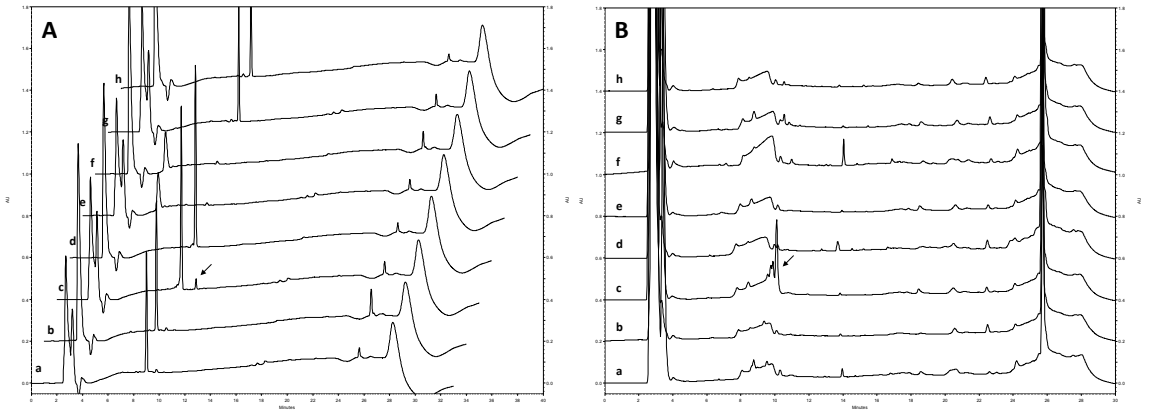

Figure 4-2. HPLC chromatograms of poly(ADP-ribosyl)ation reaction of synthetic peptides by the E988Q mutant using 1 mM NAD^+. The elution was monitored at (A) 214 nm and (B) 260 nm. (a) P1+E988Q (b) P1. (c) P2+E988Q. (d) P2. (e) PK1+E988Q. (f) PK1. (g) PK2+E988Q. (h) PK2.

The same reactions were subject to MS analysis to capture any modified peptides in solution. Samples were either separated by passing through a LC column or directly injected into ESI-MS instrument. Disappointedly, none of the samples showed MS

signals corresponding to the modified peptide, even for the P2 reaction (Figure 4-3). These results suggest that short synthetic peptides may not be suitable substrates for the E988Q mutant.

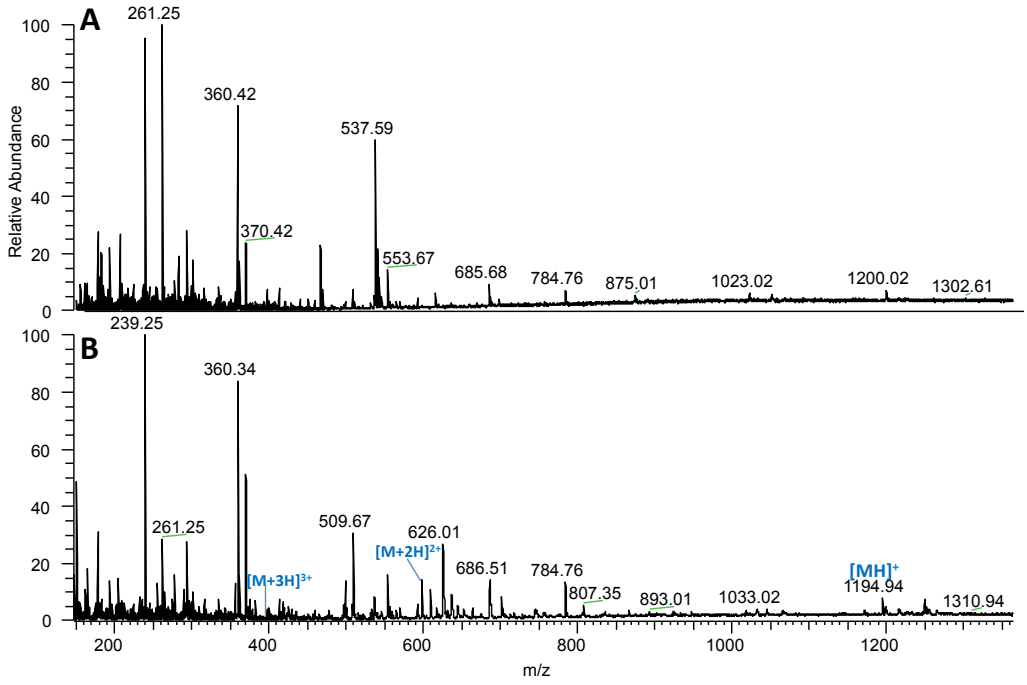

Figure 4-3. ESI-MS spectra of directly infused samples containing (A) P2+E988Q and (B) P2. The observed m/z values of different charge states of P2 are labeled. The calculated values can be found in Table 4-1.

4.3.2 MS analysis of poly(ADP-ribosyl)ated PARP-1 constructs

Since synthetic peptides were not modified by the PARP-1 E988Q mutant, MS analysis of poly(ADP-ribosyl)ated proteins was conducted to directly locate the automodification sites. Both automodification of PARP-1 and heteromodification of PARP-1 domains AB and D were carried out *in vitro*. The reaction mixtures were treated

with PARG to afford mono-ADP-ribosylated species before trypsin digestion. Tryptic digest was cleaned up by C18 spin column and subject to LC-MS analysis. The sequence coverage of the full-length PARP-1 was 70%, but peptides having ADP-ribose attached ($\Delta m/z = 541$) were poorly fragmented (Figure 4-4). This complicates the assignment of ADP-ribosylation sites to specific amino acid residue. Domains AB and D modified *in trans* also had decent sequence coverage, but similar problems existed for both constructs. Nonetheless, several modification sites could be found in these domains, suggesting that domain D is not the sole automodification center (Table 4-2).

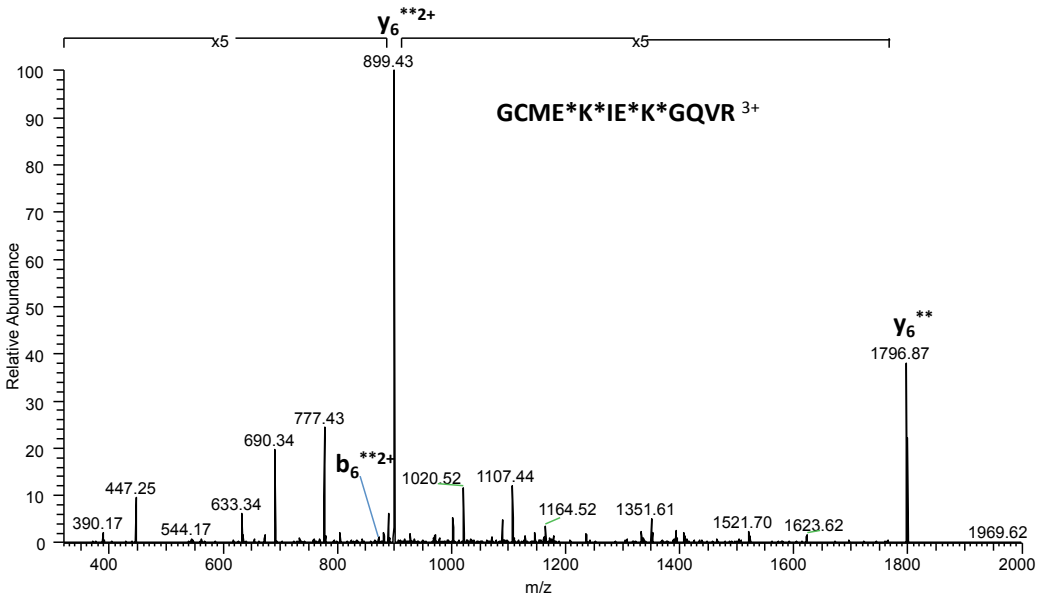

Figure 4-4. CID MS/MS spectra of a modified peptide derived from poly(ADP-ribosyl)ated PARP-1 tryptic digest. m/z values of fragmented ions are indicated. b ion is the *N*-terminal part of the molecule cleaved at the peptide bond, and y ion is the complementary *C*-terminal portion. Asterisks denote potential ADP-ribosylation sites.

Peptide	Modified residue	Domain
MAIMVQSPMFDG**K***	K47	A
KTAEAGGVTG**K***	K97	A
GQDGIGSKAE**K***	K108	A
TLGDFAA**E***YAKSNR	E116	A
TLGDFAAEYA**K***SNR	K119	A
GCM**E*****K***I**E*****K***GQVR	E130, K131, E133, K134	A
GQVRLSK**K***	K144	A
QLPGVKS**E***G**K***	E205, K207	B
RKGDEVDGVDEVA**K***	K221	B
A**E***PV**E***VVAPR	E488, E491	D

Table 4-2. Peptide ions bearing potential PARP-1 automodification sites identified by CID-MS/MS. Modification sites are labeled with asterisks, underlined and boldfaced.

4.3.3 Chemical nature of poly(ADP-ribose)–H1 linkage

Probing the chemical nature of poly(ADP-ribose)–protein linkage could potentially shed light on the type of amino acid residues to which PAR polymer is attached. PARP-1 and histone H1 were first poly(ADP-ribosyl)ated *in vitro* and the resulting poly(ADP-ribosyl)ated species were subject to different types of treatment. PARG cleaves the PAR polymers from the proteins, leaving one ADP-ribose attached. Neutral hydroxylamine could only cleave ester bond, but not Schiff base or hemiaminal, whereas strong base could cleave both types of linkage. The samples were resolved by SDS-PAGE and visualized by either Coomassie stain or anti-PAR immunoblotting.

As shown in Figure 4-5A, poly(ADP-ribosyl)ation of 113-kDa PARP-1 or 30-kDa H1 created a smear of proteins, and the PAR signal became stronger in the presence of H1 (lane 2) and higher NAD^+ concentration (lane 3). The protein band of PARP-1 shifted toward the gel interface (Figure 4-5B, land 1–3), and the smear of H1 was visible at 1

mM NAD^+ (lane 3), consistent with the trend revealed by anti-PAR immunoblotting. PARG treatment almost completely eliminated the PAR signals (Figure 4-5A, lane 4–6), and protein bands of PARP-1 and H1 shifted back to the unmodified molecular weight (Figure 4-5B, lane 4–6). Neutral hydroxylamine treatment partially reduced the PAR signals from PARP-1, and the H1 bands became visible (Figure 4-5A, lane 7–9). Samples treated with strong base, however, displayed far less PAR signals as compared to hydroxylamine treatment (Figure 4-5A, lane 10–12). The data suggest that there are at least two types of chemical linkage existing between the PAR polymer and the protein. One of them could be an ester linkage, which is sensitive to both hydroxylamine and base treatment. Another could be a Schiff base or hemiaminal linkage involving reactive amines and the reducing end of ADP-ribose. This is also in line with early observations that in addition to Glu and Asp, lysine residues could be the acceptors for PAR polymers.

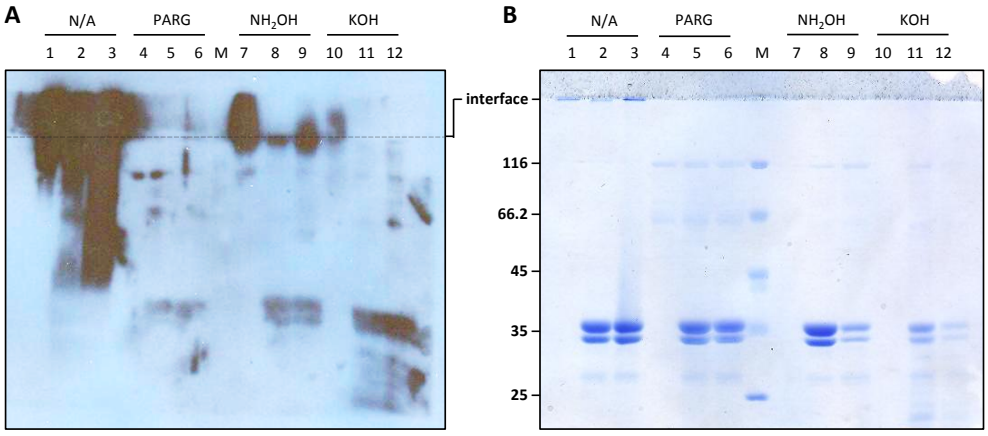

Figure 4-5. Analysis of poly(ADP-ribosyl)ated PARP-1 and H1 by enzymatic or chemical treatment. (A) Anti-PAR Western blot. (B) Coomassie stain. Lanes 1, 4, 7, and 10, 0.5 μM PARP-1+1 mM NAD^+; lanes 2, 5, 8, and 11, 0.5 μM PARP-1+20 μM H1+0.2 mM NAD^+; lanes 3, 6, 9, and 12, 0.5 μM PARP-1+20 μM H1+1 mM NAD^+. Specific treatment is indicated above the lanes.

4.3.4 ADP-ribose glycated proteins, but not poly(ADP-ribosyl)ated ones, contain protein carbonyl groups

The observation of PAR–protein linkage other than ester bond raises the possibility that lysine could also serve as the acceptor for PAR polymers. To verify the chemical nature of lysine-linked ADP-ribose, model studies of ADP-ribose–protein conjugates were carried out using peptides containing reported lysine automodification sites of PARP-1. Peptides incubated with equimolar of ADP-ribose at 37°C for 1 h did not give any newly modified products as detected by HPLC (Figure 4-6). The result could be interpreted as either the non-reactivity of these peptides toward ADP-ribose, or that the reaction proceeded too slowly to be detected within one hour's incubation.

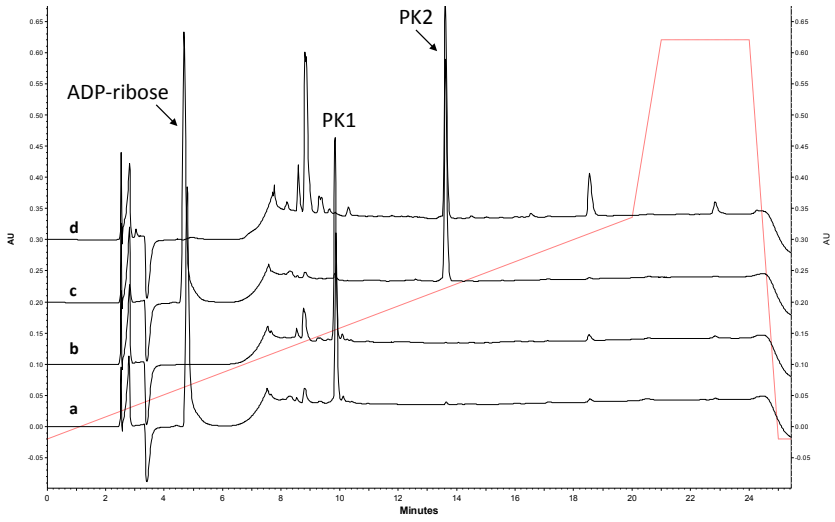

Figure 4-6. HPLC chromatograms of nonenzymatic ADP-ribose glycation reactions of model peptides monitored at 214 nm. (a) PK1. (b) PK1+ADP-ribose. (c) PK2. (d) PK2+ADP-ribose.

Protein substrates BSA and H1 were also utilized in the model study of nonenzymatic ADP-ribose conjugation reaction (*289*). BSA or H1 was incubated with 50-fold molar excess of ADP-ribose at °C in dark for either 1 day or 7 days. The reaction

mixtures were then derivatized with DNP to capture protein carbonyl groups resulting from the potential Amadori rearrangement product from the proximal ADP-ribose–lysine linkage (see Figure 4-10). For comparison, automodification of PARP-1 and heteromodification of domain D were also conducted to enzymatically generate PAR–protein linkages. The poly(ADP-ribosyl)ated proteins were subject to the same derivatization procedure to label enzymatic reaction-generated protein carbonyl groups. The DNP-labeled proteins were subsequently probed with anti-DNP antibody.

The SDS-PAGE of the resulting protein samples are shown in Figure 4-7. As expected, PARP-1 and domain D (~16 kDa) had smear band shifted upward from the unmodified protein bands (lane 1, 2). BSA, on the other hand, also had tailing bands below its original molecular weight (66 kDa) (lane 3, 4). The tailing effect could be due to prolonged incubation time, causing proteins to degrade. Similar observation can be seen for H1 (lane 5, 6). When probing the DNP-labeled protein samples, none of them showed ECL signal (data not shown). Changing the antibody concentration and adjusting the derivatization procedures did not improve the situation. It is therefore possible that either the derivatization reaction did not work, or the anti-DNP antibody is not suitable for Western Blot detection.

To ensure that the DNP derivatization reaction works as expected, and to detect protein carbonyl groups more directly, the DNP-labeled proteins from the above experiments were analyzed by HPLC equipped with a protein gel filtration column. By monitoring the elution profile at both 280 nm and 360 nm, overlapping peaks would indicate DNP-labeled protein species. Figure 4-8 shows the gel filtration elution profiles of the protein samples. Each entry (a or a′) consists of two traces, with the one having more peaks between 5 and 12.5 min being monitored at 360 nm, and the other one monitored at 280 nm. Each pair of entries (a and a′) are samples generated under the

same reaction condition (enzymatic or nonenzymatic) as designated in the figure legend. Entries with "prime" symbols are samples derivatized with DNP, whereas the plain alphabets represent controls without derivatization. From entries c′, d′, e′ and f′, it is evident that a peak around 11 min showed up in both 360 nm (DNP absorption) and 280 nm (protein) traces (arrows in the light green area), and the peak was absent in the control samples without derivatization (entry c, d, e and f). The retention time of the peak is consistent with BSA or H1. This result clearly illustrates the existence of carbonyl groups on the ADP-ribose glycated proteins, and the DNP derivatization protocol is functional. On the contrary, enzymatic poly(ADP-ribosyl)ated PARP-1 and/or domain D did not display any noticeable overlapping peaks from both 360 nm and 280 nm absorption traces (entry a′ and b′). Therefore, the data suggest that enzymatic protein poly(ADP-ribosyl)ation within one hour may not necessarily occur on the lysine residues, or the abundance was too low to be detected using DNP derivatization protocol.

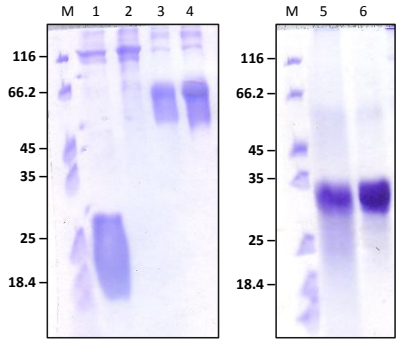

Figure 4-7. SDS-PAGE gel of enzymatically poly(ADP-ribosyl)ated proteins and nonenzymatic ADP-ribose glycation of proteins. Lane 1, 5 μM PARP-1+50 μM domain D+0.5 mM NAD^+; lane 2, 10 μM PARP-1+0.5 mM NAD^+; lane 3, BSA+ADP-ribose, 1 d; lane 4, BSA+ADP-ribose, 7 d; lane 5, H1+ADP-ribose, 7 d; lane 6, H1+ADP-ribose, 1 d. M, molecular weight marker.

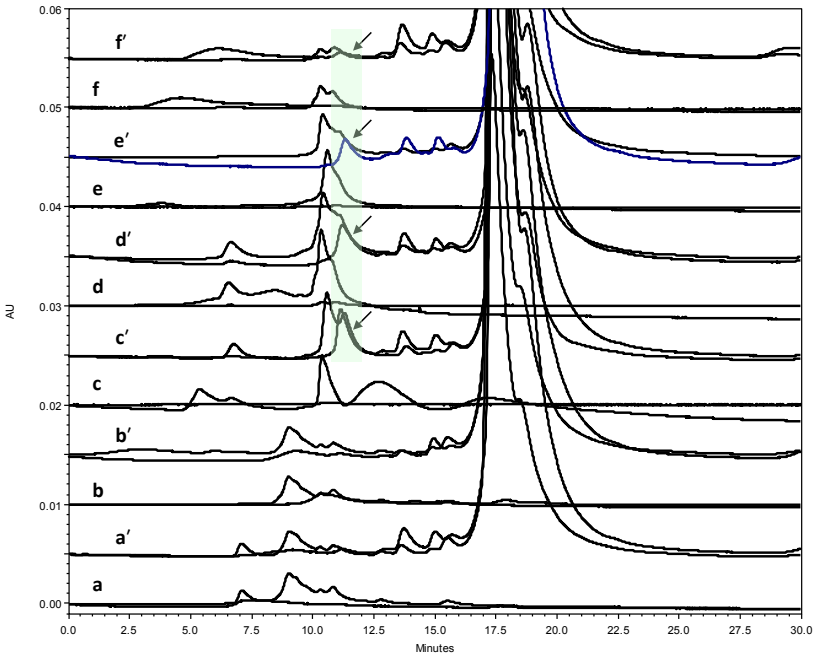

Figure 4-8. HPLC chromatograms of DNP-labeled protein species from enzymatic poly(ADP-ribosyl)ation or nonenzymatic ADP-ribose glycation reactions. For each entry, traces with more obvious peaks between 5 to 12.5 min were monitored at 280 nm. Arrows in the light green highlighted area indicate overlapping peaks from both 280 nm and 360 nm absorbance. Traces with "prime" symbols represent samples undergone DNP derivatization, whereas unlabeled alphabets represent controls. (a) and (a′), PARP-1+D+NAD^+. (b) and (b′), PARP-1+NAD^+. (c) and (c′), BSA+ADP-ribose, 1 d. (d) and (d′), BSA+ADP-ribose, 7 d. (e) and (e′), H1+ADP-ribose, 1 d. (f) and (f′), H1+ADP-ribose, 7 d.

4.4 DISCUSSION

4.4.1 Synthetic peptides are not PARP-1 substrates

Defining the amino acid residues undergone posttranslational modification is of great importance to study the biological consequence of such molecular transformation. Surprisingly, the exact locations of the automodification sites of PARP-1, a pivotal nuclear protein involved in DNA repair and other cellular processes, remain largely

unknown. This challenging problem can be attributed to several biochemical properties unique to PARP-1. One example is the lack of defined amino acid residue or sequence consensus in the modification motif. This is distinctly different from other types of posttranslational modification such as phosphorylation, methylation, acetylation, ubiquitylation…etc. In addition, the resulting PAR polymer is heterogeneous in terms of size and structure, making structural characterization a daunting task. The negatively-charged chemical nature of PAR polymer also complicates the analysis including MS. The facts that the large 113-kDa enzyme itself is the predominant acceptor of such modification, and the reaction is allosterically triggered by the presence of DNA, add another layer of complexity toward reconstitution of the reaction *in vitro*. Our previous group member, Dr. Zhihua Tao, had put substantial effort into the characterization of the automodification sites of PARP-1. The E988Q mutant of PARP-1, which only catalyzes mono-ADP-ribosylation reaction, was cleverly used to simplify the heterogeneous nature of PAR polymers. The data revealed that three amino acid residues, Asp-387, Glu-488, and Glu-491, located within domain D, are the primary modification sites by tandem MS analysis (*72*). PARP-1 with domain D deleted (ABCEF) was found to undergo automodifications as well, suggesting that ADP-ribosylation sites exist beyond domain D (*72*). To further verify these modification sites, synthetic peptides carrying these residues were used as substrates to test whether they can be poly(ADP-ribosyl)ated *in trans*. Without purification of the peptides, the MS spectra of the reaction mixture indeed showed ion patterns consistent with ADP-ribose attached onto these amino acid residues (*72*).

In light of a recent report that, rather than glutamate or aspartate residues (*12*), Lys-498, Lys-521, and Lys-524 are the true automodification sites of PARP-1, synthetic peptides carrying these lysine residues were prepared and subject to similar reaction

condition as reported by Dr. Zhihua Tao. The reaction mixture was analyzed by HPLC in an attempt to detect modified species more definitely. MS analysis of ADP-ribosylated peptide can also provide information regarding the fragmentation patterns or characteristic ions of such posttranslational modifications.

To our surprise, no modification reactions were observed for these peptide substrates, including the ones used in the previous publication (Figure 4-1 and 4-2). Direct infusion of the reaction mixtures into ESI-MS instrument did not show any signs of modification, neither (Figure 4-3). These results were perplexing at the first glance. But, it is possible that the modified peptide ions reported previously were actually derived from the enzyme E988Q itself rather than the peptide used in the reaction. Even under 500-fold molar excess of peptide to protein, with high concentrations of NAD^+, no modification of peptides was observed. Another explanation could be that the LC program or the ESI-MS analysis is affecting the stability of such modification. Similar reactions were then analyzed by HPLC using 0.1% ammonium acetate as the main component of the mobile phase instead of 0.1% TFA, but no modified peptides was observed neither (data not shown). For MS analysis, the reaction mixtures after work-up were subject to LC separation before ionization or directly injected into the instrument. Neither of them gave ion signals corresponding to modified peptides. Therefore, it is concluded that short peptides (ca. 10-15 amino acids long) may not be efficient substrates for PARP-1 heteromodification. Direct analysis of poly(ADP-ribosyl)ated protein mixtures generated *in vitro* or *in vivo*, or using chemically synthesized ADP-ribosylated peptides (*290, 291*) should be considered for future characterization of this posttranslational modification.

4.4.2 Automodification sites of PARP-1 exist beyond domain D

To circumvent the issue that short peptides are not modified by PARP-1, PARP-1 domains and the protein itself were poly(ADP-ribosyl)ated, treated with PARG, and then subject to MS analysis. Traditional CID fragmentation method, despite having the potential to cause degradation of posttranslational modifications, can still provide useful information of the possible automodification sites. In fact, several lysine and glutamate residues beyond domain D were identified to be acceptors, although the exact location of modification still needs further verification in some cases (Figure 4-4 and Table 4-2).

In order to successfully assign posttranslational modification to a specific amino acid residue by MS data, one should pay attention to sample preparation and the selection of the MS instrumentation. During the course of current studies, multiple laboratories also reported their work on the characterization of poly(ADP-ribosyl)ated proteome. Specific advancement of the reports will be discussed in the following paragraphs along with the comparison of the data presented herein.

A well-defined m/z difference between the modified and unmodified ion is crucial for the analytic software to detect and identify the targeted modification. For poly(ADP-ribosyl)ation, the strategy applied herein is to either use the E988Q mutant, which only catalyzes mono-ADP-ribosylation reaction, or digest the poly(ADP-ribosyl)ated species with PARG to get rid of the PAR polymers, leaving the proximal ADP-ribose attached to the protein. Either way would produce a modified protein (peptide) with a defined m/z difference, which is 541 Da for one ADP-ribose moiety.

Quantity of the modified species may affect the quality of MS data. Low abundance of modified proteins/peptides may lead to overlook of the signals exerted from the modified species. Enrichment protocol to concentrate only the proteins carrying modifications could enhance the signal readouts. For poly(ADP-ribosyl)ated species,

boronate resin had been demonstrated to be useful for the purification of PAR polymers (*64*). Similar protocol was thus applied here to enrich the poly(ADP-ribosyl)ated domains AB or D after *in vitro* reaction. Unfortunately, the MS results did not show significant improvement (data not shown). It is perhaps that the heteromodification reaction did not generate significant amount of modified domains AB or D so the enhancement after enrichment was only marginal. Some enrichment protocols used in the characterization of phosphoproteome had been proved useful to enrich poly(ADP-ribosyl)ated proteins after incubating with phosphodiesterase (*73, 194*). A recent publication described a novel strategy to characterize poly(ADP-ribosyl)ation proteome by combining the two methods mentioned above (*195*). Namely, modified proteins were first enriched by boronate resin column followed by elution of the proteins with hydroxylamine. Instead of using water, the researchers took advantage of the chemical sensitivity of Glu- or Asp-linked PAR polymers toward neutral hydroxylamine so that PAR-modified proteins eluted with hydroxylamine would produce a 15 Da m/z difference for each modification site distinguishable by MS. This process also reduced the heterogeneous PAR polymers into one defined chemical modification (hydroxamic acid derivatives of Glu- or Asp- residues bearing PAR polymers.) This method, being useful to identify ester linkages, is nonetheless unable to detect modifications of lysine-linked or other ADP-ribose–protein linkages.

With a properly processed protein or peptide sample in hand, the fragmentation method employed by different MS instruments should also be considered. CID is the most common and universal method to generate fragmented ions. However, the high collision energy may cause some unstable modifications to be cleaved from the peptide. Moreover, the modification itself bearing an unstable chemical linkage (e.g., phosphodiester bond in the case of poly(ADP-ribose)) may be prone to degradation by

constant collisions with gas molecules. Other fragmentation methods such as electron transfer dissociation (ETD) (*13, 292*) have been suggested for the characterization of ADP-ribosylated peptides owing to their mild ionization process, but fewer peptide backbone fragmentation may occur, hampering the detailed sequence analysis of the tandem MS spectra. Instead of analyzing protease-digested peptides, an alternative is to adopt top-down MS analysis. Ultraviolet photodissociation (UVPD) (*293*) is an emerging MS technique to directly obtain sequence information from the whole protein without protease digestion. Due to the strong yet quick photon bombardment, this method could generate a more complete peptide backbone fragmentation pattern while preserving labile posttranslational modification at the same time. UVPD has been employed in the characterization of a protein tyrosine sulfotransferase (*294*). The feasibility of this novel MS technique was tested using poly(ADP-ribosyl)ated domain D (~16 kDa), but the results were inconclusive (data not shown). The application of UVPD in the characterization of the overall protein structure will be presented in chapter 5.

Figure 4-9 summerizes the automodification sites identified in the current literature as well as in this study. Glu and Asp are the predominant residues being modified, and the automodification sites widespread throughout the entire protein, clustering at flexible the loop regions based on structural mapping (*194, 195*). Lysine residues and one arginine residue have been identified as the modification sites from *in vitro* reactions (*73*). Whether this is physiological relevant must await further examination. Due to the wide distribution of the automodification sites, identification of the modification "hot spot" or patterns under specific condition would be important to better correlate the respective physiological outcomes. Indeed, Poirier *et al*. found that the interdomain region connecting the BRCT domain and the WGR domain is the hot spot of automodification (*295*), consistent with the fact that it is in proximity to the active

site displayed in the near full-length PARP-1 crystal structure (*200*). Of note, Lys-498 was found to be the acceptor site by MS in one report (*73*).

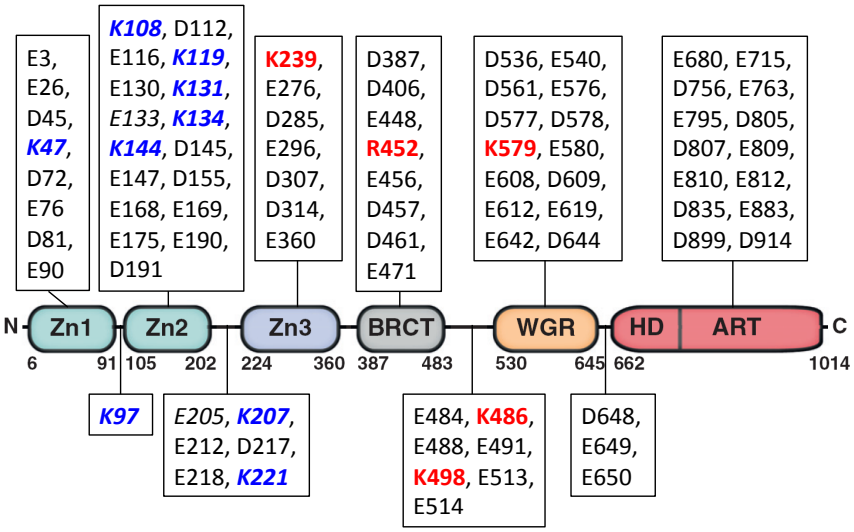

Figure 4-9. Automodification sites of PARP-1 identified by MS experiments to date (*72*, *73*, *112*, *194*, *195*, *295*). The location of each modification site is grouped according to PARP-1's domain organization. Lysine or arginine residues reported in the literature are in red and boldfaced; lysine residues reported in this chapter are in blue and italic; glutamate residue reported in this chapter is in italic.

4.4.3 Poly(ADP-ribose)–protein linkages exist in two types of chemical bonds

Identification of the automodification sites of PARP-1 is always associated with the quest of knowing what the chemical nature of PAR–protein linkage is. Before the advancement of analytical instrumentation, chemical treatment is the standard way to gain structural information of biological samples. Hydroxylamine has been used to distinguish ADP-ribose–protein linkages in the early 80s (*296*). Current data shown in

Figure 4-5 suggest that there are two types of linkages present in the enzyme-catalyzed poly(ADP-ribosyl)ation reactions. One is hydroxylamine-labile, and the other one is hydroxylamine-resistant (Figure 4-10). The hydroxylamine-labile linkage is consistent with the nucleophilic attack of neutral hydroxylamine to the ribose–protein linkage (Figure 4-10A). The hydroxylamine-resistant linkage is most likely a non-ester bond formed between a protein nucleophile and the nicotinamide ribose of NAD^+ (Figure 4-10B). Lysine, arginine, and cysteine are all possible amino acid candidates involved in such linkage.

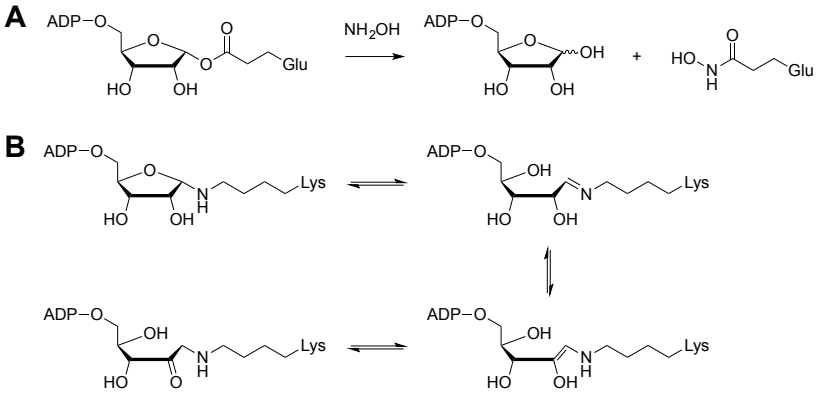

Figure 4-10. Chemical structures of possible ADP-ribose–protein linkages found in poly(ADP-ribosyl)ated PARP-1. (A) Glu-linked ADP-ribose represents an ester bond linkage. Hydroxylamine treatment gives free ADP-ribose and hydroxamic acid derivative of Glu. (B) Lys-linked ADP-ribose undergoes Amadori rearrangement to generate a 2-ketoamine species.

In the case of lysine–ADP-ribose linkage, tautomerization of the hemiaminal could lead to the production of 2-ketoamine, an Amadori rearrangement product. If poly(ADP-ribosyl)ation of lysine residues does take place, a reactive carbonyl group may present on the protein as a result of tautomerization. Such rearrangement has been characterized in detail for ADP-ribose-mediated protein glycation reaction (*297*).

Labeling the carbonyl group with a specific small molecule such as DNP could detect protein carbonylation derived from poly(ADP-ribosyl)ation of lysine.

Model reactions of ADP-ribose glycated peptides or proteins were produced to serve as a positive control for the detection of protein carbonylation derived from ADP-ribose-mediated glycation. Unfortunately, peptides containing reported PARP-1 lysine modification sites did not react with ADP-ribose under current experimental condition (Figure 4-6). Glycation of several other proteins and the derivatization with DNP seemed to work (Figure 4-7), but the detection of protein carbonylation using anti-DNP antibody did not show any signal. Alternatively, the glycated and DNP-derivatized proteins were directly analyzed by gel filtration HPLC, and the overlapping peak from the trace of both 360 nm and 280 nm absorbance strongly suggested the existence of carbonyl groups in ADP-ribose-glycated BSA and H1 (Figure 4-8, entry c′, d′, e′, and f′). However, enzymatically poly(ADP-ribosyl)ated PARP-1 and domain D did not show any significant protein species bearing absorbance at 360 nm (Figure 4-8, entry a′ and b′). The low abundance of ADP-ribosylated lysine and the low occurrence of such modification underwent Amadori rearrangement all possibly contributed to the current observation.

4.4.4 Interpretation of enzyme-catalyzed poly(ADP-ribosyl)ation of lysine residues

Considering the data presented in this chapter together with the MS results reported in the literature, it is still difficult to draw a conclusion that PARP-1-catalyzed protein poly(ADP-ribosyl)ation can indeed take place on lysine residues. Mutagenesis of Lys-498, Lys-521, and Lys-524 to arginine abolishing modification does not necessarily imply these lysine residues are the true automodification sites. Instead, these residues could play important structural roles during catalysis, such as facilitating conformational

change or maintaining overall DNA binding affinity (*199*). Advanced MS techniques should be able to provide more definitive evidence to support the chemical nature of ADP-ribose–lysine linkage, but how to optimize experimental conditions to generate poly(ADP-ribosyl)ated proteins, both *in vitro* and *in vivo*, could be the key to resolve this problem.

For *in vitro* reaction, it is clear that a streamline process of sample enrichment and derivatization are of tremendous importance to define the modified residues. However, an overlook of the "side effects" of such procedure could potentially complicate the analysis. For example, PARG treatment simplifies the PAR polymers to one ADP-ribose unit, but the remaining high concentration of ADP-ribose produced in the digestion mixture could potentially react with proteins nonenzymatically, generating ADP-ribose-glycated species. Other types of digestion leading to reactive sugar species possessing reducing ends could all potentially react with protein free amines (lysine or arginine), especially in a highly enriched sample with high density of PAR polymers.

Beyond the complication resulted from sample preparation, the endogenous NAD^+ hydrolase activity of PARP-1 could also play a role in enzymatic poly(ADP-ribosyl)ation. PARP-1's activity is triggered by binding to DNAs, and the PAR polymers being produced can reach 200-400 units. Meanwhile, the accompanied NADase activity also increases as automodification proceeds (*83*), until the balance between the DNA affinity and the charge repulsion from the negatively-charged PAR polymers is broken. The local high concentration of ADP-ribose generated form NAD^+ hydrolysis could also be reactive toward lysine residues in proximity. The high occurrence of lysine residues being identified as the acceptor (Table 4-2) in the current experimental setting may simply reflect the high concentration of free ADP-ribose produced from PARG treatment, or because of the usage of high NAD^+ concentration to drive poly(ADP-ribosyl)ation

reaction, which creates a favorable condition for the NAD^+ hydrolysis side reaction to occur, promoting nonenzymatic ADP-ribosylation of lysine.

In addition to the above considerations, an assay designed for measuring the progress of enzymatic lysine ADP-ribosylation using defined substrates and chemicals would be beneficial. Structural studies of the enzyme–substrate complex with the substrate carrying a lysine residue in the active site of PARP-1 could also provide significant insight into this enigmatic process.

Chapter 5. Macromolecular Mechanism of Human PARP-1 Automodification Reaction

5.1 INTRODUCTION

PARP-1 is a multi-modular protein containing three functional units: the DNA-binding domain, the automodification domain, and the catalytic domain (*178*). These features dictate how PARP-1 works as a DNA-dependent ADP-ribosyltransferase, which itself can serve as a substrate and undergo automodification. In the presence of genotoxic stress, PARP-1 inside the cell nucleus quickly relocalizes to bind the damaged DNA, triggering PAR polymers formation mainly on PARP-1 itself and other nuclear proteins. This self-modification property of PARP-1 and the involvement of nonspecific, structural DNA recognition to induce enzyme activity raise interesting mechanistic questions about the stoichiometry (or molecularity) of DNA-dependent poly(ADP-ribosyl)ation of PARP-1 in terms of "enzyme PARP-1," "substrate PARP-1," and DNA ligand.

Early biochemical studies suggested that dimerization or even multimerization of PARP-1 could occur during catalysis (*238, 298*). A bimolecular, namely an intermolecular mechanism of PARP-1 automodification reaction was proposed by Alvarez-Gonzalez *et al*. based on the result of their kinetic study that the initial rate is proportional to the square of enzyme concentration (*239*). Meanwhile, the molecular mechanism of receptor tyrosine kinase (RTK) on cell membranes, particularly epidermal growth factor receptor (EGFR), was also established in the early 90s. It was shown that growth factor-induced EGFR dimerization triggers *trans*-phosphorylation of EGFR and stimulates the downstream signaling cascade (*299*). The characteristics of a RTK having an allosteric ligand and catalyzing self-modification (autophosphorylation) are analogous to DNA-induced PARP-1 automodification. It is thus not surprising that researchers in the PARP field would like to consider an intermolecular process for the PARP-1

posttranslational modification reaction. In addition, biophysical studies also suggested that dimerization of PARP-1 upon binding to specific DNA structure correlate with elevated enzyme activity (*227, 241*). Therefore, the model that PARP-1 acting as a catalytic dimer and the automodification process being intermolecular is well-acknowledged in the PARP field.

Even though PARP-1 dimerization during automodification appears to be a general belief, strong evidence supporting the bi-molecularity of poly(ADP-ribosyl)ation reaction is still lacking. It remains ambiguous whether the reaction is an uni-molecular event where a single PARP-1 protein acts as both enzyme and substrate, or a bi-molecular event where the enzyme and the substrate are different proteins. Furthermore, recent solution structural studies using NMR and SAXS techniques failed to detect any dimerized species for various PARP-1 constructs including full-length PARP-1 (*188, 197, 198, 236*). An X-ray crystal structure of a near full-length PARP-1 in complex with double-strand blunt-end DNA also revealed a monomeric form of the enzyme–DNA complex (*200*). However, a structure containing only the DNA-binding domain of PARP-1 (FI and FII) was found to form a dimer at the end of an overhang DNA (*235*). Clearly, controversy about the active form of PARP-1 remains an issue to fully understand the DNA-induced PARP-1 automodification reaction.

In this chapter, an *in vitro* poly(ADP-ribosyl)ation assay using two structurally distinguishable mutants of human PARP-1 was developed and used to investigate the macromolecular mechanism of PARP-1 automodification reaction. The feasibility of this assay is based on fact that the recombination of various domains *in trans* could produce a complementary full-length PARP-1 complex, which is capable of catalyzing poly(ADP-ribosyl)ation, albeit with relatively weaker activity than the wild-type PARP-1 in a single polypeptide chain. In a typical experiment, a pair of PARP-1 constructs which have

different size and enzyme activity was used in the reaction in the presence of radioactive NAD^+ and DNA. For example, an active enzyme could be mixed with an inactive enzyme in a reaction buffer containing hot NAD^+ and DNA. Poly(ADP-ribosyl)ation could be catalyzed by the active enzyme or facilitated by the presence of other necessary domains in the solution. The reaction mixture was then treated with PARG to cleave the PAR polymers from the proteins, leaving only mono-ADP-ribosylated species. Finally, the proteins were resolved by SDS-PAGE and visualized by autoradiography. If the inactive protein constructs are ADP-ribosylated *in trans* only in the presence of a full-length active PARP-1, or a catalytically competent "PARP complex," the results could support a model that PARP-1 automodification is mediated by an intermolecular process.

The interplay between the PARP-1 domains is important for PARP-1 catalysis. Domain C, the third zinc finger-containing domain, has been shown to be essential for DNA-dependent PARP-1 automodification. Deletion of this domain largely abolished enzyme activity (*187, 188*). However, similar to the full-length PARP-1, discrepancy also exists between the reported monomeric NMR structure of domain C in solution (*188*) and the dimeric X-ray structure of domain C in crystal (*187*). Herein, a top-down MS-based method was utilized to probe the potential conformational change of domain C upon denaturation to gain insight into its native structure in solution. The results are more supportive of domain C existing in monomeric form in solution. Moreover, a chemical crosslinking experiment was also carried out to examine the protein–protein interactions involving domain C and other portions of PARP-1. No "PARP complex" with a defined molecular weight around 113 kDa was observed. But the existence of noncovalent interactions was implicated as distinct protein bands became smear after crosslinking. These results suggest that domain C is not the sole dimerization interface and interdomain contacts are more relevant during catalysis.

5.2 MATERIALS AND METHODS

5.2.1 Cloning, expression, and purification of human PARP-1 fragments and mutants in *E. coli*

DNAs encoding domains A-C (ABC, residues 1–373) and domains D-F (DEF, residues 374–1014) of human PARP-1 were cloned into MalE-pET vector by Dr. Peng Gao as described in Section 4.2.1. DNAs encoding domain C (residues 233–373) and domains ABDEF (residues 1–232 and 374–1014 as a single polypeptide chain, with two additional residues Asp and Ile in between due to primer design) of human PARP-1 were prepared and cloned into MalE-pET vector by Dr. Zhihua Tao. DNA encoding domain DEF was also cloned into the original pET-28b(+) vector (Novagen) for the expression of *N*-terminal His_6-tagged protein.

Site-directed mutagenesis was carried out using DEF/MalE-pET as the template and the primer pairs listed in Table 5-1 according to the protocol recommended by the manufacturer (Stratagene). Briefly, 5–50 ng of template DNA was PCR-amplified using 125 ng of specific primer pairs under gradient annealing temperature (55–65 °C). The reaction mixtures were incubated overnight with *Dpn*I at 37 °C to degrade the original template DNA. The resulting newly synthesized DNAs with desired mutations were individually introduced into *E. coli* XL 10-Gold (Stratagene) or DH5α (Invitrogen) strain for amplification based on their specific annealing temperature. Plasmids were then purified and sequence-verified by the ICMB DNA core facility at UT Austin. Double, triple, and quadrupole mutants were generated by cumulative mutagenesis.

Procedures for MBP-tagged protein expression and purification were essentially the same as described previously. All buffers used except for the final elution buffer contained 1 M NaCl to disrupt nonspecific protein–DNA interactions. The proteins collected from the first Ni-NTA column purification were digested with TEV protease

(5% w/w) to cleave the MBP tag during the third-time dialysis. The mixture was then passed through the Ni-NTA column again to remove all His-tagged proteins, allowing non-tagged target protein to be eluted. His-tagged DEF was purified following similar procedures without TEV protease digestion and second Ni-NTA column purification.

Mutation	Direction	Primer sequence
M890V	Forward	5′-CCCGTGACAGGCTAC**G**TGTTTGGTAAAGGGATCTATTTCGC-3′
	Reverse	5′-GCGAAATAGATCCCTTTACCAAACA**C**GTAGCCTGTCACGGG-3′
K893I	Forward	5′-GCCCGTGACAGGCTACATGTTTGGTA**TT**GGGATCTATTTCGC-3′
	Reverse	5′-GCGAAATAGATCCC**AA**TACCAAACATGTAGCCTGTCACGGGC-3′
D899N	Forward	5′-TAAAGGGATCTATTTCGCT**A**ACATGGTCTCCAAGAGTGC-3′
	Reverse	5′-GCACTCTTGGAGACCATGT**T**AGCGAAATAGATCCCTTTA -3′
E988A	Forward	5′-CCTCTCTACTATATAAC**C**AGTACATTGTCTATGATATTGCTC-3′
	Reverse	5′-GAGCAATATCATAGACAATGTACT**G**GTTATATAGTAGAGAGG-3′

Table 5-1. Primer sequences for PARP-1 site-directed mutagenesis. Mutated nucleotides were underlined and in boldface.

5.2.2 Cloning, expression, and purification of human full-length PARP-1 and mutants using baculovirus expression vector system in insect cells

The gene encoding full-length human PARP-1 was cloned into the pFastBac HT B/MBP-Tev vector as described in Section 3.2.4. To construct the full-length PARP-1 mutants, mutations were first generated in the DEF/MalE-pET vector. Taking advantage of the *Pst*I restriction enzyme site located within domain E, the DEF mutant plasmids were ligated with the *N*-terminal fragment of wild type PARP-1/MalE-pET following *Pst*I and *Xho*I digestion. The resulting full-length PARP-1 mutant genes were further cloned into the pFastBac HT B/MBP-Tev vector for protein expression in insect cells (see Section 3.2.4).

5.2.3 Poly(ADP-ribosyl)ation assay of PARP-1 and mutants using nonradioactive NAD^+

Poly(ADP-ribosyl)ation of full-length PARP-1 and/or PARP-1 fragments/mutants was performed according to the procedures described in Section 3.2.5. Briefly, full-length PARP-1, truncated domains, or combination of the two (1–10 μM) were added to a reaction mixture containing NAD^+ (50–1000 μM), 25–50 μg/mL calf thymus DNA, 250 μM DTT, 10 mM $MgCl_2$, 100 mM Tris-HCl at pH 8.0 to initiate the reaction. After incubation at room temperature for 30 min, the reaction was quenched by adding equal volume of 2× SDS-PAGE loading buffer and analyzed by SDS-PAGE. Protein signals were visualized by Coomassie stain, whereas poly(ADP-ribosyl)ation was detected by Amersham ECL Prime Western Blotting chemiluminescence substrate (GE Healthcare) using anti-PAR monoclonal primary antibody (Trevigen), and horseradish peroxidase-conjugated anti-mouse IgG secondary antibody (Sigma-Aldrich).

5.2.4 Poly(ADP-ribosyl)ation assay of PARP-1 and mutants using ^{32}P-NAD^+

A 6-μL reaction were conducted under the same condition described in Section 3.2.5. The ratio of NAD^+ to ^{32}P-NAD^+ was 0.1 mM–0.1 μCi μL^{-1}. To obtain mono-ADP-ribosylated species, samples were treated with PARG 30 min after initiation of the reaction, and were allowed to incubate for an additional 30 min at room temperature. After quenching by 6 μL 2× SDS-PAGE loading buffer, the reaction mixture was resolved by a 16 × 16 cm SDS-PAGE gel. Gels were dried (optional), exposed on a storage phosphor screen (GE Healthcare), and detected by Typhoon FLA 9500 (GE Healthcare). Gel images were processed by ImageJ (National Institutes of Health).

5.2.5 Probing the unfolding of PARP-1 domain C with mass spectrometry

To provide structural information of domain C of PARP-1 in solution, domain C was dialyzed into phosphate-buffered saline (PBS, pH 7.4) containing 0%, 25%, and 50% of acetonitrile (ACN) for differential protein denaturation for 15 min on ice. The primary amine groups of the denatured protein were then selectively labeled with *S*-ethylacetimidate (SETA) in a SETA-to-protein molar ratio of 475 on ice for 1 h. The labeling reaction was quench by adding 100-fold ammonium acetate relative to the concentration of SETA. Labeled proteins were collected by passing through a 10-kDa cut-off filtration unit and stored at −80 °C before MS analysis.

Each protein sample was diluted to 10 μM in a ACN/water/formic acid solution (60:39.5:0.5, v/v/v) prior to direct infusion into an Orbitrap Elite mass spectrometer (Thermo Scientific) equipped with a 193-nm ArF excimer laser (Coherent) as described previously (*300*). Each sample was infused at a rate of 1.2 μL/min with a spray voltage of +3.5 kV. ESI-MS spectra were collected at 120,000 resolution at m/z 400, averaged for 100 scans. MS/MS data was acquired by ultraviolet photodissociation (UVPD) for the +19 charge state envelopes of domain C including both the unmodified and SETA-modified forms. MS/MS spectra were averaged over 2,000 scans at 120,000 resolution at m/z 400. The UVPD spectra were acquired at varying laser energies, from 1.5 mJ to 2.2 mJ, using a single pulse per scan. All UVPD experiments were carried out at 5 mTorr N_2 in the higher-energy collisional dissociation (HCD) cell. MS experiments and subsequent analysis were conducted by Michael Cammarata, a graduate student in Dr. Jennifer Brodbelt's lab in the Department of Chemistry, UT Austin.

Data analysis has been described in details in a published manuscript (*301*). The structural environment of each primary amine residue (i.e., lysine and the *N*-terminal

amine) was assessed based on the SETA incorporation value (S.I.) per residue. The calculation of S.I. value was based on the following equations:

$$S.I._N = S.I._{total} \text{ at } (N) \text{ lysine} - S.I._k \text{ at } (N-1) \text{ lysine} \quad (1)$$

$$S.I._{total} = \frac{w_{av} - mass_{theo.}}{mass_{SETA}} \quad (2)$$

$$w_{av} = \frac{\Sigma(\text{product of m/z of each modified ion and its ion abundance})}{\Sigma(\text{all ion abundances in modified series})} \quad (3)$$

where w_{av} represents the weighted average of specific ion fragment bearing SETA modifications, $S.I._{total}$ represents the total S.I. value of specific ion fragment, and $S.I._N$ represents the calculated S.I. value of specific (N) lysine residue.

5.2.6 Crosslinking assay of PARP-1 domain C and ABDEF

Chemical crosslinking experiment using bis(sulfosuccinimidyl)suberate (BS^3, Thermo Scientific) as the crosslinker was performed to explore the potential protein–protein interaction within PARP-1 domains. A 100 mM sodium phosphate buffer (pH 7.5) containing 10 μM of either domain C, ABDEF, or both in the presence of 50 μg/mL calf thymus DNA or 20 μM GGAATTCC 8-mer double-strand DNA was prepared. Bovine serum albumin (BSA) and the full-length PARP-1 were used as controls. No NAD^+ was included in the reaction. BS^3 (25 mM stock concentration in water, prepared immediately before use) was added to the protein solutions to reach 20-, 50-, and 100-fold molar excess, respectively. The reaction mixtures were incubated on ice for 100 min and then quenched by adding Tris-HCl buffer (pH 7.5) to a final concentration of 50 mM. Quenched reactions were mixed with 2× SDS-PAGE loading buffer and analyzed by 12% SDS-PAGE. Protein signals were either visualized by Coomassie stain or detected by immunoblotting using anti-PARP-1 monoclonal antibody C2-10 (Trevigen) which

recognizes the 85-kDa fragment containing the automodification domain and the catalytic domain of human PARP-1.

5.3 RESULTS

5.3.1 Preparation of full-length PARP-1, domain fragments, and the mutants

PARP-1 is a modular protein comprised of six functional domains (Figure 1-11). Combination of PARP-1 domains to reconstitute its enzymatic activity has been demonstrated by our group (*188*) and Pascal's laboratory (*189*). To study the mechanism of PARP-1 automodification reaction, two pairs of complementary domain fragments were utilized in this study: ABC/DEF and ABDEF/C.

In addition to the truncated domains, mutations were also introduced into the DEF fragment as well as full-length PARP-1 in order to construct a protein which is catalytically inactive but still capable of serving as an acceptor for PAR polymers. Four amino acid point mutations, M890V, K893I, D899N, and E988A, were chosen based on the fact that PARP-1 harboring either one of these mutations had less than 0.5% activity compared to the wild type enzyme (*246, 252, 302*). As shown in Figure 5-1, these four residues are located within or near the active site of PARP-1. Met-890 is stacking with the adenine ring of the acceptor NAD^+ molecule and may also help position the catalytic base Glu-988. The M890V mutant may disrupt the binding with the acceptor substrate and have adverse effect on the proper alignment of the catalytic base. Lys-893 forms extensive hydrogen bonding with three backbone carbonyl groups from Pro-881, Pro-882, and Ala-884. Mutation of this residue to Ile could prevent these interactions and destabilize the loop structure around the NAD^+-binding pocket. Asp-899 forms a hydrogen bond with Asn-987. The catalytic base Glu-988 of the D899N mutant may have

increased mobility caused due to the adjacent mutation. It is also possible that the acceptor substrate binding may be slightly hindered in the D899N mutant. Mutations were introduced sequentially according to the observed biochemical properties (which will be presented in the following sections) and the ease of purification. The nomenclature of these mutants is shown in Table 5-2.

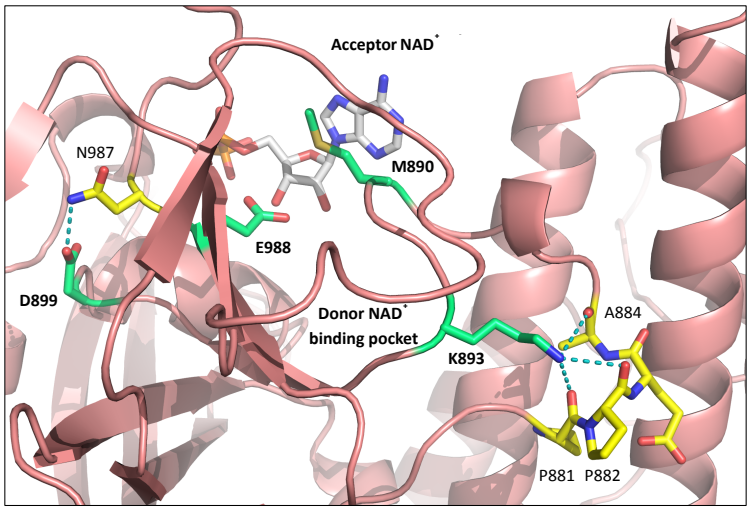

Figure 5-1. Locations of amino acid residues for targeted mutations in the PARP-1 catalytic domain (PDB: 1A26). Targeted residues are shown in green; residues forming hydrogen-bond interactions with the targeted residues are shown in yellow; the AMP moiety of carba-NAD^+ is shown in white.

Construct name	Description
PARP-1	Wild-type non-tagged PARP-1
DEF	Wild-type *N*-His_6-tagged DEF
ke-DEF	Non-tagged DEF with K893I and E988A
de-DEF / de-PARP	Non-tagged DEF or PARP-1 with D899N and E988A
mde-DEF / mde-PARP	Non-tagged DEF or PARP-1 with M890V, D899N, and E988A
mkde-DEF / mkde-PARP	Non-tagged DEF or PARP-1 with M890V, K893I, D899N, and E899A

Table 5-2. Nomenclature of PARP-1 mutants used in this study.

Shown in Figure 5-2 are the SDS-PAGE gel images containing protein constructs used in the experiments presented in this chapter. Wild-type full-length PARP-1 displayed a major band around the 116-kDa marker, matching well with the expected molecular weight of 113 kDa (lanes 6, 9, and 12). A faint band of molecular weight higher than 116 kDa was observed for batch 1 (lane 6). This band is most likely the uncleaved MBP-PARP-1 fusion protein due to insufficient activity of TEV protease. Some minor degradation was also observed. Wild-type truncated domains including DEF, ABC, and domain C were all obtained in high purity (lanes 5, 11, and 14, respectively). ABDEF (~97 kDa) was purified in fair condition, with a significant degradation band around 45 kDa (lane 13). The protein was further purified through size exclusion chromatography to get rid of the degraded protein, but the resulting ABDEF still showed signs of degradation upon storage (data not shown).

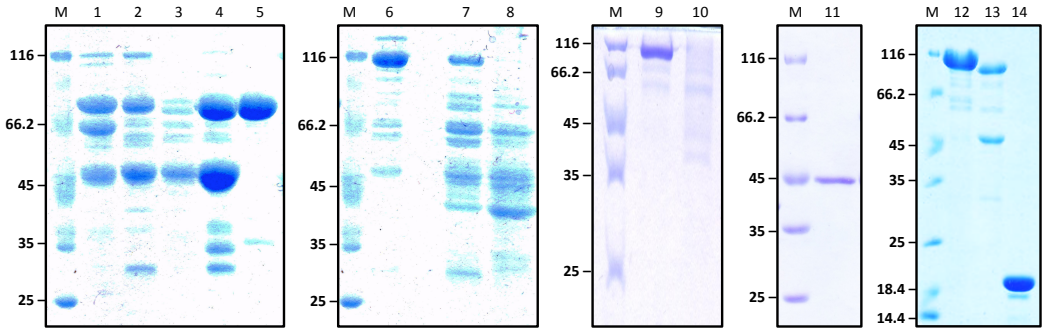

Figure 5-2. SDS-PAGE gel of purified full-length PARP-1, domain fragments, and the mutants. M, molecular weight marker; lane 1, mde-DEF; lane 2, de-DEF; lane 3, mkde-DEF; lane 4, ke-DEF; lane 5, wild-type His_6-DEF; lane 6, wild-type PARP-1 (batch 1); lane 7, de-PARP; lane 8, mde-PARP; lane 9, wild-type PARP-1 (batch 2); lane 10, mkde-PARP; lane 11, ABC; lane 12, wild-type PARP-1 (batch 3); lane 13, ABDEF; lane 14, domain C.

Handling of DEF and full-length PARP-1 mutant proteins was more problematic. All DEF mutants expressed in *E. coli* contained several degraded products in addition to the desired 71-kDa protein (lanes 1–4). Switch of the expression system to insect cells did not improve the situation (data not shown). Among the four mutants, mkde-DEF had the lowest yield upon purification (lane 3). Hence, the number of mutations of DEF was limited to two or three residues and the resulting mutants were catalytically inactive. The mde-DEF and de-DEF mutant had a faint band around 116 kDa, representing their corresponding uncleaved MBP-fusion proteins.

The expression and purification of full-length PARP-1 bearing any of the four mutations was difficult. Efforts to alter the growth conditions of the insect cells or to accelerate the purification process did not significantly improve the stability of these protein constructs. Of three mutants tested, only de-PARP showed a 113-kDa band corresponding to the molecular weight (lane 7), whereas mde-PARP and mkde-PARP were severely degraded (lanes 8 and 10, respectively). Nevertheless, the proteins were still pooled and used in the following experiments, with caveats added for data interpretation.

Overall, the wild-type proteins were obtained in high purity, while the mutant proteins of DEF and full-length PARP-1 showed noticeable degradation problems. The degradation pattern and the difference in the expected molecular weight of DEF and full-length PARP-1 proteins (71 kDa vs. 113 kDa) are two important criteria to be considered in the interpretation of the experimental results in the following sections.

5.3.2 Reconstitution of DNA-dependent poly(ADP-ribosyl)ation activity by PARP-1 domain fragments

To show that ABC/DEF and ABDEF/C, two pairs of PARP-1 truncated domains, are able to reconstitute DNA-dependent poly(ADP-ribosyl)ation activity *in vitro*, purified proteins pairs were added in 1:1 molar ratio to the PARP-1 reaction buffer containing 25–50 μg/mL calf thymus DNA in the presence or absence of NAD^+. Reactions were analyzed by SDS-PAGE followed by either Coomassie staining or anti-PAR immunoblot.

Results of the ABC/DEF pair are shown in Figure 5-3A and B. Wide-type DEF showed basal activity in the absence of ABC, as detected by anti-PAR immunoblot (lane 1), whereas DEF mutants ke-DEF and mkde-DEF did not show any poly(ADP-ribosyl)ation activity (lanes 2 and 3, respectively). Reactions containing PARP-1 showed strong poly(ADP-ribosyl)ation activity, and the smear of PARP-1 protein can be seen from the Coomassie stain (lanes 4–6). The combination of DEF and ABC successfully reconstituted the DNA-dependent poly(ADP-ribosyl)ation activity, and a slight smear of the DEF protein band was observed (lane 7). No activity was detected for the DEF mutants even in the presence of ABC (lanes 8 and 9). This observation suggests that ke-DEF and mkde-DEF are devoid of poly(ADP-ribosyl)ation activity. Whether these mutants still possess mono-ADP-ribosylation activity is unknown, since the anti-PAR antibody can only recognize PAR polymers, not mono-ADP-ribose. It is worth mentioning that as-purified wild-type DEF had already been automodified even in the absence of NAD^+ (lane 10).

Similar results were obtained from the ABDEF/C pair. The addition of C into ABDEF reaction can trigger the poly(ADP-ribosyl)ation activity. But the activity is weaker than that of the wild-type enzyme as judged by the extent of protein smear from the Coomassie stain (Figure 5-3C, lanes 4 and 6).

In short, the strategy to combine PARP-1 domain fragments *in trans* successfully reconstituted the DNA-dependent poly(ADP-ribosyl)ation activity, and the mutant enzymes prepared are catalytically inactive. These results pave the way for the design of the following experiments to determine the molecularity of PARP-1 automodification reaction.

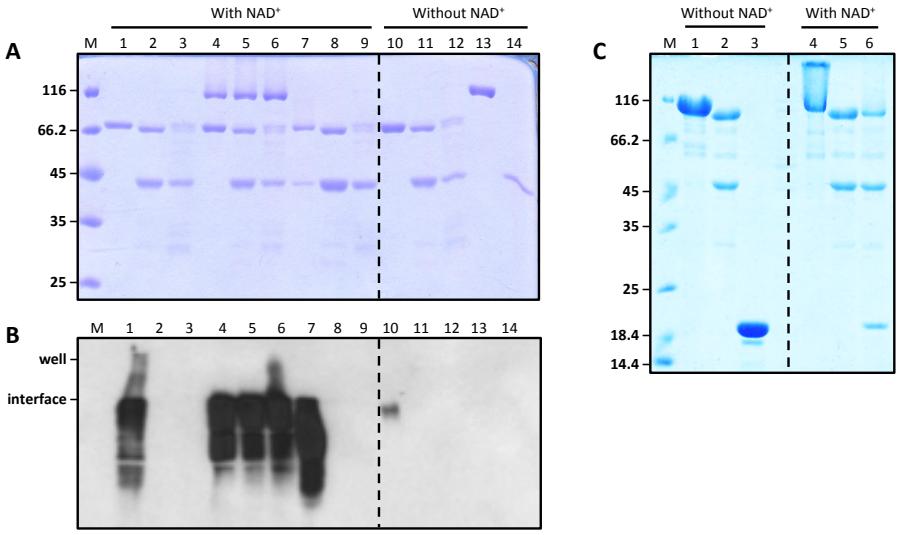

Figure 5-3. Complementation assay of DNA-dependent poly(ADP-ribosyl)ation of PARP-1. (A) SDS-PAGE gel of reactions containing ABC/DEF pair. Lane 1, DEF; lane 2, ke-DEF; lane 3, mkde-DEF; lane 4, DEF+PARP-1; lane 5, ke-DEF+PARP-1; lane 6, mkde-DEF+PARP-1; lane 7, DEF+ABC; lane 8, ke-DEF+ABC; lane 9, mkde-DEF+ABC; lane 10, DEF only; lane 11, ke-DEF only; lane 12, mkde-DEF only; lane 13, PARP-1 only; lane 14, ABC only. M, molecular weight marker. Reactions in lanes 1–9 include 50 μM NAD^+ whereas those in lanes 10–14 do not. (B) Western blotting of the same reactions performed in (A) using anti-PAR monoclonal antibody. (C) SDS-PAGE gel of reactions containing ABDEF/C pair. Lane 1, PARP-1 only; lane 2, ABDEF only; lane 3, C only; lane 4, PARP-1; lane 5, ABDEF; lane 6, ABDEF+C. Lanes 1–3 are purified proteins only whereas lanes 4–6 are poly(ADP-ribosyl)ation reactions using 1 mM NAD^+.

5.3.3 Overview of the poly(ADP-ribosyl)ation assay using PARP-1 constructs

A mix-and-match strategy was utilized here to provide experimental evidence for the macromolecular mechanism of PARP-1 automodification reaction. Namely, a wild-type enzyme is incubated with a catalytically inactive enzyme, which can still serve as the acceptor for PAR polymers. If poly(ADP-ribosyl)ation is observed for the inactive enzyme, this would suggest that an intermolecular mechanism is operating. A radioactivity-based assay was employed to achieve high sensitivity for any ADP-ribosylation events, and to offer additional mechanistic information by monitoring the hydrolysis of NAD^+ side reaction.

To distinguish between the wild-type and the inactive enzyme, minimally active PARP-1 domain DEF was selected and mutated to serve as the inactive one. DEF has been demonstrated to possess basal poly(ADP-ribosyl)ation activity in the absence of its DNA-binding domain counterpart ABC (*5*). By using two size-distinguishable PARP-1 domain constructs and taking advantage of PARP-1's domain complementarity, the protein mixture after modification can be resolved by SDS-PAGE, and radiolabeled species can be visualized by autoradiography. Solid evidence for any attachment of the ADP-ribose unit can be obtained by PARG treatment, which eliminates the smear effect associated with poly(ADP-ribosyl)ated proteins, leaving the protein-proximal ADP-ribose.

Once the property of the DEF mutant was confirmed, the same mutations were introduced into the full-length PARP-1 and poly(ADP-ribosyl)ation assay was performed in the presence of wild-type DEF. The modification of the mutant PARP-1 would further support the intermolecular mechanism.

5.3.4 Poly(ADP-ribosyl)ation of ke-DEF mutant in the presence of PARP-1 or ABC

DEF domain containing double mutations K893I and E988A was first prepared in an attempt to generate a catalytically inactive DEF mutant (ke-DEF). Poly(ADP-ribosyl)ation assay of this mutant in the presence of PARP-1 was performed along with control reactions using wild-type DEF. As shown in Figure 5-4A, PARP-1 showed robust automodification activity, with major signal seen at the gel interface (lane 2). Wild-type DEF exhibited weak activity, as the NAD^+ level was comparable to the control (lane 1 and 3). Interestingly, very long and branched polymers were attached on the DEF protein, preventing it from entering the gel (lane 3). No radioactive signal was observed for the ke-DEF reaction and NAD^+ remained in the solution (lane 4), suggesting it may not be active in the absence of other PARP-1 domains.

To examine the feasibility of detecting poly(ADP-ribosyl)ated species from different protein constructs under current experimental settings, an increasing concentrations of wild-type DEF were titrated against PARP-1. From lanes 5–8, a distinct band below PARP-1 can be observed as the concentration of DEF increased, which appears in the region corresponds to the molecular weight of unmodified DEF. PARP-1 automodification is still the dominant reaction. These results suggest that at least initiation of poly(ADP-ribosyl)ation of some DEF occurred as its concentration increased in the reactions. Whether this modification is catalyzed by DEF or PARP-1 cannot be distinguished at this point.

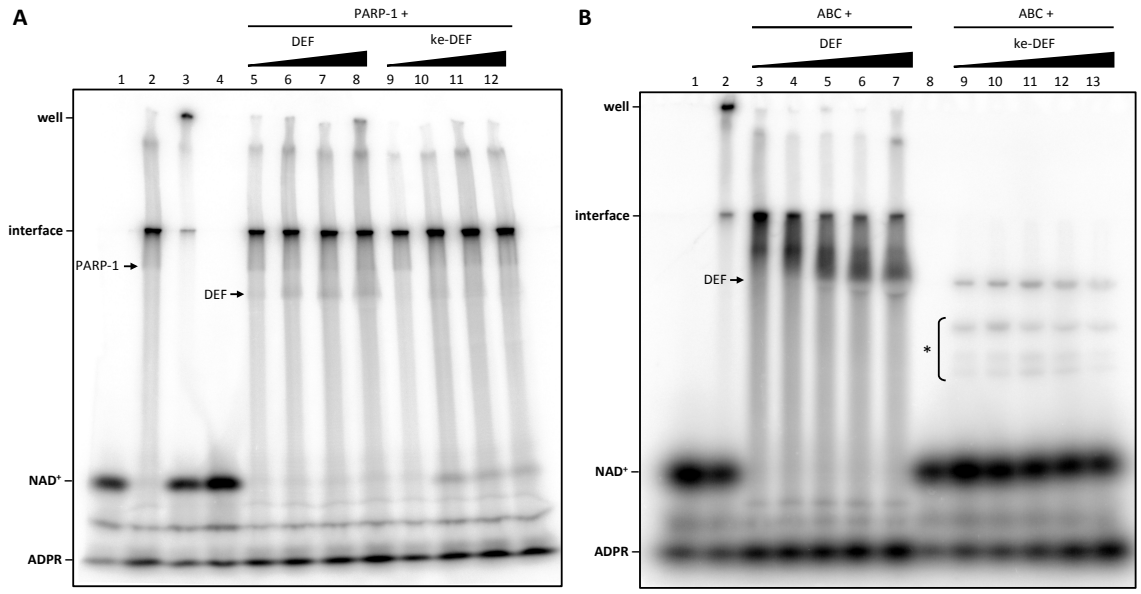

Figure 5-4. Autoradiography of poly(ADP-ribosyl)ation assays using DEF or ke-DEF incubated with (A) PARP-1 or (B) ABC in the presence of DNA and NAD^+. All reactions contain 25 μg/mL calf thymus DNA and 100 μM NAD^+ doped with ^{32}P-NAD^+. Protein concentration was 1 μM unless specified. ADPR, ADP-ribose. (A) Lane 1, NAD^+ only; lane 2, PARP-1; lane 3 DEF; lane 4, ke-DEF; lanes 5–8, PARP-1 with 1, 2, 5, and 10 μM DEF, respectively; lanes 9–12, PARP-1 with 1, 2, 5, and 10 μM ke-DEF, respectively. (B) Lane 1, NAD^+ only; lane 2, DEF; lanes 3–7, ABC with 1, 2, 5, 10, and 20 μM DEF, respectively; lane 8, ke-DEF; lanes 9–13, ABC with 1, 2, 5, 10, and 20 μM ke-DEF, respectively. Arrows indicate the expected positioning of the corresponding protein in its original molecular weight. Asterisk denotes the degraded proteins of ke-DEF.

The results of titrating ke-DEF into PARP-1 reactions were similar to those of DEF (lanes 9–12). An even weaker band was observed at the DEF region. This can be explained by the over-estimation of the concentration of ke-DEF as a result of the presence of degraded ke-DEF in the protein solution (Figure 5-2, lane 4). NAD^+ hydrolysis also decreased as ke-DEF concentration increased, suggesting that the mutant

may compete with PARP-1 for NAD^+ binding which seems to "protect" NAD^+ from hydrolysis.

The modification of ke-DEF only in the presence of PARP-1 raises the question whether this modification is catalyzed by PARP-1, or ke-DEF with the assistance from the ABC domain of PARP-1. To investigate this issue, ke-DEF was incubated with purified ABC domain and poly(ADP-ribosyl)ation assay was carried out (Figure 5-4B). In the control reactions of wild-type DEF, the strongest PAR signal was observed for DEF and ABC in a 1:1 molar ratio (lane 3). As the concentration of DEF increased, the smearing of poly(ADP-ribosyl)ated proteins weakened and shifted toward the molecular weight of unmodified DEF (lanes 3–7). This observation is consistent with the notion that ABC is required for the initiation step of poly(ADP-ribosyl)ation (Dr. Meilan Wu, unpublished results). Excess amount of DEF are competing with each other for searching available ABC, therefore less modification can occur on the protein. Meanwhile, NAD^+ was depleted in these reactions, either in the form of PAR polymers or being hydrolyzed to free ADP-ribose.

The results of ke-DEF incubated with ABC were unexpected. A total of four protein bands can be clearly seen from the gel for all reactions (lanes 9–13). The pattern of these protein bands matches with that of the purified ke-DEF (Figure 5-2, lane 4). NAD^+ was not consumed much as compared to the reaction of DEF alone (lane 2), and the addition of ABC did not increase the rate of hydrolysis. These results are mostly consistent with the explanation that ke-DEF is a mono-ADP-ribosyltransferase. The residual catalytic activity of ke-DEF even after double mutations prevent its use in the experiments for investigating intermolecular mechanism of PARP-1 automodification, as one cannot rule out the possibility that ke-DEF can be self-modified in the presence of other supporting domains such as ABC. Nonetheless, this set of experiments

demonstrated the feasibility to detect poly(ADP-ribosyl)ation of structurally distinguishable PARP-1 constructs using autoradiography.

5.3.5 Poly(ADP-ribosyl)ation of catalytically inactive mkde-DEF or mkde-PARP

To obtain a truly inactive PARP-1 mutant, four mutations were introduced into the DEF domain by site-directed mutagenesis (mkde-DEF) to ensure complete disruption of its catalytic activity. The purity of mkde-DEF was poor (Figure 5-2, lane 3), and efforts to improve its purity had limited success. The protein was still pooled and used in the poly(ADP-ribosyl)ation assay to gain some insight into the mechanistic proposal.

The mkde-DEF was first incubated with ABC to examine if any residual activity can be detected. No signal was observed for either mkde-DEF alone or in the presence of ABC (Figure 5-5A, lanes 2–6). NAD^+ remained in the samples. When increasing concentrations of mkde-DEF were titrated against PARP-1, a decreased trend of poly(ADP-ribosyl)ation around the gel interface region was observed, accompanied by the increasing amount of NAD^+ left in each reaction (lanes 7–10). No explicit band below the dark smear from PARP-1 can be seen. Several explanations are possible to account for the observation: the modified mkde-DEF protein band may be too weak to be seen on top of the overall radioactivity background; insufficient amount of mkde-DEF protein was present in the sample due to severe degradation; no modification occurred on mkde-DEF. With the current materials and method, it is difficult to distinguish between these possibilities, but at least the increasing NAD^+ remained in the samples suggest the occurrence of some inhibitory effect upon the addition of mkde-DEF.

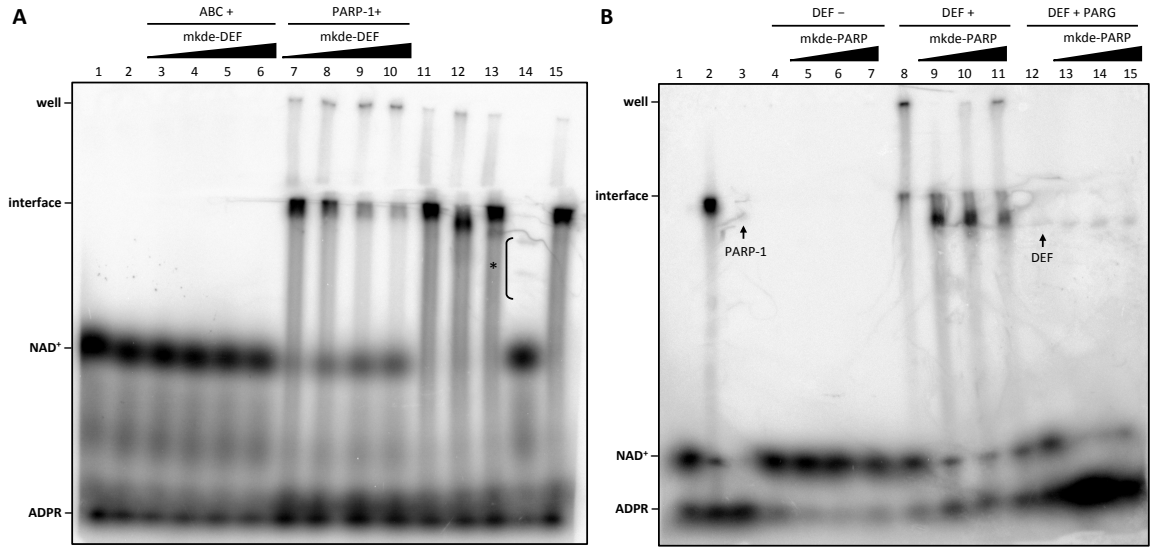

Figure 5-5. Autoradiography of poly(ADP-ribosyl)ation assays using PARP-1 bearing quadrupole mutations in the presence of DNA and NAD^+. All reactions contain 25 μg/mL calf thymus DNA and 100 μM NAD^+ doped with ^{32}P-NAD^+. Protein concentration was 1 μM unless specified. (A) mkde-DEF incubated with ABC or PARP-1. Lane 1, NAD^+ only; lane 2, mkde-PARP; lanes 3–6, ABC with 1, 2, 5, and 10 μM mkde-DEF, respectively; lanes 7–10, PARP-1 with 1, 2, 5, and 10 μM mkde-DEF, respectively; lane 11, PARP-1; lane 12, DEF+ABC; lane 13, DEF+PARP-1; lane 14, ke-DEF+ABC; lane 15, ke-DEF+PARP-1. Asterisk denotes the protein bands derived from ke-DEF. (B) mkde-PARP incubated with PARP-1 or ABC. Lane 1, NAD^+ only; lane 2, PARP-1; lane 3, PARP-1+PARG; lanes 4–7, 0, 1, 2, and 5 μM mkde-PARP, respectively; lanes 8–11, DEF with 0, 1, 2, and 5 μM mkde-PARP, respectively; lanes 12–15, DEF with 0, 1, 2, and 5 μM mkde-PARP, respectively, and then treated with PARG. Arrows indicate radiolabeled protein in its original molecular weight.

The corresponding full-length PARP-1 bearing the same mutations (mkde-PARP) was also constructed. Upon purification, the protein was again severely degraded, with no major band at 113 kDa (Figure 5-2, lane 10). The partially purified protein alone had no radiolabeled signal in the presence of NAD^+ (Figure 5-5B, lanes 4–7), and the hydrolysis of NAD^+ only slightly increased when using high concentration of mkde-PARP (lane 7).

In the absence of ABC, wild-type DEF showed signals at the well and gel interface region, as observed previously (lane 8 and Figure 5-4B lane 2). When adding 1:1 ratio of mkde-PARP to the reaction, the signal at the well region disappeared and a strong smear showed up at the DEF region (lane 9). NAD^+ was consumed more than DEF alone. This result is consistent with the notion that the ABC domain of mkde-PARP together with wild-type DEF forms an active "PARP complex" where new polymers are both initiated and extended. Increasing concentrations of mkde-PARP seemed to lower the modification level of DEF and the signal at the well region appeared again (lanes 10 and 11). To confirm if the proteins are indeed attached with PAR polymers, reactions having the same components as in lanes 8 to 11 were treated with PARG to hydrolyze the polymers, leaving mono-ADP-ribosylated proteins. As shown in lanes 12 to 15, the only protein signal can be seen corresponds to DEF. No modified mkde-PARP was observed, largely because there is no distinct major band for this protein being used (Figure 5-2, lane 10). Altogether, these results indicate that introducing mutations is possible to disrupt PARP-1's activity without interfering its ability to serve as an acceptor for PAR polymers. PARG treatment can facilitate the visualization of modified proteins to a single band, mono-ADP-ribosylated form. How many point mutations are required to inactivate a protein and how to improve the purification of the mutants are subjects need to be further defined and optimized.

5.3.6 Poly(ADP-ribosyl)ation of mde-DEF in the presence of PARP-1

In order to obtain a completely inactive mutant while retaining the protein stability for *in vitro* purification, K893I mutation was converted back to lysine to restore three peptide backbone hydrogen bond interactions (Figure 5-1). The resulting mde-DEF

was expressed and purified (Figure 5-2, lane 1). Despite having degradations around 66 kDa and 45 kDa, a major band corresponding to the correct DEF molecular weight can be seen by SDS-PAGE.

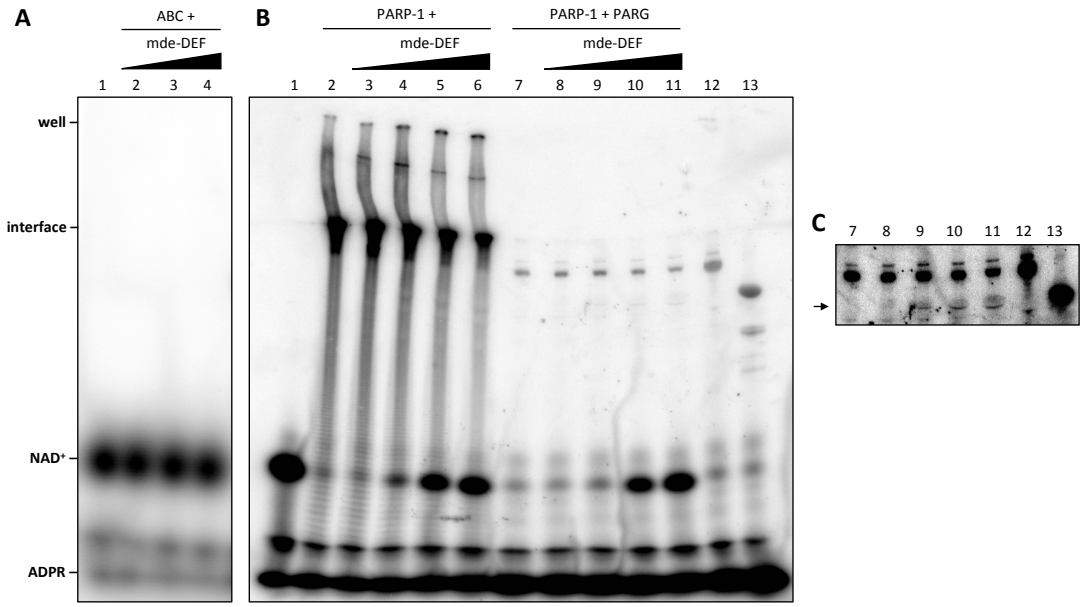

Figure 5-6. Autoradiography of poly(ADP-ribosyl)ation assays using mde-DEF incubated with (A) ABC or (B) PARP-1 in the presence of DNA and NAD^+. All reactions contain 25 μg/mL calf thymus DNA and 100 μM NAD^+ doped with ^{32}P-NAD^+. Protein concentration was 1 μM unless specified. (A) Lane 1, NAD^+ only; lanes 2–4, ABC with 1, 5, and 10 μM mde-DEF, respectively. (B) Lane 1, NAD^+ only, lanes 2–6, PARP-1 with 0, 1, 5, 10, and 25 μM mde-DEF, respectively; lanes 7–11, PARP-1 with 0, 1, 5, 10, and 25 μM mde-DEF, respectively, and then treated with PARG; lane 12, 4 μM PARP-1+PARG; lane 13, 6 μM DEF+6 μM ABC+PARG. (C) Enhanced image contrast of lanes 7–13 of (B) to show mono-ADP-ribosylated species after PARG treatment. Arrow indicates radiolabeled mde-DEF in its original molecular weight.

Incubation of the purified protein with ABC did not show any radiolabeled signal in the presence of ^{32}P-NAD^+ (Figure 5-6A, lanes 2–4), suggesting that mde-DEF is

inactive. Adding increasing amount of mde-DEF into samples containing 1 μM PARP-1 (batch 1 in Figure 5-2, lane 6) slightly reduced the overall poly(ADP-ribosyl)ation signal, and the remaining NAD^+ became more evident (Figure 5-6B, lanes 3–6), suggesting the mutant's inability to hydrolyze NAD^+. To confirm the identity of proteins which had been modified by PAR polymers, same reactions of lane 2 to 6 were treated with PARG to simplify the modified proteins to mono-ADP-ribosylated species. Clearly, a band corresponding to the molecular weight of DEF (lane 13) showed up as the mde-DEF concentration increases (Figure 5-6B and C, lanes 7–11, arrow). The signal, however, is not as strong as the one from PARP-1, even in 25-fold molar excess (lane 11). These results suggest that mde-DEF is capable of being modified by PARP-1 intermolecularly, but PARP-1 itself is still a preferred substrate.

5.3.7 Poly(ADP-ribosyl)ation of mde-PARP in the presence of DEF

To confirm the above experimental observation that mde-DEF can be modified by PARP-1 intermolecularly, full-length PARP-1 with the same point mutations were constructed (mde-PARP), and a complementary poly(ADP-ribosyl)ation assay was carried out in the presence of wild-type DEF.

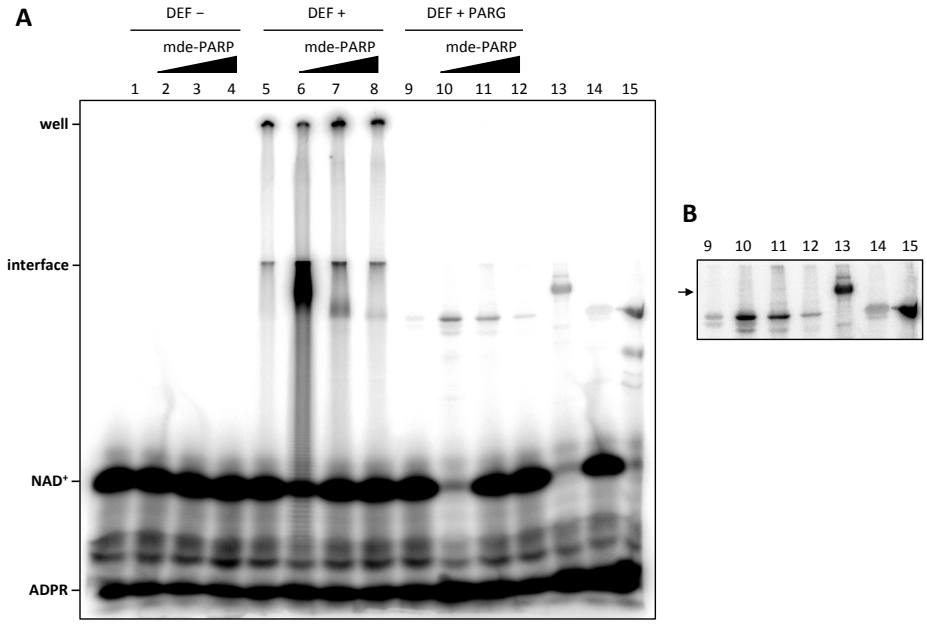

Figure 5-7. Autoradiography of poly(ADP-ribosyl)ation assays using mde-PARP incubated with DEF in the presence of DNA and NAD^+. All reactions contain 25 μg/mL calf thymus DNA and 100 μM NAD^+ doped with ^{32}P-NAD^+. Protein concentration was 1 μM unless specified. (A) Lane 1, NAD^+ only; lanes 2–4, 1, 5, and 8 μM mde-PARP, respectively; lane 5, DEF; lanes 6–8, DEF with 1, 5, and 8 μM mde-PARP, respectively; lane 9, DEF+PARG; lanes 10–12, DEF with 1, 5, and 8 μM mde-PARP, respectively, and then treated with PARG; lane 13, 5 μM PARP-1+PARG; lane 14, 5 μM DEF+PARG; lane 15, 5 μM DEF+5 μM ABC+PARG. (B) Enhanced image contrast of lanes 9–15 of (A) to show mono-ADP-ribosylated species after PARG treatment. Arrow indicates expected mde-PARP in its original molecular weight.

The purity of mde-PARP was not good, and no major band at 113 kDa can be observed (Figure 5-2, lane 8). This precludes the interpretation of mde-PARP being modified or not because there is no distinct band representing mde-PARP. Nonetheless, the mix-and-match poly(ADP-ribosyl)ation assay was still performed with caution. mde-PARP was completely inactive (Figure 5-7A, lanes 2–4). In the presence of DEF, a smear in the separating gel can be clearly observed, with the strongest one being mde-PARP and DEF in a 1:1 ratio (lane 6). As the concentration of mde-PARP increased, less DEF

was modified, probably due to the poisonous effect of inactive mde-PARP (lanes 7 and 8). Same reactions after PARG treatment gave distinct bands for DEF (lanes 9–12). There are some additional faint bands below the 71-kDa DEF major band in lane 10, and they are absent in lane 9. One possibility is that these protein bands are derived from degraded mde-PARP, and radiolabeled signals indicate that they were modified. NAD^+ was nearly depleted in lane 10, probably due to the combination of an active PARP complex and PARG to form a "PAR turnover system." The modification of DEF decreased when excess amount of mde-PARP was present, suggesting the possibility of a "dead complex" formed by mde-PARP itself which prevents the contribution of ABC domain to DEF for efficient catalysis. These results support the model that automodification of PARP-1 appears to operate in an intermolecular fashion. But an *in vitro* experiment with better defined protein materials is needed to unambiguously valid this hypothesis.

5.3.8 Poly(ADP-ribosyl)ation of de-DEF in the presence of PARP-1

From the previous section, it has been shown that both mde-DEF and mde-PARP are inactive PARP-1 mutants. To further optimize the protein stability while maintaining inactive status of the enzyme, a double mutant de-DEF was constructed for this purpose. The purified protein has a major band at 71 kDa with some degradation (Figure 5-2, lane 2). de-DEF was tested to be inactive in the presence of ABC (Figure 5-8A, lanes 2–4). When incubating with 1 μM PARP-1 (batch 1 in Figure 5-2, lane 6), no obvious difference was observed as poly(ADP-ribosyl)ation signal occupied the whole lane, and NAD^+ was depleted to similar extent (Figure 5-8B, lanes 2–6). The corresponding reactions treated with PARG showed a clearer picture. As the concentration of de-DEF increased, a band matching with the wild-type DEF molecular weight (lane 13) became

more apparent (lanes 7–11, arrow). However, PARP-1 is still the dominant automodification species. NAD^+ hydrolysis remained the same. The results, along with those obtained from mde-DEF, are in agreement with the model that de-DEF is modified intermolecularly by PARP-1 with PARP-1 being the preferred substrate.

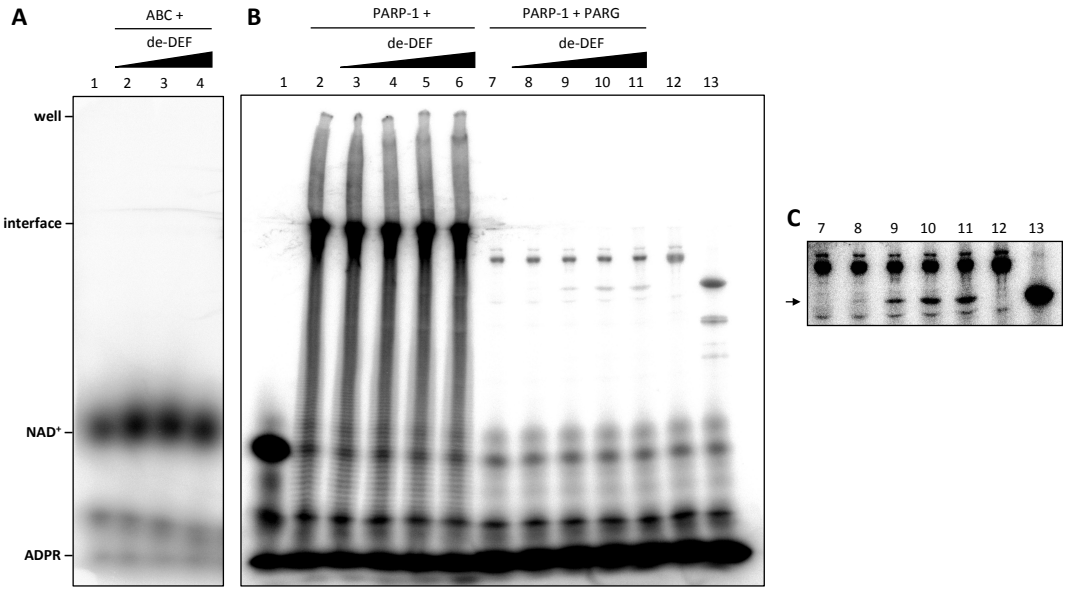

Figure 5-8. Autoradiography of poly(ADP-ribosyl)ation assays using de-DEF incubated with (A) ABC or (B) PARP-1 in the presence of DNA and NAD^+. All reactions contain 25 μg/mL calf thymus DNA and 100 μM NAD^+ doped with ^{32}P-NAD^+. Protein concentration was 1 μM unless specified. (A) Lane 1, NAD^+ only; lanes 2–4, ABC with 1, 5, and 10 μM de-DEF, respectively. (B) Lane 1, NAD^+ only, lanes 2–6, PARP-1 with 0, 1, 5, 10, and 25 μM de-DEF, respectively; lanes 7–11, PARP-1 with 0, 1, 5, 10, and 25 μM de-DEF, respectively, and then treated with PARG; lane 12, 4 μM PARP-1+PARG; lane 13, 6 μM DEF+6 μM ABC+PARG. (C) Enhanced image contrast of lanes 7–13 of (B) to show mono-ADP-ribosylated species after PARG treatment. Arrow indicates radiolabeled de-DEF in its original molecular weight.

5.3.9 Poly(ADP-ribosyl)ation of de-PARP in the presence of DEF

With the success that D899N/E988A double mutations could inactivate the enzyme while preserving certain protein stability for purification, a full-length PARP-1 containing these two mutations (de-PARP) was constructed for the complementary experiments using mutant PARP-1 and wild-type DEF. Even with some degradation bands present in the mixture, purified de-PARP has a major band around 113 kDa (Figure 5-2, lane 7). The protein has no activity in the presence of ^{32}P-NAD$^+$ (Figure 5-9A, lanes 2–4). When incubating with wild-type DEF in a 1:1 molar ratio, the active "PARP complex" lead to modified DEF which showed a smear in the gel (lane 6). Increasing de-PARP concentration attenuated the modification (lanes 7 and 8), which can be explained by the inhibitory effect from de-PARP. PARG treatment of the reactions from lanes 5 to 8 unequivocally showed that both wild-type DEF and de-PARP (arrow) were ^{32}P-labeled when the two were in equimolar amount (lane 10). When de-PARP was in excess, DEF was almost not modified at all after PARG treatment. This is identical to the situation where ABC is absent in the solution, suggesting little or no initiation took place. NAD$^+$ was not completely consumed in these reactions, perhaps because the PARP complex formed between DEF and de-PARP is much less reactive than that formed with mde-PARP. Overall, these data clearly demonstrate that DNA-dependent PARP-1 automodification reaction could proceed via an intermolecular mechanism, with the assembled full-length PARP-1 complex or a single PARP-1 polypeptide being the preferred substrate. However, one still cannot rule out the possibility that an intramolecular process is also involved based on the current experimental settings.

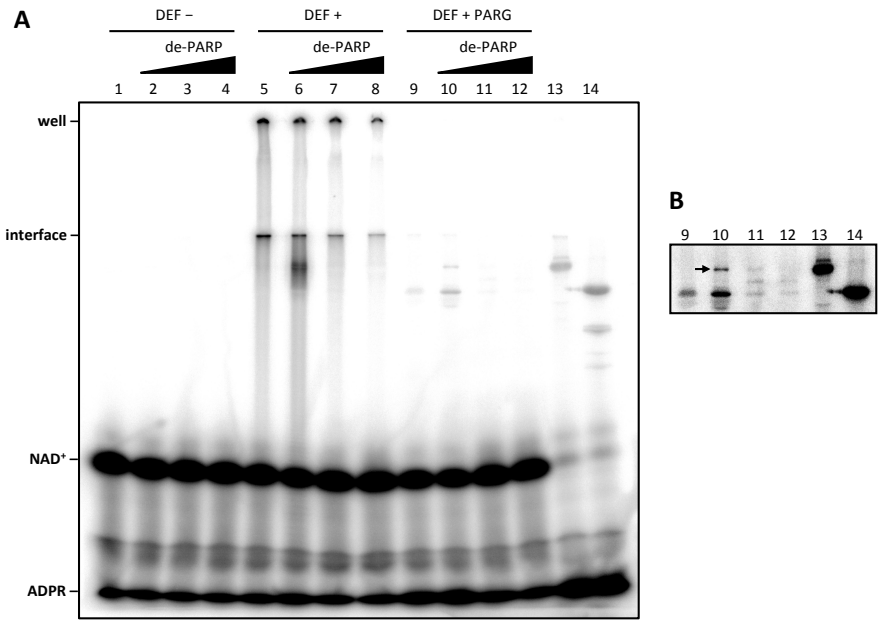

Figure 5-9. Autoradiography of poly(ADP-ribosyl)ation assays using de-PARP incubated with DEF in the presence of DNA and NAD^+. All reactions contain 25 μg/mL calf thymus DNA and 100 μM NAD^+ doped with ^{32}P-NAD^+. Protein concentration was 1 μM unless specified. (A) Lane 1, NAD^+ only; lanes 2–4, 1, 5, and 8 μM de-PARP, respectively; lane 5, DEF; lanes 6–8, DEF with 1, 5, and 8 μM de-PARP, respectively; lane 9, DEF+PARG; lanes 10–12, DEF with 1, 5, and 8 μM de-PARP, respectively, and then treated with PARG; lane 13, 5 μM PARP-1+PARG; lane 14, 5 μM DEF+5 μM ABC+PARG. (B) Enhanced image contrast of lanes 9–14 of (A) to show mono-ADP-ribosylated species after PARG treatment. Arrow indicates radiolabeled de-PARP in its original molecular weight.

5.3.10 Domain C of PARP-1 exists as a monomer in solution revealed by UVPD-MS

The mix-and-match poly(ADP-ribosyl)ation assay using distinguishable PARP-1 active enzyme and inactive substrate strongly suggests an intermolecular mechanism for the DNA-dependent PARP-1 automodification reaction. This implies that PARP-1 may be self-associated during catalysis (*238*), or more explicitly, dimerization of PARP-1 may occur during DNA-dependent poly(ADP-ribosyl)ation of PARP-1 (*239*). Domain C of

PARP-1 has been proposed to be the dimerization site for PARP-1 based on a recent crystal structure (*187*), which is in contrast to the monomeric NMR solution structure reported by our group (*188*). Herein, we employed a MS-based methodology to characterize the chemically labeled domain C, in order to evaluate the conformational change as a function of acetonitrile-induced protein denaturation. The result may provide insight into the structure of domain C under physiological conditions.

Domain C was first denatured by 25% or 50% acetonitrile for 15 min before reacting with the small molecule probe SETA which specifically labels free amino groups. Since protein conformation and local environment determine the reactivity of these amino groups, differential labeling can be achieved and then analyzed by top-down MS. UVPD is a novel MS technique which can efficiently generate a complete set of fragmented peptide ions for detection (*293*). The more fragment ions, the more sequence as well as modification information on the amino acid residues can be gathered by MS. By analyzing the spectra of the whole proteins species, the SETA incorporation value (S.I., 0–0.5) can be calculated, and the local environment of certain lysine residue can be inferred from the trend of S.I. value as a function of protein denaturation (*301*).

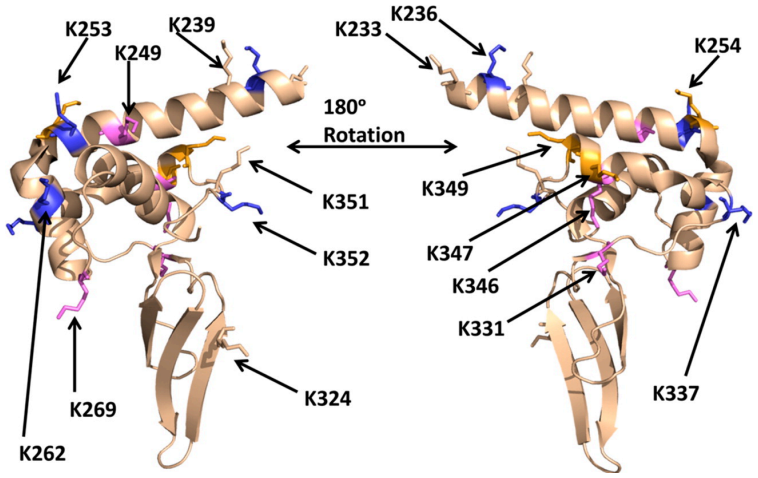

Figure 5-10. Domain C of PARP-1 (PDB:2JVN) showing the change of S.I. value of specific lysine residues as a function of protein denaturing buffer with increasing acetonitrile concentration. Blue represents decreasing SETA incorporation; pink represents increasing SETA incorporation; light brown represents no change in SETA incorporation; orange represents variable SETA incorporation. Adapted from (*301*).

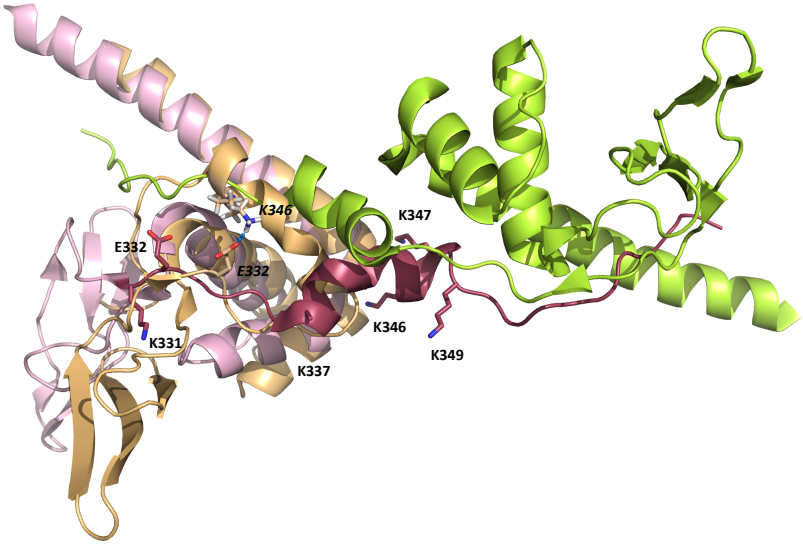

Figure 5-11. Superimposition of the domain C NMR structure (PDB: 2JVN, state 4, light brown) and the crystal structure (PDB: 2RIQ, pink and lemon). Residues 331–359 from one crystal monomer are shown in raspberry to highlight the dimerization interface. Key amino acid residues are also highlighted.

The overall trend of SETA incorporation of specific lysine residues is shown in Figure 5-10. Lysine residues with more solvent exposure have either decreasing or similar SETA incorporation, whereas more buried Lys-249, Lys-331, and Lys-346 have increasing SETA incorporation upon denaturation in 25% and 50% acetonitrile.

The loop containing residues 331–359 occupies different conformations in the NMR and in the crystal structure (Figure 5-11). The change of S.I. values of the lysine residues within this loop is of particular interest. Lys-331 showed no reactivity toward SETA in 100% aqueous buffer (*301*). It forms hydrogen bonds with Arg-330 and Glu-332 in the NMR structure, whereas being highly exposed in the crystal structure. Therefore, the result is more consistent with the monomeric form. Lys-337 has an S.I. value of 0.51 in 100% aqueous buffer, which would not be possible in the dimeric form with 27% solvent accessibility (*301*). Lys-346 had increased SETA incorporation upon denaturation, and this can be explained by the disruption of hydrogen bond interaction between Lys-346 and Glu-332 (Figure 5-11, italic highlight). Lys-347 and Lys-349 showed variable SETA incorporation. But considering the high solvent accessibility of these two residues in the dimeric crystal structure as compared to their more buried locations in the monomeric structure, the SETA trend is more consistent with the latter structure.

Despite having certain variability, the analysis suggests domain C exists in monomeric form in solution, and the primary protein dimerization interface is not located within this region.

5.3.11 Protein–protein interactions of PARP-1 domains

Domain C of PARP-1 has been shown to be important for DNA-dependent PARP-1 activation (*187-189*). Since domain C is likely not the dimerization platform for PARP-1 activation (Section 5.3.10), it is hypothesized that protein–protein interaction exists between domain C and other domains to facilitate catalysis. To probe this potential noncovalent interaction, a chemical crosslinking assay using BS^3 as the crosslinker was performed. The expected outcome was to see if there is any distinct band after crosslinking that correspond to full-length PARP-1 or other multimeric structures (dimer, trimer…etc.). Either calf thymus DNA or an 8-mer double-strand blunt end DNA was included in the reactions. BSA was used as a positive control that shows a higher molecular weight band matching with a dimeric structure (~132 kDa). Excess amount of BS^3 was used to detect the trend of chemical crosslinking.

The SDS-PAGE gels of these crosslinking reactions are shown in Figure 5-12. In the presence of 20-fold molar excess of BS^3, reactions containing ABDEF showed significant smear above its original molecular weight (lanes 9–12). PARP-1 displayed similar phenomenon (lane 13). For the positive control, BSA had a major band around 120 kDa, corresponding to the dimeric structure (lane 14) (*303*). Domain C alone did not have a smear distribution, perhaps due to the low concentration of the protein. Reactions containing both domain C and ABDEF did not have a distinct band corresponding to the molecular weight of full-length PARP-1, or any multimeric structures (lanes 10–12). Addition of DNA did not have observable effect on the smear (lanes 11 and 12). Similar results were observed for reaction treated with 50-fold and 100-fold molar excess of BS^3 reagent (Figure 5-2B), with more protein smear and reduced intensities for protein bands of their original molecular weights. Interestingly, a distinct band with molecular weight higher than 116 kDa (Figure 5-12B, lane 13, arrow) can be seen for PARP-1 under 1 mM

BS^3 treatment. This band could be a dimeric form of PARP-1, although a clearer protein resolution and other analytical methods are needed to confirm the identity of this band. Proteins after crosslinking were also detected by immunoblotting using anti-PARP-1 antibody which recognizes both the automodification and the catalytic domain of PARP-1. However, the signals were too strong and had a large smear all over the gel lanes which prevent further interpretation of the results (data not shown). In short, the chemical crosslinking assay did not provide enough evidence to verify that domain C and ABDEF form a specific protein complex which is catalytically competent. However, protein–protein interactions do exist among PARP-1 domains, and a possible dimeric structure of full-length PARP-1 could support the mechanism of its macromolecular association during catalysis.

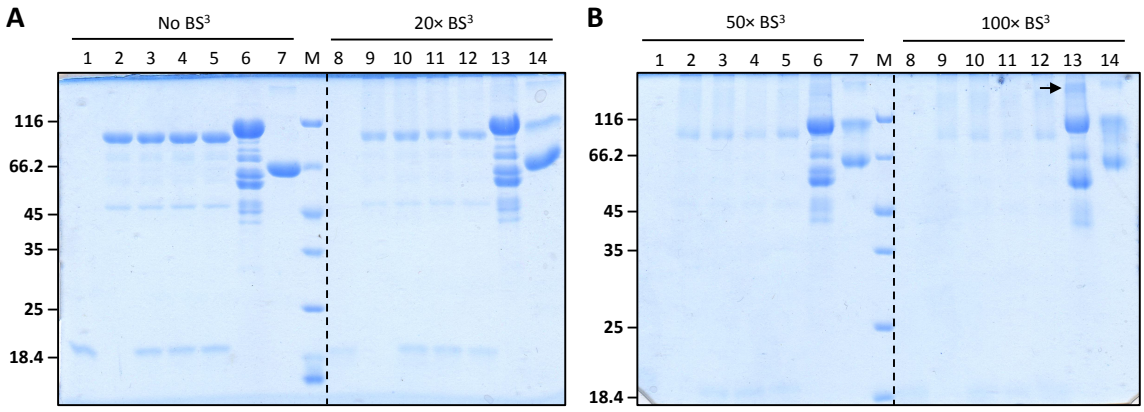

Figure 5-12. Crosslinking assay of PARP-1 domain C and ABDEF. Each protein (10 μM) was incubated in the phosphate buffer containing specific amount of crosslinking reagent BS^3 with or without 20 μM DNA. Lanes 1 and 8, domain C; lanes 2 and 9, ABDEF; lanes 3 and 10, C+ABDEF; lanes 4 and 11, C+ABDEF+calf thymus DNA; lanes 5 and 12, C+ABDEF+8-mer DNA; lanes 6 and 13, PARP-1; lanes 7 and 14, BSA. M, molecular weight marker.

5.4 DISCUSSION

5.4.1 Poly(ADP-ribosyl)ation activity can be reconstituted by PARP-1 ABC and DEF domains *in trans*

PARP-1 catalyzes auto-poly(ADP-ribosyl)ation in the presence of DNA. Unlike typical transferase-catalyzed reactions where enzymes and substrates are of different sizes, one major obstacle to study this auto-catalytic process is to distinguish between the enzyme and the substrate, both are the same species and thus have the same molecular weight. Fortunately, PARP-1 is a modular protein composed of six subdomains. It has been demonstrated that these domains do not necessarily have to be in a single polypeptide chain as for the wild-type enzyme to exert activity. For example, deletion of domain C from the full-length PARP-1 drastically reduces the DNA-dependent poly(ADP-ribosyl)ation activity. However, the catalytic activity can be restored by the addition of domain C into reactions containing ABDEF (in the same polypeptide chain), NAD^+, and DNA (*187, 188*). Taking advantage of this complementary feature, another pair of PARP-1 truncated domains, ABC/DEF, was constructed and characterized in detail. The results clearly demonstrate their ability to reconstitute poly(ADP-ribosyl)ation activity *in trans*. The successful combination of truncated PARP-1 domains to reconstitute enzyme activity has allowed the investigation of automodification reaction since the modified proteins can be readily differentiated by size.

Domain ABC (residues 1–373) and DEF (residues 374–1014) represent the DNA-binding domain and the automodification plus catalytic domain, respectively (Figure 1-11). It is known that in the absence of DNA-binding domain, DEF possesses only basal level activity (*201*). Our results showed that the as-purified wild-type DEF from the *E. coli* expression host was already modified with some PAR polymers which could only be detected by anti-PAR immunoblotting (Figure 5-3B, lane 10), but not by Coomassie

staining (Figure 5-3A, lane 10). Similar observation was also made by Dr. Meilan Wu in our laboratory via treating the protein preparation with PARG. In the presence of NAD^+, DEF alone catalyzes elongation of existing PAR polymers rather than initiating new PAR polymers, as evident by the PAR signals concentrated at well and gel interface region (Figure 5-3B, lane 1 and Figure 5-4A, lane 3). Addition of ABC domain stimulates the wild-type enzymatic activity. Consequently, NAD^+ was efficiently consumed and the proteins were poly(ADP-ribosyl)ated (Figure 5-3B, lane 7 and Figure 5-4B, lane 6). Poly(ADP-ribosyl)ation activity of similar magnitude can also be achieved by the addition of full-length PARP-1 which contributes its ABC domain to the existing DEF domain (Figure 5-3B, lane 4 and Figure 5-4A, lanes 5–8), although the effect is not obvious due to the overlapping of poly(ADP-ribosyl)ated PARP-1 and DEF species. Treating the ABC/DEF reaction mixture with PARG reduces the poly(ADP-ribosyl)ated species down to mono-ADP-ribosylated ones, which have recognizable bands on SDS-PAGE gels with defined molecular weight (Figure 5-6B, lane 13). These results demonstrate that ABC and DEF are capable of reconstituting poly(ADP-ribosyl)ation activity and set the stage for the development of a mix-and-match strategy to characterize PARP-1 automodification reaction products generated from size-distinguishable yet activity-complementary protein constructs.

5.4.2 The enzymatic and the substrate aspects of PARP-1 are separable

The challenge to study PARP-1 automodification reaction is to separate the enzymatic activity from its ability to serve as a substrate. Deletion and site-directed mutagenesis are two common ways to alter biochemical properties of the enzyme. The goal is to construct a mutant which can only serve as either an enzyme or a substrate, but

not both. These mutants, together with the wild-type enzymes, would facilitate the interpretation of experimental results because the role of enzyme and the role of substrate are clearly separated.

For typical enzymes catalyzing posttranslational modification reactions such as phosphorylation or acetylation, it is common that the location of the amino acid residues being modified are known, and the number is few and fixed. In contrast, Glu, Asp, or Lys residues found on the loop structures of PARP-1 are all possible acceptors for PAR polymers (*73*). The reported number of automodification sites of PARP-1 already exceeds ninety, and not all the residues are modified on the same protein (*295*). The wide distribution of automodification sites on PARP-1 prevents the generation of a "polymer-free" mutant by mutating every possible residue. Therefore, the only possible method to overcome this limitation is to construct a dominant-negative PARP-1 mutant devoid of enzymatic activity, while still capable of serving as a substrate.

Random mutagenesis studies of PARP-1 have revealed the importance of several amino acid residues in catalysis (*246, 252, 302*). Four mutations, M890V, K893I, D899N, and E988A, which are close to the enzyme active site, were selected based on the impaired activity of PARP-1 carrying either one of these mutations. From a structural point of view, Met-890, Lys-893, and Asp-899 may be important for the correct folding of the NAD^+-binding pocket, whereas Glu-988 is the catalytic base to facilitate the cleavage of the nicotinamide–ribose glycosidic bond (Figure 5-1). These mutations could impede the processing of NAD^+ during catalysis without pertubing other part of the enzyme.

The mutations were first introduced into the 71-kDa DEF construct. The ke-DEF mutant protein was always co-purified with several smaller protein contaminants (Figure 5-2, lane 4), suggesting the mutations may cause instability of the protein. When

incubating with NAD^+, ke-DEF did not show any poly(ADP-ribosyl)ation signals as judged from anti-PAR Western blot (Figure 5-3, lane 2). However, in the presence of ABC, DNA, and ^{32}P-NAD^+, radioactive signals were detected by autoradiography, displaying a pattern which corresponds to the protein bands of ke-DEF used in the reaction (Figure 5-4B, lanes 9–13). This finding suggests that ke-DEF, despite having no poly(ADP-ribosyl)ation activity, is still capable of catalyzing mono-ADP-ribosylation reaction. It also underscores the usefulness of radioactivity-based assay over anti-PAR immunoblotting to accurately describe reactions involving the cleavage of the nicotinamide–ribose glycosidic bond, whether it is PAR polymer initiation, elongation, or NAD^+ hydrolysis.

The observed residual activity of ke-DEF prompted the search for a completely inactive mutant. Consequently, mkde-DEF, which has all four mutations, was constructed. When ABC was added to the reaction, mkde-DEF did not show any radioactive signal on the gel (Figure 5-5A, lanes 3–6), suggesting the mutant should be completely inactive. But the protein itself was severely degraded since no band with the correct 71-kDa was discernible on SDSP-PAGE gel (Figure 5-2, lane 3). This result poses a caveat that disrupting the catalytic activity of PARP-1 domains may concomitantly result in protein degradation which complicates the interpretation of the experimental data.

To reach a compromise between inactivating the enzyme and maintaining protein stability, two more mutants, mde-DEF and de-DEF were constructed. It was hoped that these mutants may be more stable by restoring three hydrogen bonding interactions associated with Lys-893. The purity of mde-DEF and de-DEF were fair with the recognizable 71-kDa band (Figure 5-2, lanes 1 and 2). Both proteins were inactive in the presence of ABC, DNA and ^{32}P-NAD^+, and the amount of NAD^+ remained comparable to

the control (Figure 5-6A and Figure 5-8A, lanes 2–4). These data demonstrate that mde-DEF and de-DEF may be useful for the mix-and-match poly(ADP-ribosyl)ation assay as DEF is distinguishable from the full-length PARP-1 protein.

To confirm these mutations when introduced into full-length PARP-1 can also inactivate enzyme activity, equivalent mutants mkde-PARP, mde-PARP, and de-PARP were created. Only de-PARP had a correct band around 116 kDa (Figure 5-2, lane 7), whereas mde-PARP (Figure 5-2, lane 8) and mkde-PARP (Figure 5-2, lane 10) were severely degraded. Nevertheless, all proteins were still pooled and used in the experiments to see their effects on NAD^+ hydrolysis to gain additional information of the catalysis.

In short, efforts were devoted to dissecting the enzymatic activity and the substrate capacity within the same PARP-1 molecule. Dominant-negative mutants devoid of catalytic activity were successfully prepared for DEF domain and full-length PARP-1. These materials enable the subsequent study of macromolecular mechanism of DNA-dependent PARP-1 automodification reaction.

5.4.3 Intermolecular mechanism of DNA-dependent PARP-1 automodification reaction

PARP-1 automodification reaction has been considered to be an intermolecular process largely based on the kinetic study done by Alvarez-Gonzalez *et al*. in 1993 (*239*). However, their argument that PARP-1 forms a catalytic dimer based on the quadratic fitting of the initial rate data as a function of enzyme concentration does not provide molecular details of how the catalysis proceeds. If dimerization or multimerization of PARP-1 is required for its activation, a mechanism of intramolecular automodification would follow the same nonlinear concentration dependence. Likewise, if PARP-1 prefers

to form an active dimer in the presence of DNA, a linear relationship between the activity and enzyme concentration will be observed regardless of automodification being an intra- or intermolecular process. Since the activation step cannot be separated from the automodification step, the kinetic analysis of poly(ADP-ribosyl)ation as a function of PARP-1 concentration cannot be used to distinguish between an intermolecular or intramolecular mechanism.

Presented here are the results of a mix-and-match poly(ADP-ribosyl)ation assay aimed at providing biochemical evidence to unravel the mechanistic details of this reaction. mde-DEF was unable to catalyze ADP-ribosylation reaction when incubating with ABC (Figure 5-6A, lanes 2–4). But when titrating mde-DEF into reactions containing PARP-1, a decrease of overall poly(ADP-ribosyl)ated species was observed, and the consumption of NAD^+ was also reduced (Figure 5-6B, lanes 2–6). Treating the reaction mixtures with PARG revealed a protein band corresponding to mde-DEF with greater intensity than the untreated samples (Figure 5-6B, lane 8–11). Interestingly, the highest band intensity of mde-DEF was still much weaker than 1 μM PARP-1, even though the concentration of mde-DEF was 25 μM. This result clearly shows that mde-DEF can be poly(ADP-ribosyl)ated by wild-type PARP-1, which must be an intermolecular process. It also is suggests that mde-DEF competes with the activated PARP-1 molecules for poly(ADP-ribosyl)ation. The inability of mde-DEF to turnover NAD^+ may lead to reduced level of poly(ADP-ribosyl)ated species.

Similar trend was also observed for reactions containing de-DEF and PARP-1. de-DEF was clearly modified by PARP-1, and the extent of its modification was much weaker than PARP-1. The only difference is that NAD^+ was depleted in every reaction, and there was no inhibitory effect on overall poly(ADP-ribosyl)ation as the concentration of de-DEF increases. The explanation to this observation could be that de-DEF does not

bind to NAD^+ as efficiently as mde-DEF, thereby having minimal effect on the turnover of NAD^+. Another possibility is that the protein preparation of de-DEF contains much degradation products, resulting in over-estimation of de-DEF concentration to show inhibitory effect. Altogether, catalytically inactive mutants mde-DEF and de-DEF can be poly(ADP-ribosyl)ated in the presence of wild-type PARP-1. The reaction is not catalyzed by the assistance of ABC domain from PARP-1 to form a pseudo-ABC/DEF mutants complex (Figure 5-6A and 5-8A). Instead, it proceeds in an intermolecular process which PARP-1 poly(ADP-ribosyl)ates DEF mutants.

To test whether the intermolecular process also holds true for full-length PARP-1, mde-PARP and de-PARP were purified and incubated with wild-type DEF. Indeed, when present in a 1:1 ratio, de-PARP can be seen to be modified by DEF as shown in smear or as a clear band after PARG treatment (Figure 5-9, lanes 6 and 10). The lack of the 113-kDa major band of mde-PARP made it difficult to draw conclusion that the modification of mde-PARP is catalyzed by DEF. But a strong smear did appear when mixing with DEF in equimolar ratio (Figure 5-7, lanes 6 and 10). When both mutants were added in excess amount, the overall poly(ADP-ribosyl)ation signals decreased, and the pattern shift toward more like DEF alone in the absence of ABC where signals are concentrated at the well and gel interface region (Figure 5-7 and 5-9, lanes 7 and 8). This observation is consistent with the notion that full-length PARP-1 mutant forming a "dead complex," leaving wild-type DEF alone in the solution.

Taken together, the observation that a PARP-1 inactive mutant is able to be poly(ADP-ribosyl)ated by another active PARP-1 molecule is in agreement with the model that PARP-1 automodification proceeds via an intermolecular process. Although the experimental data presented here cannot rule out the possibility of an intramolecular mechanism utilized by PARP-1 during catalysis, it is difficult to rationalize the fact that

multiple automodification sites exist beyond domain D (*73, 112, 194, 195, 295*), which is in close proximity to the enzyme active site based on the monomeric, near full-length PARP-1 crystal structure (*200*). PARP-1 domains have also been shown to be able to bind PAR polymers noncovalently (*188*). Thus, it is possible that noncovalent PAR–protein interaction would be a common feature to recruit substrates more favorable to be poly(ADP-ribosyl)ated, and is important for the oligomerization of PARP-1.

The inhibitory effect on poly(ADP-ribosyl)ation due to the presence of excess amount of mutant proteins also implies that full-length PARP-1 prefers interacting with full-length PARP-1 rather than DEF, and the intermolecular modification process could be disrupted when other protein constructs alike (e.g., DEF) can compete with full-length PARP-1. In the case of mutant DEF and wild-type PARP-1, excess amount of mutant DEF outcompetes PARP-1 and the overall poly(ADP-ribosyl)ation decreases. Similarly, when excess amount of mutant PARP-1 is added into wild-type DEF, the mutant PARP-1 prefers to associate with itself and form a dead complex which is catalytically inactive, and prevent its intact ABC domain from interacting with DEF, thereby reducing the level of active "PARP complex." Characterization of such protein–protein interactions could be challenging, but may provide significant insight into this complicated catalytic process.

In conclusion, the data presented here support the model of intermolecular mechanism during DNA-dependent PARP-1 automodification reaction (Figure 1-13). Oligomerization of PARP-1, either mediated by the protein itself or in the presence of DNA, or PAR polymers, is consistent with the observation of the change in poly(ADP-ribosyl)ation, but definitive evidence awaits further investigation.

5.4.4 The role of domain C during PARP-1 catalysis

The function of domain C of PARP-1 has remained elusive for a long time. It resides within *C*-terminus of the DNA-binding domain identified by proteolytic digestion in the early 80s (*178*), and has no sequence homology to any other known domain. It was until recent structural studies that began to shed light on the role of this domain during catalysis (*187, 188*). The addition of domain C into the ABDEF deletion mutant restores its DNA-dependent poly(ADP-ribosyl)ation activity. This special property is presumably mediated by protein–protein interactions involving domain C and other parts of PARP-1 molecule. Given the fact that discrepancy exists between two structural studies (monomeric vs. dimeric), and the prevailed model of functional PARP-1 being an homodimer, it is of great interest to further examine the structural feature of domain C in solution and to probe the potential protein–protein interactions.

In collaboration with Dr. Brodbelt's lab in the Department of Chemistry, an UVPD-MS-based methodology was developed to evaluate the conformational change of domain C in solution upon denaturation. The feature of this MS technique is to use ultraviolet light for the generation of fragmented peptide ions from the whole protein without protease digestion. One major challenge for protein mass specetrometry is to produce large amount of fragmented peptide ions that cover as much protein sequence as possible. The more fragments are produced and detected by the instrument, the more information of the protein sequence can be mapped, including posttranslational modifications or any kinds of mass difference. The size of domain C is about 16 kDa, which is suitable for this top-down protein MS analysis.

To obtain structural information of domain C, the protein was first denatured using buffers containing different percentage of acetonitrile. After differential denaturation, the protein was then labeled with a small molecule probe "SETA" which

specifically reacts with primary amino groups. Only free, exposed to solvent, and deprotonated amino groups are able to react with SETA. After the reaction, the protein was subject to UVPD-MS analysis directly without protease digestion. Since the modification of specific lysine group by SETA creates a mass difference of 41 Da, MS/MS analysis can locate the modification site accurately. By examination of the total ion spectra, the SETA incorporation value S.I. for each lysine residue can be calculated. Each S.I. value reflects the local environment of specific lysine residue, and the change in S.I. value can be correlated to potential conformational change. The trend of the S.I. values of the lysine residues within a.a. 331–359 pointed toward a more exposed, solvent-accessible environment upon denaturation (Figure 5-10). This result suggests that the native conformation of domain C is more compact, in agreement with the monomeric structure observed in solution NMR experiment (Figure 5-11). Furthermore, site-directed mutagenesis of the amino acid residues involving dimerization interactions based on the crystal structure did not alter the mutant PARP-1's catalytic activity (*189*). In the near full-length PARP-1 crystal structure in complex with a blunt-end DNA, domain C (or FIII) exists in a position where dimerization is impossible to take place (*200*). These results are more consistent with domain C in a monomeric form in solution, and the potential dimerization interface does not lie within domain C.

Instead of self-dimerization, domain C may also interact with other segments of PARP-1 molecule. To investigate this protein–protein interaction, a chemical crosslinking assay of domain C and ABDEF was performed using BS^3 as the chemical crosslinker. BS^3 contains two *N*-hydroxylsulfosuccinimide (NHS) ester moieties which are reactive toward free amino groups. In the presence of 20-fold excess of BS^3 (200 μM), domain C did not crosslink to ABDEF to form a well-defined molecule with a molecular weight about 116 kDa. Rather, ABDEF showed a smear above its original

molecular weight on the SDS-PAGE gel, similar to the effect of protein poly(ADP-ribosyl)ation (Figure 5-12). The inclusion of DNA in the reactions did not have significant difference. Similar results were obtained for reactions using 50-fold or 100-fold BS^3. The aggregate formation of ABDEF was confirmed by anti-PARP immunoblot which recognizes the *C*-terminal portion of the protein. Noticeably, a relatively distinct band appeared in the PARP-1 control reactions using 100-fold BS^3 (Figure 5-12B, lane 13, arrow). The band is consistent with the species being a PARP-1 dimer, but the identity needs further verification. Except for this, chemical crosslinking assay of PARP-1 domains failed to provide clean evidence for the existence of C/ABDEF protein complex, but interdomain interactions are likely, despite being weak and transient. In addition, domain C may also interact with PAR polymers noncovalently (*188*), which may facilitate the correct orientation of PARP-1 domains poised for polymer elongation or branching.

Appendix

^{1}H NMR spectrum for 2NF-NAD^{+}

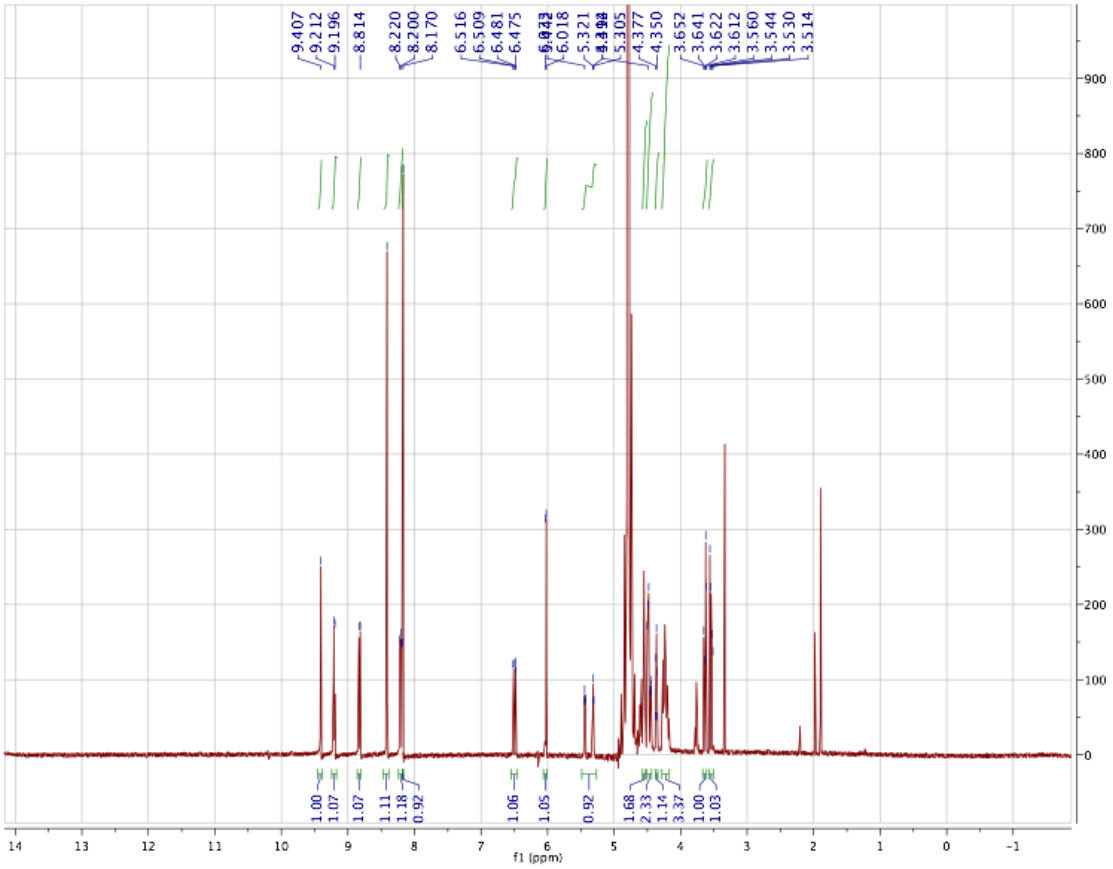

^{19}F NMR spectrum for 2NF-NAD^{+}

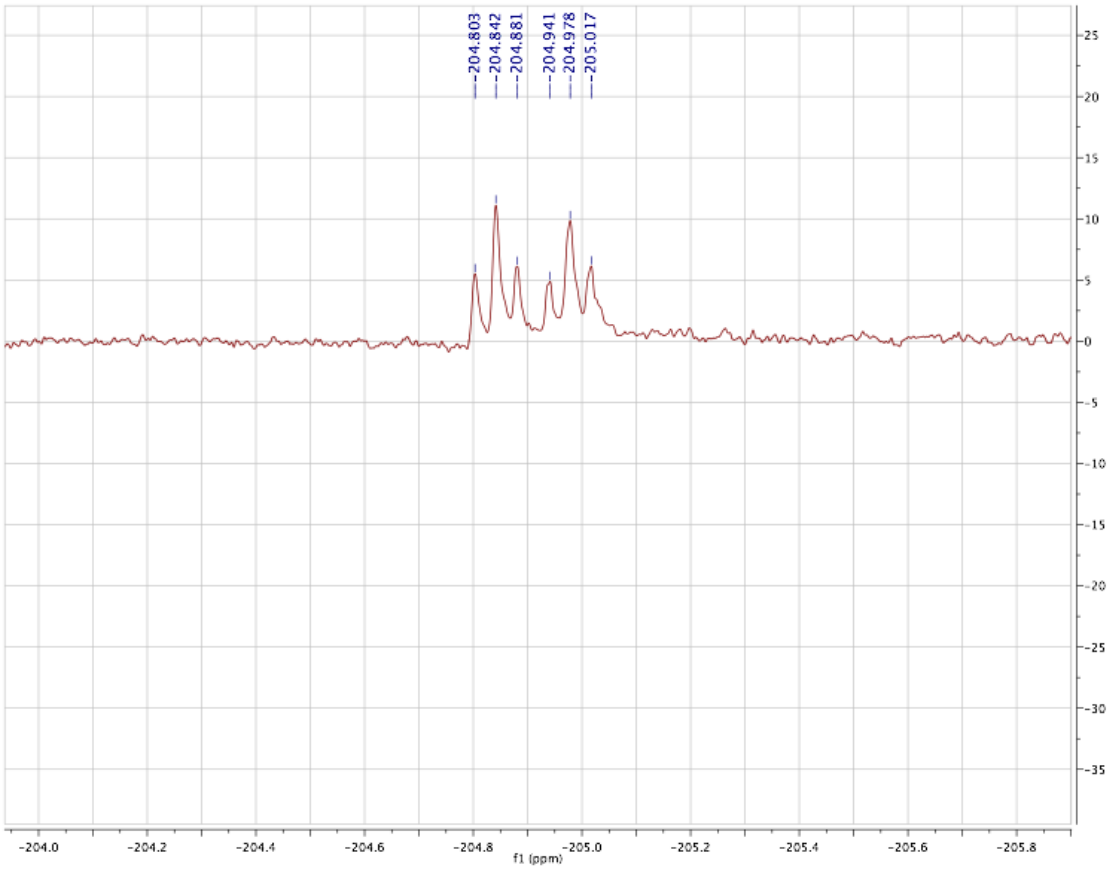

^{31}P NMR spectrum for 2NF-NAD^{+}

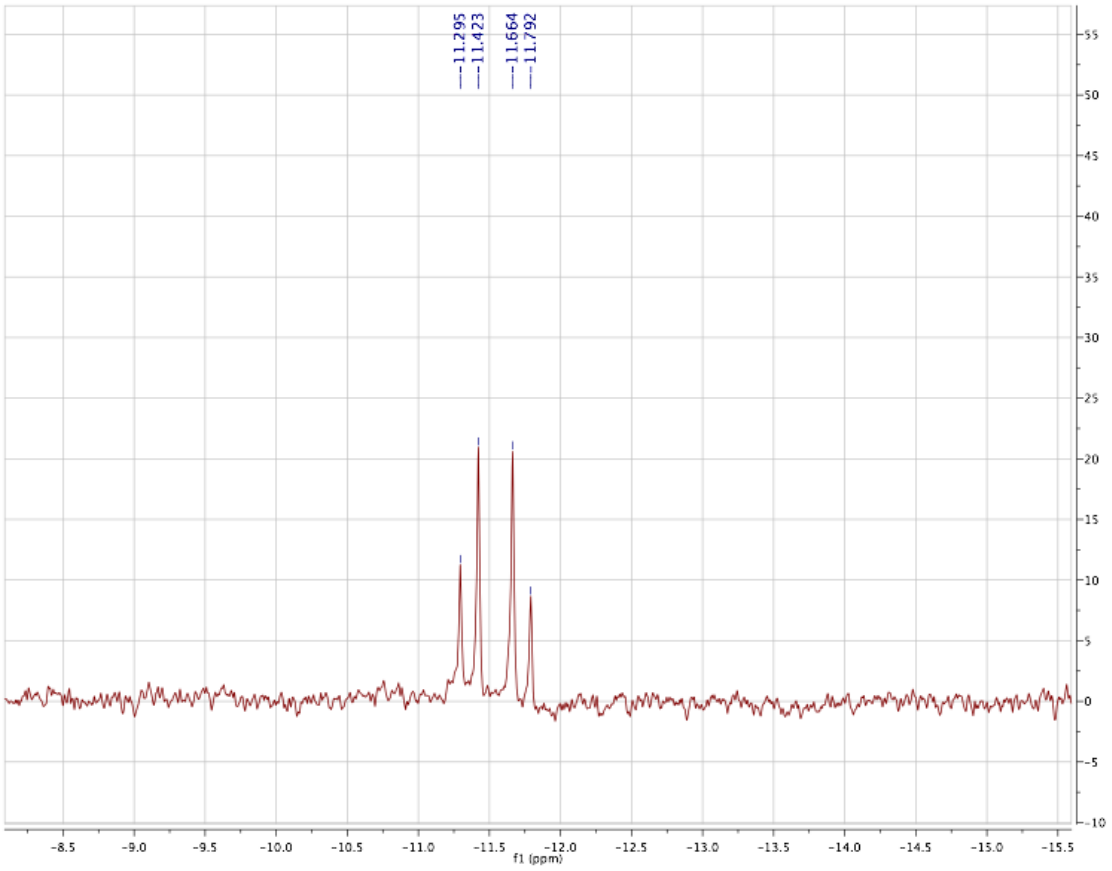

ESI-MS spectrum for 2NF-NAD$^+$

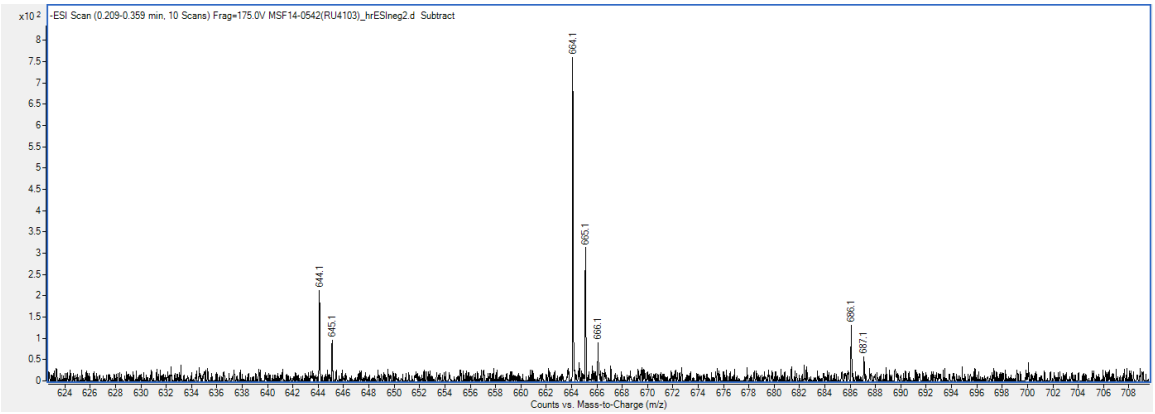

References

1. Berger, F.; Ramirez-Hernandez, M. H.; Ziegler, M. The new life of a centenarian: signalling functions of NAD(P). *Trends Biochem. Sci.* **2004,** *29*, 111-118.
2. Doherty, A. J.; Suh, S. W. Structural and mechanistic conservation in DNA ligases. *Nucleic Acids Res.* **2000,** *28*, 4051-4058.
3. Hottiger, M. O.; Hassa, P. O.; Luscher, B.; Schuler, H.; Koch-Nolte, F. Toward a unified nomenclature for mammalian ADP-ribosyltransferases. *Trends Biochem. Sci.* **2010,** *35*, 208-219.
4. Lin, H. Nicotinamide adenine dinucleotide: beyond a redox coenzyme. *Org. Biomol. Chem.* **2007,** *5*, 2541-2554.
5. D'amours, D.; Desnoyers, S.; D'Silva, I.; Poirier, G. G. Poly(ADP-ribosyl)ation reactions in the regulation of nuclear functions. *Biochem. J.* **1999,** *342*, 249-268.
6. Bürkle, A. Physiology and pathophysiology of poly(ADP-ribosyl)ation. *Bioessays* **2001,** *23*, 795-806.
7. Ame, J. C.; Spenlehauer, C.; de Murcia, G. The PARP superfamily. *Bioessays* **2004,** *26*, 882-893.
8. Hassa, P. O.; Haenni, S. S.; Elser, M.; Hottiger, M. O. Nuclear ADP-ribosylation reactions in mammalian cells: where are we today and where are we going? *Microbiol. Mol. Biol. Rev.* **2006,** *70*, 789-829.
9. Hassa, P. O.; Hottiger, M. O. The diverse biological roles of mammalian PARPs, a small but powerful family of poly-ADP-ribose polymerases. *Front. Biosci.* **2008,** *13*, 3046-3082.
10. Corda, D.; Di Girolamo, M. Functional aspects of protein mono-ADP-ribosylation. *EMBO J.* **2003,** *22*, 1953-1958.
11. Sauve, A. A.; Wolberger, C.; Schramm, V. L.; Boeke, J. D. The biochemistry of sirtuins. *Annu. Rev. Biochem.* **2006,** *75*, 435-465.
12. Altmeyer, M.; Messner, S.; Hassa, P. O.; Fey, M.; Hottiger, M. O. Molecular mechanism of poly(ADP-ribosyl)ation by PARP1 and identification of lysine residues as ADP-ribose acceptor sites. *Nucleic Acids Res.* **2009,** *37*, 3723-3738.
13. Messner, S.; Altmeyer, M.; Zhao, H.; Pozivil, A.; Roschitzki, B.; Gehrig, P.; Rutishauser, D.; Huang, D.; Caflisch, A.; Hottiger, M. O. PARP1 ADP-ribosylates lysine residues of the core histone tails. *Nucleic Acids Res.* **2010,** *38*, 6350-6362.
14. Hakme, A.; Wong, H. K.; Dantzer, F.; Schreiber, V. The expanding field of poly(ADP-ribosyl)ation reactions. *EMBO Rep.* **2008,** *9*, 1094-1100.

15. Gibson, B. A.; Kraus, W. L. New insights into the molecular and cellular functions of poly(ADP-ribose) and PARPs. *Nat. Rev. Mol. Cell Bio.* **2012,** *13*, 411-424.

16. Walsh, C. T.; Garneau-Tsodikova, S.; Gatto, G. J., Jr. Protein posttranslational modifications: the chemistry of proteome diversifications. *Angew. Chem. Int. Ed.* **2005,** *44*, 7342-7372.

17. Collier, R. J. Diphtheria toxin: mode of action and structure. *Bacteriol. Rev.* **1975,** *39*, 54-85.

18. Koch-Nolte, F.; Kernstock, S.; Mueller-Dieckmann, C.; Weiss, M. S.; Haag, F. Mammalian ADP-ribosyltransferases and ADP-ribosylhydrolases. *Front. Biosci.* **2008,** *13*, 6716-6729.

19. Glowacki, G.; Braren, R.; Firner, K.; Nissen, M.; Kuhl, M.; Reche, P.; Bazan, F.; Cetkovic-Cvrlje, M.; Leiter, E.; Haag, F.; Koch-Nolte, F. The family of toxin-related ecto-ADP-ribosyltransferases in humans and the mouse. *Protein Sci.* **2002,** *11*, 1657-1670.

20. Frye, R. A. Phylogenetic classification of prokaryotic and eukaryotic Sir2-like proteins. *Biochem. Biophys. Res. Commun.* **2000,** *273*, 793-798.

21. Otto, H.; Reche, P. A.; Bazan, F.; Dittmar, K.; Haag, F.; Koch-Nolte, F. In silico characterization of the family of PARP-like poly(ADP-ribosyl)transferases (pARTs). *BMC Genomics* **2005,** *6*, 139.

22. Choudhary, C.; Kumar, C.; Gnad, F.; Nielsen, M. L.; Rehman, M.; Walther, T. C.; Olsen, J. V.; Mann, M. Lysine acetylation targets protein complexes and co-regulates major cellular functions. *Science* **2009,** *325*, 834-840.

23. Zhao, S.; Xu, W.; Jiang, W.; Yu, W.; Lin, Y.; Zhang, T.; Yao, J.; Zhou, L.; Zeng, Y.; Li, H.; Li, Y.; Shi, J.; An, W.; Hancock, S. M.; He, F.; Qin, L.; Chin, J.; Yang, P.; Chen, X.; Lei, Q.; Xiong, Y.; Guan, K. L. Regulation of cellular metabolism by protein lysine acetylation. *Science* **2010,** *327*, 1000-1004.

24. Grozinger, C. M.; Schreiber, S. L. Deacetylase enzymes: biological functions and the use of small-molecule inhibitors. *Chem. Biol.* **2002,** *9*, 3-16.

25. Houtkooper, R. H.; Pirinen, E.; Auwerx, J. Sirtuins as regulators of metabolism and healthspan. *Nat. Rev. Mol. Cell Biol.* **2012,** *13*, 225-238.

26. Du, J.; Jiang, H.; Lin, H. Investigating the ADP-ribosyltransferase activity of sirtuins with NAD analogues and ^{32}P-NAD. *Biochemistry* **2009,** *48*, 2878-2890.

27. Du, J.; Zhou, Y.; Su, X.; Yu, J. J.; Khan, S.; Jiang, H.; Kim, J.; Woo, J.; Kim, J. H.; Choi, B. H.; He, B.; Chen, W.; Zhang, S.; Cerione, R. A.; Auwerx, J.; Hao, Q.; Lin, H. SIRT5 is a NAD-dependent protein lysine demalonylase and desuccinylase. *Science* **2011,** *334*, 806-809.

28. Jiang, H.; Khan, S.; Wang, Y.; Charron, G.; He, B.; Sebastian, C.; Du, J.; Kim, R.; Ge, E.; Mostoslavsky, R.; Hang, H. C.; Hao, Q.; Lin, H. SIRT6 regulates TNF-alpha secretion through hydrolysis of long-chain fatty acyl lysine. *Nature* **2013,** *496*, 110-113.

29. Spinelli, S. L.; Consaul, S. A.; Phizicky, E. M. A conditional lethal yeast phosphotransferase (tpt1) mutant accumulates tRNAs with a 2′-phosphate and an undermodified base at the splice junction. *RNA* **1997,** *3*, 1388-1400.

30. Culver, G. M.; McCraith, S. M.; Consaul, S. A.; Stanford, D. R.; Phizicky, E. M. A 2′-phosphotransferase implicated in tRNA splicing is essential in *Saccharomyces cerevisiae*. *J. Biol. Chem.* **1997,** *272*, 13203-13210.

31. Spinelli, S. L.; Kierzek, R.; Turner, D. H.; Phizicky, E. M. Transient ADP-ribosylation of a 2′-phosphate implicated in its removal from ligated tRNA during splicing in yeast. *J. Biol. Chem.* **1999,** *274*, 2637-2644.

32. Steiger, M. A.; Jackman, J. E.; Phizicky, E. M. Analysis of 2′-phosphotransferase (Tpt1p) from *Saccharomyces cerevisiae*: Evidence for a conserved two-step reaction mechanism. *RNA* **2005,** *11*, 99-106.

33. Takamura-Enya, T.; Watanabe, M.; Totsuka, Y.; Kanazawa, T.; Matsushima-Hibiya, Y.; Koyama, K.; Sugimura, T.; Wakabayashi, K. Mono(ADP-ribosyl)ation of 2′-deoxyguanosine residue in DNA by an apoptosis-inducing protein, pierisin-1, from cabbage butterfly. *Proc. Natl. Acad. Sci. U.S.A.* **2001,** *98*, 12414-12419.

34. Nakano, T.; Matsushima-Hibiya, Y.; Yamamoto, M.; Enomoto, S.; Matsumoto, Y.; Totsuka, Y.; Watanabe, M.; Sugimura, T.; Wakabayashi, K. Purification and molecular cloning of a DNA ADP-ribosylating protein, CARP-1, from the edible clam *Meretrix lamarckii*. *Proc. Natl. Acad. Sci. U.S.A.* **2006,** *103*, 13652-13657.

35. Nakano, T.; Matsushima-Hibiya, Y.; Yamamoto, M.; Takahashi-Nakaguchi, A.; Fukuda, H.; Ono, M.; Takamura-Enya, T.; Kinashi, H.; Totsuka, Y. ADP-ribosylation of guanosine by SCO5461 protein secreted from *Streptomyces coelicolor*. *Toxicon* **2013,** *63*, 55-63.

36. Crofts, T. S.; Seth, E. C.; Hazra, A. B.; Taga, M. E. Cobamide structure depends on both lower ligand availability and CobT substrate specificity. *Chem. Biol.* **2013,** *20*, 1265-1274.

37. Hazra, A. B.; Tran, J. L.; Crofts, T. S.; Taga, M. E. Analysis of substrate specificity in CobT homologs reveals widespread preference for DMB, the lower axial ligand of vitamin B_{12}. *Chem. Biol.* **2013,** *20*, 1275-1285.

38. Baysarowich, J.; Koteva, K.; Hughes, D. W.; Ejim, L.; Griffiths, E.; Zhang, K.; Junop, M.; Wright, G. D. Rifamycin antibiotic resistance by ADP-ribosylation:

Structure and diversity of Arr. *Proc. Natl. Acad. Sci. U.S.A.* **2008,** *105*, 4886-4891.

39. Malavasi, F.; Deaglio, S.; Funaro, A.; Ferrero, E.; Horenstein, A. L.; Ortolan, E.; Vaisitti, T.; Aydin, S. Evolution and function of the ADP ribosyl cyclase/CD38 gene family in physiology and pathology. *Physiol. Rev.* **2008,** *88*, 841-886.

40. Maggio-Hall, L. A.; Escalante-Semerena, J. C. α-5,6-dimethylbenzimidazole adenine dinucleotide (α-DAD), a putative new intermediate of coenzyme B_{12} biosynthesis in *Salmonella typhimurium*. *Microbiology* **2003,** *149*, 983-990.

41. Lee, H. C.; Aarhus, R. ADP-ribosyl cyclase: An enzyme that cyclizes NAD^+ into a calcium-mobilizing metabolite. *Cell Regul.* **1991,** *2*, 203-209.

42. Albrieux, M.; Lee, H. C.; Villaz, M. Calcium signaling by cyclic ADP-ribose, NAADP, and inositol trisphosphate are involved in distinct functions in ascidian oocytes. *J. Biol. Chem.* **1998,** *273*, 14566-14574.

43. Guse, A. H. Biochemistry, biology, and pharmacology of cyclic adenosine diphosphoribose (cADPR). *Curr. Med. Chem.* **2004,** *11*, 847-855.

44. Chambon, P.; Mandel, P.; Weill, J. D. Nicotinamide mononucleotide activation of a new DNA-dependent polyadenylic acid synthesizing nuclear enzyme. *Biochem. Biophys. Res. Commun.* **1963,** *11*, 39-43.

45. Sugimura, T.; Miwa, M. Poly(ADP-ribose): Historical perspective. *Mol. Cell. Biochem.* **1994,** *138*, 5-12.

46. Chambon, P.; Weill, J. D.; Doly, J.; Strosser, M. T.; Mandel, P. On formation of a novel adenylic compound by enzymatic extracts of liver nuclei. *Biochem. Biophys. Res. Commun.* **1966,** *25*, 638-643.

47. Nishizuk.Y; Ueda, K.; Nakazawa, K.; Hayaishi, O. Studies on polymer of adenosine diphosphate ribose. I. Enzymic formation from nicotinamide adenine dinucleotide in mammalian nuclei. *J. Biol. Chem.* **1967,** *242*, 3164-3171.

48. Reeder, R. H.; Ueda, K.; Honjo, T.; Nishizuka, Y.; Hayaishi, O. Studies on the polymer of adenosine diphosphate ribose. II. Characterization of the polymer. *J. Biol. Chem.* **1967,** *242*, 3172-3179.

49. Fujimura, S.; Hasegawa, S.; Shimizu, Y.; Sugimura, T. Polymerization of adenosine 5′-diphosphate-ribose moiety of nicotinamide-adenine dinucleotide by nuclear enzyme. I. Enzymatic reactions. *Biochim. Biophys. Acta* **1967,** *145*, 247-259.

50. Futai, M.; Mizuno, D.; Sugimura, T. Hydrolysis of polymer formed from NAD with rat liver phosphodiesterase yielding nucleoside 5′-monophosphate. *Biochem. Biophys. Res. Commun.* **1967,** *28*, 395-399.

51. Miwa, M.; Saito, H.; Sakura, H.; Saikawa, N.; Watanabe, F.; Matsushima, T.; Sugimura, T. A ^{13}C NMR-study of poly(adenosine diphosphate ribose) and its monomers: Evidence of α-(1″→2′) ribofuranosyl ribofuranoside residue. *Nucleic Acids Res*. **1977,** *4*, 3997-4006.

52. Ferro, A. M.; Oppenheimer, N. J. Structure of a poly(adenosine diphosphoribose) monomer: 2′-(5″-Phosphoribosyl)-5′-adenosine monophosphate. *Proc. Natl. Acad. Sci. U.S.A.* **1978,** *75*, 809-813.

53. Tanaka, M.; Miwa, M.; Hayashi, K.; Kubota, K.; Matsushima, T. Separation of oligo(adenosine diphosphate ribose) fractions with various chain lengths and terminal structures. *Biochemistry* **1977,** *16*, 1485-1489.

54. Hayaishi, O.; Ueda, K. Poly(ADP-ribose) and ADP-ribosylation of proteins. *Annu. Rev. Biochem*. **1977,** *46*, 95-116.

55. Tanaka, M.; Hayashi, K.; Sakura, H.; Miwa, M.; Matsushima, T.; Sugimura, T. Demonstration of high molecular-weight poly(adenosine diphosphate ribose). *Nucleic Acids Res*. **1978,** *5*, 3183-3194.

56. Miwa, M.; Saikawa, N.; Yamaizumi, Z.; Nishimura, S.; Sugimura, T. Structure of poly(adenosine-diphosphate ribose): Identification of 2′-[1″-ribosyl-2″-(or 3″-)(1‴-ribosyl)]adenosine-5′,5″,5‴-tris(phosphate) as a branch linkage. *Proc. Natl. Acad. Sci. U.S.A.* **1979,** *76*, 595-599.

57. Miwa, M.; Ishihara, M.; Takishima, S.; Takasuka, N.; Maeda, M.; Yamaizumi, Z.; Sugimura, T.; Yokoyama, S.; Miyazawa, T. The branching and linear portions of poly(adenosine diphosphate ribose) have the same α(1→2) ribose-ribose linkage. *J. Biol. Chem*. **1981,** *256*, 2916-2921.

58. De Murcia, G.; Jongstrabilen, J.; Ittel, M. E.; Mandel, P.; Delain, E. Poly(ADP-ribose) polymerase auto-modification and interaction with DNA: Electron-microscopic visualization. *EMBO J*. **1983,** *2*, 543-548.

59. Hayashi, K.; Tanaka, M.; Shimada, T.; Miwa, M.; Sugimura, T. Size and shape of poly(ADP-ribose): Examination by gel-filtration, gel-electrophoresis and electron-microscopy. *Biochem. Biophys. Res. Commun*. **1983,** *112*, 102-107.

60. Kanai, Y.; Miwa, M.; Matsushi.T; Sugimura, T. Studies on anti-poly(adenosine diphosphate ribose) antibody. *Biochem. Biophys. Res. Commun*. **1974,** *59*, 300-306.

61. Minaga, T.; Kun, E. Spectral analysis of the conformation of polyadenosine diphosphoribose: Evidence indicating secondary structure. *J. Biol. Chem*. **1983,** *258*, 725-730.

62. Minaga, T.; Kun, E. Probable helical conformation of poly(ADP-ribose): The effect of cations on spectral properties. *J. Biol. Chem*. **1983,** *258*, 5726-5730.

63. Schultheisz, H. L.; Szymczyna, B. R.; Williamson, J. R. Enzymatic synthesis and structural characterization of ^{13}C, ^{15}N-poly(ADP-ribose). *J. Am. Chem. Soc.* **2009,** *131*, 14571-14578.

64. Alvarez-Gonzalez, R.; Jacobson, M. K. Characterization of polymers of adenosine-diphosphate ribose generated in vitro and in vivo. *Biochemistry* **1987,** *26*, 3218-3224.

65. Nishizuk. Y.; Ueda, K.; Honjo, T.; Hayaishi, O. Enzymic adenosine diphosphate ribosylation of histone and poly adenosine diphosphate ribose synthesis in rat liver nuclei. *J. Biol. Chem.* **1968,** *243*, 3765-3767.

66. Nishizuk. Y.; Ueda, K.; Yoshihara. K.; Yamamura, H.; Takeda, M.; Hayaishi, O. Enzymic adenosine diphosphoribosylation of nuclear proteins. *Cold Spring Harb. Symp. Quant. Biol.* **1969,** *34*, 781-786.

67. Otake, H.; Miwa, M.; Fujimura, S.; Sugimura, T. Binding of ADP-ribose polymer with histone. *J. Biochem.* **1969,** *65*, 145-146.

68. Ueda, K.; Omachi, A.; Kawaichi, M.; Hayaishi, O. Natural occurrence of poly(ADP-ribosyl) histones in rat liver. *Proc. Natl. Acad. Sci. U.S.A.* **1975,** *72*, 205-209.

69. Bredehorst, R.; Wielckens, K.; Gartemann, A.; Lengyel, H.; Klapproth, K.; Hilz, H. Two different types of bonds linking single ADP-ribose residues covalently to proteins: Quantification in eukaryotic cells. *Eur. J. Biochem.* **1978,** *92*, 129-135.

70. Ogata, N.; Ueda, K.; Hayaishi, O. ADP-ribosylation of histone H2B: Identification of glutamic-acid residue 2 as the modification site. *J. Biol. Chem.* **1980,** *255*, 7610-7615.

71. Ogata, N.; Ueda, K.; Kagamiyama, H.; Hayaishi, O. ADP-ribosylation of histone H-1: Identification of glutamic-acid residues 2, 14, and the COOH-terminal lysine residue as modification sites. *J. Biol. Chem.* **1980,** *255*, 7616-7620.

72. Tao, Z. H.; Gao, P.; Liu, H. W. Identification of the ADP-Ribosylation sites in the PARP-1 automodification domain: Analysis and implications. *J. Am. Chem. Soc.* **2009,** *131*, 14258-14260.

73. Daniels, C. M.; Ong, S. E.; Leung, A. K. L. Phosphoproteomic approach to characterize protein mono- and poly(ADP-ribosyl)ation sites from cells. *J. Proteome Res.* **2014,** *13*, 3510-3522.

74. Alvarez-Gonzalez, R.; Althaus, F. R. Poly(ADP-ribose) catabolism in mammalian cells exposed to DNA-damaging Agents. *Mutat. Res.* **1989,** *218*, 67-74.

75. Chiarugi, A.; Dolle, C.; Felici, R.; Ziegler, M. The NAD metabolome: A key determinant of cancer cell biology. *Nat. Rev. Cancer* **2012,** *12*, 741-752.

76. Oka, S.; Kato, J.; Moss, J. Identification and characterization of a mammalian 39-kDa poly(ADP-ribose) glycohydrolase. *J. Biol. Chem.* **2006,** *281*, 705-713.

77. Kurosaki, T.; Ushiro, H.; Mitsuuchi, Y.; Suzuki, S.; Matsuda, M.; Matsuda, Y.; Katunuma, N.; Kangawa, K.; Matsuo, H.; Hirose, T.; Inayama, S.; Shizuta, Y. Primary structure of human poly(ADP-ribose) synthetase as deduced from cDNA sequence. *J. Biol. Chem.* **1987,** *262*, 15990-15997.

78. Shieh, W. M.; Ame, J. C.; Wilson, M. V.; Wang, Z. Q.; Koh, D. W.; Jacobson, M. K.; Jacobson, E. L. Poly(ADP-ribose) polymerase null mouse cells synthesize ADP-ribose polymers. *J. Biol. Chem.* **1998,** *273*, 30069-30072.

79. Ame, J. C.; Rolli, V.; Schreiber, V.; Niedergang, C.; Apiou, F.; Decker, P.; Muller, S.; Hoger, T.; Murcia, J. M. D.; de Murcia, G. PARP-2, a novel mammalian DNA damage-dependent poly(ADP-ribose) polymerase. *J. Biol. Chem.* **1999,** *274*, 17860-17868.

80. Rippmann, J. F.; Damm, K.; Schnapp, A. Functional characterization of the poly(ADP-ribose) polymerase activity of tankyrase 1, a potential regulator of telomere length. *J. Mol. Biol.* **2002,** *323*, 217-224.

81. Sbodio, J. I.; Lodish, H. F.; Chi, N. W. Tankyrase-2 oligomerizes with tankyrase-1 and binds to both TRF1 (telomere-repeat-binding factor 1) and IRAP (insulin-responsive aminopeptidase). *Biochem. J.* **2002,** *361*, 451-459.

82. Vyas, S.; Matic, I.; Uchima, L.; Rood, J.; Zaja, R.; Hay, R. T.; Ahel, I.; Chang, P. Family-wide analysis of poly(ADP-ribose) polymerase activity. *Nat. Commun.* **2014,** *5*.

83. Desmarais, Y.; Menard, L.; Lagueux, J.; Poirier, G. G. Enzymological properties of poly(ADP-ribose) polymerase: Characterization of automodification sites and NADase activity. *Biochim. Biophys. Acta* **1991,** *1078*, 179-186.

84. Ogata, N.; Ueda, K.; Kawaichi, M.; Hayaishi, O. Poly(ADP-ribose) synthetase, a main acceptor of poly(ADP-ribose) in isolated nuclei. *J. Biol. Chem.* **1981,** *256*, 4135-4137.

85. Wielckens, K.; George, E.; Pless, T.; Hilz, H. Stimulation of poly(ADP-ribosyl)ation during Ehrlich ascites tumor cell "starvation" and suppression of concomitant DNA fragmentation by benzamide. *J. Biol. Chem.* **1983,** *258*, 4098-4104.

86. Poirier, G. G.; de Murcia, G.; Jongstrabilen, J.; Niedergang, C.; Mandel, P. Poly(ADP-ribosyl)ation of polynucleosomes causes relaxation of chromatin structure. *Proc. Natl. Acad. Sci. U.S.A.* **1982,** *79*, 3423-3427.

87. Schreiber, V.; Dantzer, F.; Ame, J. C.; de Murcia, G. Poly(ADP-ribose): Novel functions for an old molecule. *Nat. Rev. Mol. Cell Biol.* **2006,** *7*, 517-528.

88. Hakme, A.; Wong, H. K.; Dantzer, F.; Schreiber, V. The expanding field of poly(ADP-ribosyl)ation reactions. *EMBO Rep*. **2008,** *9*, 1094-1100.

89. Leger, K.; Bar, D.; Savic, N.; Santoro, R.; Hottiger, M. O. ARTD2 activity is stimulated by RNA. *Nucleic Acids Res*. **2014,** *42*, 5072-5082.

90. Loseva, O.; Jemth, A. S.; Bryant, H. E.; Schuler, H.; Lehtio, L.; Karlberg, T.; Helleday, T. PARP-3 is a mono-ADP-ribosylase that activates PARP-1 in the absence of DNA. *J. Biol. Chem*. **2010,** *285*, 8054-8060.

91. De Vos, M.; Schreiber, V.; Dantzer, F. The diverse roles and clinical relevance of PARPs in DNA damage repair: Current state of the art. *Biochem. Pharmacol*. **2012,** *84*, 137-146.

92. Smith, S.; Giriat, I.; Schmitt, A.; de Lange, T. Tankyrase, a poly(ADP-ribose) polymerase at human telomeres. *Science* **1998,** *282*, 1484-1487.

93. Kaminker, P. G.; Kim, S. H.; Taylor, R. D.; Zebarjadian, Y.; Funk, W. D.; Morin, G. B.; Yaswen, P.; Campisi, J. TANK2, a new TRF1-associated poly(ADP-ribose) polymerase, causes rapid induction of cell death upon overexpression. *J. Biol. Chem*. **2001,** *276*, 35891-35899.

94. Lord, C. J.; Ashworth, A. The DNA damage response and cancer therapy. *Nature* **2012,** *481*, 287-294.

95. Kleine, H.; Poreba, E.; Lesniewicz, K.; Hassa, P. O.; Hottiger, M. O.; Litchfield, D. W.; Shilton, B. H.; Luscher, B. Substrate-assisted catalysis by PARP10 limits its activity to mono-ADP-ribosylation. *Mol. Cell* **2008,** *32*, 57-69.

96. Verheugd, P.; Forst, A. H.; Milke, L.; Herzog, N.; Feijs, K. L. H.; Kremmer, E.; Kleine, H.; Luscher, B. Regulation of NF-κB signalling by the mono-ADP-ribosyltransferase ARTD10. *Nat. Commun*. **2013,** *4*.

97. Seo, G. J.; Kincaid, R. P.; Phanaksri, T.; Burke, J. M.; Pare, J. M.; Cox, J. E.; Hsiang, T. Y.; Krug, R. M.; Sullivan, C. S. Reciprocal inhibition between intracellular antiviral signaling and the RNAi machinery in mammalian cells. *Cell Host Microbe* **2013,** *14*, 435-445.

98. Feijs, K. L. H.; Forst, A. H.; Verheugd, P.; Luscher, B. Macrodomain-containing proteins: Regulating new intracellular functions of mono(ADP-ribosyl)ation. *Nat. Rev. Mol. Cell Biol*. **2013,** *14*, 443-451.

99. Krietsch, J.; Rouleau, M.; Pic, E.; Ethier, C.; Dawson, T. M.; Dawson, V. L.; Masson, J. Y.; Poirier, G. G.; Gagné, J. P. Reprogramming cellular events by poly(ADP-ribose)-binding proteins. *Mol. Aspects. Med*. **2013,** *34*, 1066-1087.

100. Miwa, M.; Tanaka, M.; Matsushi.T; Sugimura, T. Purification and properties of a glycohydrolase from calf thymus splitting ribose-ribose linkages of poly(adenosine diphosphate ribose). *J. Biol. Chem*. **1974,** *249*, 3475-3482.

101. Davidovic, L.; Vodenicharov, M.; Affar, E. B.; Poirier, G. G. Importance of poly(ADP-ribose) glycohydrolase in the control of poly(ADP-ribose) metabolism. *Exp. Cell Res.* **2001,** *268*, 7-13.

102. Meyer, R. G.; Meyer-Ficca, M. L.; Jacobson, E. L.; Jacobson, M. K. Human poly(ADP-ribose) glycohydrolase (PARG) gene and the common promoter sequence it shares with inner mitochondrial membrane translocase 23 (TIM23). *Gene* **2003,** *314*, 181-190.

103. Meyer-Ficca, M. L.; Meyer, R. G.; Coyle, D. L.; Jacobson, E. L.; Jacobson, M. K. Human poly(ADP-ribose) glycohydrolase is expressed in alternative splice variants yielding isoforms that localize to different cell compartments. *Exp. Cell Res.* **2004,** *297*, 521-532.

104. Meyer, R. G.; Meyer-Ficca, M. L.; Whatcott, C. J.; Jacobson, E. L.; Jacobson, M. K. Two small enzyme isoforms mediate mammalian mitochondrial poly(ADP-ribose) glycohydrolase (PARG) activity. *Exp. Cell Res.* **2007,** *313*, 2920-2936.

105. Ikejima, M.; Gill, D. M. Poly(ADP-ribose) degradation by glycohydrolase starts with an endonucleolytic incision. *J. Biol. Chem.* **1988,** *263*, 11037-11040.

106. Cervantes-Laurean, D.; Jacobson, E. L.; Jacobson, M. K. Glycation and glycoxidation of histones by ADP-ribose. *J. Biol. Chem.* **1996,** *271*, 10461-10469.

107. Yu, S. W.; Andrabi, S. A.; Wang, H.; Kim, N. S.; Poirier, G. G.; Dawson, T. M.; Dawson, V. L. Apoptosis-inducing factor mediates poly(ADP-ribose) (PAR) polymer-induced cell death. *Proc. Natl. Acad. Sci. U.S.A.* **2006,** *103*, 18314-18319.

108. Andrabi, S. A.; Kim, N. S.; Yu, S. W.; Wang, H.; Koh, D. W.; Sasaki, M.; Klaus, J. A.; Otsuka, T.; Zhang, Z.; Koehler, R. C.; Hurn, P. D.; Poirier, G. G.; Dawson, V. L.; Dawson, T. M. Poly(ADP-ribose) (PAR) polymer is a death signal. *Proc. Natl. Acad. Sci. U.S.A.* **2006,** *103*, 18308-18313.

109. Menard, L.; Thibault, L.; Poirier, G. G. Reconstitution of an in vitro poly(ADP-ribose) turnover system. *Biochim Biophys. Acta* **1990,** *1049*, 45-58.

110. Okayama, H.; Honda, M.; Hayaishi, O. Novel enzyme from rat liver that cleaves an ADP-ribosyl histone linkage. *Proc. Natl. Acad. Sci. U.S.A.* **1978,** *75*, 2254-2257.

111. Oka, J.; Ueda, K.; Hayaishi, O.; Komura, H.; Nakanishi, K. ADP-ribosyl protein lyase: Purification, properties, and identification of the product. *J. Biol. Chem.* **1984,** *259*, 986-995.

112. Sharifi, R.; Morra, R.; Appel, C. D.; Tallis, M.; Chioza, B.; Jankevicius, G.; Simpson, M. A.; Matic, I.; Ozkan, E.; Golia, B.; Schellenberg, M. J.; Weston, R.; Williams, J. G.; Rossi, M. N.; Galehdari, H.; Krahn, J.; Wan, A.; Trembath, R. C.; Crosby, A. H.; Ahel, D.; Hay, R.; Ladurner, A. G.; Timinszky, G.; Williams, R.

S.; Ahel, I. Deficiency of terminal ADP-ribose protein glycohydrolase TARG1/C6orf130 in neurodegenerative disease. *EMBO J*. **2013,** *32*, 1225-1237.

113. Luo, X.; Kraus, W. L. On PAR with PARP: Cellular stress signaling through poly(ADP-ribose) and PARP-1. *Genes Dev*. **2012,** *26*, 417-32.

114. Sauermann, G.; Wesierskagadek, J. Poly(ADP-ribose) effectively competes with DNA for Histone H-4 binding. *Biochem. Biophys. Res. Commun*. **1986,** *139*, 523-529.

115. Panzeter, P. L.; Realini, C. A.; Althaus, F. R. Noncovalent interactions of poly(adenosine diphosphate ribose) with histones. *Biochemistry* **1992,** *31*, 1379-1385.

116. Pleschke, J. M.; Kleczkowska, H. E.; Strohm, M.; Althaus, F. R. Poly(ADP-ribose) binds to specific domains in DNA damage checkpoint proteins. *J. Biol. Chem*. **2000,** *275*, 40974-40980.

117. Gagné, J. P.; Isabelle, M.; Lo, K. S.; Bourassa, S.; Hendzel, M. J.; Dawson, V. L.; Dawson, T. M.; Poirier, G. G. Proteome-wide identification of poly(ADP-ribose) binding proteins and poly(ADP-ribose)-associated protein complexes. *Nucleic Acids Res*. **2008,** *36*, 6959-6976.

118. Wang, Y. F.; Kim, N. S.; Haince, J. F.; Kang, H. C.; David, K. K.; Andrabi, S. A.; Poirier, G. G.; Dawson, V. L.; Dawson, T. M. Poly(ADP-ribose) (PAR) binding to apoptosis-inducing factor is critical for PAR polymerase-1-dependent cell death (parthanatos). *Sci. Signal*. **2011,** *4*.

119. Pehrson, J. R.; Fried, V. A. MacroH2A, a core histone containing a large nonhistone region. *Science* **1992,** *257*, 1398-1400.

120. Karras, G. I.; Kustatscher, G.; Buhecha, H. R.; Allen, M. D.; Pugieux, C.; Sait, F.; Bycroft, M.; Ladurner, A. G. The macro domain is an ADP-ribose binding module. *EMBO J*. **2005,** *24*, 1911-1920.

121. Ahel, D.; Horejsi, Z.; Wiechens, N.; Polo, S. E.; Garcia-Wilson, E.; Ahel, I.; Flynn, H.; Skehel, M.; West, S. C.; Jackson, S. P.; Owen-Hughes, T.; Boulton, S. J. Poly(ADP-ribose)-dependent regulation of DNA repair by the chromatin remodeling enzyme ALC1. *Science* **2009,** *325*, 1240-1243.

122. Gottschalk, A. J.; Timinszky, G.; Kong, S. E.; Jin, J. J.; Cai, Y.; Swanson, S. K.; Washburn, M. P.; Florens, L.; Ladurner, A. G.; Conaway, J. W.; Conaway, R. C. Poly(ADP-ribosyl)ation directs recruitment and activation of an ATP-dependent chromatin remodeler. *Proc. Natl. Acad. Sci. U.S.A*. **2009,** *106*, 13770-13774.

123. Timinszky, G.; Till, S.; Hassa, P. O.; Hothorn, M.; Kustatscher, G.; Nijmeijer, B.; Colombelli, J.; Altmeyer, M.; Stelzer, E. H. K.; Scheffzek, K.; Hottiger, M. O.; Ladurner, A. G. A macrodomain-containing histone rearranges chromatin upon sensing PARP1 activation. *Nat. Struct. Mol. Biol*. **2009,** *16*, 923-929.

124. Slade, D.; Dunstan, M. S.; Barkauskaite, E.; Weston, R.; Lafite, P.; Dixon, N.; Ahel, M.; Leys, D.; Ahel, I. The structure and catalytic mechanism of a poly(ADP-ribose) glycohydrolase. *Nature* **2011,** *477*, 616-620.

125. Kim, I. K.; Kiefer, J. R.; Ho, C. M. W.; Stegeman, R. A.; Classen, S.; Tainer, J. A.; Ellenberger, T. Structure of mammalian poly(ADP- ribose) glycohydrolase reveals a flexible tyrosine clasp as a substrate-binding element. *Nat. Struct. Mol. Biol.* **2012,** *19*, 653-656.

126. Peterson, F. C.; Chen, D. W.; Lytle, B. L.; Rossi, M. N.; Ahel, I.; Denu, J. M.; Volkman, B. F. Orphan macrodomain protein (human C6orf130) is an *O*-acyl-ADP-ribose deacylase: Solution structure and catalytic properties. *J. Biol. Chem.* **2011,** *286*, 35955-35965.

127. Jankevicius, G.; Hassler, M.; Golia, B.; Rybin, V.; Zacharias, M.; Timinszky, G.; Ladurner, A. G. A family of macrodomain proteins reverses cellular mono-ADP-ribosylation. *Nat. Struct. Mol. Biol.* **2013,** *20*, 508-514.

128. Rosenthal, F.; Feijs, K. L. H.; Frugier, E.; Bonalli, M.; Forst, A. H.; Imhof, R.; Winkler, H. C.; Fischer, D.; Caflisch, A.; Hassa, P. O.; Luscher, B.; Hottiger, M. O. Macrodomain-containing proteins are new mono-ADP-ribosylhydrolases. *Nat. Struct. Mol. Biol.* **2013,** *20*, 502-507.

129. Ahel, I.; Ahel, D.; Matsusaka, T.; Clark, A. J.; Pines, J.; Boulton, S. J.; West, S. C. Poly(ADP-ribose)-binding zinc finger motifs in DNA repair/checkpoint proteins. *Nature* **2008,** *451*, 81-85.

130. Eustermann, S.; Brockmann, C.; Mehrotra, P. V.; Yang, J. C.; Loakes, D.; West, S. C.; Ahel, I.; Neuhaus, D. Solution structures of the two PBZ domains from human APLF and their interaction with poly(ADP-ribose). *Nat. Struct. Mol. Biol.* **2010,** *17*, 241-243.

131. Kashima, L.; Idogawa, M.; Mita, H.; Shitashige, M.; Yamada, T.; Ogi, K.; Suzuki, H.; Toyota, M.; Ariga, H.; Sasaki, Y.; Tokino, T. CHFR protein regulates mitotic checkpoint by targeting PARP-1 Protein for ubiquitination and degradation. *J. Biol. Chem.* **2012,** *287*, 12975-12984.

132. Aravind, L. The WWE domain: A common interaction module in protein ubiquitination and ADP ribosylation. *Trends Biochem. Sci.* **2001,** *26*, 273-275.

133. Wang, Z. Z.; Michaud, G. A.; Cheng, Z. H.; Zhang, Y.; Hinds, T. R.; Fan, E. K.; Cong, F.; Xu, W. Q. Recognition of the iso-ADP-ribose moiety in poly(ADP-ribose) by WWE domains suggests a general mechanism for poly (ADP-ribosyl)ation-dependent ubiquitination. *Genes Dev.* **2012,** *26*, 235-240.

134. Kang, H. C.; Lee, Y. I.; Shin, J. H.; Andrabi, S. A.; Chi, Z. K.; Gagné, J. P.; Lee, Y. J.; Ko, H. S.; Lee, B. D.; Poirier, G. G.; Dawson, V. L.; Dawson, T. M. Iduna is a poly(ADP-ribose) (PAR)-dependent E3 ubiquitin ligase that regulates DNA damage. *Proc. Natl. Acad. Sci. U.S.A.* **2011,** *108*, 14103-14108.

135. Andrabi, S. A.; Kang, H. C.; Haince, J. F.; Lee, Y. I.; Zhang, J.; Chi, Z. K.; West, A. B.; Koehler, R. C.; Poirier, G. G.; Dawson, T. M.; Dawson, V. L. Iduna protects the brain from glutamate excitotoxicity and stroke by interfering with poly(ADP-ribose) polymer-induced cell death. *Nat. Med.* **2011,** *17*, 692-699.

136. Zhang, Y.; Liu, S. M.; Mickanin, C.; Feng, Y.; Charlat, O.; Michaud, G. A.; Schirle, M.; Shi, X. Y.; Hild, M.; Bauer, A.; Myer, V. E.; Finan, P. M.; Porter, J. A.; Huang, S. M. A.; Cong, F. RNF146 is a poly(ADP-ribose)-directed E3 ligase that regulates axin degradation and Wnt signalling. *Nat. Cell Biol.* **2011,** *13*, 623-629.

137. DaRosa, P. A.; Wang, Z. Z.; Jiang, X. M.; Pruneda, J. N.; Cong, F.; Klevit, R. E.; Xu, W. Q. Allosteric activation of the RNF146 ubiquitin ligase by a poly(ADP-ribosyl)ation signal. *Nature* **2015,** *517*, 223-226.

138. Li, M.; Lu, L. Y.; Yang, C. Y.; Wang, S. M.; Yu, X. C. The FHA and BRCT domains recognize ADP-ribosylation during DNA damage response. *Genes Dev.* **2013,** *27*, 1752-1768.

139. Li, M.; Yu, X. C. Function of BRCA1 in the DNA damage response is mediated by ADP-ribosylation. *Cancer Cell* **2013,** *23*, 693-704.

140. Zhang, F.; Chen, Y. B.; Li, M.; Yu, X. C. The oligonucleotide/oligosaccharide-binding fold motif is a poly(ADP-ribose)-binding domain that mediates DNA damage response. *Proc. Natl. Acad. Sci. U.S.A.* **2014,** *111*, 7278-7283.

141. Min, W.; Bruhn, C.; Grigaravicius, P.; Zhou, Z. W.; Li, F.; Kruger, A.; Siddeek, B.; Greulich, K. O.; Popp, O.; Meisezahl, C.; Calkhoven, C. F.; Burkle, A.; Xu, X. Z.; Wang, Z. Q. Poly(ADP-ribose) binding to Chk1 at stalled replication forks is required for S-phase checkpoint activation. *Nat. Commun.* **2013,** *4*.

142. Reinhardt, H. C.; Yaffe, M. B. Phospho-Ser/Thr-binding domains: Navigating the cell cycle and DNA damage response. *Nat. Rev. Mol. Cell Biol.* **2013,** *14*, 563-580.

143. Flynn, R. L.; Zou, L. Oligonucleotide/oligosaccharide-binding fold proteins: A growing family of genome guardians. *Crit. Rev. Biochem. Mol. Biol.* **2010,** *45*, 266-275.

144. Lautier, D.; Lagueux, J.; Thibodeau, J.; Menard, L.; Poirier, G. G. Molecular and biochemical features of poly(ADP-ribose) metabolism. *Mol. Cell. Biochem.* **1993,** *122*, 171-193.

145. Sancar, A.; Lindsey-Boltz, L. A.; Unsal-Kacmaz, K.; Linn, S. Molecular mechanisms of mammalian DNA repair and the DNA damage checkpoints. *Annu. Rev. Biochem.* **2004,** *73*, 39-85.

146. Satoh, M. S.; Lindahl, T. Role of Poly(ADP-ribose) formation in DNA repair. *Nature* **1992,** *356*, 356-358.

147. Realini, C. A.; Althaus, F. R. Histone shuttling by poly(ADP-ribosylation). *J. Biol. Chem.* **1992,** *267*, 18858-18865.

148. Krishnakumar, R.; Gamble, M. J.; Frizzell, K. M.; Berrocal, J. G.; Kininis, M.; Kraus, W. L. Reciprocal binding of PARP-1 and histone H1 at promoters specifies transcriptional outcomes. *Science* **2008,** *319*, 819-821.

149. Muthurajan, U. M.; Hepler, M. R. D.; Hieb, A. R.; Clark, N. J.; Kramer, M.; Yao, T. T.; Luger, K. Automodification switches PARP-1 function from chromatin architectural protein to histone chaperone. *Proc. Natl. Acad. Sci. U.S.A.* **2014,** *111*, 12752-12757.

150. Jackson, S. P.; Bartek, J. The DNA-damage response in human biology and disease. *Nature* **2009,** *461*, 1071-1078.

151. Ciccia, A.; Elledge, S. J. The DNA damage response: Making it safe to play with knives. *Mol. Cell* **2010,** *40*, 179-204.

152. Robert, I.; Karicheva, O.; San Martin, B. R.; Schreiber, V.; Dantzer, F. Functional aspects of PARylation in induced and programmed DNA repair processes: Preserving genome integrity and modulating physiological events. *Mol. Aspects Med.* **2013,** *34*, 1138-1152.

153. Kraus, W. L.; Lis, J. T. PARP goes transcription. *Cell* **2003,** *113*, 677-683.

154. Kim, M. Y.; Zhang, T.; Kraus, W. L. Poly(ADP-ribosyl)ation by PARP-1: "PAR-laying" NAD^+ into a nuclear signal. *Genes Dev.* **2005,** *19*, 1951-1967.

155. Krishnakumar, R.; Kraus, W. L. The PARP side of the nucleus: Molecular actions, physiological outcomes, and clinical targets. *Mol. Cell* **2010,** *39*, 8-24.

156. Luo, X.; Kraus, W. L. On PAR with PARP: Cellular stress signaling through poly(ADP-ribose) and PARP-1. *Genes Dev.* **2012,** *26*, 417-432.

157. Kaufmann, S. H.; Desnoyers, S.; Ottaviano, Y.; Davidson, N. E.; Poirier, G. G. Specific proteolytic cleavage of poly(ADP-ribose) polymerase: An early marker of chemotherapy-induced apoptosis. *Cancer Res.* **1993,** *53*, 3976-3985.

158. Yu, S. W.; Wang, H. M.; Poitras, M. F.; Coombs, C.; Bowers, W. J.; Federoff, H. J.; Poirier, G. G.; Dawson, T. M.; Dawson, V. L. Mediation of poly(ADP-ribose) polymerase-1-dependent cell death by apoptosis-inducing factor. *Science* **2002,** *297*, 259-263.

159. Ha, H. C.; Snyder, S. H. Poly(ADP-ribose) polymerase is a mediator of necrotic cell death by ATP depletion. *Proc. Natl. Acad. Sci. U.S.A.* **1999,** *96*, 13978-13982.

160. Cipriani, G.; Rapizzi, E.; Vannacci, A.; Rizzuto, R.; Moroni, F.; Chiarugi, A. Nuclear poly(ADP-ribose) polymerase-1 rapidly triggers mitochondrial dysfunction. *J. Biol. Chem.* **2005,** *280*, 17227-17234.

161. Pellegrini-Giampietro, D. E.; Peruginelli, F.; Meli, E.; Cozzi, A.; Chjarugi, A.; Moroni, F. Poly(ADP-ribose) polymerase inhibitors attenuate post-ischemic neurodegeneration of the necrotic but not of the apoptotic type. *Eur. J. Neurosci.* **2000,** *12*, 234-234.

162. Thomas, C.; Tulin, A. V. Poly-ADP-ribose polymerase: Machinery for nuclear processes. *Mol. Aspects Med.* **2013,** *34*, 1124-1137.

163. Ryu, K. W.; Kim, D. S.; Kraus, W. L. New facets in the regulation of gene expression by ADP-ribosylation and poly(ADP-ribose) polymerases. *Chem. Rev.* **2015,** *115*, 2453-81.

164. Tao, Z. H.; Gao, P.; Liu, H. W. Studies of the expression of human poly(ADP-ribose) polymerase-1 in *Saccharomyces cerevisiae* and identification of PARP-1 substrates by yeast proteome microarray screening. *Biochemistry* **2009,** *48*, 11745-11754.

165. Virag, L.; Szabo, C. The therapeutic potential of poly(ADP-ribose) polymerase inhibitors. *Pharmacol. Rev.* **2002,** *54*, 375-429.

166. Purnell, M. R.; Whish, W. J. D. Novel inhibitors of poly(ADP-ribose) synthetase. *Biochem. J.* **1980,** *185*, 775-777.

167. Durkacz, B. W.; Omidiji, O.; Gray, D. A.; Shall, S. $(ADP\text{-}ribose)_n$ participates in DNA excision repair. *Nature* **1980,** *283*, 593-596.

168. Ferraris, D. V. Evolution of poly(ADP-ribose) polymerase-1 (PARP-1) inhibitors. From concept to clinic. *J. Med. Chem.* **2010,** *53*, 4561-4584.

169. Wahlberg, E.; Karlberg, T.; Kouznetsova, E.; Markova, N.; Macchiarulo, A.; Thorsell, A. G.; Pol, E.; Frostell, A.; Ekblad, T.; Oncu, D.; Kull, B.; Robertson, G. M.; Pellicciari, R.; Schuler, H.; Weigelt, J. Family-wide chemical profiling and structural analysis of PARP and tankyrase inhibitors. *Nat. Biotechnol.* **2012,** *30*, 283-288.

170. Plummer, R.; Jones, C.; Middleton, M.; Wilson, R.; Evans, J.; Olsen, A.; Curtin, N.; Boddy, A.; McHugh, P.; Newell, D.; Harris, A.; Johnson, P.; Steinfeldt, H.; Dewji, R.; Wang, D.; Robson, L.; Calvert, H. Phase I study of the poly(ADP-ribose) polymerase inhibitor, AG014699, in combination with temozolomide in patients with advanced solid tumors. *Clin. Cancer. Res.* **2008,** *14*, 7917-7923.

171. Buki, K. G.; Bauer, P. I.; Mendeleyev, J.; Hakam, A.; Kun, E. Destabilization of Zn^{2+} coordination in ADP-ribose transferase (polymerizing) by 6-nitroso-1,2-benzopyrone coincidental with inactivation of the polymerase but not the DNA-binding function. *FEBS Lett.* **1991,** *290*, 181-185.

172. Patel, A. G.; De Lorenzo, S. B.; Flatten, K. S.; Poirier, G. G.; Kaufmann, S. H. Failure of iniparib to inhibit poly(ADP-ribose) polymerase in vitro. *Clin. Cancer. Res.* **2012,** *18*, 1655-1662.

173. Mateo, J.; Ong, M.; Tan, D. S. P.; Gonzalez, M. A.; de Bono, J. S. Appraising iniparib, the PARP inhibitor that never was—what must we learn? *Nat. Rev. Clin. Oncol.* **2013,** *10*, 688-696.

174. Deeks, E. D. Olaparib: First global approval. *Drugs* **2015,** *75*, 231-240.

175. Jagtap, P.; Szabo, C. Poly(ADP-ribose) polymerase and the therapeutic effects of its inhibitors. *Nat. Rev. Drug Discov.* **2005,** *4*, 421-440.

176. Curtin, N. J.; Szabo, C. Therapeutic applications of PARP inhibitors: Anticancer therapy and beyond. *Mol. Aspects Med.* **2013,** *34*, 1217-1256.

177. De Lorenzo, S. B.; Patel, A. G.; Hurley, R. M.; Kaufmann, S. H. The elephant and the blind men: Making sense of PARP inhibitors in homologous recombination deficient tumor cells. *Front. Oncol.* **2013,** *3*, 228.

178. Kameshita, I.; Matsuda, Z.; Taniguchi, T.; Shizuta, Y. Poly(ADP-ribose) synthetase: Separation and identification of three proteolytic fragments as the substrate-binding domain, the DNA-binding domain, and the automodification domain. *J. Biol. Chem.* **1984,** *259*, 4770-4776.

179. De Murcia, G.; de Murcia, J. M. Poly(ADP-ribose) polymerase: A molecular nick-sensor. *Trends Biochem. Sci.* **1994,** *19*, 172-176.

180. Langelier, M. F.; Pascal, J. M. PARP-1 mechanism for coupling DNA damage detection to poly(ADP-ribose) synthesis. *Curr. Opin. Struct. Biol.* **2013,** *23*, 134-143.

181. Ikejima, M.; Noguchi, S.; Yamashita, R.; Ogura, T.; Sugimura, T.; Gill, D. M.; Miwa, M. The zinc fingers of human poly(ADP-ribose) polymerase are differentially required for the recognition of DNA breaks and nicks and the consequent enzyme activation: Other structures recognize intact DNA. *J. Biol. Chem.* **1990,** *265*, 21907-21913.

182. Gradwohl, G.; de Murcia, J. M.; Molinete, M.; Simonin, F.; Koken, M.; Hoeijmakers, J. H. J.; de Murcia, G. The second zinc-finger domain of poly(ADP-ribose) polymerase determines specificity for single-stranded breaks in DNA. *Proc. Natl. Acad. Sci. U.S.A.* **1990,** *87*, 2990-2994.

183. Lonskaya, I.; Potaman, V. N.; Shlyakhtenko, L. S.; Oussatcheva, E. A.; Lyubchenko, Y. L.; Soldatenkov, V. A. Regulation of poly(ADP-ribose) polymerase-1 by DNA structure-specific binding. *J. Biol. Chem.* **2005,** *280*, 17076-17083.

184. Petrucco, S.; Percudani, R. Structural recognition of DNA by poly(ADP-ribose)polymerase-like zinc finger families. *FEBS J.* **2008,** *275*, 883-893.

185. Schreiber, V.; Molinete, M.; Boeuf, H.; de Murcia, G.; Menissier-de Murcia, J. The human poly(ADP-ribose) polymerase nuclear-localization signal is a bipartite

element functionally separate from DNA-binding and catalytic activity. *EMBO J.* **1992,** *11*, 3263-3269.

186. Trucco, C.; Flatter, E.; Fribourg, S.; de Murcia, G.; Menissier-de Murcia, J. Mutations in the amino-terminal domain of the human poly(ADP-ribose) polymerase that affect its catalytic activity but not its DNA binding capacity. *FEBS Lett.* **1996,** *399*, 313-316.

187. Langelier, M. F.; Servent, K. M.; Rogers, E. E.; Pascal, J. M. A third zinc-binding domain of human poly(ADP-ribose) polymerase-1 coordinates DNA-dependent enzyme activation. *J. Biol. Chem.* **2008,** *283*, 4105-4114.

188. Tao, Z. H.; Gao, P.; Hoffman, D. W.; Liu, H. W. Domain C of human poly(ADP-ribose) polymerase-1 is important for enzyme activity and contains a novel zinc-ribbon motif. *Biochemistry* **2008,** *47*, 5804-5813.

189. Langelier, M. F.; Ruhl, D. D.; Planck, J. L.; Kraus, W. L.; Pascal, J. M. The Zn3 domain of human poly(ADP-ribose) polymerase-1 (PARP-1) functions in both DNA-dependent poly(ADP-ribose) synthesis activity and chromatin compaction. *J. Biol. Chem.* **2010,** *285*, 18877-18887.

190. Kawaichi, M.; Ueda, K.; Hayaishi, O. Multiple autopoly(ADP-ribosyl)ation of rat liver poly(ADP-ribose) synthetase: Mode of modification and properties of automodified synthetase. *J. Biol. Chem.* **1981,** *256*, 9483-9489.

191. Cherney, B. W.; Mcbride, O. W.; Chen, D.; Alkhatib, H.; Bhatia, K.; Hensley, P.; Smulson, M. E. cDNA sequence, protein structure, and chromosomal location of the human gene for poly(ADP-ribose) polymerase. *Proc. Natl. Acad. Sci. U.S.A.* **1987,** *84*, 8370-8374.

192. Alkhatib, H. M.; Chen, D.; Cherney, B.; Bhatia, K.; Notario, V.; Giri, C.; Stein, G.; Slattery, E.; Roeder, R. G.; Smulson, M. E. Cloning and expression of cDNA for human poly(ADP-ribose) polymerase. *Proc. Natl. Acad. Sci. U.S.A.* **1987,** *84*, 1224-1228.

193. Uchida, K.; Morita, T.; Sato, T.; Ogura, T.; Yamashita, R.; Noguchi, S.; Suzuki, H.; Nyunoya, H.; Miwa, M.; Sugimura, T. Nucleotide sequence of a full-length cDNA for human fibroblast poly(ADP-ribose) polymerase. *Biochem. Biophys. Res. Commun.* **1987,** *148*, 617-622.

194. Chapman, J. D.; Gagne, J. P.; Poirier, G. G.; Goodlett, D. R. Mapping PARP-1 auto-ADP-ribosylation sites by liquid chromatography-tandem mass spectrometry. *J. Proteome Res.* **2013,** *12*, 1868-80.

195. Zhang, Y. J.; Wang, J. Q.; Ding, M.; Yu, Y. H. Site-specific characterization of the Asp- and Glu-ADP-ribosylated proteome. *Nat. Methods* **2013,** *10*, 981-984.

196. Bork, P.; Hofmann, K.; Bucher, P.; Neuwald, A. F.; Altschul, S. F.; Koonin, E. V. A superfamily of conserved domains in DNA damage-responsive cell cycle checkpoint proteins. *FASEB J*. **1997,** *11*, 68-76.

197. Loeffler, P. A.; Cuneo, M. J.; Mueller, G. A.; DeRose, E. F.; Gabel, S. A.; London, R. E. Structural studies of the PARP-1 BRCT domain. *BMC Struct. Biol*. **2011,** *11*, 37.

198. Mansoorabadi, S. O.; Wu, M.; Tao, Z.; Gao, P.; Pingali, S. V.; Guo, L.; Liu, H. W. Conformational activation of poly(ADP-ribose) polymerase-1 upon DNA binding revealed by small-angle X-ray scattering. *Biochemistry* **2014,** *53*, 1779-1788.

199. Huambachano, O.; Herrera, F.; Rancourt, A.; Satoh, M. S. Double-stranded DNA binding domain of poly(ADP-ribose) polymerase-1 and molecular insight into the regulation of its activity. *J. Biol. Chem*. **2011,** *286*, 7149-7160.

200. Langelier, M. F.; Planck, J. L.; Roy, S.; Pascal, J. M. Structural basis for DNA damage-dependent poly(ADP-ribosyl)ation by human PARP-1. *Science* **2012,** *336*, 728-732.

201. Simonin, F.; Menissier-de Murcia, J.; Poch, O.; Muller, S.; Gradwohl, G.; Molinete, M.; Penning, C.; Keith, G.; de Murcia, G. Expression and site-directed mutagenesis of the catalytic domain of human poly(ADP-ribose) polymerase in *Escherichia coli*: Lysine-893 is critical for activity. *J. Biol. Chem*. **1990,** *265*, 19249-19256.

202. Ruf, A.; de Murcia, J. M.; de Murcia, G. M.; Schulz, G. E. Structure of the catalytic fragment of poly(ADP-ribose) polymerase from chicken. *Proc. Natl. Acad. Sci. U.S.A*. **1996,** *93*, 7481-7485.

203. Ruf, A.; Rolli, V.; de Murcia, G.; Schulz, G. E. The mechanism of the elongation and branching reaction of poly(ADP-ribose) polymerase as derived from crystal structures and mutagenesis. *J. Mol. Biol*. **1998,** *278*, 57-65.

204. Pic, E.; Gagné, J. P.; Poirier, G. G. Mass spectrometry-based functional proteomics of poly(ADP-ribose) polymerase-1. *Expert Rev. Proteomics* **2011,** *8*, 759-774.

205. Hassa, P. O.; Haenni, S. S.; Buerki, C.; Meier, N. I.; Lane, W. S.; Owen, H.; Gersbach, M.; Imhof, R.; Hottiger, M. O. Acetylation of poly(ADP-ribose) polymerase-1 by p300/CREB-binding protein regulates coactivation of NF-κB-dependent transcription. *J. Biol. Chem*. **2005,** 280, 40450-40464.

206. Kauppinen, T. M.; Chin, W. Y.; Suh, S. W.; Wiggins, A. K.; Huang, E. J.; Swanson, R. A. Direct phosphorylation and regulation of poly(ADP-ribose) polymerase-1 by extracellular signal-regulated kinases 1/2. *Proc. Natl. Acad. Sci. U.S.A*. **2006,** *103*, 7136-7141.

207. Cohen-Armon, M.; Visochek, L.; Rozensal, D.; Kalal, A.; Geistrikh, I.; Klein, R.; Bendetz-Nezer, S.; Yao, Z.; Seger, R. DNA-independent PARP-1 activation by phosphorylated ERK2 increases Elk1 activity: A link to histone acetylation. *Mol. Cell* **2007,** *25*, 297-308.

208. Messner, S.; Schuermann, D.; Altmeyer, M.; Kassner, I.; Schmidt, D.; Schar, P.; Muller, S.; Hottiger, M. O. SUMOylation of poly(ADP-ribose) polymerase 1 inhibits its acetylation and restrains transcriptional coactivator function. *FASEB J.* **2009,** *23*, 3978-3989.

209. Zilio, N.; Williamson, C. T.; Eustermann, S.; Shah, R.; West, S. C.; Neuhaus, D.; Ulrich, H. D. DNA-dependent SUMO modification of PARP-1. *DNA Repair* **2013,** *12*, 761-773.

210. Wang, T.; Simbulan-Rosenthal, C. M.; Smulson, M. E.; Chock, P. B.; Yang, D. C. H. Polyubiquitylation of PARP-1 through ubiquitin K48 is modulated by activated DNA, NAD^+, and dipeptides. *J. Cell. Biochem.* **2008,** *104*, 318-328.

211. Vivelo, C. A.; Leung, A. K. Proteomics approaches to identify mono-(ADP-ribosyl)ated and poly(ADP-ribosyl)ated proteins. *Proteomics* **2015,** *15*, 203-17.

212. Dania, N.; Stilla, A.; Marchegiani, A.; Tamburro, A.; Till, S.; Ladurner, A. G.; Corda, D.; Di Girolamo, M. Combining affinity purification by ADP-ribose-binding macro domains with mass spectrometry to define the mammalian ADP-ribosyl proteome. *Proc. Natl. Acad. Sci. U.S.A.* **2009,** *106*, 4243-4248.

213. Troiani, S.; Lupi, R.; Perego, R.; Depaolini, S. R.; Thieffine, S.; Bosotti, R.; Rusconi, L. Identification of candidate substrates for poly(ADP-ribose) polymerase-2 (PARP2) in the absence of DNA damage using high-density protein microarrays. *FEBS J.* **2011,** *278*, 3676-3687.

214. Isabelle, M.; Moreel, X.; Gagné, J. P.; Rouleau, M.; Ethier, C.; Gagne, P.; Hendzel, M. J.; Poirier, G. G. Investigation of PARP-1, PARP-2, and PARG interactomes by affinity-purification mass spectrometry. *Proteome Sci.* **2010,** *8*, 22.

215. Gagné, J. P.; Pic, E.; Isabelle, M.; Krietsch, J.; Ethier, C.; Paquet, E.; Kelly, I.; Boutin, M.; Moon, K. M.; Foster, L. J.; Poirier, G. G. Quantitative proteomics profiling of the poly(ADP-ribose)-related response to genotoxic stress. *Nucleic Acids Res.* **2012,** *40*, 7788-7805.

216. Jungmichel, S.; Rosenthal, F.; Altmeyer, M.; Lukas, J.; Hottiger, M. O.; Nielsen, M. L. Proteome-wide identification of poly(ADP-ribosyl)ation targets in different genotoxic stress responses. *Mol. Cell* **2013,** *52*, 272-285.

217. Westcott, N. P.; Hang, H. C. Chemical reporters for exploring ADP-ribosylation and AMPylation at the host-pathogen interface. *Curr. Opin. Chem. Biol.* **2014,** *23*, 56-62.

218. Jiang, H.; Kim, J. H.; Frizzell, K. M.; Kraus, W. L.; Lin, H. N. Clickable NAD analogues for labeling substrate proteins of poly(ADP-ribose) polymerases. *J. Am. Chem. Soc.* **2010,** *132*, 9363-9372.

219. Carter-O'Connell, I.; Jin, H.; Morgan, R. K.; David, L. L.; Cohen, M. S. Engineering the substrate specificity of ADP-Ribosyltransferases for identifying direct protein targets. *J. Am. Chem. Soc.* **2014,** *136*, 5201-5204.

220. Juarez-Salinas, H.; Sims, J. L.; Jacobson, M. K. Poly(ADP-ribose) levels in carcinogen-treated cells. *Nature* **1979,** *282*, 740-741.

221. Benjamin, R. C.; Gill, D. M. ADP-ribosylation in mammalian cell ghosts: Dependence of poly(ADP-ribose) synthesis on strand breakage in DNA. *J. Biol. Chem.* **1980,** *255*, 493-501.

222. Benjamin, R. C.; Gill, D. M. Poly(ADP-ribose) synthesis in vitro programmed by damaged DNA: A comparison of DNA molecules containing different types of strand breaks. *J. Biol. Chem.* **1980,** *255*, 502-508.

223. Mazen, A.; Menissier-de Murcia, J.; Molinete, M.; Simonin, F.; Gradwohl, G.; Poirier, G.; de Murcia, G. Poly(ADP-ribose) polymerase: A novel finger protein. *Nucleic Acids Res.* **1989,** *17*, 4689-4698.

224. Lecam, E.; Fack, F.; Menissier-de Murcia, J.; Cognet, J. A. H.; Barbin, A.; Sarantoglou, V.; Revet, B.; Delain, E.; de Murcia, G. Conformational analysis of a 139 base-pair DNA fragment containing a single-stranded break and its interaction with human poly(ADP-ribose) polymerase. *J. Mol. Biol.* **1994,** *235*, 1062-1071.

225. Soldatenkov, V. A.; Potaman, V. N. DNA-binding properties of poly(ADP-ribose) polymerase: A target for anticancer therapy. *Curr. Drug Targets* **2004,** *5*, 357-365.

226. D'Silva, I.; Pelletier, J. D.; Lagueux, J.; D'Amours, D.; Chaudhry, M. A.; Weinfeld, M.; Lees-Miller, S. P.; Poirier, G. G. Relative affinities of poly(ADP-ribose) polymerase and DNA-dependent protein kinase for DNA strand interruptions. *Biochim. Biophys. Acta* **1999,** *1430*, 119-126.

227. Pion, E.; Ullmann, G. M.; Ame, J. C.; Gerard, D.; de Murcia, G.; Bombarda, E. DNA-induced dimerization of poly(ADP-ribose) polymerase-1 triggers its activation. *Biochemistry* **2005,** *44*, 14670-14681.

228. Zhu, G. Y.; Chang, P.; Lippard, S. J. Recognition of platinum-DNA damage by poly(ADP-ribose) polymerase-1. *Biochemistry* **2010,** *49*, 6177-6183.

229. Fekete, A.; Kenesi, E.; Hunyadi-Gulyas, E.; Durgo, H.; Berko, B.; Dunai, Z. A.; Bauer, P. I. The guanine-quadruplex structure in the muman *c-myc* gene's promoter is converted into B-DNA form by the human poly(ADP-ribose) polymerase-1. *PLoS One* **2012,** *7*, e42690.

230. Kim, M. Y.; Mauro, S.; Gevry, N.; Lis, J. T.; Kraus, W. L. NAD^+-dependent modulation of chromatin structure and transcription by nucleosome binding properties of PARP-1. *Cell* **2004,** *119*, 803-814.

231. Pinnola, A.; Naumova, N.; Shah, M.; Tulin, A. V. Nucleosomal core histones mediate dynamic regulation of poly(ADP-ribose) polymerase 1 protein binding to chromatin and induction of its enzymatic activity. *J. Biol. Chem.* **2007,** *282*, 32511-32519.

232. Clark, N. J.; Kramer, M.; Muthurajan, U. M.; Luger, K. Alternative modes of binding of poly(ADP-ribose) polymerase 1 to free DNA and nucleosomes. *J. Biol. Chem.* **2012,** *287*, 32430-32439.

233. Langelier, M. F.; Planck, J. L.; Roy, S.; Pascal, J. M. Crystal structures of Poly(ADP-ribose) polymerase-1 (PARP-1) zinc fingers bound to DNA: Structural and functional insights into DNA-dependent PARP-1 activity. *J. Biol. Chem.* **2011,** *286*, 10690-10701.

234. Hassler, M.; Ladurner, A. G. Towards a structural understanding of PARP1 activation and related signalling ADP-ribosyl-transferases. *Curr. Opin. Struct. Biol.* **2012,** *22*, 721-729.

235. Ali, A. A. E.; Timinszky, G.; Arribas-Bosacoma, R.; Kozlowski, M.; Hassa, P. O.; Hassler, M.; Ladurner, A. G.; Pearl, L. H.; Oliver, A. W. The zinc-finger domains of PARP1 cooperate to recognize DNA strand breaks. *Nat. Struct. Mol. Biol.* **2012,** *19*, 685-692.

236. Lilyestrom, W.; van der Woerd, M. J.; Clark, N.; Luger, K. Structural and biophysical studies of human PARP-1 in complex with damaged DNA. *J. Mol. Biol.* **2010,** *395*, 983-994.

237. Eustermann, S.; Videler, H.; Yang, J. C.; Cole, P. T.; Gruszka, D.; Veprintsev, D.; Neuhaus, D. The DNA-binding domain of human PARP-1 interacts with DNA single-strand breaks as a monomer through its second zinc finger. *J. Mol. Biol.* **2011,** *407*, 149-170.

238. Bauer, P. I.; Buki, K. G.; Hakam, A.; Kun, E. Macromolecular association of ADP-ribosyltransferase and its correlation with enzymatic activity. *Biochem. J.* **1990,** *270*, 17-26.

239. Mendoza-Alvarez, H.; Alvarez-Gonzalez, R. Poly(ADP-ribose) polymerase is a catalytic dimer and the automodification reaction is intermolecular. *J. Biol. Chem.* **1993,** *268*, 22575-22580.

240. Panzeter, P. L.; Althaus, F. R. DNA strand break-mediated partitioning of poly(ADP-ribose) polymerase function. *Biochemistry* **1994,** *33*, 9600-9605.

241. Pion, E.; Bombarda, E.; Stiegler, P.; Ullmann, G. M.; Mely, Y.; de Murcia, G.; Gerard, D. Poly(ADP-ribose) polymerase-1 dimerizes at a 5′ recessed DNA end in vitro: A fluorescence study. *Biochemistry* **2003,** *42*, 12409-12417.

242. Steffen, J. D.; Tholey, R. M.; Langelier, M. F.; Planck, J. L.; Schiewer, M. J.; Lal, S.; Bildzukewicz, N. A.; Yeo, C. J.; Knudsen, K. E.; Brody, J. R.; Pascal, J. M. Targeting PARP-1 allosteric regulation offers therapeutic potential against cancer. *Cancer Res*. **2014,** *74*, 31-37.

243. Mao, Z. Y.; Hine, C.; Tian, X.; Van Meter, M.; Au, M.; Vaidya, A.; Seluanov, A.; Gorbunova, V. SIRT6 promotes DNA repair under stress by activating PARP1. *Science* **2011,** *332*, 1443-1446.

244. Domenighini, M.; Montecucco, C.; Ripka, W. C.; Rappuoli, R. Computer modelling of the NAD binding site of ADP-ribosylating toxins: Active-site structure and mechanism of NAD binding. *Mol. Microbiol*. **1991,** *5*, 23-31.

245. Douglas, C. M.; Collier, R. J. *Pseudomonas aeruginosa* exotoxin A: Alterations of biological and biochemical properties resulting from mutation of glutamic acid 553 to aspartic acid. *Biochemistry* **1990,** *29*, 5043-5049.

246. Marsischky, G. T.; Wilson, B. A.; Collier, R. J. Role of glutamic acid 988 of human poly-ADP-ribose polymerase in polymer formation: Evidence for active-site similarities to the ADP-ribosylating toxins. *J. Biol. Chem*. **1995,** *270*, 3247-3254.

247. Alvarez-Gonzalez, R. 3′-Deoxy-NAD^+ as a substrate for poly(ADP-ribose) polymerase and the reaction mechanism of poly(ADP-ribose) elongation. *J. Biol. Chem*. **1988,** *263*, 17690-17696.

248. Mendoza-Alvarez, H.; Alvarez-Gonzalez, R. Biochemical characterization of mono(ADP-ribosyl)ated poly(ADP-ribose) polymerase. *Biochemistry* **1999,** *38*, 3948-3953.

249. Wang, Y.; Rosner, D.; Grzywa, M.; Marx, A. Chain-terminating and clickable NAD^+ analogues for labeling the target proteins of ADP-ribosyltransferases. *Angew. Chem. Int. Ed*. **2014,** *53*, 8159-8162.

250. Ruf, A.; Rolli, V.; de Murcia, G.; Schulz, G. E. The mechanism of the elongation and branching reaction of poly(ADP-ribose) polymerase as derived from crystal structures and mutagenesis. *J. Mol. Biol*. **1998,** *278*, 57-65.

251. Bell, C. E.; Eisenberg, D. Crystal structure of diphtheria toxin bound to nicotinamide adenine dinucleotide. *Biochemistry* **1996,** *35*, 1137-1149.

252. Rolli, V.; O'Farrell, M.; Menissier-de Murcia, J.; de Murcia, G. Random mutagenesis of the poly(ADP-ribose) polymerase catalytic domain reveals amino acids involved in polymer branching. *Biochemistry* **1997,** *36*, 12147-12154.

253. Taniguchi, T. Reaction mechanism for automodification of poly(ADP-ribose) synthetase. *Biochem. Biophys. Res. Commun.* **1987,** *147*, 1008-1012.

254. Zahradka, P.; Ebisuzaki, K. A Shuttle mechanism for DNA-protein interactions: The regulation of poly(ADP-ribose) polymerase. *Eur. J. Biochem.* **1982,** *127*, 579-585.

255. Menard, L.; Thibault, L.; Poirier, G. G. Reconstitution of an in vitro poly(ADP-ribose) turnover system. *Biochim. Biophys. Acta* **1990,** *1049*, 45-58.

256. Thomassin, H.; Menard, L.; Hengartner, C.; Kirkland, J. B.; Poirier, G. G. Poly(ADP-ribosyl)ation of chromatin in an in-vitro poly(ADP-ribose)-turnover system. *Biochim. Biophys. Acta* **1992,** *1137*, 171-181.

257. Kun, E.; Kirsten, E.; Mendeleyev, J.; Ordahl, C. P. Regulation of the enzymatic catalysis of poly(ADP-ribose) polymerase by dsDNA, polyamines, Mg^{2+}, Ca^{2+}, histones H-1 and H-3 and ATP. *Biochemistry* **2004,** *43*, 210-216.

258. Carrico, I. S.; Carlson, B. L.; Bertozzi, C. R. Introducing genetically encoded aldehydes into proteins. *Nat. Chem. Biol.* **2007,** *3*, 321-322.

259. Cannon, B.; Kuhnlein, J.; Yang, S. H.; Cheng, A.; Schindler, D.; Stark, J. M.; Russell, R.; Paull, T. T. Visualization of local DNA unwinding by Mre11/Rad50/Nbs1 using single-molecule FRET. *Proc. Natl. Acad. Sci. U.S.A.* **2013,** *110*, 18868-18873.

260. van Oijen, A. M. Single-molecule approaches to characterizing kinetics of biomolecular interactions. *Curr. Opin. Biotechnol.* **2011,** *22*, 75-80.

261. Cornish, P. V.; Ha, T. A survey of single-molecule techniques in chemical biology. *ACS Chem. Biol.* **2007,** *2*, 53-61.

262. Joo, C.; Balci, H.; Ishitsuka, Y.; Buranachai, C.; Ha, T. Advances in single-molecule fluorescence methods for molecular biology. *Annu. Rev. Biochem.* **2008,** *77*, 51-76.

263. Selvin, P. R.; Ha, T. *Single-molecule techniques: a laboratory manual*. Cold Spring Harbor Laboratory Press: Cold Spring Harbor, N.Y., 2008; p vii, 507 p.

264. Wang, Y. F.; Guo, L.; Golding, I.; Cox, E. C.; Ong, N. P. Quantitative transcription factor binding kinetics at the single-molecule Level. *Biophys. J.* **2009,** *96*, 609-620.

265. Prescher, J. A.; Bertozzi, C. R. Chemistry in living systems. *Nat. Chem. Biol.* **2005,** *1*, 13-21.

266. Shi, X.; Jung, Y.; Lin, L. J.; Liu, C.; Wu, C.; Cann, I. K.; Ha, T. Quantitative fluorescence labeling of aldehyde-tagged proteins for single-molecule imaging. *Nat. Methods* **2012,** *9*, 499-503.

267. Jorgensen, T. J.; Chen, K.; Chasovskikh, S.; Roy, R.; Dritschilo, A.; Uren, A. Binding kinetics and activity of human poly(ADP-ribose) polymerase-1 on oligo-deoxyribonucleotide substrates. *J. Mol. Recognit.* **2009,** *22*, 446-452.

268. Nottbohm, A. C.; Dothager, R. S.; Putt, K. S.; Hoyt, M. T.; Hergenrother, P. J. A colorimetric substrate for poly(ADP-ribose) polymerase-1, VPARP, and tankyrase-1. *Angew. Chem. Int. Ed.* **2007,** *46*, 2066-2069.

269. Ueda, K.; Hayaishi, O. ADP-ribosylation. *Annu. Rev. Biochem.* **1985,** *54*, 73-100.

270. Handlon, A. L.; Xu, C.; Mullersteffner, H. M.; Schuber, F.; Oppenheimer, N. J. 2′-Ribose substituent effects on the chemical and enzymatic hydrolysis of NAD^+. *J. Am. Chem. Soc.* **1994,** *116*, 12087-12088.

271. Oppenheimer, N. J. NAD hydrolysis: chemical and enzymatic mechanisms. *Mol. Cell. Biochem.* **1994,** *138*, 245-251.

272. Berti, P. J.; Blanke, S. R.; Schramm, V. L. Transition state structure for the hydrolysis of NAD^+ catalyzed by diphtheria toxin. *J. Am. Chem. Soc.* **1997,** *119*, 12079-12088.

273. Bellocchi, D.; Costantino, G.; Pellicciari, R.; Re, N.; Marrone, A.; Coletti, C. Poly(ADP-ribose)-polymerase-catalyzed hydrolysis of NAD^+: QM/MM simulation of the enzyme reaction. *Chemmedchem* **2006,** *1*, 533-539.

274. Dudev, T.; Lim, C. Factors controlling the mechanism of NAD^+ non-redox reactions. *J. Am. Chem. Soc.* **2010,** *132*, 16533-16543.

275. Alvarez-Gonzalez, R. Synthesis and purification of deoxyribose analogs of NAD^+ by affinity chromatography and strong-anion-exchange high-performance liquid-chromatography. *J. Chromatogr.* **1988,** *444*, 89-95.

276. Alvarez-Gonzalez, R.; Moss, J.; Niedergang, C.; Althaus, F. R. Selective probing of ADP-ribosylation reactions with oxidized 2′-deoxy-nicotinamide adenine-dinucleotide. *Biochemistry* **1988,** *27*, 5378-5383.

277. Pongdee, R.; Liu, H. W. Elucidation of enzyme mechanisms using fluorinated substrate analogues. *Bioorg. Chem.* **2004,** *32*, 393-437.

278. Cen, Y.; Sauve, A. A. Diastereocontrolled electrophilic fluorinations of 2-deoxyribonolactone: syntheses of all corresponding 2-deoxy-2-fluorolactones and 2′-deoxy-2′-fluoro-NAD^+s. *J. Org. Chem.* **2009,** *74*, 5779-5789.

279. Imai, K. I.; Fujii, S.; Takanoha.K; Furukawa, Y.; Masuda, T.; Honjo, M. Studies on phosphorylation. IV. Selective phosphorylation of primary hydroxyl group in nucleosides. *J. Org. Chem.* **1969,** *34*, 1547-1550.

280. Franchetti, P.; Pasqualini, M.; Petrelli, R.; Ricciutelli, M.; Vita, P.; Cappellacci, L. Stereoselective synthesis of nicotinamide β-riboside and nucleoside analogs. *Bioorg. Med. Chem. Lett.* **2004,** *14*, 4655-4658.

281. Graeff, R.; Liu, Q.; Kriksunov, I. A.; Kotaka, M.; Oppenheimer, N.; Hao, Q.; Lee, H. C. Mechanism of cyclizing NAD to cyclic ADP-ribose by ADP-ribosyl cyclase and CD38. *J. Biol. Chem.* **2009,** *284*, 27629-27636.

282. Liu, Q.; Graeff, R.; Kriksunov, I. A.; Jiang, H.; Zhang, B.; Oppenheimer, N.; Lin, H.; Potter, B. V.; Lee, H. C.; Hao, Q. Structural basis for enzymatic evolution from a dedicated ADP-ribosyl cyclase to a multifunctional NAD hydrolase. *J. Biol. Chem.* **2009,** *284*, 27637-45.

283. Egea, P. F.; Muller-Steffner, H.; Kuhn, I.; Cakir-Kiefer, C.; Oppenheimer, N. J.; Stroud, R. M.; Kellenberger, E.; Schuber, F. Insights into the mechanism of bovine CD38/NAD^+ glycohydrolase from the X-ray structures of its Michaelis complex and covalently-trapped intermediates. *PLoS One* **2012,** *7*.

284. Kuhn, I.; Kellenberger, E.; Cakir-Kiefer, C.; Muller-Steffner, H.; Schuber, F. Probing the catalytic mechanism of bovine CD38/NAD^+ glycohydrolase by site directed mutagenesis of key active site residues. *Biochim. Biophys. Acta* **2014,** *1844*, 1317-1331.

285. Everse, J.; Anderson, B.; You, K. S. *The Pyridine nucleotide coenzymes*. Academic Press: New York, 1982; p xxxv, 389 p.

286. Ji, D.; Wang, L.; Hou, S.; Liu, W.; Wang, J.; Wang, Q.; Zhao, Z. K. Creation of bioorthogonal redox systems depending on nicotinamide flucytosine dinucleotide. *J. Am. Chem. Soc.* **2011,** *133*, 20857-20862.

287. Yates, S. P.; Merrill, A. R. Characterization of oxidized nicotinamide adenine dinucleotide (NAD^+) analogues using a high-pressure-liquid-chromatography-based NAD^+-glycohydrolase assay and comparison with fluorescence-based measurements. *Anal. Biochem.* **2005,** *340*, 41-51.

288. Wondrak, G. T.; Cervantes-Laurean, D.; Jacobson, E. L.; Jacobson, M. K. Histone carbonylation in vivo and in vitro. *Biochem. J.* **2000,** *351*, 769-777.

289. Cervantes-Laurean, D.; Minter, D. E.; Jacobson, E. L.; Jacobson, M. K. Protein glycation by ADP-ribose: studies of model conjugates. *Biochemistry* **1993,** *32*, 1528-1534.

290. van der Heden van Noort, G. J.; van der Horst, M. G.; Overkleeft, H. S.; van der Marel, G. A.; Filippov, D. V. Synthesis of mono-ADP-ribosylated oligopeptides using ribosylated amino acid building blocks. *J. Am. Chem. Soc.* **2010,** *132*, 5236-5240.

291. Moyle, P. M.; Muir, T. W. Method for the synthesis of mono-ADP-ribose conjugated peptides. *J. Am. Chem. Soc.* **2010,** *132*, 15878-15880.

292. Hengel, S. M.; Goodlett, D. R. A Review of Tandem mass spectrometry characterization of adenosine diphosphate-ribosylated peptides. *Int. J. Mass Spectrom.* **2012,** *312*, 114-121.

293. Brodbelt, J. S. Photodissociation mass spectrometry: new tools for characterization of biological molecules. *Chem. Soc. Rev.* **2014,** *43*, 2757-2783.

294. Han, S. W.; Lee, S. W.; Bahar, O.; Schwessinger, B.; Robinson, M. R.; Shaw, J. B.; Madsen, J. A.; Brodbelt, J. S.; Ronald, P. C. Tyrosine sulfation in a Gram-negative bacterium. *Nat. Commun.* **2012,** *3*, 1153.

295. Gagné, J. P.; Ethier, C.; Defoy, D.; Bourassa, S.; Langelier, M. F.; Riccio, A. A.; Pascal, J. M.; Moon, K. M.; Foster, L. J.; Ning, Z.; Figeys, D.; Droit, A.; Poirier, G. G. Quantitative site-specific ADP-ribosylation profiling of DNA-dependent PARPs. *DNA Repair (Amst.)* **2015,** *30*, 68-79.

296. Moss, J.; Yost, D. A.; Stanley, S. J. Amino acid-specific ADP-ribosylation. *J. Biol. Chem.* **1983,** *258*, 6466-6470.

297. Jacobson, E. L.; Cervantes-Laurean, D.; Jacobson, M. K. ADP-ribose in glycation and glycoxidation reactions. *Adv. Exp. Med. Biol.* **1997,** *419*, 371-379.

298. Buki, K. G.; Bauer, P. I.; Hakam, A.; Kun, E. Identification of domains of poly(ADP-ribose) polymerase for protein binding and self-association. *J. Biol. Chem.* **1995,** *270*, 3370-3377.

299. Schlessinger, J. Ligand-induced, receptor-mediated dimerization and activation of EGF receptor. *Cell* **2002,** *110*, 669-672.

300. Shaw, J. B.; Li, W.; Holden, D. D.; Zhang, Y.; Griep-Raming, J.; Fellers, R. T.; Early, B. P.; Thomas, P. M.; Kelleher, N. L.; Brodbelt, J. S. Complete protein characterization using top-down mass spectrometry and ultraviolet photodissociation. *J. Am. Chem. Soc.* **2013,** *135*, 12646-12651.

301. Cammarata, M.; Lin, K. Y.; Pruet, J.; Liu, H. W.; Brodbelt, J. Probing the unfolding of myoglobin and domain C of PARP-1 with covalent labeling and top-down ultraviolet photodissociation mass spectrometry. *Anal. Chem.* **2014,** *86*, 2534-2542.

302. Simonin, F.; Poch, O.; Delarue, M.; de Murcia, G. Identification of potential active-site residues in the human poly(ADP-ribose) polymerase. *J. Biol. Chem.* **1993,** *268*, 8529-8535.

303. Squire, P. G.; Moser, P.; O'Konski, C. T. The hydrodynamic properties of bovine serum albumin monomer and dimer. *Biochemistry* **1968,** *7*, 4261-4272.

Vita

Ke-Yi Lin was born in Taipei, Taiwan. After graduating from Kuang Jen Catholic High School in 2001, Ke-Yi entered the School of Pharmacy, National Taiwan University and received his B.S. degree in Pharmacy in 2005. He passed the Pharmacist Board Examination of Taiwan in September 2005. Following sixteen months' military service in the R.O.C. Air Force, Ke-Yi worked as a pharmacist at Sheng-Hsin Clinic in New Taipei City from 2007 to 2008. In the summer of 2008, Ke-Yi was admitted to the graduate program in the Division of Medicinal Chemistry, College of Pharmacy at the University of Texas at Austin. He joined Dr. Hung-wen Liu's research laboratory in the spring of 2009 and began studying the catalytic mechanism of human poly(ADP-ribose) polymerase-1 for his doctoral research.

E-mail: keyi.lin@utexas.edu

This manuscript was typed by the author.